UNIVERSITAT ROVIRA I VIRGILI

DESIGN AND CONTROL OF A BIDIRECTIONAL DC/DC CONVERTER FOR AN ELECTRIC VEHICLE APPLICATION.

Laura Albiol Rendillo

Dipòsit Legal: T 1361-2015

ADVERTIMENT. L'accés als continguts d'aquesta tesi doctoral i la seva utilització ha de respectar els drets de la persona autora. Pot ser utilitzada per a consulta o estudi personal, així com en activitats o materials d'investigació i docència en els termes establerts a l'art. 32 del Text Refós de la Llei de Propietat Intel·lectual (RDL 1/1996). Per altres utilitzacions es requereix l'autorització prèvia i expressa de la persona autora. En qualsevol cas, en la utilització dels seus continguts caldrà indicar de forma clara el nom i cognoms de la persona autora i el títol de la tesi doctoral. No s'autoritza la seva reproducció o altres formes d'explotació efectuades amb finalitats de lucre ni la seva comunicació pública des d'un lloc aliè al servei TDX. Tampoc s'autoritza la presentació del seu contingut en una finestra o marc aliè a TDX (framing). Aquesta reserva de drets afecta tant als continguts de la tesi com als seus resums i índexs.

ADVERTENCIA. El acceso a los contenidos de esta tesis doctoral y su utilización debe respetar los derechos de la persona autora. Puede ser utilizada para consulta o estudio personal, así como en actividades o materiales de investigación y docencia en los términos establecidos en el art. 32 del Texto Refundido de la Ley de Propiedad Intelectual (RDL 1/1996). Para otros usos se requiere la autorización previa y expresa de la persona autora. En cualquier caso, en la utilización de sus contenidos se deberá indicar de forma clara el nombre y apellidos de la persona autora y el título de la tesis doctoral. No se autoriza su reproducción u otras formas de explotación efectuadas con fines lucrativos ni su comunicación pública desde un sitio ajeno al servicio TDR. Tampoco se autoriza la presentación de su contenido en una ventana o marco ajeno a TDR (framing). Esta reserva de derechos afecta tanto al contenido de la tesis como a sus resúmenes e índices.

WARNING. Access to the contents of this doctoral thesis and its use must respect the rights of the author. It can be used for reference or private study, as well as research and learning activities or materials in the terms established by the 32nd article of the Spanish Consolidated Copyright Act (RDL 1/1996). Express and previous authorization of the author is required for any other uses. In any case, when using its content, full name of the author and title of the thesis must be clearly indicated. Reproduction or other forms of for profit use or public communication from outside TDX service is not allowed. Presentation of its content in a window or frame external to TDX (framing) is not authorized either. These rights affect both the content of the thesis and its abstracts and indexes.

Laura Albiol Tendillo

DESIGN AND CONTROL OF A BIDIRECTIONAL DC/DC CONVERTER FOR AN ELECTRIC VEHICLE APPLICATION

DOCTORAL THESIS

Department of Electronic, Electric
and Automatic Engineering

UNIVERSITAT ROVIRA I VIRGILI

UNIVERSITAT ROVIRA I VIRGILI
DESIGN AND CONTROL OF A BIDIRECTIONAL DC/DC CONVERTER FOR AN ELECTRIC VEHICLE APPLICATION.
Laura Albiol Rendillo
Dipòsit Legal: T 1361-2015

Laura Albiol Tendillo

DESIGN AND CONTROL OF A BIDIRECTIONAL DC/DC CONVERTER FOR AN ELECTRIC VEHICLE APPLICATION

DOCTORAL THESIS

Supervised by Dr. Enric Vidal Idiarte
and Dr. Javier Maixé Altés

Department of Electronic, Electric
and Automatic Engineering

UNIVERSITAT ROVIRA I VIRGILI
Tarragona
2015

UNIVERSITAT ROVIRA I VIRGILI
DESIGN AND CONTROL OF A BIDIRECTIONAL DC/DC CONVERTER FOR AN ELECTRIC VEHICLE APPLICATION.
Laura Albiol Rendillo
Dipòsit Legal: T 1361-2015

UNIVERSITAT ROVIRA I VIRGILI
DESIGN AND CONTROL OF A BIDIRECTIONAL DC/DC CONVERTER FOR AN ELECTRIC VEHICLE APPLICATION.
Laura Albiol Rendillo
Dipòsit Legal: T 1361-2015

UNIVERSITAT
ROVIRA I VIRGILI
Departament d'Enginyeria Electrònica,
Elèctrica i Automàtica

Avinguda Països Catalans, 26
43007 Tarragona
Tel. +34 977 55 96 10
Fax +34 977 55 96 05

WE STATE that the present study, entitled "Design and Control of a Bidirectional DC/DC Converter for an Electric Vehicle Application", presented by Laura Albiol Tendillo for the award of the degree of Doctor, has been carried out under our supervision at the Department of Electronic, Electric and Automatic Engineering of this university.

Tarragona, 2 June 2015

Doctoral Thesis Supervisor	Doctoral Thesis Supervisor
Dr. Enric Vidal Idiarte	Dr. Javier Maixé Altés

A la meva família,
gràcies al vostre suport incansable
he aconseguit arribar fins aquí.

UNIVERSITAT ROVIRA I VIRGILI
DESIGN AND CONTROL OF A BIDIRECTIONAL DC/DC CONVERTER FOR AN ELECTRIC VEHICLE APPLICATION.
Laura Albiol Rendillo
Dipòsit Legal: T 1361-2015

Acknowledgements

First of all, I would like to express my gratitude to my thesis supervisors, Dr. Enric Vidal-Idiarte and Dr. Javier Maixé-Altés. They have shown their trust and support, both when I was a research technician and along the thesis. Their guidance and technical observations have been essential to the completion of my work.

I also want to remark the undoubted help that my colleagues in the Automatic Control and Industrial Electronics Group (GAEI) have offered. All the hours working together in the laboratory have resulted in a valuable friendship, so thank you Toni León, Josep M. Bosque, Adrià Marcos, Freddy Flores, Sylvia Méndez, Harrynson Ramírez, Ricardo Bonache, Reham Haroun, Albert Teixidó, Carlos Olalla, Mirko Bodetto, Xavi Alsina, Sai Wu-Fu and Toni Martínez. I would like to especially thank the latter, Toni Martínez, who has critically helped me with the experimental part of my thesis.

All the professors of the department have been really supportive, but I would like to mention Roberto Giral, who assisted me with the interleaving of converters; Luis Martinez, who gave excellent advice to organize and publish papers; Angel Cid, for searching new perspectives and applications to my work; and Javier Calvente, for solving questions related to the analysis of DC/DC converters.

Moreover, I would like to thank my family (and particularly my parents Àlvaro and Remei, my sister Marta and her partner Marc, my aunt Àngels and my grandparents Miguel and Ángela) for their priceless withstanding during the entire thesis. They have not stopped to encourage me in any moment. I am also very grateful with my friends who have been incessantly caring and understanding. Last, but not least, I would like to thank Joan, for sharing with me the good and bad moments of the final part of my PhD, and motivating me to push forward.

UNIVERSITAT ROVIRA I VIRGILI
DESIGN AND CONTROL OF A BIDIRECTIONAL DC/DC CONVERTER FOR AN ELECTRIC VEHICLE APPLICATION.
Laura Albiol Rendillo
Dipòsit Legal: T 1361-2015

Abstract

The present thesis deals with the analysis, design and control of a DC/DC converter for the powertrain of an electric vehicle. The objective is to develop an integral solution of DC/DC converter and control that supports bidirectional operation, in order to recover energy during regenerative braking.

The proposed DC/DC converter topology is a bidirectional boost converter with output filter. The stability of this topology is analysed considering the electric vehicle application. A motor drive can behave as a constant power load, which has negative incremental impedance, and thus holds unstable effects. An RC snubber is presented to avoid the instability, and a 1.5-kW prototype is designed.

Sliding-mode control is the chosen control method for the current loop of the bidirectional boost converter with output filter, due to its robustness and disturbances rejection capability. The stability of the converter under sliding mode control is corroborated according to the Routh-Hurwitz criterion. Then, the voltage PI control is designed by means of the small-signal transfer functions of the bidirectional boost converter with output filter. As the Middlebrook criterion is accomplished, the stable DC/DC converter will remain stable when the load is connected. An analogue implementation of both the current sliding-mode and the voltage PI controller for the designed converter is presented, and validated by simulation and experimental tests.

In order to increase the power rating of the system, as it should be done for a real electric vehicle application, several converters are interleaved. A ring-configuration interleaved system with sliding-mode control is proposed and analysed, and later the analogue control circuit is developed. Finally, in the adopted solution for this thesis three 1.5-kW converters are interleaved, and the feasibility of the system is proven both by simulation and experimental results.

Focusing on the electric vehicle application, a 4.5-kW powertrain emulator will be used to verify the design of the converter and the control under a realistic driving profile. The features of the emulator are set, and then a Matlab/Simulink model is developed in order to test the model in the first instance. Later, the experimental set-up is implemented, and results show the stability of the interleaved bidirectional boost converters with output filter under a driving profile, both during traction and regenerative braking.

Contents

UNIVERSITAT ROVIRA I VIRGILI
DESIGN AND CONTROL OF A BIDIRECTIONAL DC/DC CONVERTER FOR AN ELECTRIC VEHICLE APPLICATION.
Laura Albiol Rendillo
Dipòsit Legal: T 1361-2015

UNIVERSITAT ROVIRA I VIRGILI
DESIGN AND CONTROL OF A BIDIRECTIONAL DC/DC CONVERTER FOR AN ELECTRIC VEHICLE APPLICATION.
Laura Albiol Rendillo
Dipòsit Legal: T 1361-2015

List of figures

UNIVERSITAT ROVIRA I VIRGILI
DESIGN AND CONTROL OF A BIDIRECTIONAL DC/DC CONVERTER FOR AN ELECTRIC VEHICLE APPLICATION.
Laura Albiol Rendillo
Dipòsit Legal: T 1361-2015

List of tables

List of abbreviations and symbols

BBCOF	Bidirectional Boost Converter with Output Filter
EMI	Electro-Magnetic Interferences
EV	Electric Vehicle
GHG	Greenhouse Gases
HEV	Hybrid Electric Vehicle
ICE	Internal Combustion Engine
IM	Induction Machine
PMSM	Permanent Magnet Synchronous Machine
SRM	Switched Reluctance Machine
ZOH	Zero-Order Hold

B	damping coefficient [N·m·s]
C_1	capacitance of the boost converter from the BBCOF [F]
C_2	capacitance of the output filter from the BBCOF [F]
C_d	RC snubber capacitance [Ω]
d	duty cycle
f_s	switching frequency [Hz]
$G_c(s)$	transfer function of the voltage controller
$h(t)$	current reference in interleaving obtained from the voltage controller [A]
i_a, i_b, i_c	currents of the motor phases [A]
i_{C1}	current in C_1 capacitor of the BBCOF [A]
i_{C2}	current in C_2 capacitor of the BBCOF [A]
I_{CPL}	value current of the current source of the CPL model [A]
i_d	d-axis current [A]
I_{dc}	current consumed from the DC bus [A]
i_{L1}	current in L_1 inductor of the BBCOF [A]
i_{L2}	current in L_2 inductor of the BBCOF [A]
i_o	load current source of the BBCOF [A]
i_{ph}	phase current of a SRM [A]
i_q	q-axis current [A]
i_{ref}	time-varying current reference for the BBCOF [A]
J	rotor inertia [kg·m^2]
k	constant current reference for the BBCOF [A]
k_e	motor electrical constant [V/krpm]
k_i	gain of the BBCOF current sensor
k_{Ii}	integral gain of the PMSM current controller
k_{Ip}	proportional gain of the PMSM current controller
k_t	motor torque constant [N·m/A]
k_v	gain of the BBCOF voltage sensor
L_1	inductance of the boost converter from the BBCOF [H]
L_2	inductance of the output filter from the BBCOF [H]

UNIVERSITAT ROVIRA I VIRGILI
DESIGN AND CONTROL OF A BIDIRECTIONAL DC/DC CONVERTER FOR AN ELECTRIC VEHICLE APPLICATION.
Laura Albiol Rendillo
Dipòsit Legal: T 1361-2015

L_{lr}	rotor leakage inductance of an IM[H]
L_{ls}	stator leakage inductance of an IM [H]
L_{ph}	phase inductance of a SRM [H]
L_s	stator self-inductance per phase in a PMSM [H]
N	number of interleaved converters
P	number of poles of the machine
P_{CPL}	power of the CPL model [W]
P_n	nominal power of the BBCOF [W]
Q_1	low-side switch of the BBCOF
Q_2	high-side switch of the BBCOF
R_{CPL}	resistance of the CPL model [Ω]
R_d	RC snubber resistance [Ω]
R_{L1}	parasitic resistance of the L1 inductor [Ω]
R_{L2}	parasitic resistance of the L2 inductor [Ω]
R_{load}	load resistance for the BBCOF [Ω]
R_r	rotor resistance [Ω]
R_s	stator resistance [Ω]
s	slip of an asynchronous machine
S	sliding surface [A]
t	time [s]
$T(s)$	loop gain
T_e	electromagnetic torque [N·m]
T_L	load torque [N·m]
u	control signal of the BBCOF
u_{eq}	equivalent control of the BBCOF
V	Lyapunov function [A]
v_{C1}	voltage in C_1 capacitor of the BBCOF [V]
v_{C2}	voltage in C_2 capacitor of the BBCOF [V]
V_d	d-axis voltage [V]
V_{dc}	DC bus voltage [V]
v_{err}	error between the voltage reference and the sensed voltage [V]
v_g	source voltage [V]
v_{L1}	voltage in L_1 inductor of the BBCOF [V]
v_{L2}	voltage in L_2 inductor of the BBCOF [V]
v_o	voltage at the output of the BBCOF [V]
$v_{o,ref}$	voltage reference for the BBCOF [V]
V_q	q-axis voltage [V]
V_s	stator voltage [V]
x	vector of state-space variables
$Z_i(s)$	input impedance of the PMSM drive
$Z_o(s)$	output impedance of the BBCOF
Δi_{L1}	peak current ripple in L_1 inductor [A]
Δi_{L2}	peak current ripple in L_2 inductor [A]
Δv_{C1}	peak voltage ripple in C_1 capacitor [V]
Δv_{C2}	peak voltage ripple in C_2 capacitor [V]
ϑ	electrical rotor position [rad]
λ_f	flux linkage established by the permanent magnets [V·s]
ω_e	electric angular speed [rad/s]
ω_p	pole pulsation of the controller [rad/s]
ω_r	rotor angular speed [rad/s]
ω_z	zero pulsation of the controller [rad/s]

1 Introduction

1.1 The electric vehicle

1.1.1 History of the electric vehicle

Although the electric vehicle (EV) may seem a relatively novel invention, its origins go back to the XIX century. The first EV was invented in 1828 by Slovak-Hungarian priest Ányos Jedlik. It was a toy car that used an electric motor as a propelling force [1]. The motor consisted of a rudimental combination of electromagnets sequentially switched by commutators, which offered both low power and low efficiency.

Successive EV were developed with electromagnet-based motors and using electrochemical cells as a source of energy. Although quite limited, their features overcame those of the internal combustion engine (ICE) vehicles, first invented in 1826 by the American inventor Samuel Morey.

Further development was achieved with the use of a lead-acid rechargeable battery, by Gaston Planté in 1859. Moreover, the efficiency of the DC electric motors was improved thanks to the improvements introduced by Zénobe Gramme in 1873 [2]. The first commercial EV vehicle dates from 1893. This design from Paul Pouchain was able to carry six passengers at 16 km/h. Until 1910s, EV outnumbered ICE vehicles. However, the mass production of ICE vehicles introduced by Henry Ford in 1910 and the invention of the automobile starter in 1920 by Charles Kettering finished the prevalence of the EV over ICE vehicles. Moreover, the large-scale oil production that started in 1920 offered extended driving range to the ICE vehicles, with a lower production cost. This combination of factors made EVs less attractive [3], and after the 1920s their use became very restricted.

Interest was focused again on EV after the oil embargo of 1973 for price and energy availability reasons [4]. Moreover, there is a growing concern on environmental issues concerning ICE vehicles, the constantly growing energy demand and the depletion of fossil fuels [5]. As a consequence, several governments have incentivised both the development and the purchase of EVs [6]. Therefore, EVs constitute a powerful alternative, although some technological problems still have to be suppressed [7].

UNIVERSITAT ROVIRA I VIRGILI
DESIGN AND CONTROL OF A BIDIRECTIONAL DC/DC CONVERTER FOR AN ELECTRIC VEHICLE APPLICATION.
Laura Albiol Rendillo
Dipòsit Legal: T 1361-2015

1.1.2 Motivation

In the EU transportation accounts for one quarter of the GHG emissions, becoming the second gas-emitting source after energy [8]. Accordingly, the EU has established several GHG reduction policies, including that ICE vehicles constitute only the half of the urban transport in 2030, and become eradicated on 2050 [9].

However, there is criticism on EVs as they are regarded as zero-emission vehicles, although obtaining the electricity used to charge the EVs is a GHG-emitting process. Therefore, do EVs reduce the emissions compared to gasoline vehicles? The answer is clearly affirmative, but the reduction is subjected to the proportion of the electricity sources found in every region [10]. With the aim to assess the emissions reduction attained with the use of EV instead of ICE vehicles, the particular case of Europe will be studied. Fig. 1.1 shows the 2012 Europe electricity grid mix, according to the Eurostat statistics [11].

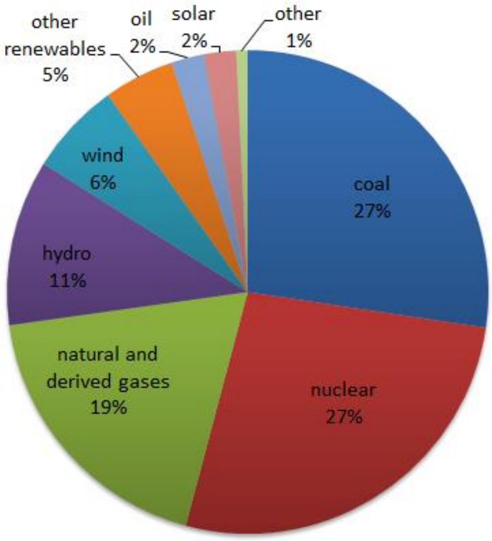

Fig. 1.1. 2012 European energy consumption by electricity source.

In order to compare the emissions of a fuel-powered vehicle to those of an electrical one, the concept of l/100 km is used. In Table 1.I, the equivalent consumption of every energy source is presented [10]. For example, an EV only powered by electricity from coal would produce the same GHG emissions that a 7.84 l/100 km gasoline vehicle. The reference vehicle is a Nissan Leaf [12], with a consumption of 0.21 kWh/km. Combining the data in Fig. 1.1 and Table 1.I, an EV charged in the average European grid would have an equivalent 3.34 l/100 km approximately, according to GHG emissions. No gasoline vehicle can equal this emission rating, therefore EV do reduce the emissions that cause the climate change. However, there is plenty of scope for emission reduction, progressively dropping generation based on non-renewable products and improving the efficiency of electricity generation. These facts partially explain the market growing interest towards hybrid and electric vehicles, as stated in Fig. 1.2 [13]. According to the represented data, in 2050 there will be no ICE vehicles, and the vast majority of cars will be either plug-in hybrids or electric.

Table 1.I. EV consumption equivalent by electricity source

coal	7.84 l/100 km
oil	7.35 l/100 km
natural and derived gases	4.36 l/100 km
solar	0.47 l/100 km
nuclear	0.12 l/100 km
wind	0.06 l/100 km
hydro	0.04 l/100 km

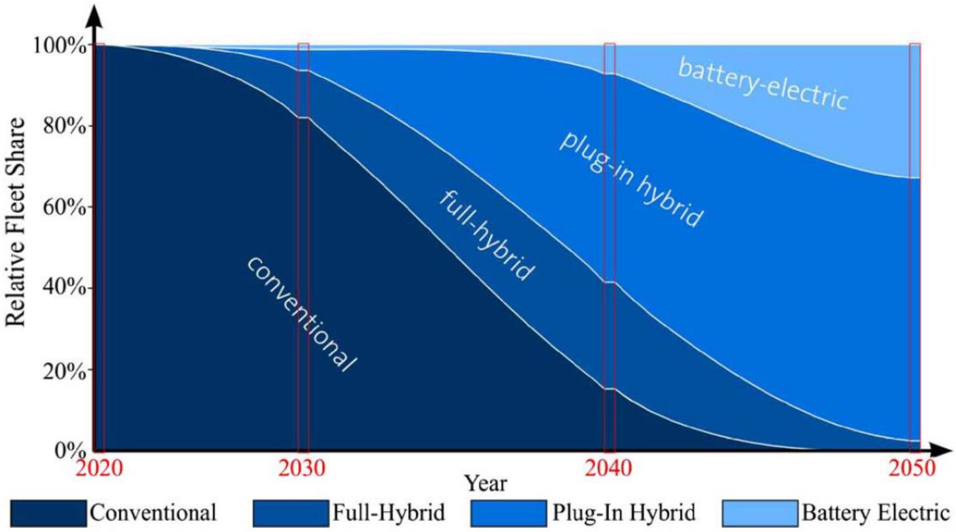

Fig. 1.2. Predicted vehicle fleet composition.

1.1.3 Current deployment

Currently, there are several HEVs and EVs commercially available. While the EVs are fully-powered by the battery, HEVs have more or less intensive usage of the battery depending on the model. Considering on the penetration of electrical energy in the HEV architecture, i.e. the power ratio between the ICE and the electric machines, it is possible to distinguish the following degrees of hybridization [14]:

- **Micro HEV**: the electric machine has a reduced power rating (1.5 to 3 kW [15]), and it is only used during start-up operation as an alternator, while the engine is used for propulsion. The efficiency gain resides in stopping the engine every time the vehicle is halted, usually known as start-stop system. Some examples of micro HEV vehicles are Ford Fiesta and Honda Civic.
- **Mild HEV**: the electric machine has a low power rating (10 to 20 kW). Apart from the start-stop functionality, the electric machine can provide extra power during acceleration or braking. The battery is only recharged by regenerative braking. Peugeot 308 e-HDi and BMW ActiveHybrid 7 are two mild HEV commercially available.
- **Full Hybrid**: the electric machine has an intermediate to high power rating (40 to 80 kW), allowing the vehicle to run solely on electricity depending on its speed and the state of charge of the battery –the limits vary in every model. Moreover, the engine

UNIVERSITAT ROVIRA I VIRGILI
DESIGN AND CONTROL OF A BIDIRECTIONAL DC/DC CONVERTER FOR AN ELECTRIC VEHICLE APPLICATION.
Laura Albiol Rendillo
Dipòsit Legal: T 1361-2015

and the electrical machine can operate simultaneously to provide the maximum performance. The battery recharge is produced by regenerative braking.

- **Plug-in Hybrid**: it has the features of a full hybrid, but it can also be recharged by plugging it in the grid. For high power ratings of the electrical machine, the engine actuates as a range extender, operating at its most efficient point and recharging the battery during propulsion.

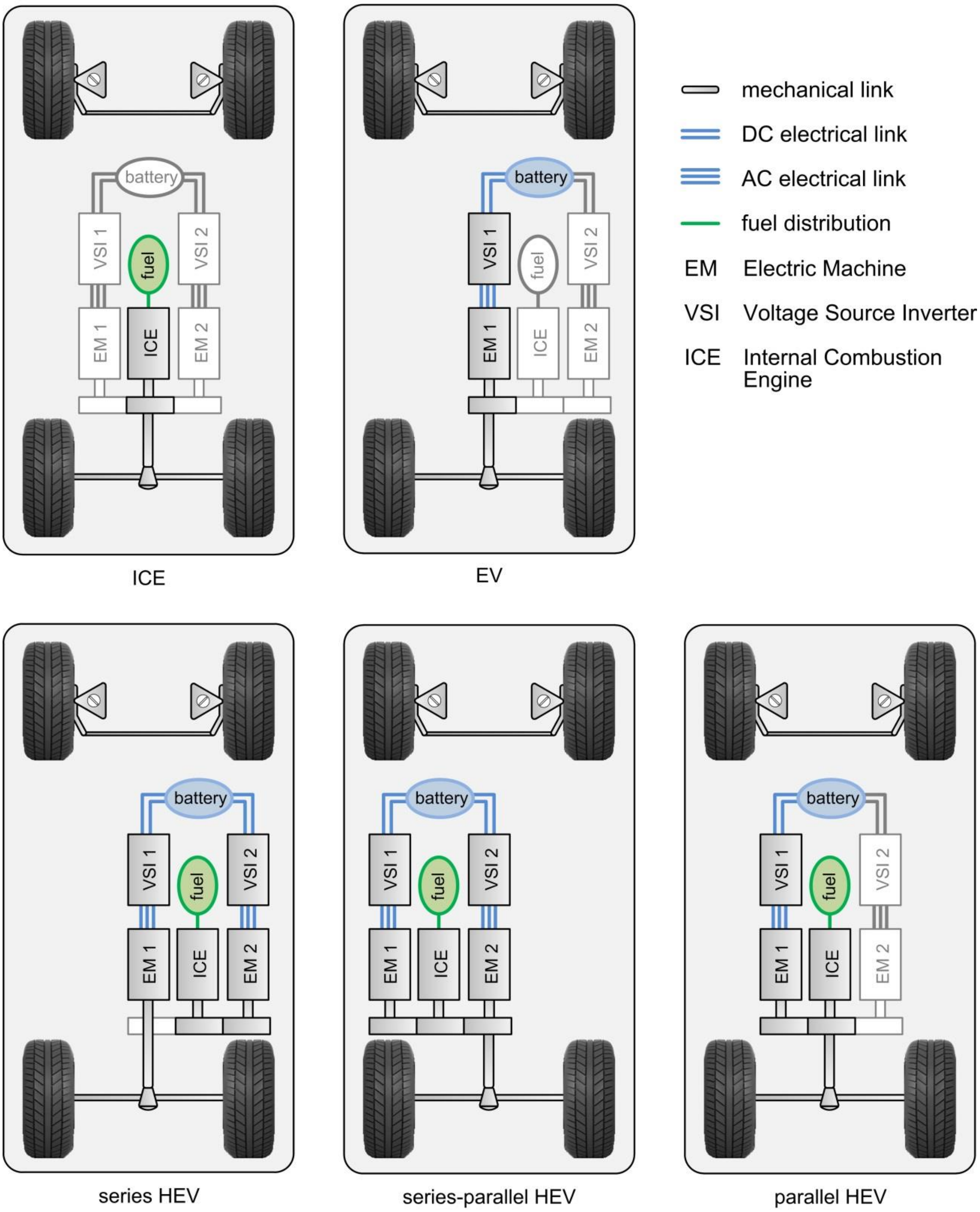

ICE EV

series HEV series-parallel HEV parallel HEV

Fig. 1.3. ICE, HEV and EV configurations.

These functionalities are reached by using different powertrain architectures, which can be classified as follows:

- **Parallel HEV:** the vehicle can be driven by the engine, the electric machine or both simultaneously. In order to do so, the electric machine and the engine have to be mechanically coupled. This architecture is particularly efficient when driving at constant high speeds, since the engine works at its most efficient point and the electrical machine supplies extra power when it is necessary [16].
- **Series HEV**: the vehicle is driven by the electric machine, which is powered from the battery. The engine is coupled with another electric machine that actuates as a generator and charges the battery during vehicle operation, depending on the driving conditions. This architecture is more efficient in urban driving cycles with frequent stop/start manoeuvres, since the motor does not run when the vehicle is halted, and starting an electric motor consumes less energy than starting an engine.
- **Series-parallel HEV:** this architecture permits the vehicle to work either as a parallel or a series HEV. Consequently, the two electric machines and the engine have to be mechanically coupled by a planetary gear unit [17].

The different HEVs architectures are represented in Fig. 1.3, together with an ICE vehicle and an electric one. All the architectures can be seen as a special case of the series-parallel HEV architecture in which some parts have been removed.

These architectures do not directly correspond to one of the aforementioned degrees of hybridization. As a rough approach, the parallel architecture is used in low degrees of hybridization, since a low power electrical machine would be unable to drive the vehicle, and the series architecture is used in high degrees of hybridization, since the engine is used to charge the battery on the go. The detailed relationship is stated in Table 1.II [14, 18].

Table 1.II. Degree of hybridization by architecture type.

		ICE	HEV				EV
			micro	mild	full	plug-in	
ICE		x					
HEV	parallel		x	x	x	x	
	series-parallel				x	x	
	series				x	x	
EV							x

1.2 DC/DC converter

Both HEV and EV have electric motors that are powered from the battery via a voltage source inverter. For vehicle performance optimization, it is interesting to maintain the battery rated voltage relatively low, since this means using fewer cells connected in series. However, from the motor point of view, it is necessary to have a high-voltage DC bus because the rated voltage and the power delivered by the motor are directly dependant. Moreover, in the case of permanent magnet synchronous machines, it is especially convenient to a have high-voltage

DC bus to displace the flux-weakening region to the high-speed region [19]. An additional advantageous feature of the introduction of a DC/DC converter is having a regulated DC voltage, which results in better performance of the motor drive [20]. As a consequence, a DC/DC bidirectional converter is usually inserted between the battery and the inverter, in order to match the different voltage rating of these two elements [21], as depicted in Fig. 1.4.

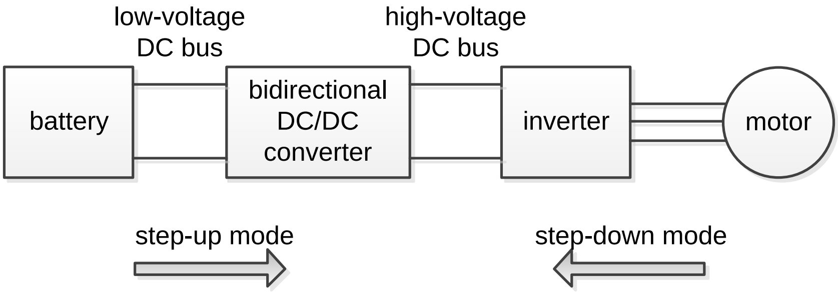

Fig. 1.4. Emplacement of the DC/DC converter in the traction system of an EV.

This DC/DC converter has to be bidirectional in order to enable power delivery from the battery to the motor (step-up motor) and battery recharging during regenerative braking (step-down mode). Galvanic isolation is not needed, opposed to the DC/DC converter between the high voltage and the 12 V-battery. The basic non-isolated second-order topologies available are boost [22, 23] and buck-boost [24-26] converters, Fig. 1.5.a and b respectively, and higher order converters include Ćuk [27, 28] and SEPIC [29-32] converters, Fig. 1.6.a and Fig. 1.6.b respectively. Generally, the DC/DC converter used in the powertrain of the electric and hybrid electric vehicles is a boost-type converter [33]. Considering this, this thesis studies a bidirectional boost converter with output filter (BBCOF). BBCOF is a competitive solution as intermediate voltage step-up stage in EVs, since this converter presents a significant reduction of the EMI level in comparison with conventional boost structures [34]. BBCOF also offers indirectly improved reliability, since the implementation of the filter capacitors require components of smaller capacitance in comparison to a conventional boost converter, which allows the natural introduction of high-quality capacitors such as polypropylene, ceramic multilayer, etc. In a clear-cut contrast, the use of a conventional boost converter would require for the same level of output ripple much bigger capacitance which eventually must be implemented by means of electrolytic capacitors, this resulting in a poorer reliability and bigger losses.

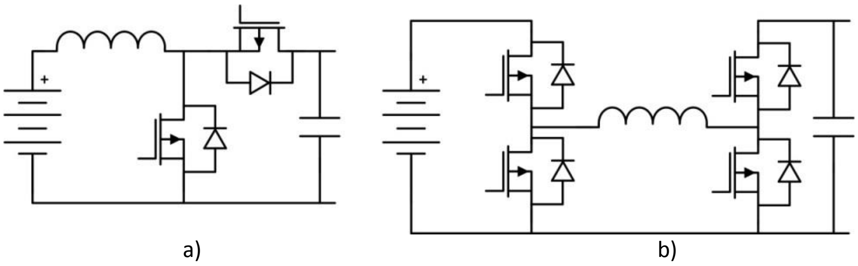

a) b)

Fig. 1.5. Basic second-order DC/DC converter topologies for the EV powertrain: a) boost and b) buck-boost converter.

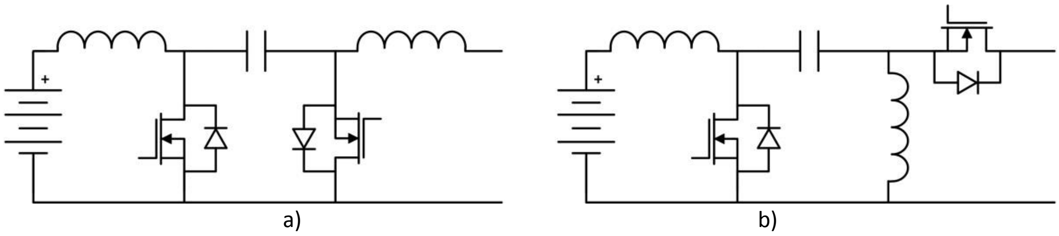

a) b)

Fig. 1.6. Fourth-order DC/DC converter topologies for the EV powertrain: a) Ćuk and b) SEPIC converter.

In [35] the following essential design criteria for DC/DC converters for automotive are considered:

- light weight
- high efficiency
- small volume
- low electromagnetic interference
- low current ripple drawn from the battery

These points have to be considered during the design of the selected DC/DC converter, i.e. the BBCOF.

1.3 Control of DC/DC converters

Previous research on the control of bidirectional DC-DC converters has led to different solutions, such as using two PWM controllers [36], an adaptive control by means of two PI controllers [37], and a set of two hysteretic controllers for a dual active bridge, one for each full bridge converter, that are alternated when the operation mode of the converter changes [38].

Recently, some solutions on the bidirectional control of DC/DC converters with a seamless transition between the operating modes have been published. A seamless transition in a bidirectional DC-DC converter is a transition between operation modes with uninterrupted power delivery and stable output voltage [39]. In [40], a bidirectional control for a soft-switching half-bridge DC-DC converter for the electric vehicle is presented. The seamless variation is guaranteed by inserting an additional switching pattern when changing from one operation mode to the other. A bidirectional control of a dual active bridge is presented in [38]. The gate signals are selected according to the sign of the demanded current, and the change is also performed seamlessly. Similarly, in [41] a seamless mode change strategy is accomplished by switching between two different controls according to a certain threshold of the demanded current for a bidirectional resonant converter. In [42], a certain duty cycle is set, and then current is allowed to circulate in both directions. Two different controls are used depending on the current ripple in order to avoid instability.

In [43], a sliding-mode control strategy is used in battery energy storage applications to control the output current of a bidirectional buck converter with an output LCL-filter, which results in a higher attenuation of the high frequency harmonics in the battery current than the usual

L-filter. A single sliding-mode controller is used for the battery current in both step-up and step-down modes. However, the output voltage is not regulated.

This thesis proposes the sliding-mode control approach for an EV bidirectional boost converter with output filter as the solution to achieve a seamless mode change strategy with a single controller guaranteeing output voltage regulation. The sliding-mode approach is the natural way to control variable structure systems like switching converters and it features robustness and design simplicity at the expense of variable switching frequency [44]-[45].

1.4 Electric machines

The electric machine is the key element in the powertrain of an EV, since its features determine the performance of the entire vehicle. Most EV use either induction or permanent magnet synchronous machines as traction motors [46]. Recently, switched reluctance machines have gathered significant interest for researchers and automakers. These three machine types are strong candidates for the powertrain of EV and HEV since they have the torque-speed characteristic shown in Fig. 1.7 [47].

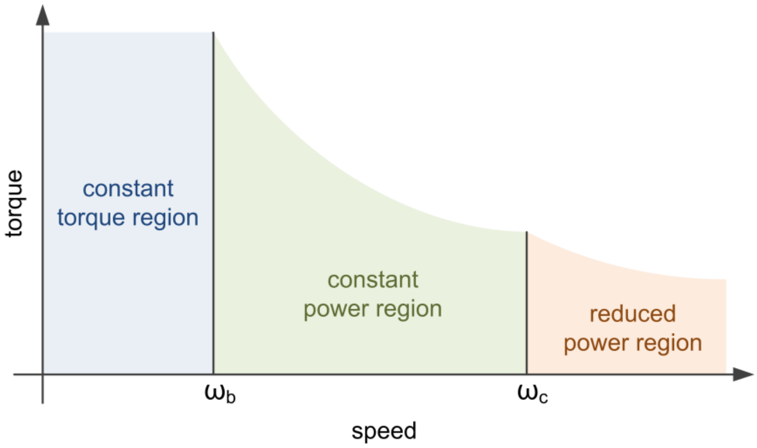

Fig. 1.7. Ideal torque-speed characteristic.

Moreover, the selected machine has to accomplish the following set of specifications [48]:

- High torque density and power density
- Wide speed range and wide constant power region
- High efficiency over wide speed and torque ranges
- High torque for starting and hill climbing
- High power for high-speed cruising
- High overload capacity for overtaking
- High reliability and robustness
- Reasonable cost
- Low acoustic noise
- Low torque ripple

1.4.1 Induction machines

Induction machines (IM) are a mature technology with a relatively low cost and ease of control [46]. Two types of induction machines can be distinguished depending on the rotor construction, the squirrel cage and the wound motor induction machine, although the former is more popular due to its robustness [33]. The arrangement of an IM with squirrel cage rotor is shown in Fig. 1.8.a. The voltage applied to the stator windings generates a magnetic field. Since this voltage is AC, the direction of the magnetic field rotates at the same frequency than the applied voltage. When this moving magnetic field crosses a conductor, in this case, a squirrel cage bar, a voltage is induced in the terminals of the bar. As the bars are connected as seen in Fig. 1.8.b, the induced voltage causes a current conduction through the rotor bars. According to the Lorentz law, when there is a conductor with circulating current exposed to a magnetic field, this conductor experiments a force that provokes its movement. Consequently, torque is produced, and the rotor spins. The same phenomenon takes place in a wounded-rotor IM, but bars are replaced by rotor windings.

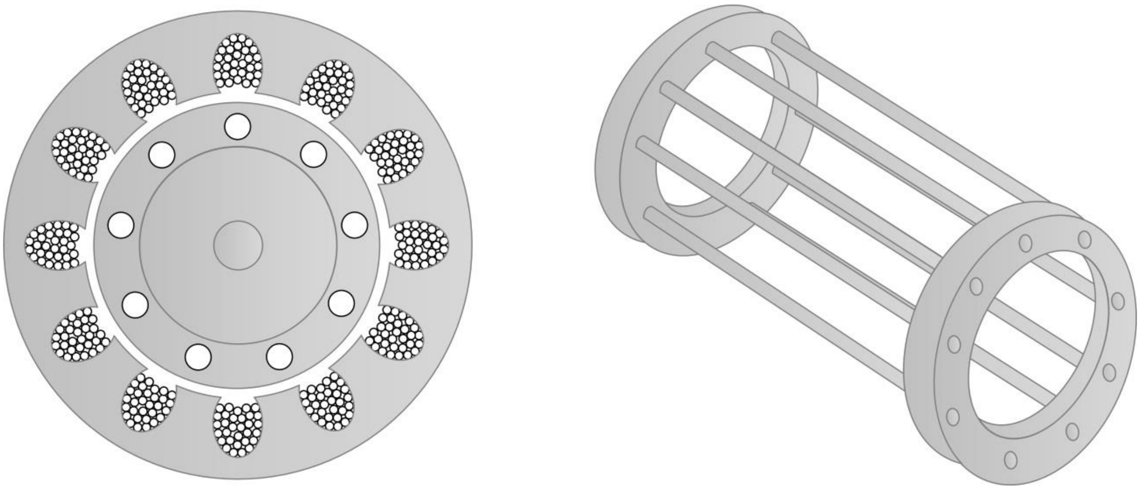

Fig. 1.8. Representation of an IM: a) frontal view of the stator and squirrel cage rotor, and b) perspective of the squirrel cage.

For torque production, it is necessary that the magnetic field crosses the rotor conductors. This means that in case the magnetic field and the rotor rotated at the same speed there would be no torque production, and the rotor would reduce its speed. Consequently, IMs are asynchronous machines, i.e. the magnetic field and the rotor have different rotating speeds. This speed difference is evaluated with the slip figure [49], defined as

$$s = \frac{\omega_e - (P/2)\omega_r}{\omega_e}, \tag{1.1}$$

where ω_e is the electric angular speed, ω_r is the rotor angular speed and P is the number of poles of the machine. Then, the electromagnetic torque generated by the motor is

$$T_e = \frac{P}{2}\frac{3r_r}{\omega_e s}\frac{V_s^2}{\left(R_s + \frac{R_r}{s}\right)^2 + \omega_e^2\left(L_{ls} + L_{lr}\right)^2}, \tag{1.2}$$

UNIVERSITAT ROVIRA I VIRGILI
DESIGN AND CONTROL OF A BIDIRECTIONAL DC/DC CONVERTER FOR AN ELECTRIC VEHICLE APPLICATION.
Laura Albiol Rendillo
Dipòsit Legal: T 1361-2015

where R_s is the stator resistance, R_r the rotor resistance, L_{ls} the stator leakage inductance, L_{lr} the rotor leakage inductance and V_s the stator voltage. Knowing the generated electromagnetic torque, the dynamics of the mechanical part can be obtained from the following equation, valid for any type of motor

$$T_e = J\frac{d}{dt}\omega_r + B\omega_r + T_L\,, \tag{1.3}$$

where J is the rotor inertia, B is the damping coefficient and T_L is the load torque. Consequently, the motor speed and torque can be controlled by means of the stator voltage and the electric angular speed, i.e. the frequency.

1.4.2 Permanent magnet synchronous machines

Permanent magnet synchronous machines (PMSM) are eligible for the powertrain of an electric vehicle due to their high power density and efficiency, despite the cost of the rare earth magnets and their limited availability. The stator is wounded, whereas the rotor has rare earth magnets inserted. The distribution of the earth magnets has a direct effect on the drive characteristics and performance. The most typical PMSM structures are the surface-mounted magnet in Fig. 1.9.a, with constant reluctance and low power density, the inset magnet in Fig. 1.9.b, with variable reluctance and low power density, and the interior magnet in Fig. 1.9.c and Fig. 1.9.d. The difference between these two interior distributions is that the flux-concentrating distribution of Fig. 1.9.d offers higher air gap field density with the same magnets, although the shaft has to be made of a non-ferromagnetic material.

To generate the electromagnetic torque, the stator windings are fed with an AC voltage, in the same way that the field in IM is created. The magnets in the rotor will align with the rotating stator field, making the motor spin. As magnets follow the rotation of the stator field, PMSMs are, as their name indicates, synchronous machines. The expression for the electromagnetic torque is

$$T_e = \frac{3}{2}\frac{P}{2}\lambda_f i_q = k_e i_q\,, \tag{1.4}$$

where λ_f is the flux linkage established by the permanent magnets, and k_e is the motor torque constant. Consequently, the electromagnetic torque is proportional to i_q, the q-axis current of the PMSM [50], which can be calculated as

$$i_q = \frac{2}{3}\left(\sin(\theta)i_a + \sin\left(\theta - \frac{2\pi}{3}\right)i_b + \sin\left(\theta + \frac{2\pi}{3}\right)i_c\right), \tag{1.5}$$

where θ is the electrical rotor position, and i_a, i_b and i_c are the currents of the motor phases. Then, the dynamics of the mechanical part can be calculated with (1.3). Therefore the motor can be controlled by means of the phase currents. Considering the dq modelling of the machine, the PMSM can be controlled like a DC machine by i_q.

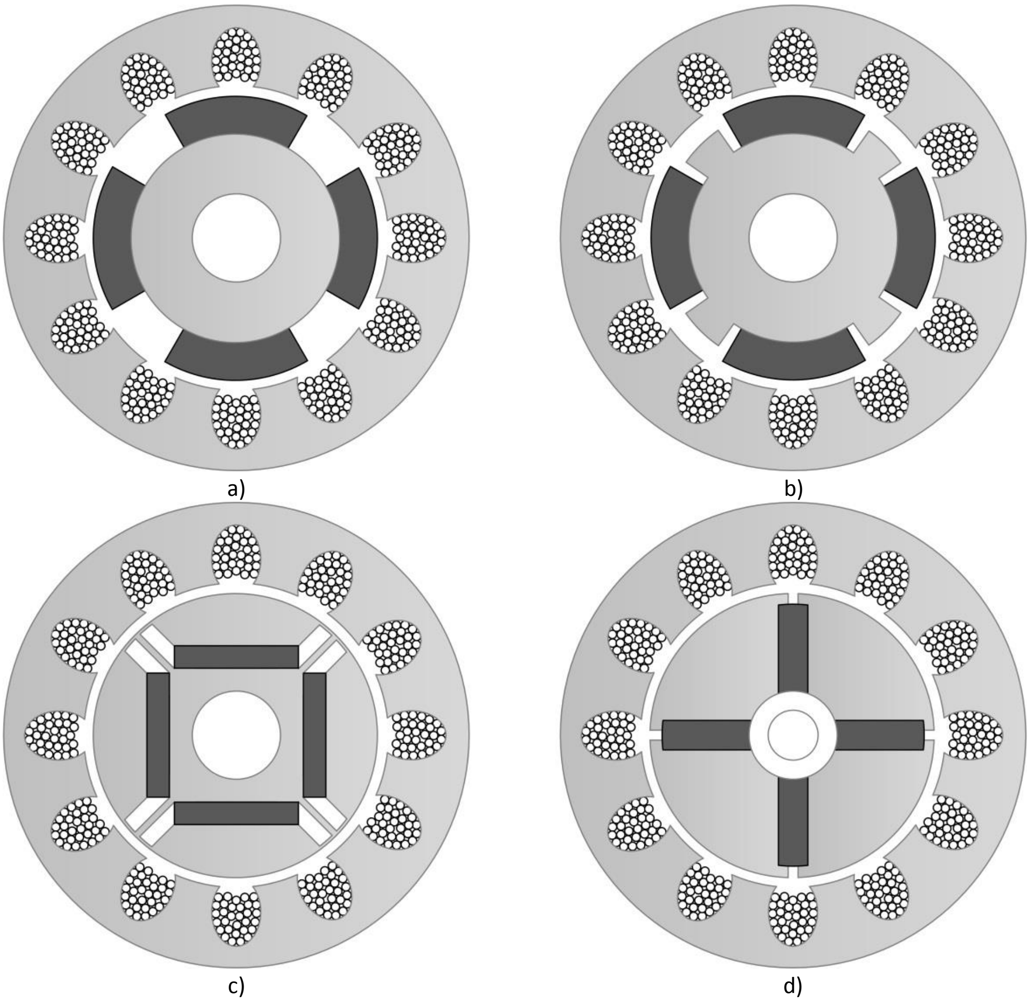
a)
b)
c)
d)

Fig. 1.9. Typical PMSM structures: a) surface magnet, b) inset magnet, c) interior magnet and d) interior magnet (with axial flux).

1.4.3 Switched reluctance machines

Switched reluctance machines consist of a wounded stator and a stacked iron rotor with salient poles, as shown in Fig. 1.10. These salient poles offer different reluctance along the outer circumference of the rotor. When the stator windings are fed with a DC voltage, the rotor moves to offer the minimum reluctance. If the phase B' from Fig. 1.10 were fed, the nearest rotor pole would align, in this case poles 4 and 8 would align with phase B'. By sequentially changing the excited phase the rotor spin is accomplished.

The instantaneous electromagnetic torque produced can be expressed as

$$T_e = \frac{1}{2} i_{ph}{}^2 \frac{d}{d\theta} L_{ph}(\theta), \tag{1.6}$$

where i_{ph} is the phase current, L_{ph} is the phase inductance and θ is the rotor position.

The main advantages of this machine are the reliability and the reduced cost, with a reasonable power density. This combination makes switched reluctance machines a matter of interest. However, the high noise levels generated are preventing their use in commercial vehicles.

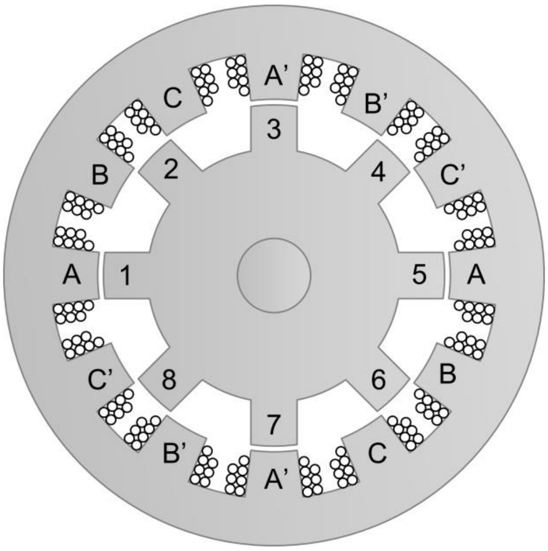

Fig. 1.10. Section of a three-phase 12/8 SRM.

1.5 Research objectives and outline

Having demonstrated the environmental and energy related advantages of the EVs, and noticed the prevalence of EVs with a DC/DC converter in their powertrain, the objective of this thesis is to develop a solution for the powertrain DC/DC converter of an electric vehicle. Several aspects of the solution have been examined minutely. The first of them is the selection of an appropriate topology of bidirectional DC/DC converter for the herein considered application, which finally is a bidirectional boost converter with output filter. On this decision, the stability of the system has to be thoroughly analysed in view of the fact that the load is a motor drive, and thus has a destabilising effect. According to the results of the stability analysis, the converter has to be designed. The design of the converter is an iterative process that will have to be re-examined during the development of the thesis.

As part of the DC/DC system solution, this thesis also has to cover the controller of the converter. Sliding mode is proposed as the current controller technique of the converter, with an outer voltage control loop. This technique is thought to enable the bidirectional operation of the converter with no need to determine if power is flowing from the motor to the source or vice versa, and this point has to be demonstrated.

The last step of the solution is to propose a method to increase the power rating of the design, to match the rating of a commercial EV. Paralleling several converters and establishing a ring-configuration sliding-mode control achieves this objective, with the added value of ripple reduction.

Then, this thesis focuses on verifying the proposed solution by means of a powertrain emulator of 4.5 kW, according to the available facilities. The specifications for the emulator have to be set and once designed, its model in Matlab/Simulink will be obtained. The

UNIVERSITAT ROVIRA I VIRGILI
DESIGN AND CONTROL OF A BIDIRECTIONAL DC/DC CONVERTER FOR AN ELECTRIC VEHICLE APPLICATION.
Laura Albiol Rendillo
Dipòsit Legal: T 1361-2015

experimental setup will be used to evaluate the operation of the solution under a driving profile, and moreover the experimental results will be compared to the results obtained with the model.

This thesis document is organised as follows. The present chapter establishes the need for EV vehicles and explains the basics of the powertrain of an EV. In chapter 2 the open-loop stability analysis of the proposed converter, a BBCOF, is performed. Part of the design and implementation of this converter is also covered. The system is simulated to validate the both the analysis and the design of the BBCOF. Chapter 3 focuses on sliding-mode control and its feasibility for the proposed converter. In order to verify this point, a stability analysis is performed. Moreover, the output voltage controller is designed. The design of the controller and its implementation is tested by means of simulation and also experimentally. In chapter 4, interleaved connection is proposed to increase the power rating of the system. First the analysis is performed, then the stability is verified and at last the circuit implementation is described. The study is also validated by simulation and experimentally. Chapter 5 presents the EV powertrain emulation system used to verify the analysis, design and control of the interleaved BBCOF with sliding-mode ring-configuration control. The system is described, modelled, simulated and tested experimentally. Chapter 6 shows preliminary simulation results of the digital version of the BBCOF controller. Finally, the conclusions and future work of this thesis are developed in chapter 7.

UNIVERSITAT ROVIRA I VIRGILI
DESIGN AND CONTROL OF A BIDIRECTIONAL DC/DC CONVERTER FOR AN ELECTRIC VEHICLE APPLICATION.
Laura Albiol Rendillo
Dipòsit Legal: T 1361-2015

2 Bidirectional boost converter with output filter

2.1 Introduction

As mentioned in chapter 1, a bidirectional DC/DC converter is usually inserted between the battery and the electric drive in most EVs. In order to obtain a good power rating from the motor with a reasonable number of battery cells, a bidirectional boost converter with output filter (BBCOF) is proposed in this thesis.

Fig. 2.1.a shows the electrical architecture of the BBCOF, altogether with the rest of the EV traction system previously described in Fig. 1.4, i.e. the battery, the inverter and the motor.

During the step-up mode, the power is flowing from the battery to the converter and the inverter, and so the motor is performing a traction operation. The inverter bus voltage is higher than the battery voltage. Consequently, during step-up mode the MOSFET in Q_1 and the diode in Q_2 conduct alternatively, as depicted in Fig. 2.1.b.

Conversely, during step-down mode the power flows from the inverter and motor to the battery, performing regenerative braking. The inverter bus voltage continues being higher than the battery voltage, and the diode in Q_1 and the MOSFET in Q_2 conduct alternatively, as shown in Fig. 2.1c.

2.2 Output impedance and constant power loads

BBCOF are known to be stable with resistive loads. However, tightly regulated motor drives behave as constant power loads (CPLs), with negative impedance at their input terminals [51]. Therefore, a deeper stability study must be done, analysing the BBBCOF loaded with a CPL.

2.2.1 CPL concept

The motor drive for the traction system of the electric vehicle has two control loops. The outer loop regulates the motor speed, whereas the inner loop regulates the motor torque. If the speed is tightly regulated and the load has a one-to-one torque speed characteristic, speed and torque are both constant. In this situation the power is also constant, since it is the product of speed by torque, as seen in Fig. 2.2.a. Considering that the drive has a fixed efficiency, the electrical power at the input of the motor drive will also be constant. Consequently, as depicted in Fig. 2.2.b, when voltage applied to a CPL increases, the current decreases. Conversely, when the applied voltage decreases, the current increases. Therefore,

UNIVERSITAT ROVIRA I VIRGILI
DESIGN AND CONTROL OF A BIDIRECTIONAL DC/DC CONVERTER FOR AN ELECTRIC VEHICLE APPLICATION.
Laura Albiol Rendillo
Dipòsit Legal: T 1361-2015

the incremental impedance is negative, and this has a destabilising effect on the systems feeding the CPL, in this case the BBCOF.

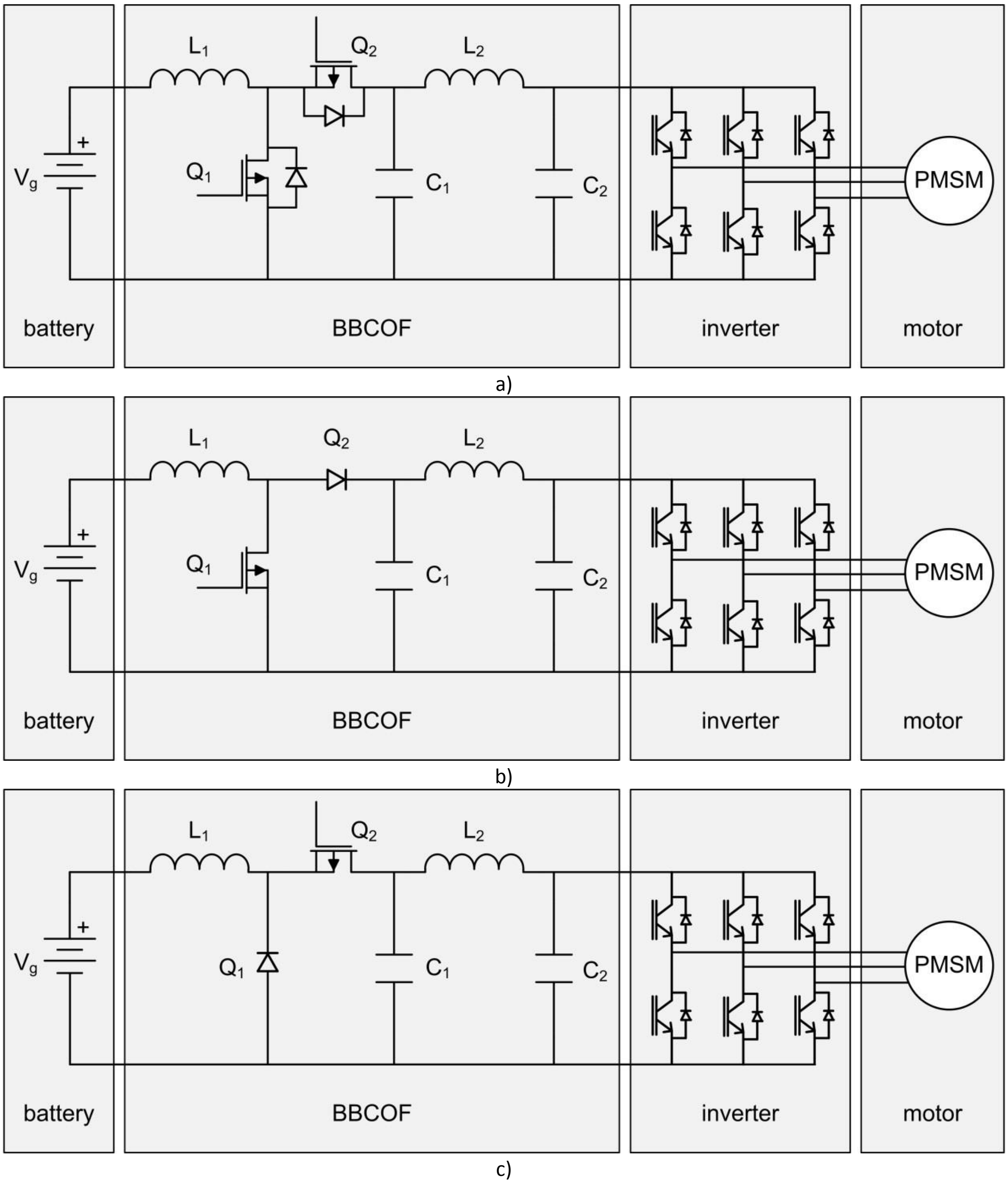

Fig. 2.1. Electrical architecture of an EV traction system: a) general view, b) during step-up mode and c) during step-down mode.

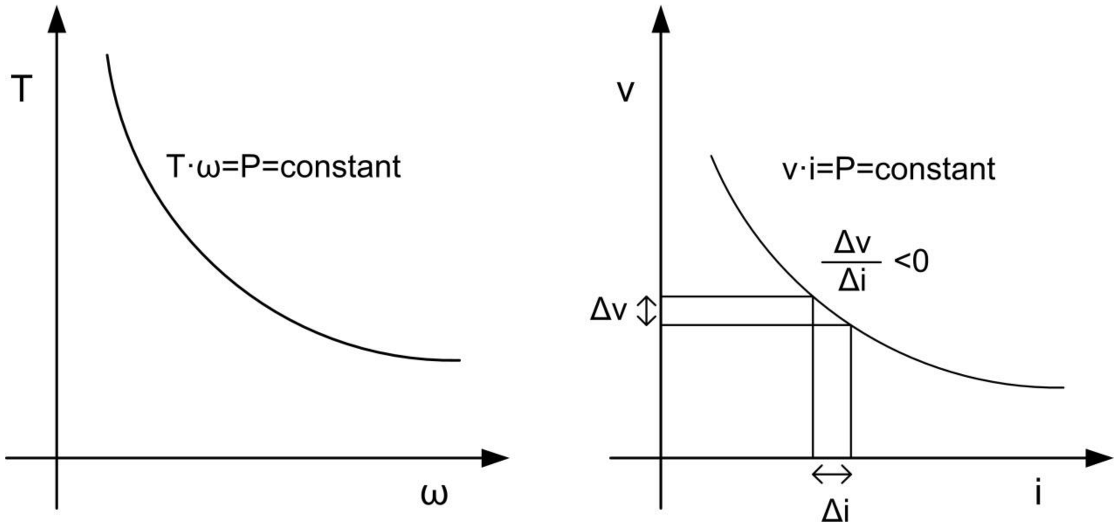

a) b)

Fig. 2.2. Characteristics of a constant power load: a) from the mechanical and b) from the electrical point of view.

To understand the destabilising effect of a CPL, it is useful to compare the connection of a standard voltage source to both a resistive load and a CPL. This connection is represented generically in Fig. 2.3. An equilibrium point exists where the v-i characteristic of the source and the load match. However, the stability of this equilibrium point needs to be discussed. In the case of a resistive load, corresponding to Fig. 2.4.a, if there is a perturbation that reduces the current by Δi, the source voltage becomes greater than the load voltage, so there is a positive voltage in the terminals of the wire inductance. This positive voltage makes the current increase, and the perturbation is compensated. Consequently, it is a stable equilibrium point. In contrast, when the load is a CPL as in Fig. 2.4.b, with the same current perturbation the source voltage becomes lesser than the load voltage, and thus the voltage across the wire inductance is negative, and current decreases again. So the equilibrium point reached with a voltage source and a CPL is unstable.

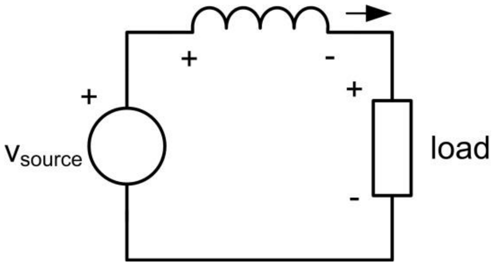

Fig. 2.3. Connection of a voltage source to a generic load considering the wire inductance.

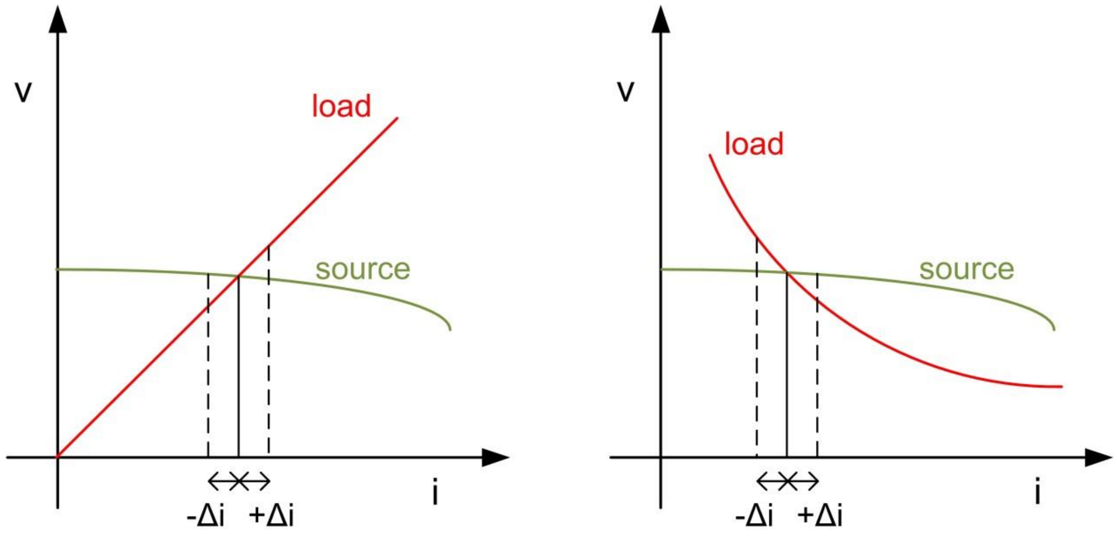

a) b)

Fig. 2.4. Characteristics of a typical voltage source with: a) a resistive load and b) a CPL.

2.2.2 CPL model

From the electrical point of view, a CPL is a load element which consumes, or delivers, a constant product of voltage by current, as in Fig. 2.2.b. The expression of the current curve is

$$i = \frac{P}{v} \tag{2.1}$$

For a given operating point, with voltage equal to *V* and current equal to *I*, the CPL current curve can be approximated by a line tangent to the current curve at the operating point. The slope of this line is the same that the current derivative at the operating point .

$$\left.\frac{\partial}{\partial v} i\right|_{\substack{v=V\\ i=I}} = -\left.\frac{P}{v^2}\right|_{\substack{v=V\\ i=I}} = -\frac{P}{V^2} \tag{2.2}$$

Therefore, the line equation is

$$i = -\frac{P}{V^2} v + c \tag{2.3}$$

where *c* is the crossing point with the y-axis. To determine its value, it is necessary to evaluate (2.3) at the operating point

$$\frac{P}{V} = -\frac{P}{V^2} V + c \tag{2.4}$$

Finally, the CPL can be approximated, for a given operating point, as:

$$i = -\frac{P}{V^2} v + 2\frac{P}{V} \tag{2.5}$$

This CPL approximated expression can be translated into an electrical model shown in Fig. 2.5, where

$$R_{CPL} = -\frac{V^2}{P} \tag{2.6}$$

$$I_{CPL} = 2\frac{P}{V} \tag{2.7}$$

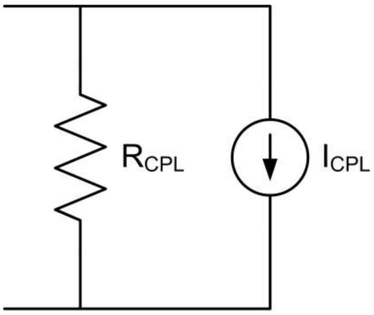

Fig. 2.5. CPL electrical model.

2.2.3 Stability of the converter with a CPL during step-up mode

Several solutions have been presented in the literature to damp the negative impedance effect associated with constant power loads, which can be roughly classified into control-based and hardware-based techniques. Control-based techniques consist on modifying the control action strategy of the inverter by introducing compensation in the current reference of the bus voltage deviations [52]. Instead, hardware-based techniques aggregate a network to the circuitry to damp the resonant effect of the CPL [53]. As inverter control is not the purpose of this thesis, the selected option is to modify the hardware of the converter by adding a resistance.

To study the effect of the negative incremental impedance of the motor drive on the stability of the BBCOF, the CPL shown in Fig. 2.6 is replaced by the corresponding CPL electrical model, described in Fig. 2.5. The obtained system is represented in Fig. 2.7.

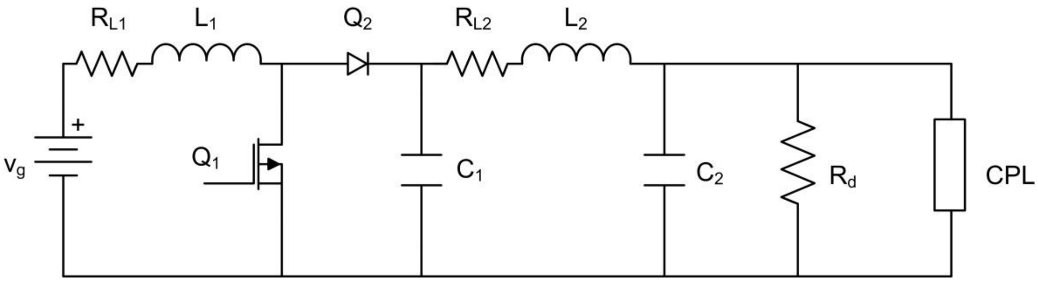

Fig. 2.6. BBCOF, CPL load and aggregate resistance R_d during step-up operation mode.

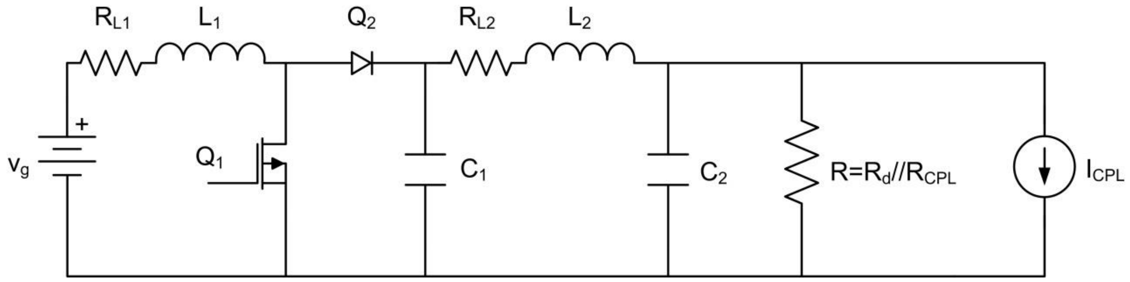

Fig. 2.7. Modified BBCOF, with the equivalent CPL electrical model during step-up mode.

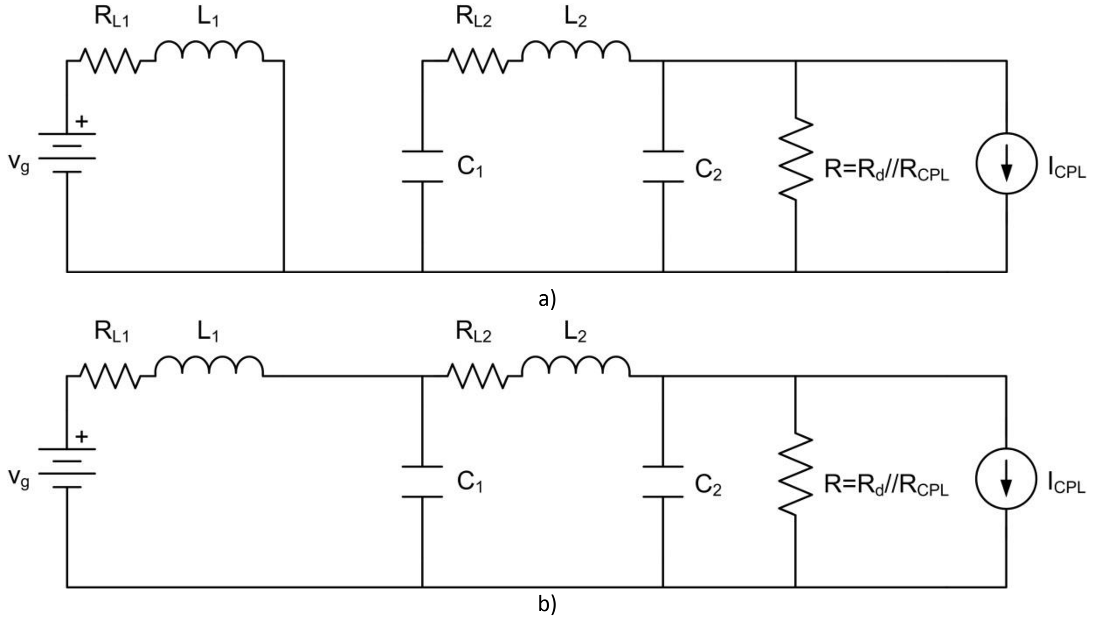

Fig. 2.8. BBCOF, CPL load and aggregate resistance during step-up mode when a) Q1 MOSFET is active, and b) during Q1 MOSFET cut-off.

The system resulting of the conduction of Q_1 MOSFET is represented in Fig. 2.8.a, and its state variables have the following expressions:

$$\frac{\mathrm{d}}{\mathrm{d}t} i_{L1}(t) = \frac{1}{L_1}\left(v_g(t) - R_{L1} i_{L1}(t)\right) \tag{2.8}$$

$$\frac{\mathrm{d}}{\mathrm{d}t} i_{L2}(t) = \frac{1}{L_2}\left(v_{C1}(t) - R_{L2} i_{L2}(t) - v_{C2}(t)\right) \tag{2.9}$$

$$\frac{\mathrm{d}}{\mathrm{d}t} v_{C1}(t) = \frac{1}{C_1}\left(-i_{L2}(t)\right) \tag{2.10}$$

$$\frac{\mathrm{d}}{\mathrm{d}t} v_{C2}(t) = \frac{1}{C_2}\left(i_{L2}(t) - \frac{v_{C2}(t)}{R} - I_{CPL}\right), \tag{2.11}$$

where R_{L1} and R_{L2} are the parasitic resistances of inductors L_1 and L_2, respectively.

During the rest of the period, current is flowing through Q_2 diode, as depicted in Fig. 2.8.b, and the expressions of the state variables are:

UNIVERSITAT ROVIRA I VIRGILI
DESIGN AND CONTROL OF A BIDIRECTIONAL DC/DC CONVERTER FOR AN ELECTRIC VEHICLE APPLICATION.
Laura Albiol Rendillo
Dipòsit Legal: T 1361-2015

$$\frac{\mathrm{d}}{\mathrm{d}t} i_{L1}(t) = \frac{1}{L_1}\left(v_g(t) - R_{L1} i_{L1}(t) - v_{C1}(t)\right) \tag{2.12}$$

$$\frac{\mathrm{d}}{\mathrm{d}t} i_{L2}(t) = \frac{1}{L_2}\left(v_{C1}(t) - R_{L2} i_{L2}(t) - v_{C2}(t)\right) \tag{2.13}$$

$$\frac{\mathrm{d}}{\mathrm{d}t} v_{C1}(t) = \frac{1}{C_1}\left(i_{L1}(t) - i_{L2}(t)\right) \tag{2.14}$$

$$\frac{\mathrm{d}}{\mathrm{d}t} v_{C2}(t) = \frac{1}{C_2}\left(i_{L2}(t) - \frac{v_{C2}(t)}{R} - I_{CPL}\right) \tag{2.15}$$

The system can be described during the whole commutation period by means of the following averaged expressions:

$$\frac{\mathrm{d}}{\mathrm{d}t} i_{L1}(t) = \frac{1}{L_1}\left(v_g(t) - R_{L1} i_{L1}(t) - v_{C1}(t)\cdot\left(1 - d(t)\right)\right) \tag{2.16}$$

$$\frac{\mathrm{d}}{\mathrm{d}t} i_{L2}(t) = \frac{1}{L_2}\left(v_{C1}(t) - R_{L2} i_{L2}(t) - v_{C2}(t)\right) \tag{2.17}$$

$$\frac{\mathrm{d}}{\mathrm{d}t} v_{C1}(t) = \frac{1}{C_1}\left(i_{L1}(t)\cdot\left(1 - d(t)\right) - i_{L2}(t)\right) \tag{2.18}$$

$$\frac{\mathrm{d}}{\mathrm{d}t} v_{C2}(t) = \frac{1}{C_2}\left(i_{L2}(t) - \frac{v_{C2}(t)}{R} - I_{CPL}\right), \tag{2.19}$$

where *d(t)* represents the duty cycle, i.e. the proportion of the conduction time of Q_1 MOSFET over the commutation period, and its value is between 0 and 1.

These expressions are nonlinear. To obtain linear equations to determine the stability of the system around the equilibrium point, the state variables at steady state are considered as a sum of their steady state value at the equilibrium point and their small signal variations, as follows:

$$i_{L1}(t) = I_{L1} + \tilde{i}_{L1}(t) \tag{2.20}$$

$$i_{L2}(t) = I_{L2} + \tilde{i}_{L2}(t) \tag{2.21}$$

$$v_{C1}(t) = V_{C1} + \tilde{v}_{C1}(t) \tag{2.22}$$

$$v_{C2}(t) = V_{C2} + \tilde{v}_{C2}(t), \tag{2.23}$$

where the steady state values are obtained by equalling the state variable derivatives (2.16)-(2.19) to zero:

$$I_{L1} = -\frac{\mathrm{D}RI_{CPL} - RI_{CPL} - V_g}{\mathrm{D}^2R + \mathrm{D}^2R_{L2} - 2\mathrm{D}R - 2\mathrm{D}R_{L2} + R + R_{L1} + R_{L2}} \tag{2.24}$$

$$I_{L2} = \frac{(\mathrm{D}-1)\left(\mathrm{D}RI_{CPL} - RI_{CPL} - V_g\right)}{\mathrm{D}^2R + \mathrm{D}^2R_{L2} - 2\mathrm{D}R - 2\mathrm{D}R_{L2} + R + R_{L1} + R_{L2}} \tag{2.25}$$

$$V_{C1} = -\frac{\mathrm{D}RV_g + \mathrm{D}R_{L2}V_g + RI_{CPL}R_{L1} - RV_g - R_{L2}V_g}{\mathrm{D}^2R + \mathrm{D}^2R_{L2} - 2\mathrm{D}R - 2\mathrm{D}R_{L2} + R + R_{L1} + R_{L2}} \tag{2.26}$$

$$V_{C2} = -\frac{R\left(\mathrm{D}^2I_{CPL}R_{L2} - 2\mathrm{D}I_{CPL}R_{L2} + \mathrm{D}V_g + I_{CPL}R_{L1} + I_{CPL}R_{L2} - V_g\right)}{\mathrm{D}^2R + \mathrm{D}^2R_{L2} - 2\mathrm{D}R - 2\mathrm{D}R_{L2} + R + R_{L1} + R_{L2}}, \tag{2.27}$$

and the capital letters denote the steady state value of the respective instantaneous values of the state and control variables. Hence, the linearized expression of $i_{L1}(t)$ is calculated as

$$\begin{aligned}\frac{\mathrm{d}}{\mathrm{d}t}\tilde{i}_{L1}(t) &= \frac{\partial}{\partial i_{L1}(t)}\left(\frac{d}{dt}i_{L1}(t)\right)\Bigg|_{*}\cdot\tilde{i}_{L1}(t) + \frac{\partial}{\partial i_{L2}(t)}\left(\frac{d}{dt}i_{L1}(t)\right)\Bigg|_{*}\cdot\tilde{i}_{L2}(t) + \\ &+ \frac{\partial}{\partial v_{C1}(t)}\left(\frac{d}{dt}i_{L1}(t)\right)\Bigg|_{*}\cdot\tilde{v}_{C1}(t) + \frac{\partial}{\partial v_{C2}(t)}\left(\frac{d}{dt}i_{L1}(t)\right)\Bigg|_{*}\cdot\tilde{v}_{C2}(t) + \\ &+ \frac{\partial}{\partial d(t)}\left(\frac{d}{dt}i_{L1}(t)\right)\Bigg|_{*}\cdot\tilde{d}(t)\end{aligned}, \tag{2.28}$$

where the subscript * indicates the steady state. Hence, evaluating the previous expression, the linearized expression on $i_{L1}(t)$ around the steady state is

$$\frac{\mathrm{d}}{\mathrm{d}t}\tilde{i}_{L1}(t) = \frac{1}{L_1}\left(\tilde{v}_g(t) - R_{L1}\tilde{i}_{L1}(t) - \tilde{v}_{C1}(t)\cdot(1-D) + V_{C1}\tilde{d}(t)\right) \tag{2.29}$$

Following the same procedure for the rest of state variables, the following dynamics representation is obtained

$$\frac{\mathrm{d}}{\mathrm{d}t}\tilde{i}_{L2}(t) = \frac{1}{L_2}\left(\tilde{v}_{C1}(t) - R_{L2}\tilde{i}_{L2}(t) - \tilde{v}_{C2}(t)\right) \tag{2.30}$$

$$\frac{\mathrm{d}}{\mathrm{d}t}\tilde{v}_{C1}(t) = \frac{1}{C_1}\left(\tilde{i}_{L1}(t)\cdot(1-D) - I_{L1}\tilde{d} - \tilde{i}_{L2}(t)\right) \tag{2.31}$$

$$\frac{\mathrm{d}}{\mathrm{d}t}\tilde{v}_{C2}(t) = \frac{1}{C_2}\left(\tilde{i}_{L2}(t) - \frac{\tilde{v}_{C2}(t)}{R}\right) \tag{2.32}$$

With these linearized expressions, it is possible to obtain the output voltage to control transfer function, $\tilde{v}_{C2}(s)/\tilde{d}(s)$. The first step is to obtain a unique equation defining the relation between $\tilde{v}_{C2}(t)$ and $\tilde{d}(t)$. Isolating $\tilde{i}_{L1}(t)$ in (2.31) and calculating its derivative:

$$\tilde{i}_{L1}(t)=\frac{-C_1\frac{\mathrm{d}}{\mathrm{d}t}\tilde{v}_{C1}(t)-I_{L1}\tilde{d}-\tilde{i}_{L2}(t)}{D-1} \tag{2.33}$$

$$\frac{\mathrm{d}}{\mathrm{d}t}\tilde{i}_{L1}(t)=\frac{-C_1\frac{\mathrm{d}^2}{\mathrm{d}t^2}\tilde{v}_{C1}(t)-I_{L1}\frac{\mathrm{d}}{\mathrm{d}t}\tilde{d}-\frac{\mathrm{d}}{\mathrm{d}t}\tilde{i}_{L2}(t)}{D-1} \tag{2.34}$$

Using (2.33) and (2.34) in (2.29), the dependency on $\tilde{i}_{L1}(t)$ is eliminated:

$$\begin{aligned}&\frac{\left(-C_1\frac{\mathrm{d}^2}{\mathrm{d}t^2}\tilde{v}_{C1}(t)-I_{L1}\frac{\mathrm{d}}{\mathrm{d}t}\tilde{d}-\frac{\mathrm{d}}{\mathrm{d}t}\tilde{i}_{L2}(t)\right)L_1}{D-1}=\tilde{v}_g(t)-\\&-\frac{\left(-C_1\frac{\mathrm{d}}{\mathrm{d}t}\tilde{v}_{C1}(t)-I_{L1}\tilde{d}-\tilde{i}_{L2}(t)\right)R_{L1}}{D-1}+\tilde{v}_{C1}(t)\cdot(D-1)+V_{C1}\tilde{d}(t)\end{aligned} \tag{2.35}$$

To eliminate the dependency on $\tilde{v}_{C1}(t)$, the expression for this variable is extracted from (2.30), and the first and second derivatives are calculated

$$\tilde{v}_{C1}(t)=L_2\frac{\mathrm{d}}{\mathrm{d}t}\tilde{i}_{L2}(t)+R_{L2}\tilde{i}_{L2}(t)+\tilde{v}_{C2}(t) \tag{2.36}$$

$$\frac{\mathrm{d}}{\mathrm{d}t}\tilde{v}_{C1}(t)=L_2\frac{\mathrm{d}^2}{\mathrm{d}t^2}\tilde{i}_{L2}(t)+R_{L2}\frac{\mathrm{d}}{\mathrm{d}t}\tilde{i}_{L2}(t)+\frac{\mathrm{d}}{\mathrm{d}t}\tilde{v}_{C2}(t) \tag{2.37}$$

$$\frac{\mathrm{d}^2}{\mathrm{d}t^2}\tilde{v}_{C1}(t)=L_2\frac{\mathrm{d}^3}{\mathrm{d}t^3}\tilde{i}_{L2}(t)+R_{L2}\frac{\mathrm{d}^2}{\mathrm{d}t^2}\tilde{i}_{L2}(t)+\frac{\mathrm{d}^2}{\mathrm{d}t^2}\tilde{v}_{C2}(t), \tag{2.38}$$

and later substituted in (2.35):

$$\begin{aligned}&\frac{\left(-\left(L_2\frac{\mathrm{d}^3}{\mathrm{d}t^3}\tilde{i}_{L2}(t)+R_{L2}\frac{\mathrm{d}^2}{\mathrm{d}t^2}\tilde{i}_{L2}(t)+\frac{\mathrm{d}^2}{\mathrm{d}t^2}\tilde{v}_{C2}(t)\right)C_1-I_{L1}\frac{\mathrm{d}}{\mathrm{d}t}\tilde{d}-\frac{\mathrm{d}}{\mathrm{d}t}\tilde{i}_{L2}(t)\right)L_1}{D-1}=\tilde{v}_g(t)-\\&-\frac{\left(-\left(L_2\frac{\mathrm{d}^2}{\mathrm{d}t^2}\tilde{i}_{L2}(t)+R_{L2}\frac{\mathrm{d}}{\mathrm{d}t}\tilde{i}_{L2}(t)+\frac{\mathrm{d}}{\mathrm{d}t}\tilde{v}_{C2}(t)\right)C_1-I_{L1}\tilde{d}-\tilde{i}_{L2}(t)\right)R_{L1}}{D-1}+\\&+\left(L_2\frac{\mathrm{d}}{\mathrm{d}t}\tilde{i}_{L2}(t)+R_{L2}\tilde{i}_{L2}(t)+\tilde{v}_{C2}(t)\right)\cdot(D-1)+V_{C1}\tilde{d}(t)\end{aligned} \tag{2.39}$$

The expression for $\tilde{i}_{L2}(t)$ can be obtained from (2.32):

$$\tilde{i}_{L2}(t)=C_2\frac{\mathrm{d}}{\mathrm{d}t}\tilde{v}_{C2}(t)+\frac{\tilde{v}_{C2}(t)}{R}, \tag{2.40}$$

and its first, second and third derivatives are the following

$$\frac{\mathrm{d}}{\mathrm{d}t}\tilde{i}_{L2}(t)=C_2\frac{\mathrm{d}^2}{\mathrm{d}t^2}\tilde{v}_{C2}(t)+\frac{1}{R}\frac{\mathrm{d}}{\mathrm{d}t}\tilde{v}_{C2}(t), \tag{2.41}$$

$$\frac{\mathrm{d}^2}{\mathrm{d}t^2}\tilde{i}_{L2}(t)=C_2\frac{\mathrm{d}^3}{\mathrm{d}t^3}\tilde{v}_{C2}(t)+\frac{1}{R}\frac{\mathrm{d}^2}{\mathrm{d}t^2}\tilde{v}_{C2}(t), \tag{2.42}$$

$$\frac{\mathrm{d}^3}{\mathrm{d}t^3}\tilde{i}_{L2}(t)=C_2\frac{\mathrm{d}^4}{\mathrm{d}t^4}\tilde{v}_{C2}(t)+\frac{1}{R}\frac{\mathrm{d}^3}{\mathrm{d}t^3}\tilde{v}_{C2}(t), \tag{2.43}$$

Using (2.40)-(2.43) in (2.39), the linear expression connecting $\tilde{v}_{C2}(t)$ and $\tilde{d}(t)$ is

$$\begin{aligned}
&\frac{1}{D-1}\left(\begin{array}{l}\left(\begin{array}{l}L_2\left(C_2\frac{\mathrm{d}^4}{\mathrm{d}t^4}\tilde{v}_{C2}(t)+\frac{1}{R}\frac{\mathrm{d}^3}{\mathrm{d}t^3}\tilde{v}_{C2}(t)\right)-\\ R_{L2}\left(C_2\frac{\mathrm{d}^3}{\mathrm{d}t^3}\tilde{v}_{C2}(t)+\frac{1}{R}\frac{\mathrm{d}^2}{\mathrm{d}t^2}\tilde{v}_{C2}(t)\right)+\frac{\mathrm{d}^2}{\mathrm{d}t^2}\tilde{v}_{C2}(t)\end{array}\right)C_1-\\ -I_{L1}\frac{\mathrm{d}}{\mathrm{d}t}\tilde{d}-C_2\frac{\mathrm{d}^2}{\mathrm{d}t^2}\tilde{v}_{C2}(t)-\frac{1}{R}\frac{\mathrm{d}}{\mathrm{d}t}\tilde{v}_{C2}(t)\end{array}\right)L_1=\\
&=\tilde{v}_g(t)-\frac{1}{D-1}\left(\begin{array}{l}-\left(\begin{array}{l}L_2\left(C_2\frac{\mathrm{d}^3}{\mathrm{d}t^3}\tilde{v}_{C2}(t)+\frac{1}{R}\frac{\mathrm{d}^2}{\mathrm{d}t^2}\tilde{v}_{C2}(t)\right)+\\ +R_{L2}\left(C_2\frac{\mathrm{d}^2}{\mathrm{d}t^2}\tilde{v}_{C2}(t)+\frac{1}{R}\frac{\mathrm{d}}{\mathrm{d}t}\tilde{v}_{C2}(t)\right)+\frac{\mathrm{d}}{\mathrm{d}t}\tilde{v}_{C2}(t)\end{array}\right)C_1-\\ -I_{L1}\tilde{d}-C_2\frac{\mathrm{d}}{\mathrm{d}t}\tilde{v}_{C2}(t)-\frac{\tilde{v}_{C2}(t)}{R}\end{array}\right)R_{L1}+\\
&+\left(\begin{array}{l}L_2\left(C_2\frac{\mathrm{d}^2}{\mathrm{d}t^2}\tilde{v}_{C2}(t)+\frac{1}{R}\frac{\mathrm{d}}{\mathrm{d}t}\tilde{v}_{C2}(t)\right)+\\ +R_{L2}\left(C_2\frac{\mathrm{d}}{\mathrm{d}t}\tilde{v}_{C2}(t)+\frac{\tilde{v}_{C2}(t)}{R}\right)+\tilde{v}_{C2}(t)\end{array}\right)\cdot(D-1)+V_{C1}\tilde{d}(t)
\end{aligned} \tag{2.44}$$

Doing the Laplace transform and collecting terms, the output voltage to control transfer function is finally obtained

$$\frac{\tilde{v}_{C2}(s)}{\tilde{d}(s)}=\frac{-R\left(I_{L1}sL_1+\mathrm{D}V_{C1}+I_{L1}R_{L1}-V_{C1}\right)}{a\cdot s^4+b\cdot s^3+c\cdot s^2+d\cdot s+e}, \tag{2.45}$$

where

$$\begin{aligned}
a&=RC_1C_2L_1L_2\\
b&=RC_1C_2L_1R_{L2}+RC_1C_2L_2R_{L1}+C_1L_1L_2\\
c&=\mathrm{D}^2RC_2L_2+RC_1C_2R_{L1}R_{L2}-2\mathrm{D}RC_2L_2+RC_1L_1+RC_2L_1+RC_2L_2+C_1L_1R_{L2}+\\
&\quad+C_1L_2R_{L1}\\
d&=\mathrm{D}^2RC_2R_{L2}-2\mathrm{D}RC_2R_{L2}+\mathrm{D}^2L_2+RC_1R_{L1}+RC_2R_{L1}+RC_2R_{L2}+C_1R_{L1}R_{L2}-\\
&\quad-2\mathrm{D}L_2+L_1+L_2\\
e&=\mathrm{D}^2R+\mathrm{D}^2R_{L2}-2\mathrm{D}R-2\mathrm{D}R_{L2}+R+R_{L1}+R_{L2}
\end{aligned} \tag{2.46}$$

From the denominator of the transfer function in (2.45) several conditions can be extracted, since coefficients *a*, *b*, *c*, *d* and *e* have to be positive to ensure the system stability applying the Routh-Hurwitz stability criterion. Taking into account that L_1, L_2, C_1, C_2, R_{L1} and R_{L2} are positive, and the value of D is comprised between 0 and 1, the resulting stability conditions are:

$$R > 0 \tag{2.47}$$

$$R > -\frac{C_1 L_1 L_2}{C_1 C_2 L_1 R_{L2} + C_1 C_2 L_2 R_{L1}} \tag{2.48}$$

$$R > -\frac{C_1 L_1 R_{L2} + C_1 L_2 R_{L1}}{(\mathrm{D}-1)^2 C_2^2 L_2 ` + C_1 R_{L1} R_{L2} + C_1 L_1 + C_2 L_1} \tag{2.49}$$

$$R > -\frac{(\mathrm{D}-1)^2 L_2 + L_1 + C_1 R_{L1} R_{L2}}{(\mathrm{D}-1)^2 C_2 R_{L2} + C_1 R_{L1} + C_2 R_{L1}} \tag{2.50}$$

$$R > -\frac{(\mathrm{D}-1)^2 R_{L2} + R_{L1}}{(\mathrm{D}-1)^2} \tag{2.51}$$

Among the previous expressions, the most restrictive condition is (2.47). Consequently, it is necessary to guarantee that R is greater than zero under any circumstances. Therefore,

$$R_{\min} = \frac{1}{\frac{1}{R_d} + \frac{1}{R_{CPL}}} > 0\,, \tag{2.52}$$

which can be rearranged as

$$R_d < -R_{CPL\min} \tag{2.53}$$

According to the CPL electrical model shown in Fig. 2.5, (2.53) can be expressed in terms of CPL power

$$R_d < \frac{{V_{C2}}^2}{P_{CPL,\max}}\,, \tag{2.54}$$

If the BBCOF output filter design accomplishes (2.54), the stability of its operation during the step-up mode is guaranteed. Therefore, without the aggregate resistance R_d, the system would be unstable, which justifies its inclusion.

2.2.4 Stability of the converter with a CPL during step-down mode

The same procedure is followed to determine the stability of the BBCOF during the step-down mode, depicted in Fig. 2.9. The circuit modified with the inclusion of the electrical model of the CPL is represented in Fig. 2.10. During the conduction of the Q_2 MOSFET, the system equations extracted from Fig. 2.11.a. correspond to

$$\frac{\mathrm{d}}{\mathrm{d}t} i_{L1}(t) = \frac{1}{L_1}\left(v_g(t) - R_{L1} i_{L1}(t) - v_{C1}(t)\right) \tag{2.55}$$

$$\frac{\mathrm{d}}{\mathrm{d}t} i_{L2}(t) = \frac{1}{L_2}\left(v_{C1}(t) - R_{L2} i_{L2}(t) - v_{C2}(t)\right) \tag{2.56}$$

$$\frac{\mathrm{d}}{\mathrm{d}t} v_{C1}(t) = \frac{1}{C_1}\left(i_{L1}(t) - i_{L2}(t)\right) \tag{2.57}$$

$$\frac{\mathrm{d}}{\mathrm{d}t} v_{C2}(t) = \frac{1}{C_2}\left(i_{L2}(t) - \frac{v_{C2}(t)}{R} + I_{CPL}\right) \tag{2.58}$$

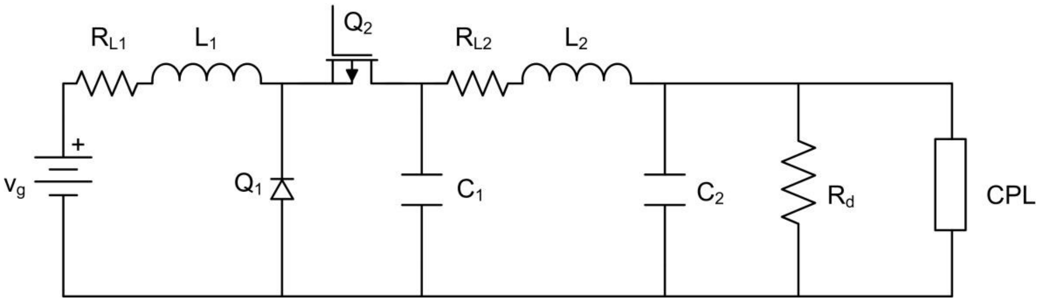

Fig. 2.9. BBCOF filter, CPL load and aggregate resistance R_d during step-down operation mode.

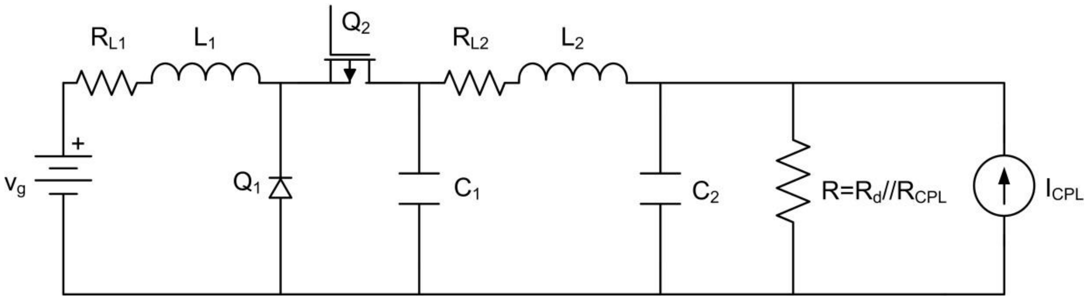

Fig. 2.10. Simplified BBCOF, CPL load and aggregate resistance during step-down mode.

During the rest of the period, represented in Fig. 2.11.b, the state variable expressions are

$$\frac{\mathrm{d}}{\mathrm{d}t} i_{L1}(t) = \frac{1}{L_1}\left(v_g(t) - R_{L1} i_{L1}(t)\right) \tag{2.59}$$

$$\frac{\mathrm{d}}{\mathrm{d}t} i_{L2}(t) = \frac{1}{L_2}\left(v_{C1}(t) - R_{L2} i_{L2}(t) - v_{C2}(t)\right) \tag{2.60}$$

$$\frac{\mathrm{d}}{\mathrm{d}t} v_{C1}(t) = \frac{1}{C_1}\left(-i_{L2}(t)\right) \tag{2.61}$$

$$\frac{\mathrm{d}}{\mathrm{d}t} v_{C2}(t) = \frac{1}{C_2}\left(i_{L2}(t) - \frac{v_{C2}(t)}{R} + I_{CPL}\right) \tag{2.62}$$

UNIVERSITAT ROVIRA I VIRGILI
DESIGN AND CONTROL OF A BIDIRECTIONAL DC/DC CONVERTER FOR AN ELECTRIC VEHICLE APPLICATION.
Laura Albiol Rendillo
Dipòsit Legal: T 1361-2015

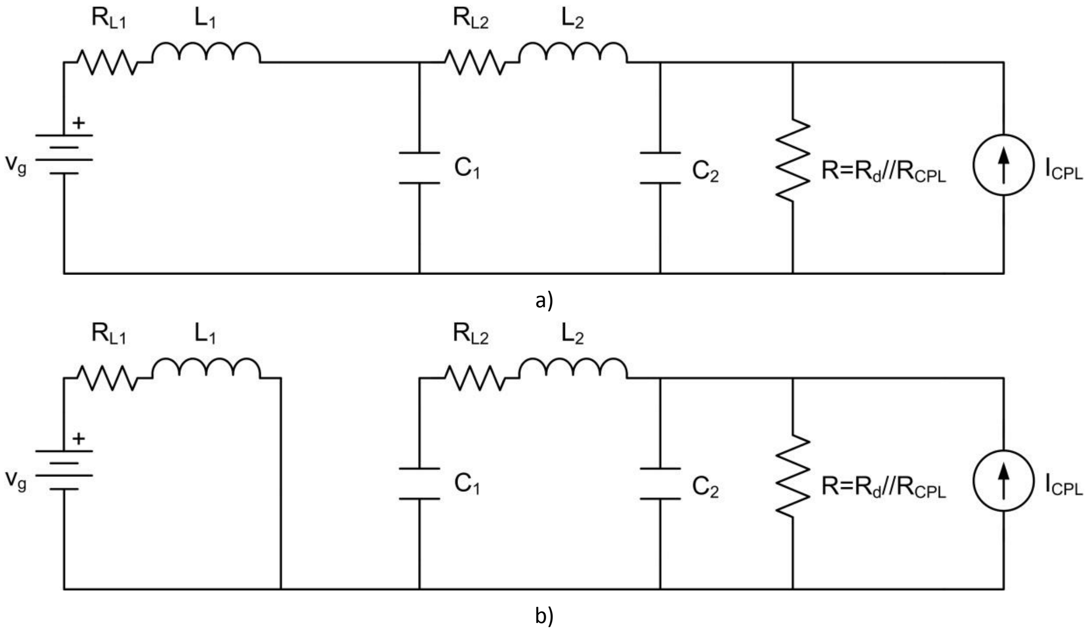

a)

b)

Fig. 2.11. BBCOF, CPL load and aggregate resistance during step-down mode when a) Q2 MOSFET is active, and b) during Q2 MOSFET cut-off.

Again, the switched system can be represented by a series of averaged equations using the control variable *d*. In order to maintain the nomenclature, *d* value is 1 when the current is circulating through Q_1 switch, in this case through the diode, and is 0 when the Q_2 MOSFET is active. Consequently, the averaged state variable expressions are

$$\frac{\mathrm{d}}{\mathrm{d}t}i_{L1}(t)=\frac{1}{L_1}\left(v_g(t)-R_{L1}i_{L1}(t)-v_{C1}(t)\cdot\left(1-d(t)\right)\right) \tag{2.63}$$

$$\frac{\mathrm{d}}{\mathrm{d}t}i_{L2}(t)=\frac{1}{L_2}\left(v_{C1}(t)-R_{L2}i_{L2}(t)-v_{C2}(t)\right) \tag{2.64}$$

$$\frac{\mathrm{d}}{\mathrm{d}t}v_{C1}(t)=\frac{1}{C_1}\left(i_{L1}(t)\cdot\left(1-d(t)\right)-i_{L2}(t)\right) \tag{2.65}$$

$$\frac{\mathrm{d}}{\mathrm{d}t}v_{C2}(t)=\frac{1}{C_2}\left(i_{L2}(t)-\frac{v_{C2}(t)}{R}+I_{CPL}\right) \tag{2.66}$$

The only difference between (2.63)-(2.66) and (2.16)-(2.19) is the sign of the CPL current source in (2.66). As done previously for the step-up mode analysis, the averaged state variable expressions have to be linearized around steady state considering (2.20)-(2.23):

$$\frac{\mathrm{d}}{\mathrm{d}t}\tilde{i}_{L1}(t)=\frac{1}{L_1}\left(\tilde{v}_g(t)-R_{L1}\tilde{i}_{L1}(t)-\tilde{v}_{C1}(t)\cdot(1-D)+V_{C1}\tilde{d}(t)\right) \tag{2.67}$$

$$\frac{\mathrm{d}}{\mathrm{d}t}\tilde{i}_{L2}(t)=\frac{1}{L_2}\left(\tilde{v}_{C1}(t)-R_{L2}\tilde{i}_{L2}(t)-\tilde{v}_{C2}(t)\right) \tag{2.68}$$

UNIVERSITAT ROVIRA I VIRGILI
DESIGN AND CONTROL OF A BIDIRECTIONAL DC/DC CONVERTER FOR AN ELECTRIC VEHICLE APPLICATION.
Laura Albiol Rendillo
Dipòsit Legal: T 1361-2015

$$\frac{\mathrm{d}}{\mathrm{d}t}\tilde{v}_{C1}(t)=\frac{1}{C_1}\left(\tilde{i}_{L1}(t)\cdot(1-D)-I_{L1}\tilde{d}-\tilde{i}_{L2}(t)\right) \tag{2.69}$$

$$\frac{\mathrm{d}}{\mathrm{d}t}\tilde{v}_{C2}(t)=\frac{1}{C_2}\left(\tilde{i}_{L2}(t)-\frac{\tilde{v}_{C2}(t)}{R}\right) \tag{2.70}$$

Note that the linearized expressions of the state variables in step-up and step-down are identical. Subsequently, the transfer function $\tilde{v}_{C2}(s)/\tilde{d}(s)$ for the step-down mode is (2.45), and the stability conditions (2.47)-(2.51) are also maintained. The most restrictive stability condition, (2.47), forces the R resistance to be positive. For the CPL model corresponding to the step-down operation, R_{CPL} is already positive, so the step-down operation will be stable as long as R_d is positive, condition which is compatible with the R_d restriction for the step-up mode (2.54). In a nutshell, stability can be guaranteed if the value of R_d satisfies the following condition

$$0<R_d<\frac{{V_{C2}}^2}{P_{CPL,\max}} \tag{2.71}$$

2.2.5 Stability of the converter during the mode transition

During the transition from step-up to step-down mode and vice versa, there is an instant when the current consumed (or delivered) by the inverter is null. According to the CPL model, at this point the value of the current source I_{CPL} is 0, and the R_{CPL} resistance is infinite, so the system can be modelled as in Fig. 2.12.

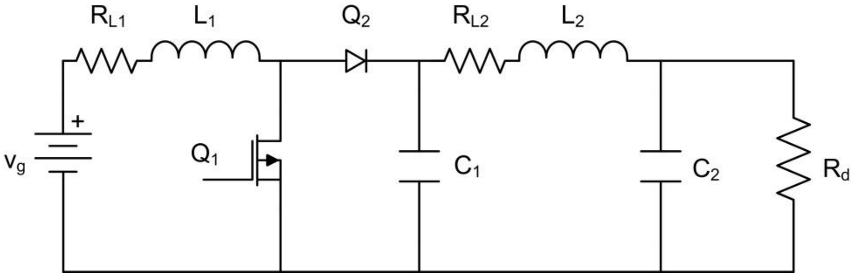

Fig. 2.12. BBCOF and CPL load during mode transitions.

From the step-down mode stability analysis, it is known that the value of the current source I_{CPL} does not modify the transfer function $\tilde{v}_{C2}(s)/\tilde{d}(s)$. Particularising (2.45) for an infinite CPL resistance, the transfer function of the converter during transitions is

$$\frac{\tilde{v}_{C2}(s)}{\tilde{d}(s)}=\frac{-R_d\left(I_{L1}sL_1+\mathrm{D}V_{C1}+I_{L1}R_{L1}-V_{C1}\right)}{a\cdot s^4+b\cdot s^3+c\cdot s^2+d\cdot s+e}, \tag{2.72}$$

where

$$\begin{aligned}
&a = R_d C_1 C_2 L_1 L_2 \\
&b = R_d C_1 C_2 L_1 R_{L2} + R_d C_1 C_2 L_2 R_{L1} + C_1 L_1 L_2 \\
&c = \mathrm{D}^2 R_d C_2 L_2 + R_d C_1 C_2 R_{L1} R_{L2} - 2\mathrm{D} R_d C_2 L_2 + R_d C_1 L_1 + R_d C_2 L_1 + R_d C_2 L_2 + C_1 L_1 R_{L2} + \\
&\quad + C_1 L_2 R_{L1} \\
&d = \mathrm{D}^2 R_d C_2 R_{L2} - 2\mathrm{D} R_d C_2 R_{L2} + \mathrm{D}^2 L_2 + R_d C_1 R_{L1} + R_d C_2 R_{L1} + R_d C_2 R_{L2} + C_1 R_{L1} R_{L2} - \\
&\quad - 2\mathrm{D} L_2 + L_1 + L_2 \\
&e = \mathrm{D}^2 R_d + \mathrm{D}^2 R_{L2} - 2\mathrm{D} R_d - 2\mathrm{D} R_{L2} + R_d + R_{L1} + R_{L2}
\end{aligned} \tag{2.73}$$

The effect of not including the resistance R$_d$ can be derived by calculating the limit of the transfer function when this resistance tends to infinity:

$$\frac{\tilde{v}_{C2}(s)}{\tilde{d}(s)} = \frac{-I_{L1} L_1 s - \mathrm{D} V_{C1} - I_{L1} R_{L1} + V_{C1}}{a \cdot s^4 + b \cdot s^3 + c \cdot s^2 + d \cdot s + e}, \tag{2.74}$$

where

$$\begin{aligned}
&a = C_1 C_2 L_1 L_2 \\
&b = R_{L1} C_1 C_2 L_2 + R_{L2} C_1 C_2 L_1 \\
&c = \mathrm{D}^2 C_2 L_2 + R_{L1} R_{L2} C_1 C_2 - 2\mathrm{D} C_2 L_2 + C_1 L_1 + C_2 L_1 + C_2 L_2\ , \\
&d = \mathrm{D}^2 R_{L2} C_2 - 2\mathrm{D} R_{L2} C_2 + R_{L1} C_1 + R_{L1} C_2 + R_{L2} C_2 \\
&e = \mathrm{D}^2 - 2\mathrm{D} + 1
\end{aligned} \tag{2.75}$$

If the parasitic resistances of the inductors are neglected, the transfer function is

$$\frac{\tilde{v}_{C2}(s)}{\tilde{d}(s)} = \frac{-I_{L1} L_1 s - \mathrm{D} V_{C1} - I_{L1} R_{L1} + V_{C1}}{C_1 C_2 L_1 L_2 s^4 + \left(\mathrm{D}^2 C_2 L_2 - 2\mathrm{D} C_2 L_2 + C_1 L_1 + C_2 L_1 + C_2 L_2\right) s^2 + (D-1)^2} \tag{2.76}$$

Note that the missing terms of s^3 and s denote the system instability. Consequently, unless the aggregate resistance R$_d$ is connected, the BBCOF will be unstable. This instability is predictable, since without R$_d$ the BBCOF is unloaded.

2.2.6 R$_d$ dissipation reduction

As proven in the previous analysis, R$_d$ is necessary to ensure the stability of the BBCOF connected to a CPL. However, this solution adds dissipation to the converter, impoverishing the BBCOF efficiency. An effective solution to this phenomenon is to connect a damping capacitor (C$_d$) in series with the aggregate resistance R$_d$. The capacitor prevents DC dissipation, but has to be designed so that the corner frequency of the R$_d$-C$_d$ snubber is considerably lower than the resonance peak frequency of the converter [53]. Then, a factor of 5 between both frequencies is chosen, and then the expression for the snubber capacitor is

$$C_d = \frac{1}{2\pi R_d \frac{1}{5} f_r}, \tag{2.77}$$

where f_r is the resonance peak frequency. In case that $C_1 >> C_2$, the resonance peak frequency of the BBCOF can be considered as [54]

$$f_r = \frac{1}{2\pi\sqrt{L_2 C_1}} \tag{2.78}$$

2.3 Converter implementation

The design of the passive components of the BBCOF is performed between chapters 2 and 4, according to the following steps:

1) **L_1 design:** a ripple criterion is adopted for the current ripple in L_1 inductor, and correspondingly the value for L_1 is obtained.
2) **L_2 design:** the value of L_2 inductor is constrained to approximately one tenth of L_1, according to the converter design rules described in [54].
3) **C_2 design:** the value of C_2 capacitor is chosen so that the resonance peak of the output impedance of the BBCOF is below 0 dB.
4) **C_1 design:** C_1 is constrained to approximately one fifth of C_2, also according to the design rules found in [54].

The stability of the designed BBCOF has been already demonstrated by the previous analysis, provided that the RC snubber is added to the circuit. Then, once the passive components are designed, it will be verified if the Middlebrook criterion is accomplished, and consequently if the BBCOF remains stable when the studied load is connected.

2.3.1 Ripple analysis of the BBCOF

The small-ripple approximation [55] is used for the converter analysis. This approximation is based on the fact that, in any well-designed converter, the ripple of the variable states found after a switching element should be much smaller than the DC component. Then, neglecting the damping network and the resistive losses in the inductors, the waveforms of interest to calculate the ripple of the circuit state variables are represented and analysed below. The first element to be analysed is the inductor L_1, with pulsating voltage characteristics, which has the current waveform shown in Fig. 2.13 [55]. The values of the current slopes are extracted from (2.16).

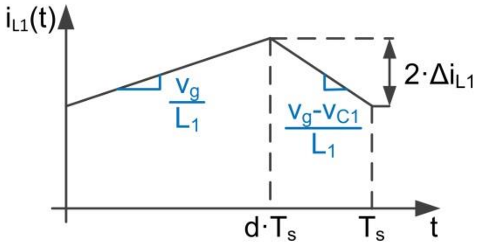

Fig. 2.13. Current waveform in inductor L_1.

From this representation, the current ripple Δi_{L1} is calculated

$$\Delta i_{L1} = \frac{1}{2}\frac{v_g}{L_1} dT_s , \tag{2.79}$$

and therefore, the value of inductor L_1 can be expressed as

$$L_1 = \frac{1}{2}\frac{v_g}{\Delta i_{L1}} dT_s \tag{2.80}$$

In a similar manner, the value of the voltage ripple in capacitor C_1 can be represented as in Fig. 2.14 according to (2.18), since the current in the capacitor is also pulsating.

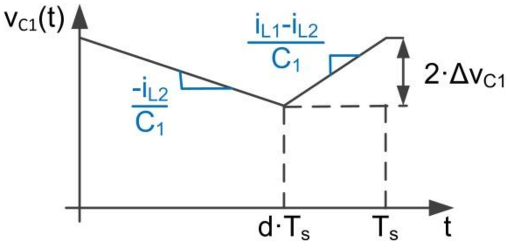

Fig. 2.14. Voltage waveform in capacitor C_1.

The voltage ripple Δi_{L1} is deduced graphically, and the analytical value of capacitor C_1 can be isolated according to the voltage ripple.

$$C_1 = \frac{1}{2}\frac{i_{L2}}{\Delta v_{C1}} dT_s \tag{2.81}$$

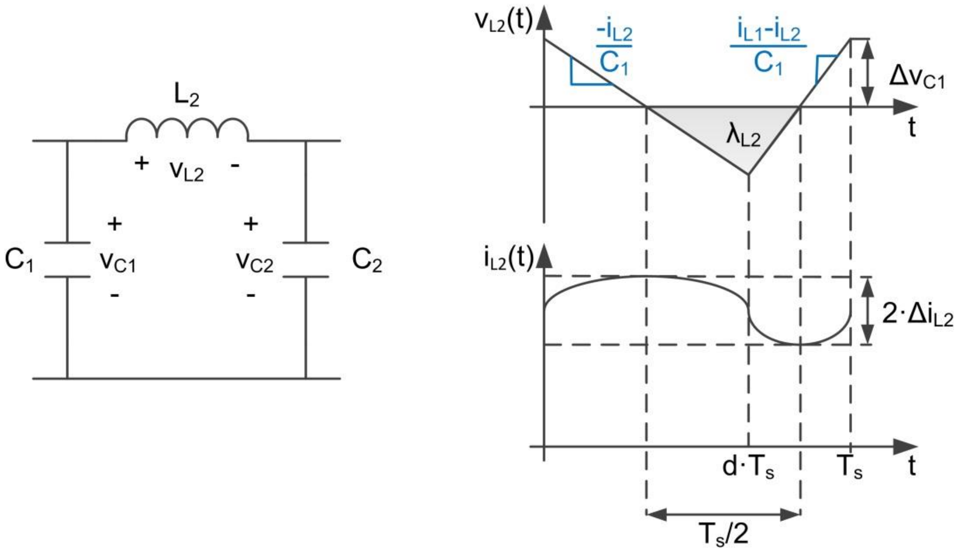

a) b)

Fig. 2.15. Considerations for ripple calculation in inductor L_2: a) C_1 ripple distribution between L_2 and C_2, and b) voltage and current waveforms of inductor L_2.

The other two elements, C_2 and L_2, have nonpulsating current and voltage, respectively. Therefore, the ripple of the previous components is the only component for the state variables of L_2 and C_2, and thus the small-ripple approximation in no longer applicable. Consequently, the ripple in these elements has to be estimated considering the switching ripple, neglected for C_1 and L_1. In the study of inductor L_2, the ripple in C_1 has to be considered. Recalling the relevant part of the BBCOF topology for this analysis in Fig. 2.15.a, for a well-designed converter almost all the voltage ripple in C_1 will fall across L_2, so that the voltage in C_2 is continuous. Therefore, the voltage and current waveforms of inductor L_2 are the ones represented in Fig. 2.15.b.

The shaded area in Fig. 2.15.b is the inductor total flux linkage, which is defined as

$$\lambda_{L2} = L_2\left(2\Delta i_{L2}\right), \tag{2.82}$$

but can also be calculated from its graphical representation

$$\lambda_{L2} = \int_{\frac{1}{2}dTs}^{dT_s+\frac{1}{2}(1-d)T_s} v_{L2}\left(t\right)dt = \frac{1}{4}T_s\Delta v_{C1} \tag{2.83}$$

Equating (2.82) and (2.83), the value of the inductor L_2 is obtained according to the voltage ripple in C_1 and the current ripple of C_1 and L_2, respectively

$$L_2 = \frac{1}{8}\frac{\Delta v_{C1}T_s}{\Delta i_{L2}} \tag{2.84}$$

To study the value of capacitor C_2, it is assumed from the analysis of Fig. 2.16.a that the current ripple in inductor L_2 will entirely circulate through C_2 and not through the load, and so the load current will be continuous. In Fig. 2.16.b the voltage of inductor L_2 is depicted, and the current waveforms of L_2 and C_2 are extracted. Since the current in L_2 is

$$i_{L2}\left(t\right) = \frac{1}{L_2}\int v_{L2}\left(t\right)dt\,, \tag{2.85}$$

the time-dependent expressions for the current in capacitor C_2 are known, and thus the shaded area, which is the total charge of C_2 capacitor, can be calculated

$$q_{C2} = \int_0^{dT_s} \frac{-i_{L2}}{2C_1L_2}t^2\,dt = \frac{1}{8}\frac{i_{L2}d^3T_s^3}{C_1L_2} \tag{2.86}$$

As well, it is defined as

$$q_{C2} = C_2\left(2\Delta v_{C2}\right) \tag{2.87}$$

As a result, the following expression for the value of C_2 capacitor is found

$$C_2 = \frac{1}{16}\frac{i_{L2}d^3T_s^3}{C_1L_2\Delta v_{C2}} \tag{2.88}$$

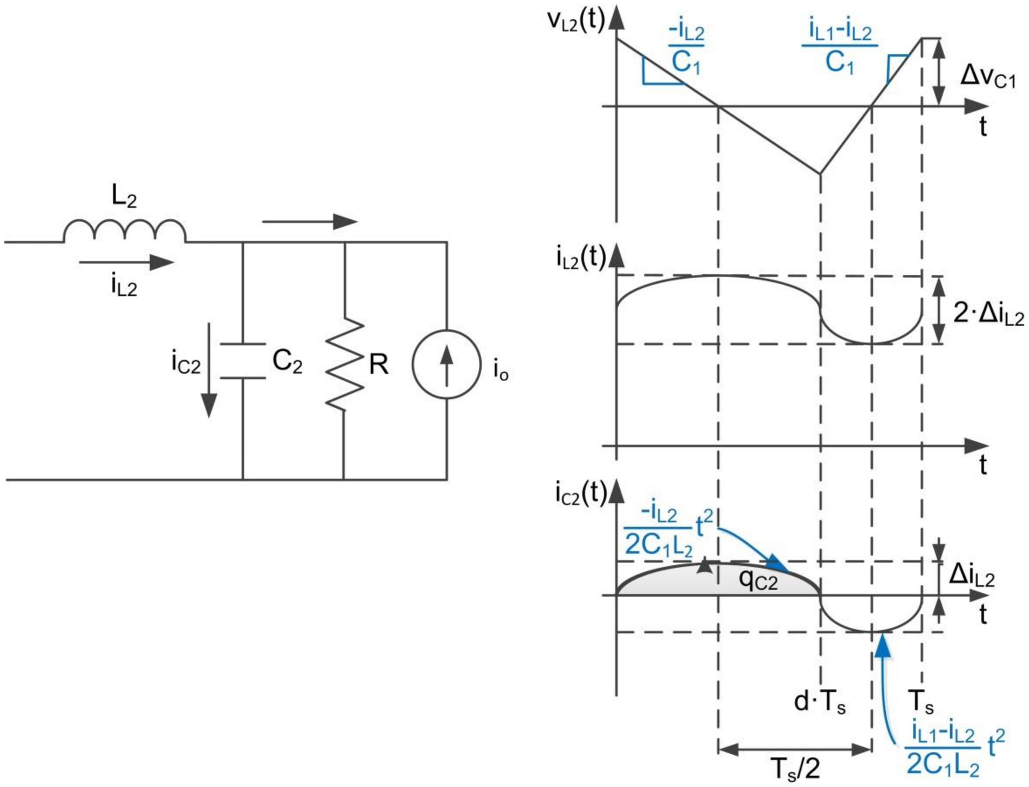

a) b)

Fig. 2.16. Considerations for ripple calculation in capacitor C_2: a) L_2 ripple distribution between C_2 and the load, and b) voltage and current waveforms of inductor L_2, and current waveform of capacitor C_2.

Once the expressions for the component values are known, the design criteria in Table 2.I have been established to proceed. Note that the values of L_2 and C_1 have been constrained according to L_1 and C_2, respectively, in order to accomplish the design rules in [54] that make sure that the converter impedance is not degraded. Consequently, the values of the inductors can be automatically derived from (2.80)

$$L_1 = \frac{1}{2}\frac{200\,V}{1.3125\,A}\left(1-\frac{200\,V}{350\,V}\right)\frac{1}{40\,kHz} \simeq 816\ \mu H \tag{2.89}$$

$$L_2 = \frac{L_1}{10} = 81.6\ \mu H \tag{2.90}$$

Considering the desired capacitance ratio, the expression for C_2 can be rewritten as follows

$$C_2 = \frac{5}{16}\frac{i_{L2} d^3 T_s^{\,3}}{C_2 L_2 \Delta v_{C2}} \tag{2.91}$$

With the adopted design criteria it is also possible to determine the values of the damping network that stabilises the BBCOF. The damping resistance must accomplish (2.71)

$$0 < R_d < \frac{V_{C2}^{\ 2}}{P_{CPL,\max}} = \frac{(350\,V)^2}{1.5\,kW} = 81.67\,\Omega, \tag{2.92}$$

so R_d has been fixed to the commercial value of 75 Ω. The damping capacitor that avoids dissipation at low frequencies has the following value, according to (2.77) and (2.78),

$$C_d = \frac{1}{2\pi R_d \frac{1}{5} f_r} = \frac{1}{\frac{1}{5} 75\,\Omega \frac{1}{\sqrt{81.6\,\mu H \cdot 1\,\mu F}}} = 602\,nF \tag{2.93}$$

In order to maintain a minimum ratio of 5 between the resonance peak frequency and the corner frequency of the RC snubber, a 820 nF value is chosen for C_d. Although the value of the capacitors is designed in chapter 4, the values of all the components are summarised in Table 2.II. The values of the inductors' parasitic inductance have been measured and included in the table.

Table 2.I. Design criteria for the BBCOF.

input voltage V_g	200 V
output voltage V_{C2}	350 V
rated power P_n	1.5 kW
switching frequency f_s	40 kHz
input current ripple $\Delta i_{L1,\%}$	17.5%
input current ripple Δi_{L1}	1.3125 A
output voltage ripple $\Delta v_{C2,\%}$	0.5%
inductance ratio L_1/L_2	10
capacitance ratio C_2/C_1	5

Table 2.II. Component values of the designed BBCOF.

inductance L_1	816 μH
parasitic resistance R_{L1}	45 mΩ
inductance L_2	82 μH
parasitic resistance R_{L2}	20 mΩ
capacitance C_1	1 μF
capacitance C_2	6.2 μF
damping resistance R_d	75 Ω
damping capacitor C_d	820 nF

2.3.2 Relocating the RC snubber

From the simple inspection of the expression for the resonance peak frequency, it can be observed that the two elements that form the resonant tank are C_1 and L_2, provided that C_2>>C_1. It is straightforward that introducing the RC snubber between these components, the damping effect is greater, but it has been corroborated by repeating the analysis in section 2.2.3 relocating the aggregate resistance as specified in Fig. 2.17. The following transfer function has been obtained

$$\frac{\tilde{v}_{C2}(s)}{\tilde{d}(s)} = \frac{-R_{CPL}R_D\left(IL1sL_1 + DVC1 + IL1R_{L1} - VC1\right)}{a \cdot s^4 + b \cdot s^3 + c \cdot s^2 + d \cdot s + e}, \tag{2.94}$$

UNIVERSITAT ROVIRA I VIRGILI
DESIGN AND CONTROL OF A BIDIRECTIONAL DC/DC CONVERTER FOR AN ELECTRIC VEHICLE APPLICATION.
Laura Albiol Rendillo
Dipòsit Legal: T 1361-2015

where

$$
\begin{aligned}
a &= R_d C_1 C_2 L_1 L_2 R_{CPL} \\
b &= R_d C_1 C_2 L_1 R_{CPL} R_{L2} + R_d C_1 C_2 L_2 R_{CPL} R_{L1} + R_d C_1 L_1 L_2 + C_2 L_1 L_2 R_{CPL} \\
c &= D^2 R_d C_2 L_2 R_{CPL} + R_d C_1 C_2 R_{CPL} R_{L1} R_{L2} - 2DR_d C_2 L_2 R_{CPL} + R_d C_1 L_1 R_{CPL} + \\
&\quad + R_d C_1 L_1 R_{L2} + R_d C_1 L_2 R_{L1} + R_d C_2 L_1 R_{CPL} + R_d C_2 L_2 R_{CPL} + C_2 L_1 R_{CPL} R_{L2} + \\
&\quad + C_2 L_2 R_{CPL} R_{L1} + L_1 L_2 \\
d &= D^2 R_d C_2 R_{CPL} R_{L2} - 2DR_d C_2 R_{CPL} R_{L2} + D^2 R_d L_2 + R_d C_1 R_{CPL} R_{L1} + R_d C_1 R_{L1} R_{L2} + \\
&\quad + R_d C_2 R_{CPL} R_{L1} + R_d C_2 R_{CPL} R_{L2} + C_2 R_{CPL} R_{L1} R_{L2} - 2DR_d L_2 + R_d L_1 + R_d L_2 + L_1 R_{CPL} + \\
&\quad + L_1 R_{L2} + L_2 R L_1 \\
e &= \mathrm{D}^2 R_d R_{CPL} + \mathrm{D}^2 R_d R_{L2} - 2\mathrm{D} R_d R_{CPL} - 2\mathrm{D} R_d R_{L2} + R_d R_{CPL} + R_d R_{L1} + R_d R_{L2} + \\
&\quad + R_{CPL} R_{L1} + R_{L1} R_{L2}
\end{aligned}
\tag{2.95}
$$

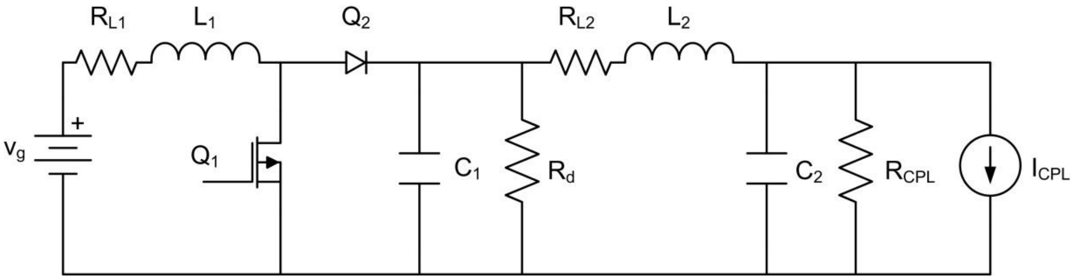

Fig. 2.17. BBCOF with the aggregate resistance in parallel with C_1.

The frequency responses of the BBCOF with the aggregate resistance in parallel with C_1, and the BBCOF with the relocated aggregate resistance are compared in Fig. 2.18. It can be observed that the attenuation of the resonance peak by placing the aggregate resistance in parallel with C_1 is remarkable, and thus justifies relocating the RC snubber as suggested.

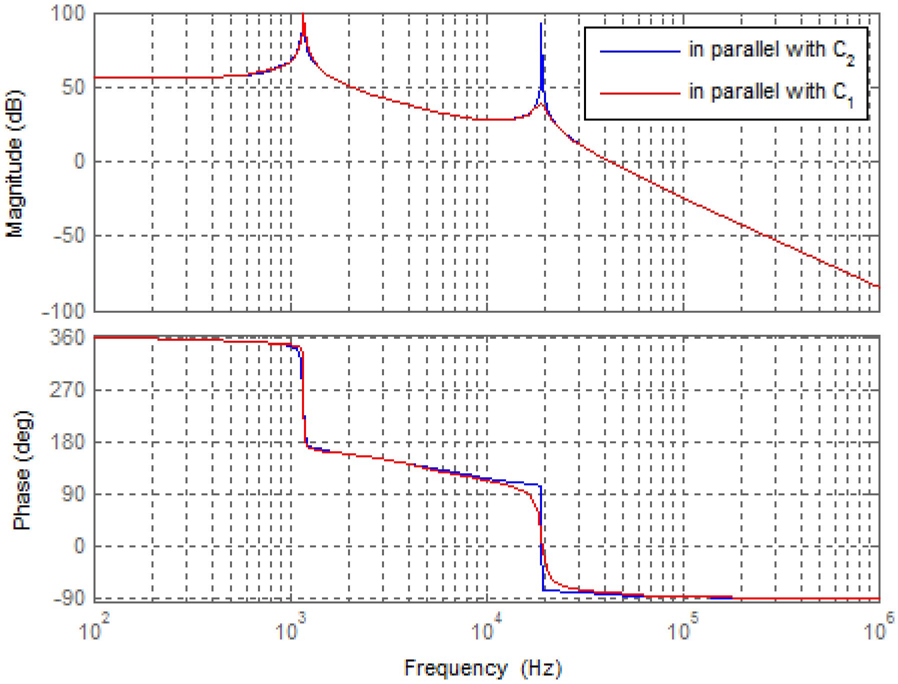

Fig. 2.18. Frequency response of the BBCOF with the damping network in parallel with C_2 and C_1.

2.3.3 External diodes for MOSFET switches

MOSFETs are switching devices that only block positive voltages but, due to their body diode, exhibit current-bidirectional operation. The v-i characteristic of an ideal MOSFET is represented in Fig. 2.19.a. However the switching speed of the body diode is much lower than the MOSFET switching speed. This phenomenon causes high peak-currents during diode turn-off, leading to MOSFET failure [55]. To avoid this problem, two additional diodes are used, one in series and one in antiparallel to the MOSFET, as depicted in Fig. 2.19.b.

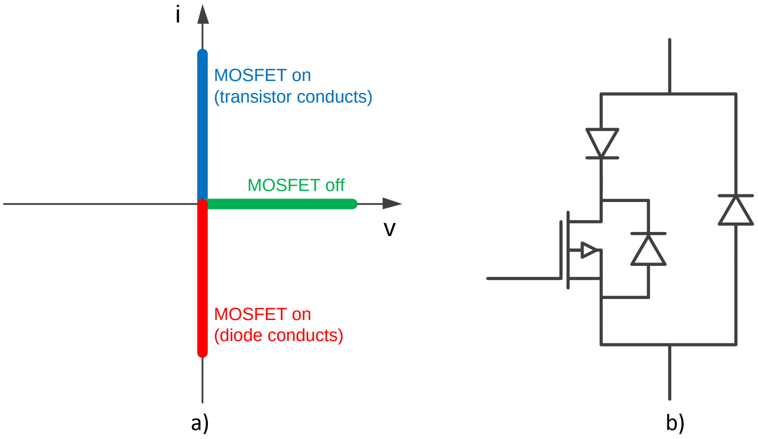

Fig. 2.19. MOSFET considerations for the BBCOF: a) v-i characteristic of an ideal MOSFET, and b) connection of the additional diodes.

2.3.4 Component selection

The final component selection for the BBCOF is shown in Fig. 2.20. It has 600 V-rated switching elements, Infineon IPW60R041C6 MOSFETs and Infineon IDH16S60C diodes. An IR2110 driver is used to generate the gate signals for the MOSFETS of the converter. C1, C21 and C22 are metallized polypropylene (MKP) capacitors. The output filter C_2 is the parallel association of the MKP capacitors C21 and C22 with the ceramic capacitors C23, C24 and C25. This combination of capacitor technologies offers improved filtering and reliability capabilities. The damping capacitor C_d is the parallel association of two 220 nF and four 100 nF capacitors, although not represented in Fig. 2.20. The input current is sensed by the current transducer LEM LTS 15-NP, with a gain k_{sens} of 0.092, and the output voltage is sensed by means of the voltage divider formed by R1, R2, R3 and R4.

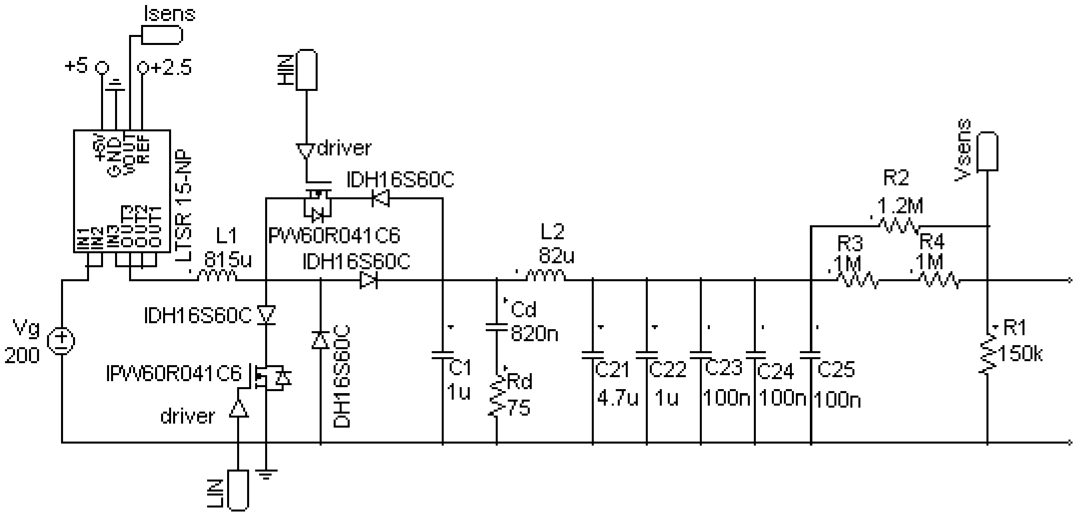

Fig. 2.20. Schematic of the 1.5 kW BBCOF implementation.

2.4 Simulation results

The designed converter has been simulated using PSIM, and its schematic is reproduced in Fig. 2.21. The gating signals of the MOSFETs have been set to have 350 V at the output. The constant power load is modelled by a voltage-controlled current source, with the value defined in (2.1). The current is limited to the maximum current consumption of the 1.5 kW load at 350 V, i.e. 4.29 A. A zero-order hold (ZOH) is inserted after voltage sensing to avoid time step influence on the simulation results. The frequency has been set 20 times lower than the BBCOF switching frequency.

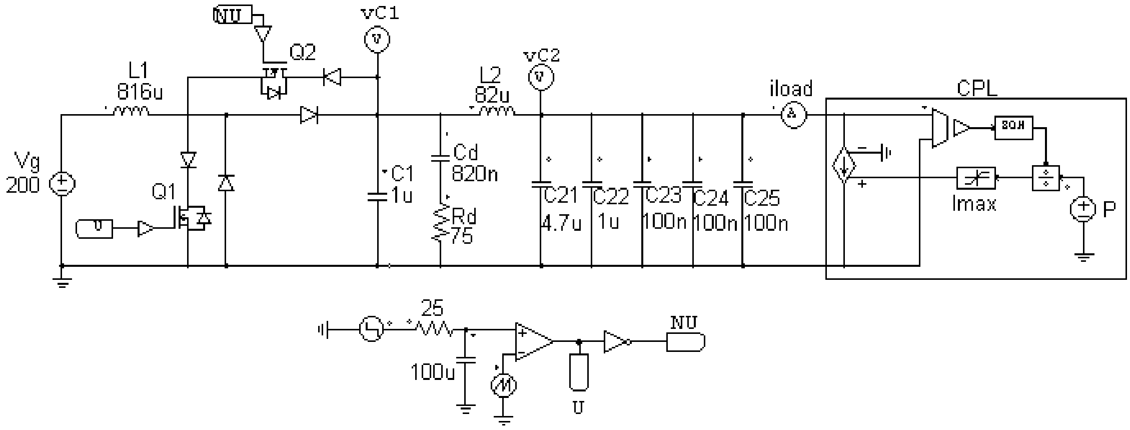

Fig. 2.21. Schematic of the PSIM simulation of the designed converter.

The step-up operation has been simulated by fixing the power reference source P to 1.5 kW, and the results are reproduced in Fig. 2.22. After the start-up transient, the BBCOF output voltage v_{C2} is 350 V, and it can be observed that the converter is delivering power to the load, since the current circulating through L_1 is positive. On the contrary, setting the power reference source to -1.5 kW forces the step-down operation in Fig. 2.23. The current i_{L1} is negative, and the output voltage of the converter is 350 V. From these results, it can be concluded that the operation of the BBCOF with a CPL is stable in both operation modes, as analysed in sections 2.2.3 and 2.2.4. The high ripple during in the input current and output voltage during start-up is due to the open-loop start-up operation of the BBCOF with a CPL.

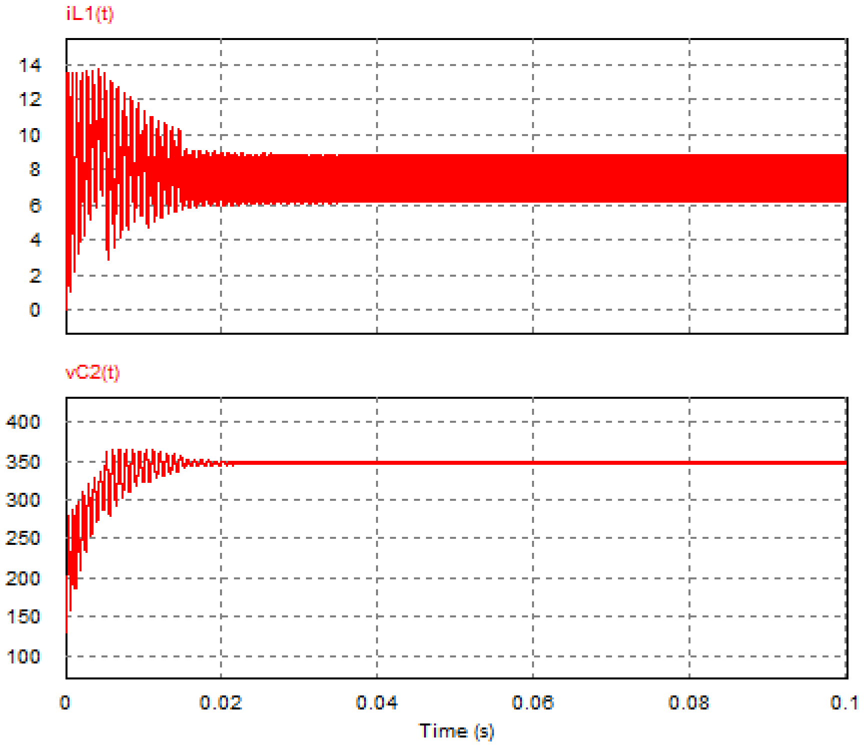

Fig. 2.22. Simulation results of the designed converter under step-up operation.

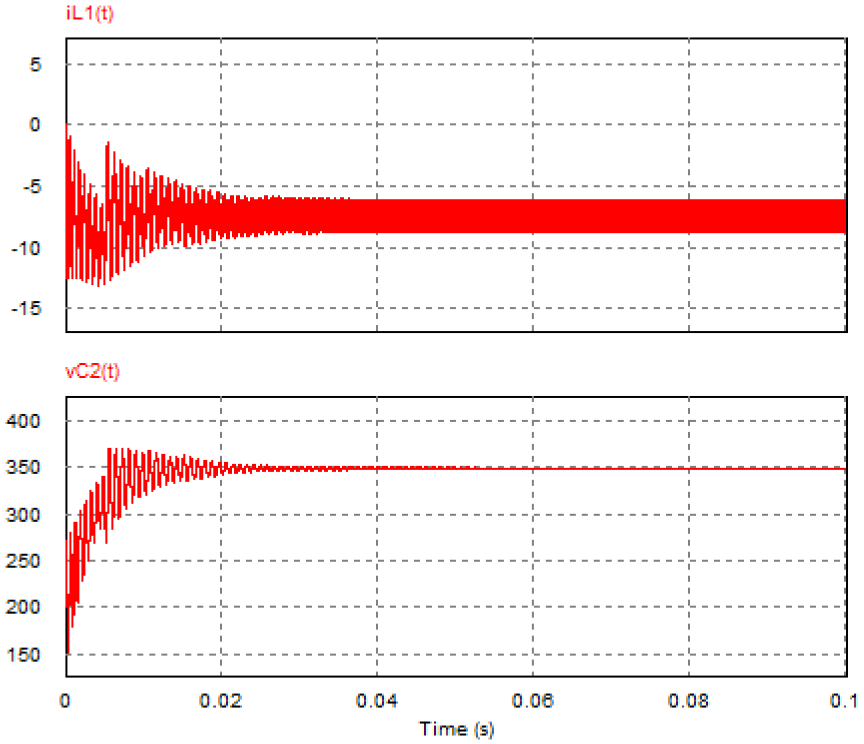

Fig. 2.23. Simulation results of the designed converter under step-down operation.

The input current and output voltage ripple have also been verified in this simulation, as shown in Fig. 2.24. The input current ripple value is 1.32 A as set by the design criteria. The output voltage ripple is 0.74 V, which slightly differs from the 0.525 V criterion due to the approximations made during the ripple analysis. It represents an output ripple of 0.211%, which is still considered valid for this application.

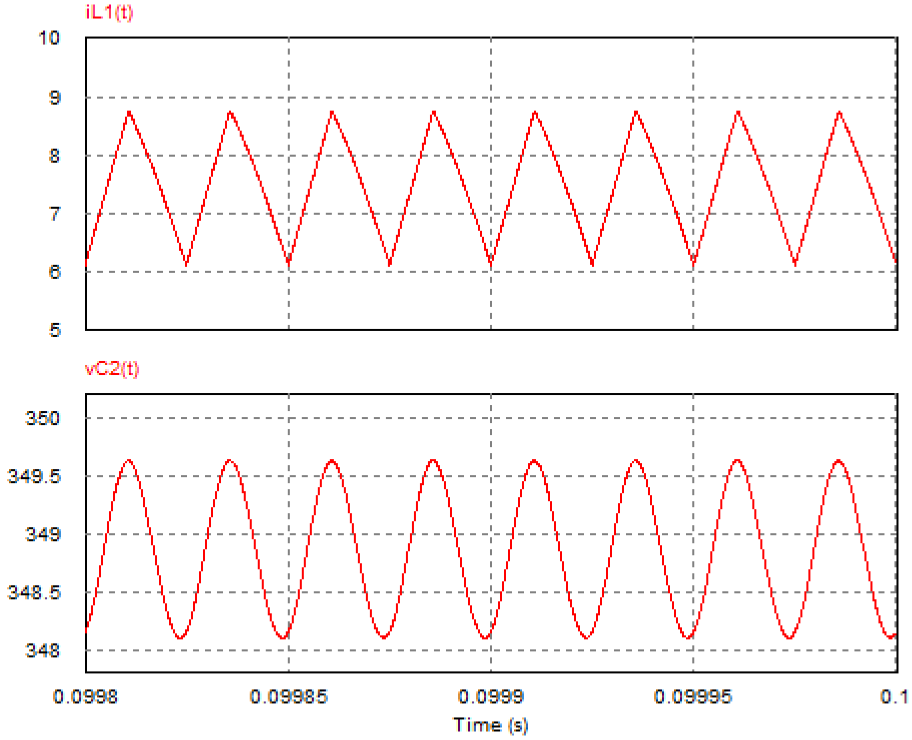

Fig. 2.24. Simulated input current and output voltage ripple at 1.5 kW step-up operation.

2.5 Conclusions

This chapter analyses thoroughly the DC/DC converter chosen for the powertrain of the EV, i.e. the BBCOF. As the motor drive behaves as a constant-power load, with incremental negative impedance, this effect has been considered in the stability study of the converter. It has been proven that the BBCOF is stable during step-up and step-down operations, as well as during transitions, by means of an RC snubber connected in parallel to the capacitor of the boost converter.

Moreover, the design of the converter is partly covered in this chapter. The calculation of the ripple yields the specification for the inductor values, whereas the value of the capacitors for the BBCOF will be derived in successive chapters. Component selection for the voltage and power rating of the implemented converters is also covered in detail.

The model of the converter has been developed with PSIM, and results are in good agreement with the conclusions drawn during the stability analysis of the system.

3 Sliding-mode control

3.1 Introduction

Sliding mode refers to the phenomenon in which a dynamic system described by differential equations has a high-frequency (ideally infinite) switching motion. The cause of this high-frequency switching motion is that either the control or the dynamics of the system is discontinuous. As DC/DC converters are systems which inherently have a discontinuous control, it is straightforward to consider sliding mode for their control [44].

Sliding mode is an effective method to control complex nonlinear systems with uncertainty conditions, at the expense of operating at variable frequency. Due to its advantages, sliding-mode control has been extensively covered in the literature. Regarding to topics related with power electronics, sliding-mode control has been proposed for DC power distribution systems [56], inductive power transfer [57] and power factor correction [58, 59] among other applications. Sliding-mode control has been widely used in renewable energy systems. In [60, 61] it is employed for power conditioning of renewable generation. [62] proposed a second-order sliding-mode control for wind energy conversion, and several solutions for impedance matching [63] and MPPT tracking [64-66] for photovoltaic applications are also discussed.

Sliding-mode control has been considered for several DC/DC topologies recently in the literature, as buck [67, 68], boost [45, 69], quadratic boost [70] and resonant converters [71, 72], certifying the interest on this control technique.

The aim of the proposed sliding-mode control is to regulate the output voltage of the BBCOF, i.e. the high-voltage DC bus of the EV traction system. This sliding-mode control is required to regulate the output voltage of the converter with seamless transitions regardless of the operation mode [73]. As in most DC/DC converters, the fast dynamics of the BBCOF is associated with the input current, whereas the slow dynamics is related to the output voltage [44]. Fig. 3.1 details the structure of the proposed cascaded control, with an inner loop that regulates the input current, and an outer one that regulates the output voltage.

UNIVERSITAT ROVIRA I VIRGILI
DESIGN AND CONTROL OF A BIDIRECTIONAL DC/DC CONVERTER FOR AN ELECTRIC VEHICLE APPLICATION.
Laura Albiol Rendillo
Dipòsit Legal: T 1361-2015

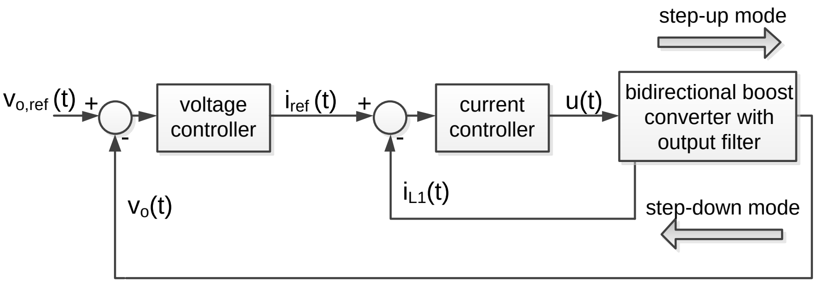

Fig. 3.1. Two-loop control architecture.

3.1.1 State-space representation of the BBCOF

In order to simplify the calculus, the sliding-mode control analysis is performed with the matrix expressions of the converter. The state-space variables and their derivatives are defined, respectively, as

$$x(t)=\begin{bmatrix} i_{L1}(t) \\ i_{L2}(t) \\ v_{C1}(t) \\ v_{C2}(t) \\ v_{Cd}(t) \end{bmatrix}; \quad \dot{x}(t)=\begin{bmatrix} \dot{i}_{L1}(t) \\ \dot{i}_{L2}(t) \\ \dot{v}_{C1}(t) \\ \dot{v}_{C2}(t) \\ \dot{v}_{Cd}(t) \end{bmatrix} \tag{3.1}$$

The dynamics of the BBCOF can be expressed by means of the following state-space representation

$$\begin{cases} \dot{x}(t)=A_1x+B_1, & for\ u=1 \\ \dot{x}(t)=A_2x+B_2, & for\ u=0 \end{cases}, \tag{3.2}$$

where *u* represents the control, i.e. the switching state of the Q_1 MOSFET in Fig. 3.2, where *u*= 1 corresponds to the on state of the switch, and *u*=0 to the off state. The matrices A_1, A_2, B_1 and B_2 can be derived from the analysis of Fig. 3.2 and the obtained expressions are shown in Table 3.I.

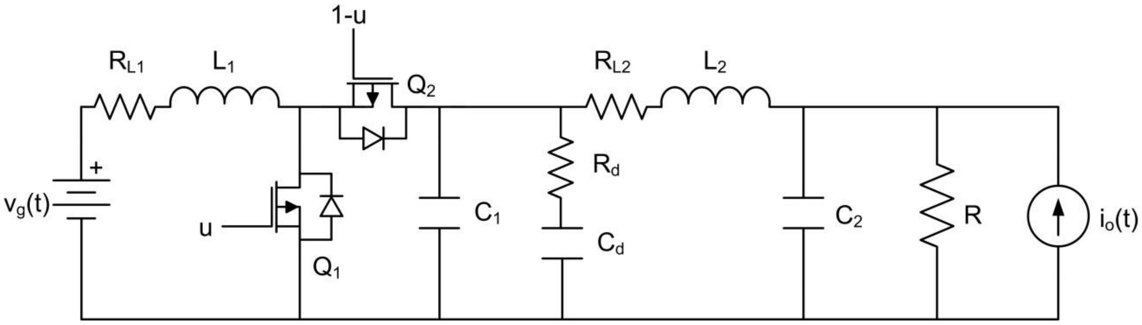

Fig. 3.2. BBCOF with time-dependant sources.

Table 3.I. Matrix description of the BBCOF.

A_1	A_2	B_1	B_2
$\begin{bmatrix} \frac{-R_{L1}}{L_1} & 0 & 0 & 0 & 0 \\ 0 & \frac{-R_{L2}}{L_2} & \frac{1}{L_2} & \frac{-1}{L_2} & 0 \\ 0 & \frac{-1}{C_1} & \frac{-1}{C_1 R_d} & 0 & \frac{1}{C_1 R_d} \\ 0 & \frac{1}{C_2} & 0 & \frac{-1}{C_2 R} & 0 \\ 0 & 0 & \frac{1}{C_d R_d} & 0 & \frac{-1}{C_d R_d} \end{bmatrix}$	$\begin{bmatrix} \frac{-R_{L1}}{L_1} & 0 & \frac{-1}{L_1} & 0 & 0 \\ 0 & \frac{-R_{L2}}{L_2} & \frac{1}{L_2} & \frac{-1}{L_2} & 0 \\ \frac{1}{C_1} & \frac{-1}{C_1} & \frac{-1}{C_1 R_d} & 0 & \frac{1}{C_1 R_d} \\ 0 & \frac{1}{C_2} & 0 & \frac{-1}{C_2 R} & 0 \\ 0 & 0 & \frac{1}{C_d R_d} & 0 & \frac{-1}{C_d R_d} \end{bmatrix}$	$\begin{bmatrix} \frac{\tilde{v}_g(t)}{L_1} \\ 0 \\ 0 \\ \frac{\tilde{i}_o(t)}{C_2} \\ 0 \end{bmatrix}$	$\begin{bmatrix} \frac{\tilde{v}_g(t)}{L_1} \\ 0 \\ 0 \\ \frac{\tilde{i}_o(t)}{C_2} \\ 0 \end{bmatrix}$

3.2 Sliding-mode current control

The general bilinear description of a variable structure system with two states is

$$\dot{x}(t) = \left[A \cdot x(t) + \delta\right] + \left[B \cdot x(t) + \gamma\right] u(t), \tag{3.3}$$

where

$$\begin{aligned} &A = A_2;\ B = A_1 - A_2 \\ &\delta = B_2;\ \gamma = B_1 - B_2 \end{aligned} \tag{3.4}$$

The sliding surface to seamlessly control [34] the bidirectional flux of energy in the converter is defined as

$$S\left(x(t)\right) = i_{L1}(t) - k = 0, \tag{3.5}$$

where k is the constant value of the current reference. The system will exhibit a sliding motion if the following condition is accomplished

$$S\left(x(t)\right) \cdot \dot{S}\left(x(t)\right) < 0 \tag{3.6}$$

According to (3.3), the derivative of the sliding surface in (3.5) will be given by

$$\dot{S}\left(x(t)\right) = \frac{d\,i_{L1}(t)}{d\,t} = \frac{1}{L_1}\left[v_{C1}(t)\left(u(t)-1\right) + v_g - R_{L1} i_{L1}(t)\right] \tag{3.7}$$

Since the control action can be defined as

$$u(t) = \frac{1}{2}\left[1 - sign\left(S\left(x(t)\right)\right)\right], \tag{3.8}$$

then, omitting the resistive losses in the inductor L_1, the condition in (3.6) can be reformulated as

$$S\left(x(t)\right) \cdot \dot{S}\left(x(t)\right) = \frac{1}{L_1}\left(-\frac{v_{C1}(t)}{2} S\left(x(t)\right) - \frac{v_{C1}(t)}{2}\left|S\left(x(t)\right)\right| + v_g S\left(x(t)\right)\right) < 0 \tag{3.9}$$

Therefore, two reachability conditions can be derived from (3.9), depending on the sign of the sliding surface

$$v_{C1}(t) > v_g \quad if\ S(x(t)) > 0 \tag{3.10}$$

$$v_g > 0 \quad if\ S(x(t)) < 0 \tag{3.11}$$

The system motion will be attracted to the sliding surface once the capacitor voltage v_{c1} exceeds the source voltage v_g as depicted in Fig. 3.3.

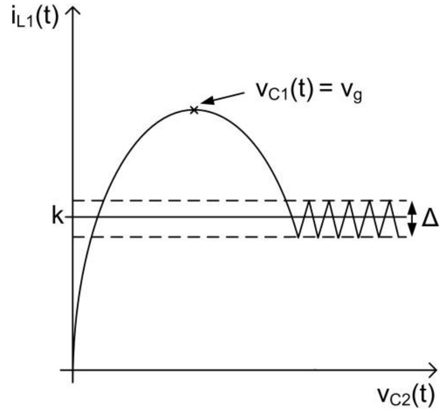

Fig. 3.3. Representation of the attraction domain of the sliding surface.

3.2.1 Stability under sliding-mode control

The equivalent control u_{eq} is the control action that constraints the motion of the system on the surface once it is reached. For sliding mode to exist locally on *S(x(t))*=0, the corresponding equivalent control has to satisfy

$$0 < u_{eq} < 1, \tag{3.12}$$

which is equivalent to the previously obtained reachability conditions (3.10) and (3.11). The existence condition of the equivalent control [44] is given by

$$\frac{\delta}{\delta u}\left(\frac{d}{dt}S(x(t),t)\right) = \alpha\left[B\cdot x(t)+\gamma\right] \neq 0 \tag{3.13}$$

The partial derivative of the sliding surface with respect to the control is not null, and hence the existence condition is fulfilled.

$$\alpha\left[B\cdot x(t)+\gamma\right] = \frac{1}{L_1}v_{C1}(t) \neq 0 \tag{3.14}$$

From the calculus of the existence condition with constant current control in (3.5), it is proven that the sliding-mode will exist, and so i_{L1} will converge to *k*. Then, the ideal switching dynamics is obtained after substituting u_{eq} in (3.3).

$$\frac{d}{dt}i_{L1}(t)=0 \tag{3.15}$$

$$\frac{d}{dt}i_{L2}(t)=\frac{v_{C1}(t)-R_{L2}i_{L2}(t)-v_{C2}(t)}{L_2} \tag{3.16}$$

$$\frac{d}{dt}v_{C1}(t)=-\frac{R_d i_{L1}(t)\left(u_{eq}(t)-1\right)+R_d i_{L2}(t)+v_{C1}(t)-v_{Cd}(t)}{C_1R_d} \tag{3.17}$$

$$\frac{d}{dt}v_{C2}(t)=\frac{Ri_{L2}(t)+Ri_o(t)-v_{C2}(t)}{C_2R} \tag{3.18}$$

$$\frac{d}{dt}v_{Cd}(t)=\frac{v_{C1}(t)-v_{Cd}(t)}{C_dR_d} \tag{3.19}$$

By equalling the derivatives of the state variables to zero, the following steady state values are found

$$I_{L1}=k \tag{3.20}$$

$$I_{L2}=-\frac{\frac{1}{2}RI_o+\frac{1}{2}\sqrt{R^2I_o{}^2-4RR_{L1}k^2-4R_{L1}R_{L2}k^2+4V_gRk+4V_gR_{L2}k}}{R+R_{L2}} \tag{3.21}$$

$$V_{C1}=\frac{1}{2}RI_o-\frac{1}{2}\sqrt{R^2I_o{}^2-4RR_{L1}k^2-4R_{L1}R_{L2}k^2+4V_gRk+4V_gR_{L2}k} \tag{3.22}$$

$$V_{C2}=-\frac{R\left(\frac{1}{2}RI_o+\frac{1}{2}\sqrt{R^2I_o{}^2-4RR_{L1}k^2-4R_{L1}R_{L2}k^2+4V_gRk+4V_gR_{L2}k}\right)}{R+R_{L2}}+RI_o \tag{3.23}$$

$$V_{Cd}=\frac{1}{2}RI_o-\frac{1}{2}\sqrt{R^2I_o{}^2-4RR_{L1}k^2-4R_{L1}R_{L2}k^2+4V_gRk+4V_gR_{L2}k}\,, \tag{3.24}$$

where I_{L1}, I_{L2}, V_{C1}, V_{C2}, V_{Cd} ,V_g and I_o denote the steady state values of $i_{L1}(t)$, $i_{L2}(t)$, $v_{C1}(t)$, $v_{C2}(t)$, $v_{Cd}(t)$, $v_g(t)$and $i_o(t)$, respectively. Note that equations (3.15)-(3.19) correspond to a fourth-order system. The order reduction is caused by the addition of the sliding-mode current control, which regulates $i_{L1}(t)$. Therefore, (3.16)-(3.19) are used to calculate the characteristic polynomial. The first step is to isolate $v_{cd}(t)$ in (3.17)

$$v_{Cd}(t)=C_1R_d\frac{\mathrm{d}}{\mathrm{d}t}v_{C1}(t)+\frac{k\left(R_{L1}k-v_g(t)+v_{C1}(t)\right)R_d}{v_{C1}(t)}-kR_d+R_di_{L2}(t)+v_{C1}(t) \tag{3.25}$$

The derivative of $v_{cd}(t)$ is found by evaluating (3.25) in (3.19)

$$\frac{\mathrm{d}}{\mathrm{d}t}v_{Cd}\left(t\right)=\frac{-C_1R_d\frac{\mathrm{d}}{\mathrm{d}t}vC1\left(t\right)-\frac{k\left(R_{L1}k-v_g\left(t\right)+v_{C1}\left(t\right)\right)R_d}{v_{C1}\left(t\right)}+kR_d-R_di_{L2}\left(t\right)}{C_dR_d} \tag{3.26}$$

The result of using (3.26) in the expression of the derivative of $v_{C1}(t)$ (3.17) is

$$\frac{\mathrm{d}}{\mathrm{d}t}v_{C1}\left(t\right)=-\frac{\frac{k\left(R_{L1}k-v_g\left(t\right)+v_{C1}\left(t\right)\right)R_d}{v_{C1}\left(t\right)}-kR_d+R_di_{L2}\left(t\right)+v_{C1}\left(t\right)-v_{Cd}\left(t\right)}{C_1R_d} \tag{3.27}$$

Differentiating (3.27), the following expression for the second derivative of $v_{C1}(t)$ is obtained

$$\frac{\mathrm{d}^2}{\mathrm{d}t^2}v_{C1}\left(t\right)=-\frac{1}{C_1R_d}\left(\begin{array}{l}\frac{k\left(-\frac{\mathrm{d}}{\mathrm{d}t}v_g\left(t\right)+\frac{\mathrm{d}}{\mathrm{d}t}v_{C1}\left(t\right)\right)R_d}{v_{C1}\left(t\right)}+\frac{\mathrm{d}}{\mathrm{d}t}i_{L2}\left(t\right)R_d+\frac{\mathrm{d}}{\mathrm{d}t}v_{C1}\left(t\right)-\\-\frac{k\left(R_{L1}k-v_g\left(t\right)+v_{C1}\left(t\right)\right)R_d\frac{\mathrm{d}}{\mathrm{d}t}v_{C1}\left(t\right)}{{v_{C1}}^2\left(t\right)}-\frac{\mathrm{d}}{\mathrm{d}t}v_{Cd}\left(t\right)\end{array}\right) \tag{3.28}$$

By using (3.26) in (3.28), the second derivative of $v_{C1}(t)$ can be expressed as

$$\frac{d^2}{dt^2}v_{C1}(t)=\frac{-1}{C_dC_1R_d{v_{C1}}^2(t)}\left(\begin{array}{l}\left(R_dC_dk\left(v_g(t)-kR_{L1}\right)+\left(C_1+C_d\right){v_{C1}}^2(t)\right)\frac{d}{dt}v_{C1}(t)-\\-kR_dv_{C1}(t)C_d\frac{d}{dt}v_g(t)+R_dC_d{v_{C1}}^2(t)\frac{d}{dt}i_{L2}(t)+\\+R_{L1}k^2v_{C1}(t)+{v_{C1}}^2(t)i_{L2}(t)-kv_{C1}(t)v_g(t)\end{array}\right) \tag{3.29}$$

In parallel, an expression for $v_{C1}(t)$ and its first and second derivatives can be obtained from (3.16)

$$v_{C1}\left(t\right)=L_2\frac{\mathrm{d}}{\mathrm{d}t}i_{L2}\left(t\right)+R_{L2}i_{L2}\left(t\right)+v_{C2}\left(t\right) \tag{3.30}$$

$$\frac{d}{dt}v_{C1}\left(t\right)=L_2\frac{\mathrm{d}^2}{\mathrm{d}t^2}i_{L2}\left(t\right)+R_{L2}\frac{d}{dt}i_{L2}\left(t\right)+\frac{d}{dt}v_{C2}\left(t\right) \tag{3.31}$$

$$\frac{d^2}{dt^2}v_{C1}\left(t\right)=L_2\frac{\mathrm{d}^3}{\mathrm{d}t^3}i_{L2}\left(t\right)+R_{L2}\frac{d^2}{dt^2}i_{L2}\left(t\right)+\frac{d^2}{dt^2}v_{C2}\left(t\right) \tag{3.32}$$

Evaluating (3.30)-(3.32) in (3.29), the system dynamics is expressed by a function with dependencies on *$i_{L2}(t)$*, *$v_{C2}(t)$* and *k*, not reproduced here due to its extension. The dependency on $i_{L2}(t)$) is eliminated by substituting in this function the expressions of $i_{L2}(t)$ and its first, second and third derivatives obtained from (3.18)

$$i_{L2}(t) = C_2 \frac{\mathrm{d}}{\mathrm{d}t} v_{C2}(t) - i_o(t) + \frac{v_{C2}(t)}{R} \tag{3.33}$$

$$\frac{d}{dt} i_{L2}(t) = C_2 \frac{\mathrm{d}^2}{\mathrm{d}t^2} v_{C2}(t) - \frac{d}{dt} i_o(t) + \frac{1}{R}\frac{d}{dt} v_{C2}(t) \tag{3.34}$$

$$\frac{d^2}{dt^2} i_{L2}(t) = C_2 \frac{\mathrm{d}^3}{\mathrm{d}t^3} v_{C2}(t) - \frac{d^2}{dt^2} i_o(t) + \frac{1}{R}\frac{d^2}{dt^2} v_{C2}(t) \tag{3.35}$$

$$\frac{d^3}{dt^3} i_{L2}(t) = C_2 \frac{\mathrm{d}^4}{\mathrm{d}t^4} v_{C2}(t) - \frac{d^3}{dt^3} i_o(t) + \frac{1}{R}\frac{d^3}{dt^3} v_{C2}(t) \tag{3.36}$$

Therefore, the expression that relates the dynamics of $i_{L2}(t)$ and the current reference k is found. By linearizing around steady state and doing the Laplace transform the transfer function of the system is obtained, and annotated as (8.1) in section 8.1. The study of the characteristic polynomial gives the stability conditions that the system should accomplish to be stable. In order to simplify this study, the inductor losses R_{L1} and R_{L2} have been neglected. As they are dissipative elements, the stability conditions obtained after this simplification will be slightly stricter, but it is not an inconvenience. Therefore, the obtained characteristic polynomial is

$$p = as^4 + bs^3 + cs^2 + ds + e, \tag{3.37}$$

where

$$\begin{aligned}
a &= C_1C_2C_dL_2R^3R_dV_{C2}{}^2 \\
b &= C_2C_dL_2R^3R_dV_gk + C_1C_2L_2R^3V_{C2}{}^2 + C_1C_dL_2R^2R_dV_{C2}{}^2 + C_2C_dL_2R^3V_{C2}{}^2 \\
c &= C_1C_dR^3R_dV_{C2}{}^2 + C_2C_dR^3R_dV_{C2}{}^2 + C_2L_2R^3V_gk + C_dL_2R^2R_dV_gk + \\
&\quad + C_1L_2R^2V_{C2}{}^2 + C_dL_2R^2V_{C2}{}^2 \\
d &= C_dR^3R_dV_gk + C_1R^3V_{C2}{}^2 + C_2R^3V_{C2}{}^2 + C_dR^3V_{C2}{}^2 + C_dR^2R_dV_{C2}{}^2 + L_2R^2V_gk \\
e &= R^3V_gk + R^2V_{C2}{}^2
\end{aligned} \tag{3.38}$$

Following the Routh-Hurwitz stability criterion, the study of this characteristic polynomial proves that the system is stable as long as R is positive, since all the terms have to be positive. This condition is in good agreement with the study of the stability of a BBCOF with a CPL load, since the BBCOF operation will be stable providing that the aggregate resistance presented in section 2.2.3 is inserted.

3.3 Small-signal analysis of the BBCOF with sliding mode control

For the small-signal analysis, the BBCOF can be seen as three different transfer functions describing the relation between the perturbation inputs of the system, i.e. output current, input voltage and current reference, and the output. Consequently, the two-loop system architecture of Fig. 3.1 can be represented as in Fig. 3.4.

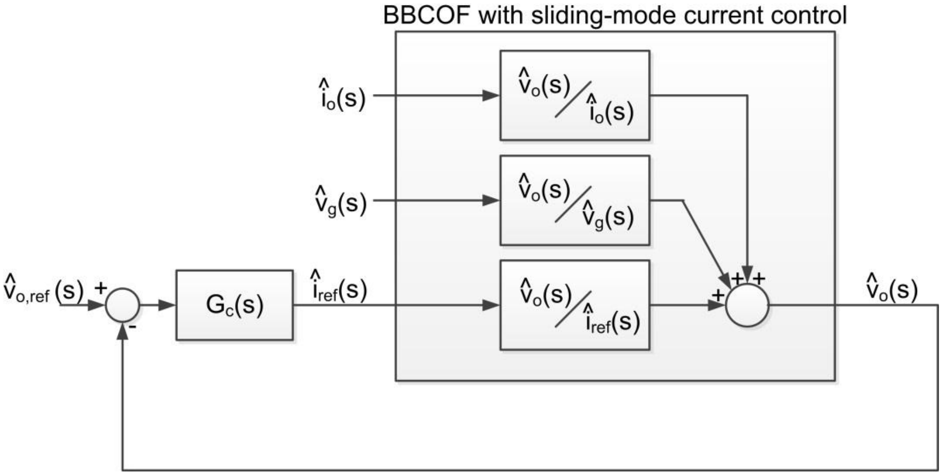

Fig. 3.4. Small-signal model of the BBCOF with sliding-mode current control and PI voltage control loop.

Note that in the preceding stability analysis of the BBCOF, the slow dynamics of the voltage control loop have been neglected. However, it is necessary to consider a time-varying current reference in order to design the output voltage controller. Consequently, the proposed sliding surface is

$$S(t)=i_{L1}(t)-i_{ref}(t)=0, \tag{3.39}$$

which can be rewritten in matrix form as

$$S(x(t),t)=\alpha\cdot x(t)-i_{ref}(t), \tag{3.40}$$

where

$$\alpha=\begin{bmatrix}1 & 0 & 0 & 0 & 0\end{bmatrix} \tag{3.41}$$

Then, the derivative of the sliding surface with respect to time is

$$\frac{d}{dt}S(x(t),t)=-\frac{d}{dt}i_{ref}(t)+\alpha\cdot\dot{x}(t) \tag{3.42}$$

By combining (3.3) and (3.42), the sliding surface time-derivative is expressed in terms of the state-space variables and the derivative of the current reference as follows

$$\frac{d}{dt}S(x(t),t)=-\frac{d}{dt}i_{ref}(t)+\alpha\left\{A\cdot x(t)+\delta+\left[B\cdot x(t)+\gamma\right]u\right\} \tag{3.43}$$

The sliding motion will exist if the following condition is accomplished

$$\frac{\delta}{\delta u}\left(\frac{d}{dt}S\left(x(t),t\right)\right)=\alpha\left[B\cdot x(t)+\gamma\right]\neq 0 \tag{3.44}$$

The partial derivative of (3.43) with respect to the control is not null, and hence the existence condition is fulfilled.

$$\alpha\left[B\cdot x(t)+\gamma\right]=\frac{1}{L_1}v_{C1}(t)\neq 0 \tag{3.45}$$

By imposing the condition(3.46), the equivalent control (3.47) is obtained.

$$\left.\frac{d}{dt}S\left(x(t),t\right)\right|_{u=ueq}=0 \tag{3.48}$$

$$u_{eq}=\frac{\frac{d}{dt}i_{ref}(t)-\alpha\cdot A\cdot x(t)}{\alpha\cdot B\cdot x(t)+\alpha\cdot\gamma} \tag{3.49}$$

Particularizing the equivalent control for the BBCOF leads to

$$-\frac{d}{dt}i_{ref}(t)+\alpha\left\{A\cdot x(t)+\delta+\left[B\cdot x(t)+\gamma\right]u_{eq}(t)\right\}=0 \tag{3.50}$$

$$u_{eq}(t)=\frac{L_1\frac{d}{dt}i_{ref}(t)-v_g+v_{C1}(t)}{v_{C1}(t)} \tag{3.51}$$

And thus the state variables derivatives, considering (3.39) and (3.51) are

$$\dot{i}_{L1}(t)=0 \tag{3.52}$$

$$\dot{i}_{L2}(t)=\frac{v_{C1}(t)-i_{L2}(t)R_{L2}-v_{C2}(t)}{L_2} \tag{3.53}$$

$$\begin{aligned}\dot{v}_{C1}(t)=&-\frac{i_{ref}(t)\left(\left(\dot{i}_{ref}(t)\right)L_1+R_{L1}i_{ref}(t)-v_g(t)+v_{C1}(t)\right)}{C_1v_{C1}(t)}+\\&+\frac{v_{Cd}(t)-\left(i_{L2}(t)-i_{ref}(t)\right)R_d-v_{C1}(t)}{C_1R_d}\end{aligned} \tag{3.54}$$

$$\dot{v}_{C2}(t)=\frac{Ri_{L2}(t)+Ri_o(t)-v_{C2}(t)}{C_2R} \tag{3.55}$$

$$\dot{v}_{Cd}(t)=\frac{v_{C1}(t)-v_{Cd}(t)}{C_dR_d} \tag{3.56}$$

Deriving and combining (3.53)-(3.56), it is possible to obtain an expression relating the system inputs and output, following a procedure similar to the used in the stability analysis of the BBCOF with a CPL, seen in section 3.2. The first step is to derivate (3.54)

$$\begin{aligned}\frac{d^2}{dt^2}v_{C1}(t) = &-\frac{\left(\frac{d}{dt}i_{ref}(t)\right)^2 L_1}{C_1 v_{C1}(t)} + \frac{i_{ref}(t)\left(\frac{d}{dt}i_{ref}(t)\right)L_1\left(\frac{d}{dt}v_{C1}(t)\right)}{C_1 {v_{C1}}^2(t)} - \\ &-\frac{i_{ref}(t)\left(\frac{d^2}{dt^2}i_{ref}(t)\right)L_1}{C_1 v_{C1}(t)} - \frac{2i_{ref}(t)R_{L1}\left(\frac{d}{dt}i_{ref}(t)\right)}{C_1 v_{C1}(t)} + \frac{{i_{ref}}^2(t)R_{L1}\left(\frac{d}{dt}v_{C1}(t)\right)}{C_1 {v_{C1}}^2(t)} + \\ &+\frac{\left(\frac{d}{dt}i_{ref}(t)\right)v_g(t)}{C_1 v_{C1}(t)} - \frac{i_{ref}(t)v_g(t)\left(\frac{d}{dt}v_{C1}(t)\right)}{C_1 {v_{C1}}^2(t)} + \frac{i_{ref}(t)\left(\frac{d}{dt}v_g(t)\right)}{C_1 v_{C1}(t)} - \\ &-\frac{\frac{d}{dt}i_{L2}(t)}{C_1} - \frac{\frac{d}{dt}v_{C1}(t)}{C_1 R_d} + \frac{\frac{d}{dt}v_{Cd}(t)}{R_1 C_d}\end{aligned} \tag{3.57}$$

The next step is to eliminate the dependency on $v_{Cd}(t)$. With this aim, the expression for $v_{Cd}(t)$ is isolated from (3.54)

$$v_{Cd}(t) = \frac{1}{v_{C1}(t)}\left(\begin{array}{l}\left(\frac{\mathrm{d}}{\mathrm{d}t}v_{C1}(t)\right)C_1 v_{C1}(t)R_d + i_{ref}(t)\left(\frac{\mathrm{d}}{\mathrm{d}t}i_{ref}(t)\right)L_1 R_d + {i_{ref}}^2(t)R_{L1}R_d - \\ -i_{ref}(t)v_g(t)R_d + i_{L2}(t)v_{C1}(t)R_d + {v_{C1}}^2(t)\end{array}\right) \tag{3.58}$$

The derivative of $v_{Cd}(t)$ is obtained by substituting (3.58) in (3.56):

$$\frac{\mathrm{d}}{\mathrm{d}t}v_{Cd}(t) = \frac{v_{C1}(t)}{C_d R_d} - \frac{1}{C_d R_d v_{C1}(t)}\left(\begin{array}{l}\left(\frac{\mathrm{d}}{\mathrm{d}t}v_{C1}(t)\right)C_1 v_{C1}(t)R_d + i_{ref}(t)\left(\frac{\mathrm{d}}{\mathrm{d}t}i_{ref}(t)\right)L_1 R_d + \\ +{i_{ref}}^2(t)R_{L1}R_d - i_{ref}(t)v_g(t)R_d + i_{L2}(t)v_{C1}(t)R_d + \\ +{v_{C1}}^2(t)\end{array}\right) \tag{3.59}$$

Replacing (3.59) in (3.57)

$$\begin{aligned}\frac{d^2}{dt^2}v_{C1}(t)=&-\frac{\left(\frac{d}{dt}i_{ref}(t)\right)^2L_1}{C_1v_{C1}(t)}+\frac{i_{ref}(t)\left(\frac{d}{dt}i_{ref}(t)\right)L_1\left(\frac{d}{dt}v_{C1}(t)\right)}{C_1{v_{C1}}^2(t)}-\\&-\frac{i_{ref}(t)\left(\frac{d^2}{dt^2}i_{ref}(t)\right)L_1}{C_1v_{C1}(t)}-\frac{2i_{ref}(t)R_{L1}\left(\frac{d}{dt}i_{ref}(t)\right)}{C_1v_{C1}(t)}+\frac{{i_{ref}}^2(t)R_{L1}\left(\frac{d}{dt}v_{C1}(t)\right)}{C_1{v_{C1}}^2(t)}+\\&+\frac{\left(\frac{d}{dt}i_{ref}(t)\right)v_g(t)}{C_1v_{C1}(t)}-\frac{i_{ref}(t)v_g(t)\left(\frac{d}{dt}v_{C1}(t)\right)}{C_1{v_{C1}}^2(t)}+\frac{i_{ref}(t)\left(\frac{d}{dt}v_g(t)\right)}{C_1v_{C1}(t)}-\\&-\frac{\frac{d}{dt}i_{L2}(t)}{C_1}-\frac{\frac{d}{dt}v_{C1}(t)}{C_1R_d}-\frac{\frac{d}{dt}v_{C1}(t)}{R_dC_d}-\frac{i_{ref}(t)\left(\frac{d}{dt}i_{ref}(t)\right)L_1}{C_1R_dC_dv_{C1}(t)}-\frac{{i_{ref}}^2(t)\mathrm{R}_{L1}}{C_1R_dC_dv_{C1}(t)}+\\&+\frac{i_{ref}(t)v_g(t)}{C_1R_dC_dv_{C1}(t)}-\frac{i_{L2}(t)}{C_1R_dC_d}\end{aligned}\tag{3.60}$$

To eliminate the dependency on $v_{C1}(t)$, the variable is isolated from (3.53), and its first and second derivatives are calculated as follows

$$v_{C1}(t)=L_2\frac{\mathrm{d}}{\mathrm{d}t}i_{L2}(t)+R_{L2}i_{L2}(t)+v_{C2}(t)\tag{3.61}$$

$$\frac{d}{dt}v_{C1}(t)=L_2\frac{\mathrm{d}^2}{\mathrm{d}t^2}i_{L2}(t)+R_{L2}\frac{d}{dt}i_{L2}(t)+\frac{d}{dt}v_{C2}(t)\tag{3.62}$$

$$\frac{d^2}{dt^2}v_{C1}(t)=L_2\frac{\mathrm{d}^3}{\mathrm{d}t^3}i_{L2}(t)+R_{L2}\frac{d^2}{dt^2}i_{L2}(t)+\frac{d^2}{dt^2}v_{C2}(t)\tag{3.63}$$

Using (3.61)-(3.63) in (3.60), the cumbersome expression obtained –not reproduced for the sake of brevity– has dependency on the output voltage, the three small-signal converter inputs and *$i_{L2}(t)$*. To eliminate this dependency, the expression for *$i_{L2}(t)$* is isolated from (3.55) and derived

$$i_{L2}(t)=C_2\frac{\mathrm{d}}{\mathrm{d}t}v_{C2}(t)-i_o(t)+\frac{v_{C2}(t)}{R}\tag{3.64}$$

$$\frac{\mathrm{d}}{\mathrm{d}t}i_{L2}(t)=C_2\frac{\mathrm{d}^2}{\mathrm{d}t^2}v_{C2}(t)-\frac{\mathrm{d}}{\mathrm{d}t}i_o(t)+\frac{1}{R}\frac{\mathrm{d}}{\mathrm{d}t}v_{C2}(t)\tag{3.65}$$

$$\frac{\mathrm{d}^2}{\mathrm{d}t^2}i_{L2}(t)=C_2\frac{\mathrm{d}^3}{\mathrm{d}t^3}v_{C2}(t)-\frac{\mathrm{d}^2}{\mathrm{d}t^2}i_o(t)+\frac{1}{R}\frac{\mathrm{d}^2}{\mathrm{d}t^2}v_{C2}(t)\tag{3.66}$$

$$\frac{\mathrm{d}^3}{\mathrm{d}t^3}i_{L2}(t)=C_2\frac{\mathrm{d}^4}{\mathrm{d}t^4}v_{C2}(t)-\frac{\mathrm{d}^3}{\mathrm{d}t^3}i_o(t)+\frac{1}{R}\frac{\mathrm{d}^3}{\mathrm{d}t^3}v_{C2}(t)\tag{3.67}$$

Replacing (3.64)-(3.67) in the combination of (3.60)-(3.63), a nonlinear expression is obtained, and it is annotated in Appendix as (8.2). Note that this expression is only dependent on the system inputs and output defined in Fig. 3.4, but it is nonlinear. In order to obtain the output voltage to any of the inputs transfer function, it is necessary to obtain a linear expression that uniquely relates the output voltage and the input. With this aim, function (8.2), denominated *g(t)* for simplicity, is linearized by using the first term of the Taylor expansion around steady state. *g(t)* is a function with the following form

$$g(t) = f\left(v_{C2}(t), i_o(t), v_g(t), i_{ref}(t)\right), \tag{3.68}$$

and the values of these variables evaluated at steady state are

$$v_{C2}(t)\big|_* = \mathrm{V}_{C2};\quad i_o(t)\big|_* = \mathrm{I}_o;\quad v_g(t)\big|_* = \mathrm{V}_g;\quad i_{ref}(t)\big|_* = I_{ref}, \tag{3.69}$$

where * denotes the steady state. Then, this function can be approximated as

$$\begin{gathered} g(t) \approx f\left(V_{C2}, I_o, V_g, I_{ref}\right) + \left(\frac{\partial}{\partial v_{C2}(t)} g(t)\right)\bigg|_* \tilde{v}_{C2}(t) + \left(\frac{\partial}{\partial i_o(t)} g(t)\right)\bigg|_* \tilde{i}_o(t) + \\ + \left(\frac{\partial}{\partial v_g(t)} g(t)\right)\bigg|_* \tilde{v}_g(t) + \left(\frac{\partial}{\partial i_{ref}(t)} g(t)\right)\bigg|_* \tilde{i}_{ref}(t) \end{gathered}, \tag{3.70}$$

where the superscript ~ denotes the small-signal variations of the variable. Consequently, the system is perceived as a superposition of a steady-state part and a small-signal part

$$x(t) = X + \tilde{x}(t) \tag{3.71}$$

3.3.1 Output current to output voltage transfer function

To obtain the output current to output voltage transfer function, the small-signal variations of other two inputs, $v_g(t)$ and $i_{ref}(t)$, are neglected

$$\tilde{v}_g(t) = 0;\quad \tilde{i}_{ref}(t) = 0, \tag{3.72}$$

and the description of the small-signal part is

$$g(t)\Big|_{\substack{\tilde{v}_g(t)=0 \\ \tilde{i}_{ref}(t)=0}} = \left(\frac{\partial}{\partial v_{C2}(t)} g(t)\right)\bigg|_* \tilde{v}_{C2}(t) + \left(\frac{\partial}{\partial i_o(t)} g(t)\right)\bigg|_* \tilde{i}_o(t) \tag{3.73}$$

Applying (3.73) to (8.2) and doing the Laplace transform, the transfer function (8.3) is obtained, and annotated in Appendix for brevity. However, if the resistive losses of the inductors are omitted, the output current to output voltage transfer function is

$$\left.\frac{\tilde{v}_{C2}(s)}{\tilde{i}_o(s)}\right|_{R_{L1}, R_{L2}=0} = \frac{num_1(s)}{den_1(s)}, \tag{3.74}$$

where

$$\begin{aligned} num_1(s) = {} & R^3 C_1 C_d L_2 R_d {V_{C2}}^2 s^3 + R^3 \left(C_d L_2 R_d I_{ref} V_g + C_1 L_2 {V_{C2}}^2 + C_d L_2 {V_{C2}}^2 \right) s^2 + \\ & + R^3 \left(C_d R_d {V_{C2}}^2 + L_2 I_{ref} V_g \right) s + R^3 {V_{C2}}^2 \end{aligned} , \tag{3.75}$$

$$den_1(s) = a_1 s^4 + b_1 s^3 + c_1 s^2 + d_1 s + e_1 , \tag{3.76}$$

and

$$\begin{aligned} a_1 &= C_1 C_2 C_d L_2 R^3 R_d {V_{C2}}^2 \\ b_1 &= R^2 \left(C_2 C_d L_2 R R_d I_{ref} V_g + C_1 C_2 L_2 R {V_{C2}}^2 + C_1 C_d L_2 R_d {V_{C2}}^2 + C_2 C_d L_2 R {V_{C2}}^2 \right) \\ c_1 &= R^2 \begin{pmatrix} C_1 C_d R R_d {V_{C2}}^2 + C_2 C_d R R_d {V_{C2}}^2 + C_2 L_2 R I_{ref} V_g + C_d L_2 R_d I_{ref} V_g + \\ + C_1 L_2 {V_{C2}}^2 + C_d L_2 {V_{C2}}^2 \end{pmatrix} \\ d_1 &= R^2 \left(C_d R R_d I_{ref} V_g + C_1 R {V_{C2}}^2 + C_2 R {V_{C2}}^2 + C_d R {V_{C2}}^2 + C_d R_d {V_{C2}}^2 + L_2 I_{ref} V_g \right) \\ e_1 &= R^2 \left(R I_{ref} V_g + {V_{C2}}^2 \right) \end{aligned} \tag{3.77}$$

3.3.2 Input voltage to output voltage transfer function

In this case, the neglected variables are

$$\tilde{i}_o(t) = 0; \quad \tilde{i}_{ref}(t) = 0 , \tag{3.78}$$

Thus the small-signal part of the linear approximation of (8.2) is

$$g(t)\Big|_{\substack{\tilde{i}_o(t)=0 \\ \tilde{i}_{ref}(t)=0}} = \left(\frac{\partial}{\partial v_{C2}(t)} g(t) \right)\Bigg|_{*} \tilde{v}_{C2}(t) + \left(\frac{\partial}{\partial v_g(t)} g(t) \right)\Bigg|_{*} \tilde{v}_g(t) \tag{3.79}$$

The result of applying (3.79) to (8.2) and doing the Laplace transform is (8.4). Omitting the inductor losses, the simplified expression is

$$\frac{\tilde{v}_{C2}(s)}{\tilde{v}_g(s)}\Bigg|_{R_{L1}, R_{L2}=0} = \frac{C_d R^3 R_d I_{ref} V_{C2} s + R^3 I_{ref} V_{C2}}{den_1(s)} \tag{3.80}$$

As expected, the transfer function denominator is the same that in the output current to output voltage transfer function, defined at (3.76) and (3.77).

3.3.3 Current reference to output voltage transfer function

To evaluate the effects of current reference small-signal variations in the output voltage, the rest of the inputs are neglected

$$\tilde{i}_o(t) = 0; \quad \tilde{v}_g(t) = 0 , \tag{3.81}$$

and then the description of the small-signal part is

$$g(t)\Big|_{\substack{\tilde{i}_o(t)=0 \\ \tilde{v}_g(t)=0}} = \left(\frac{\partial}{\partial i_o(t)} g(t) \right)\Bigg|_{*} \tilde{i}_o(t) + \left(\frac{\partial}{\partial v_g(t)} g(t) \right)\Bigg|_{*} \tilde{v}_g(t) \tag{3.82}$$

Applying (3.82) to (8.2) and doing the Laplace transform, the obtained transfer function is (8.5) , found in Appendix. Omitting the resistive losses of the inductors, the simplified expression is

$$\left.\frac{\tilde{v}_{C2}(s)}{\tilde{i}_{ref}(s)}\right|_{R_{L1},R_{L2}=0}=\frac{-R^3C_dL_1R_dI_{ref}V_{C2}s^2-R^3\left(-C_dR_dV_g+L_1I_{ref}\right)V_{C2}s+R^3V_gV_{C2}}{den_1(s)} \qquad (3.83)$$

3.4 Output voltage controller

The output voltage controller $G_c(s)$ depicted in Fig. 3.4 gives the current reference to the sliding-mode current controller. A PI controller with an additional pole, at the frequency of the non-minimum-phase zero of the converter, will be used. The voltage and current sensors used in the converter add gains to the system, which have to be considered during the design of the voltage controller. After considering the sensor gains, the system can be represented by the block diagram in Fig. 3.5.

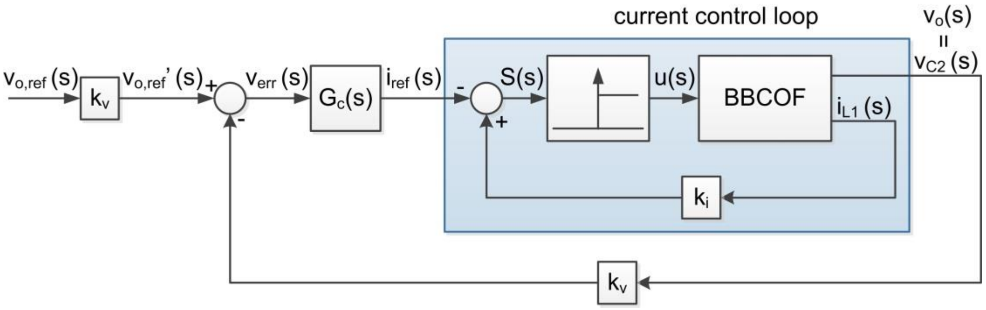

Fig. 3.5. Small-signal model of the converter in the frequency domain considering the gain of the sensors, with $i_o(s)=0$ and $v_g(s)=0$.

Note that the gain of the current sensor appears in the feedback of the sliding-mode current control. It is possible to represent an equivalent system that eliminates the gain from the feedback loop, by moving the sensor gain and adding another gain block, as depicted in Fig. 3.6. This disposition enables the designer to see that the output-input transfer function of the current control loop is not modified with the inclusion of the current sensor. The only difference comes to the magnitude of the hysteresis margins when non-ideal surface switching is considered.

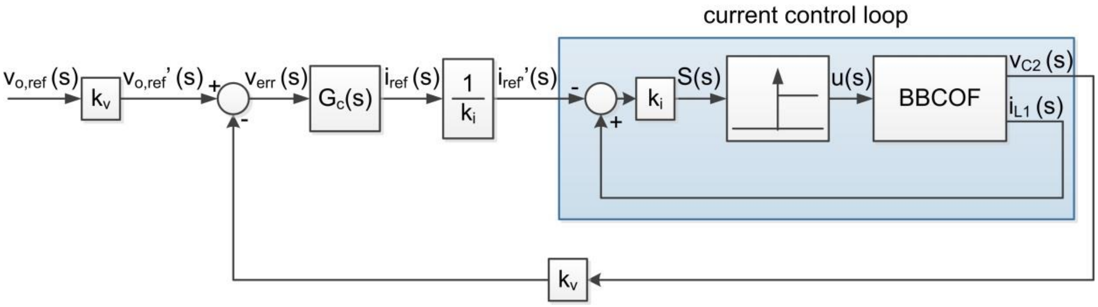

Fig. 3.6. Modified small-signal model to eliminate the gain in the current feedback loop.

Then, the plant of the voltage control loop is the already calculated $\tilde{v}_{C2}(s)/\tilde{i}_{ref}(s)$ transfer function with the $1/k_i$ gain, as seen in Fig. 3.7. This representation is the one used to adjust the PI with additional pole voltage controller.

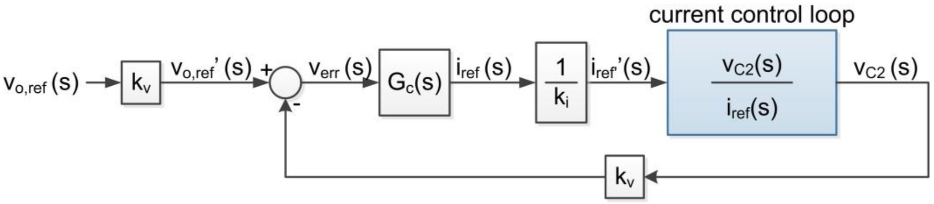

Fig. 3.7. Small-signal model of the output voltage loop.

The transfer function of the voltage controller is

$$G_c(s) = k\frac{(1+s/\omega_z)}{s(1+s/\omega_p)}, \tag{3.84}$$

with gain *k*, and zero and additional pole frequencies ω_z and ω_p, respectively. The design of these three values is performed with Matlab/Sisotool. $\tilde{v}_{C2}(s)/\tilde{i}_{ref}(s)$ in (8.5) has been evaluated with the values of the components detailed in Table 2.II, and then the additional pole is located the frequency of the non-minimum-phase zero of the BBCOF. The zero and the gain are designed in order to achieve the desired phase margin with the maximum bandwidth. Moreover, the bandwidth of the current loop has been determined with Matlab, and it is approximately 10 kHz. As the bandwidth of the voltage controller has to be significantly lower than this value, at least 10 times, an approximate design value of 500 Hz has been adopted. Finally,

$$G_c(s) = 590\frac{1+s/1920}{s(1+s/33200)} \tag{3.85}$$

The frequency response of the open-loop gain is depicted in Fig. 3.8. As it can be observed, the designed control for the BBCOF has a phase margin of 47.2°, a gain margin of 20.8 dB and a 457 Hz bandwidth.

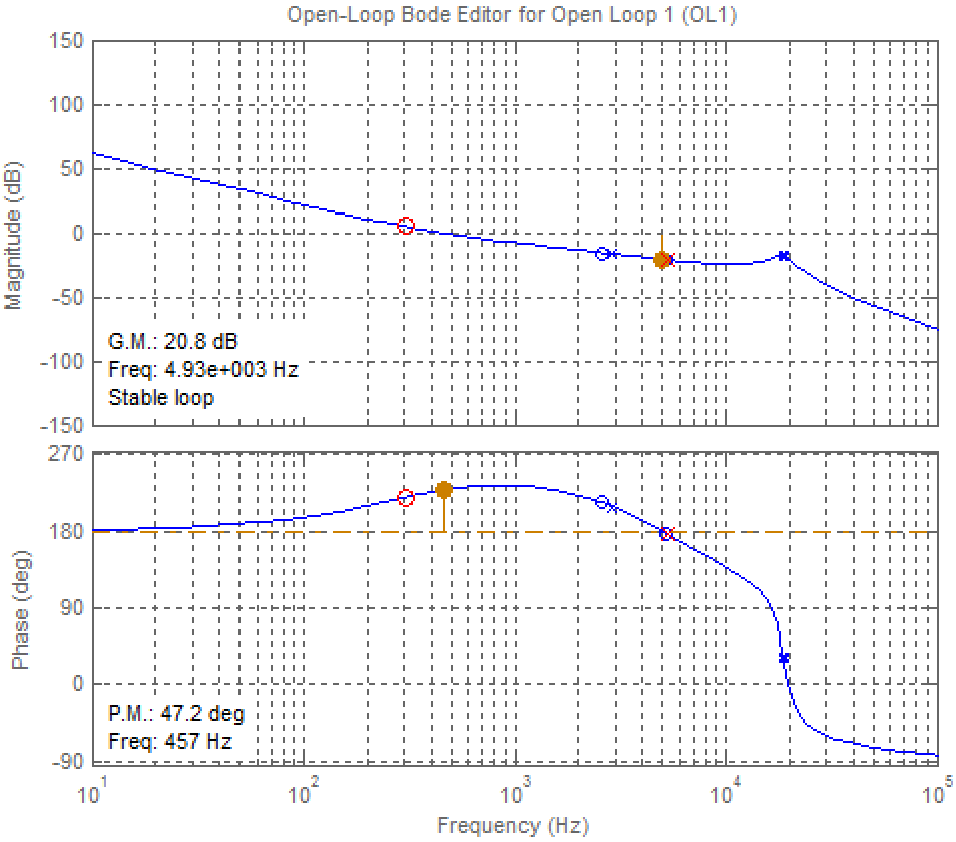

Fig. 3.8. Bode diagram of T(s) for the designed converter and control.

3.4.1 Analogue implementation of the output voltage controller

The designed PI controller with an additional pole has been implemented analogously by means of the circuit in Fig. 3.9. The values of the elements have to be adjusted in order to obtain a transfer function as close to the designed (3.85) as possible.

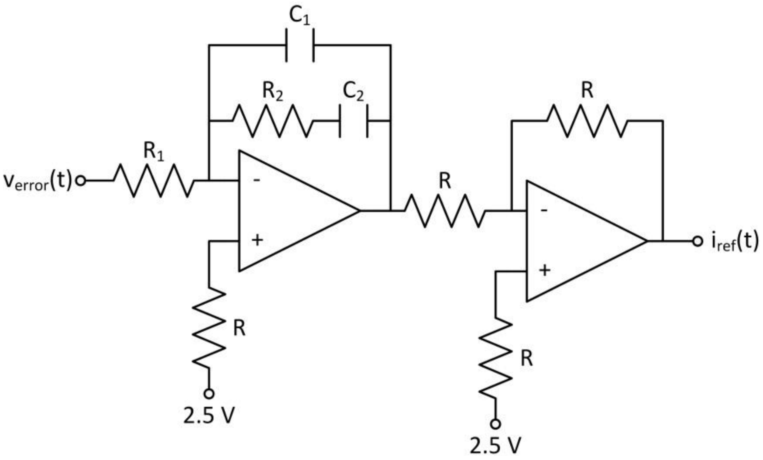

Fig. 3.9. Analogue implementation of the PI voltage controller with an additional pole.

The current reference $i_{ref}(t)$ to voltage error $v_{error}(t)$ transfer function obtained with the proposed circuit is the following

$$G_{c,circuit}(s)=\frac{1}{R_1(C_1+C_2)}\frac{1+R_2C_2s}{s\left(1+\frac{R_2C_1C_2}{C_1+C_2}s\right)}, \tag{3.86}$$

where $G_{c,circuit}(s)$ is the transfer function of the controller implemented by means of the analogue circuit described above. Then, the design of the circuit elements of Fig. 3.9 has been done identifying values. First, an arbitrary value of 10 kΩ is set for R_2. Therefore, the value of C_2 should be

$$C_2=\frac{1}{1950R_2}=52\ nF \tag{3.87}$$

As this value is not commercial, C_2 will be composed of two parallel capacitors of 47 and 4.7 nF, and so the real value of C_2 in the analogue control circuit will be of 51.7 nF. Next, the ideal value of C_1 can be deduced

$$C_1=\frac{C_2}{33200C_2R_2-1}=3.2\ nF \tag{3.88}$$

In order to obtain this value, C_1 will be the parallel association of two capacitors of values 2.2 and 1 nF. Finally, the resistor R1 will be adjusted to get the designed gain according to

$$R_1=\frac{1}{590(C_1+C_2)}=30.9\ k\Omega \tag{3.89}$$

Two parallel resistors of 39 and 150 kΩ will be used to obtain a resistance of 31 kΩ. The values of the design PI controller are detailed in Table 3.II.

Table 3.II. Component values of the designed PI controller.

resistance R	10 kΩ
resistance R_1	31 kΩ
resistance R_2	10 kΩ
capacitance C_1	3.2 nF
capacitance C_2	52 nF

3.5 Output impedance of the BBCOF

As seen previously in section 2.3.1, the inductances of the BBCOF, L_1 and L_2, are design fixing a ripple specification for the current in L_1, and then choosing L_2 value ten times smaller according to the stability design criteria in [54]. The same criteria establish that the value of C_1 capacitor has to be at least 5 times bigger than C_2. However, the selection of the C_2 capacitor is not made according to ripple specifications, but to output impedance design. From the small signal description of the system in Fig. 3.4, the closed-loop output voltage to current voltage transfer function is represented in Fig. 3.10.

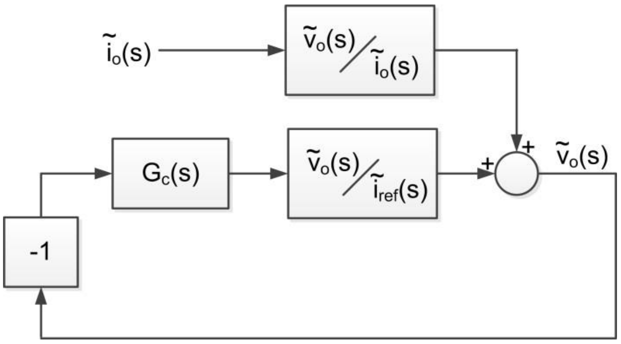

Fig. 3.10. Closed-loop small-signal output voltage to output current relation.

By analysing the block diagram, the closed-loop output current to output voltage transfer function is obtained

$$Z_{o,CL}(s) = \frac{Z_o(s)}{1+T(s)} = \frac{Z_o(s)}{1+G_c(s)\dfrac{\tilde{v}_o(s)}{\tilde{i}_{ref}(s)}}, \tag{3.90}$$

where $Z_o(s)$ is the output impedance transfer function $\tilde{v}_{o(s)}/\tilde{i}_{o(s)}$ and $T(s)$ represents the open-loop gain of the system. This output impedance transfer function has been evaluated with the controller and the converter design values, found in Table 2.II and Table 3.II, respectively. The obtained frequency response is depicted in Fig. 3.11. Note that there is a resonance peak that surpasses the 0 dB limit at approximately 22 kHz. This means that the harmonics in the vicinity of 22 kHz will be amplified instead of attenuated. The effects of the resonance peak are critical, since these frequencies are relatively near to the common switching frequencies of motor drives. This problem will be addressed during the design of the interleaved system in section 4.3, which in fact is the one that will be loaded with a PMSM drive.

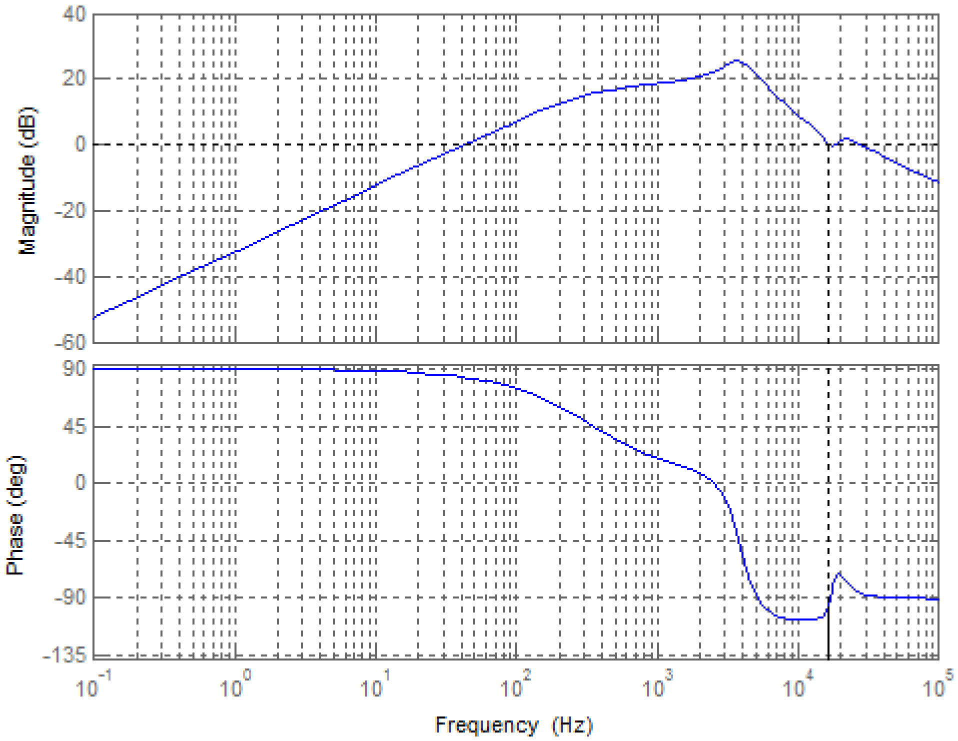

Fig. 3.11. $Z_o(s)$ bode representation for the designed converter.

3.5.1 Middlebrook criterion verification

Moreover, in order to ensure the stability of the loaded converter the Middlebrook criterion has to be accomplished, i.e. the magnitude of the frequency response of the output impedance of the BBCOF has to be lower than the magnitude of the input impedance of the load, the CPL load, modelled as in Fig. 2.5. This comparison has been performed for several power ratings of the CPL, both positive and negative to verify the Middlebrook criterion in step-up and step-down mode, respectively. Results are shown in Fig. 3.12 to Fig. 3.24.

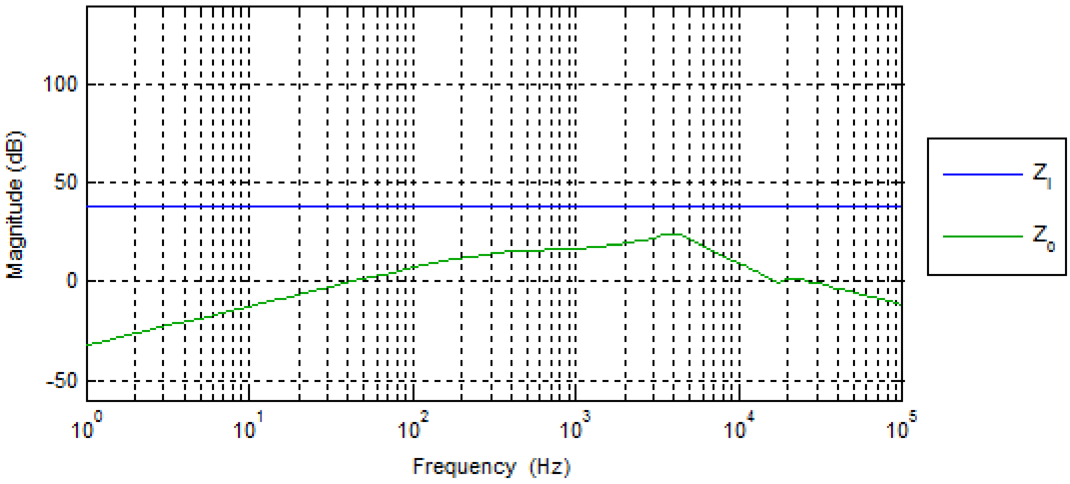

Fig. 3.12. Impedance comparison with P=1.5 kW.

UNIVERSITAT ROVIRA I VIRGILI
DESIGN AND CONTROL OF A BIDIRECTIONAL DC/DC CONVERTER FOR AN ELECTRIC VEHICLE APPLICATION.
Laura Albiol Rendillo
Dipòsit Legal: T 1361-2015

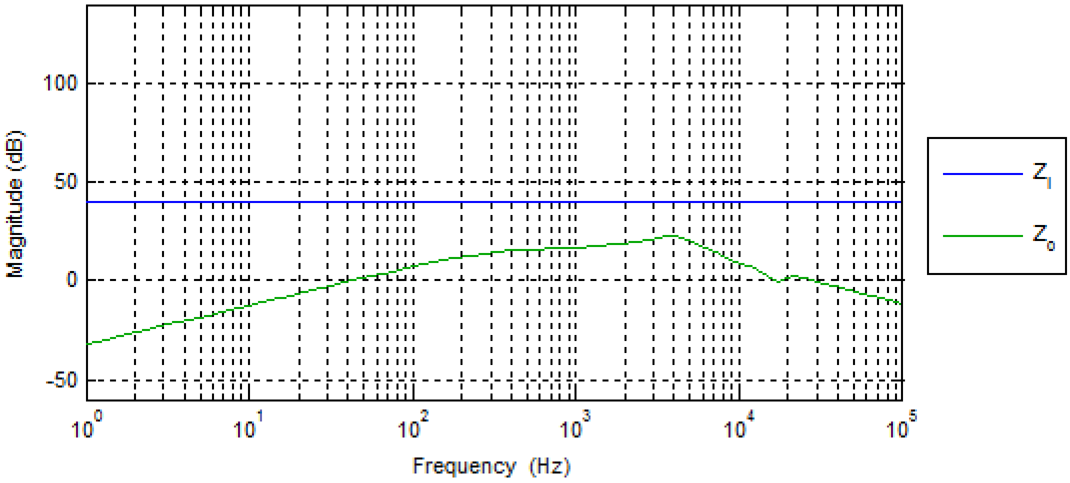

Fig. 3.13. Impedance comparison with P=1.25 kW.

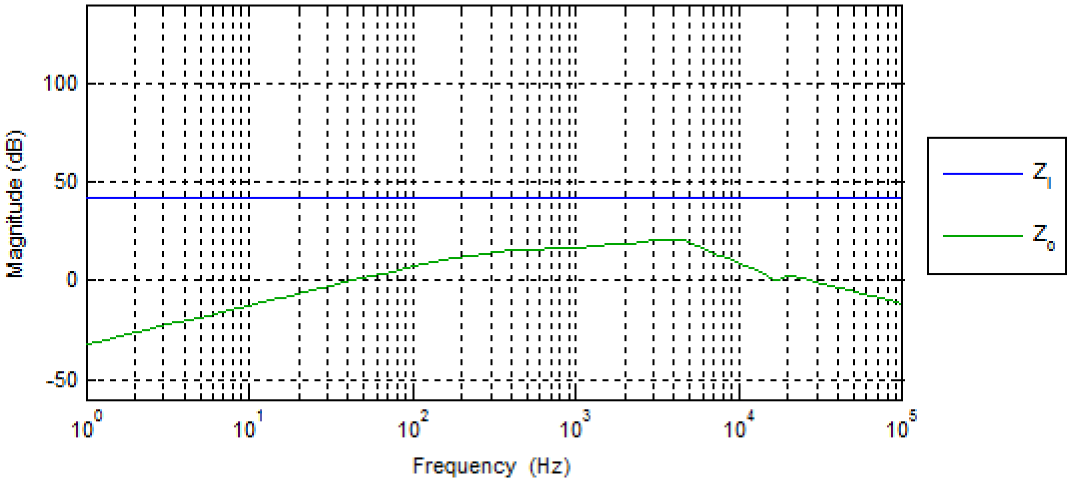

Fig. 3.14. Impedance comparison with P=1 kW.

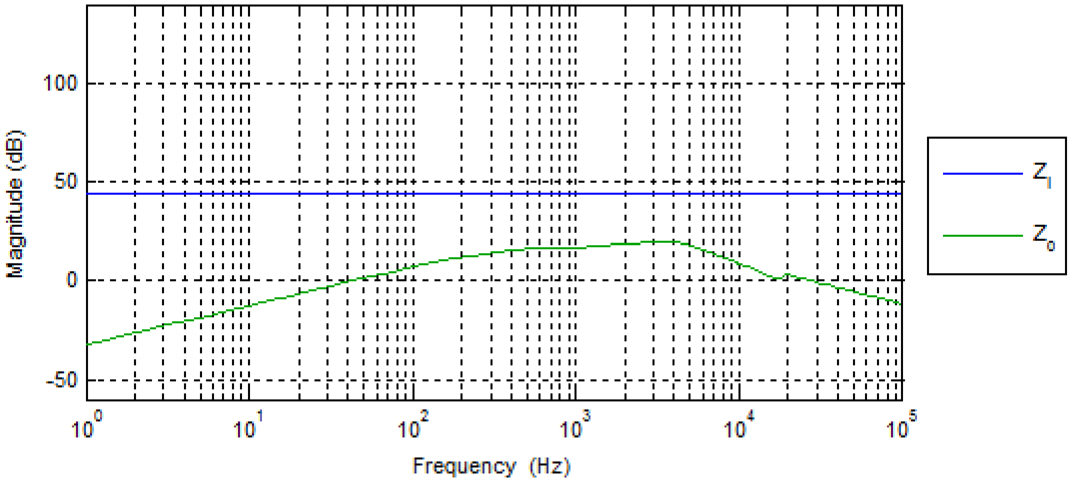

Fig. 3.15. Impedance comparison with P=750 W.

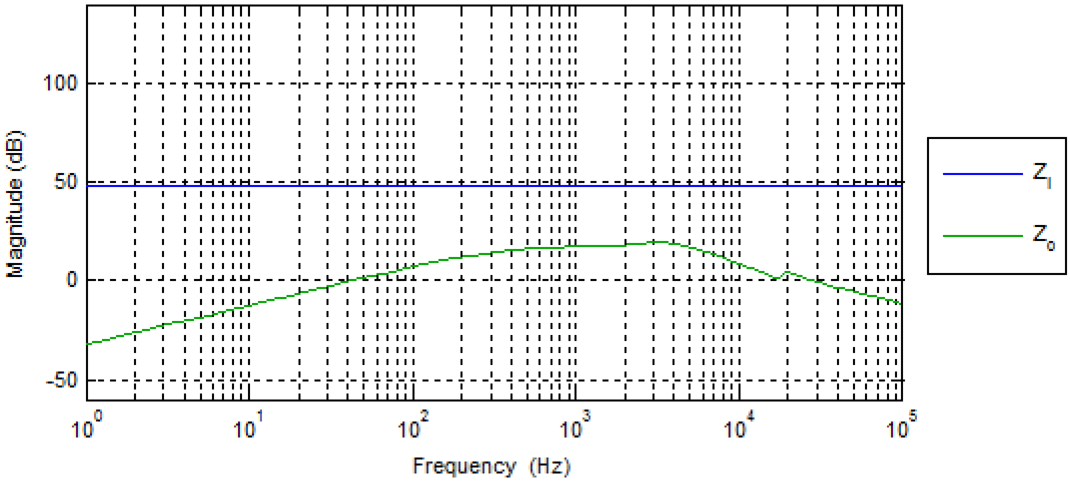

Fig. 3.16. Impedance comparison with P=500 W.

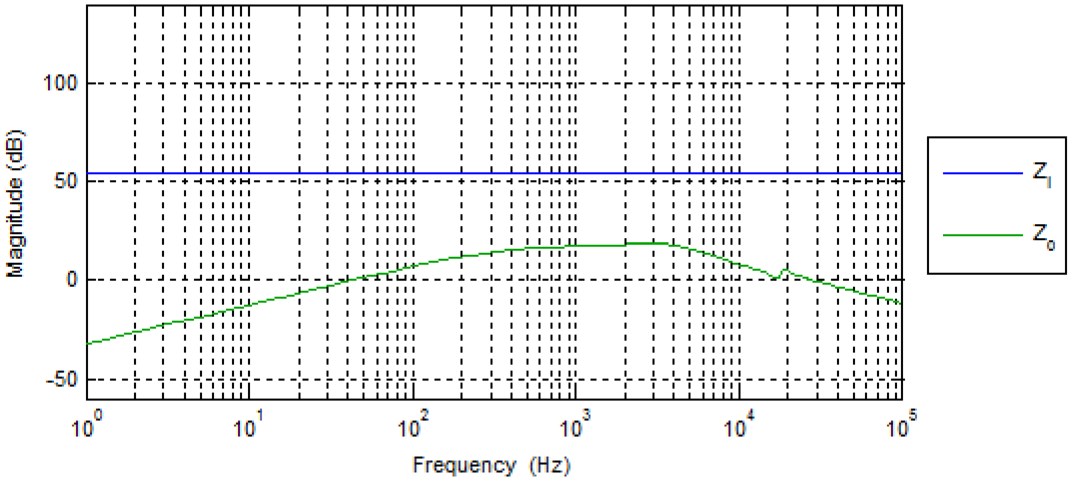

Fig. 3.17. Impedance comparison with P=250 W.

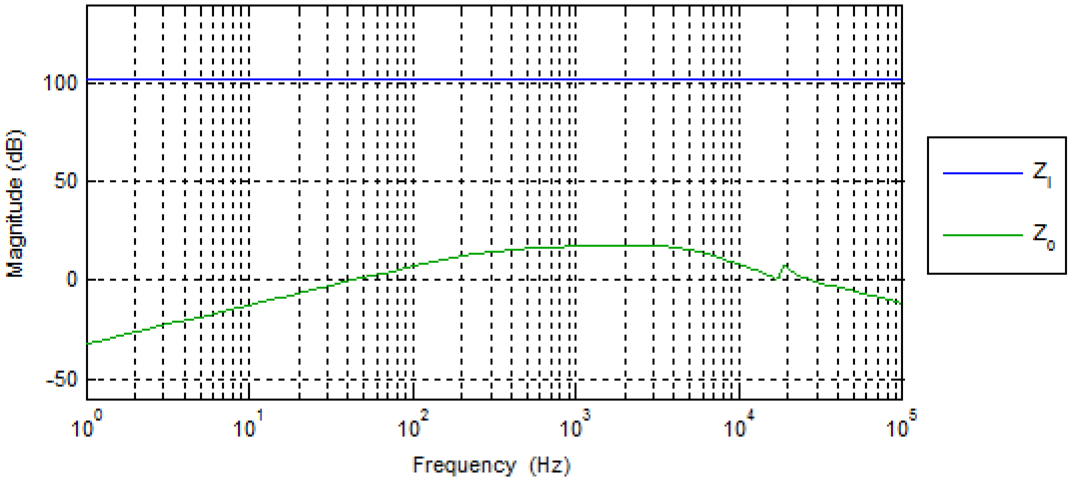

Fig. 3.18. Impedance comparison with P=-1 W (approximately null power).

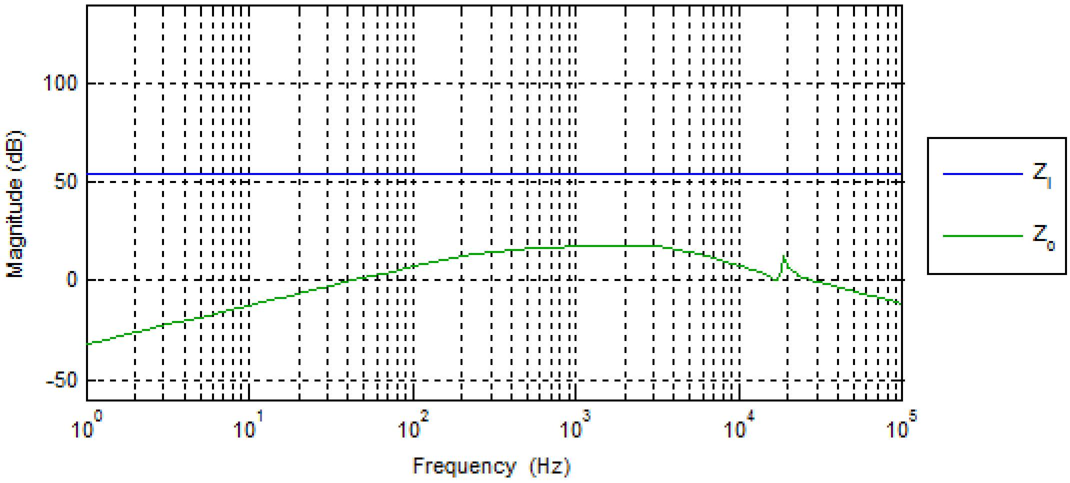

Fig. 3.19. Impedance comparison with P=-250 W.

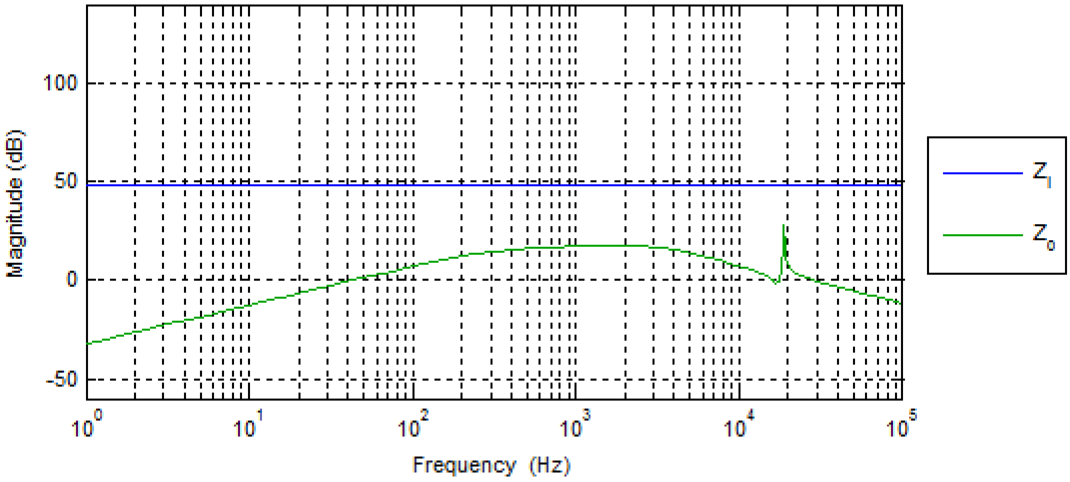

Fig. 3.20. Impedance comparison with P=-500 W.

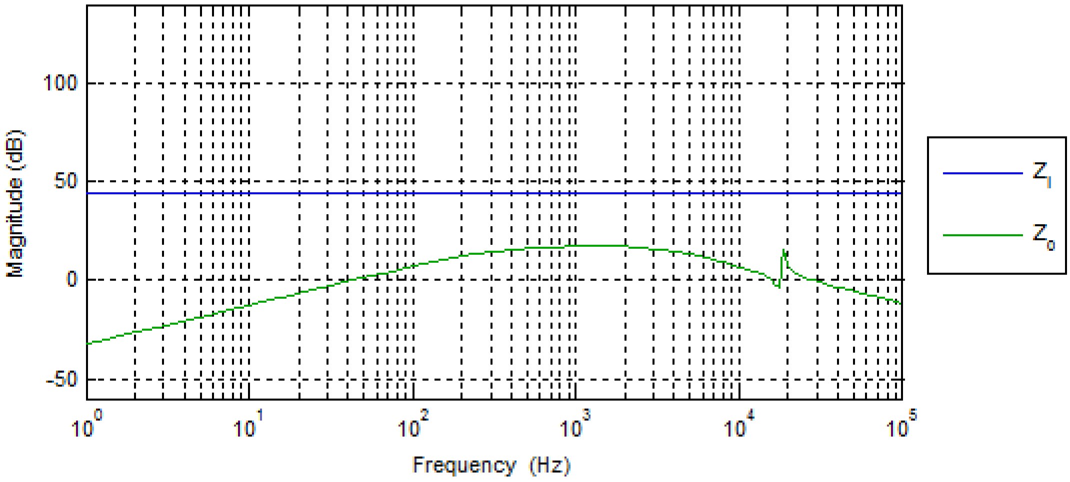

Fig. 3.21. Impedance comparison with P=-750 W.

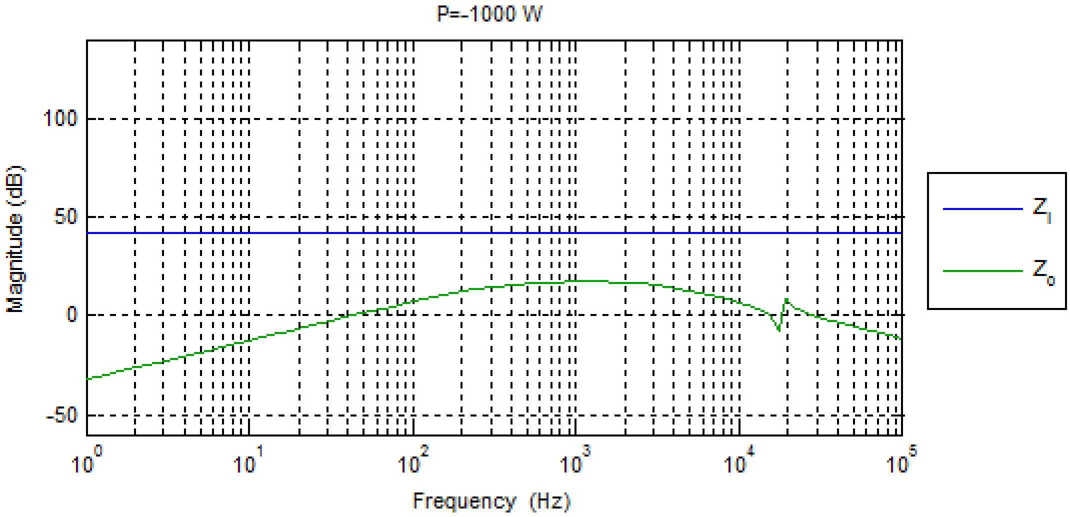

Fig. 3.22. Impedance comparison with P=-1 kW.

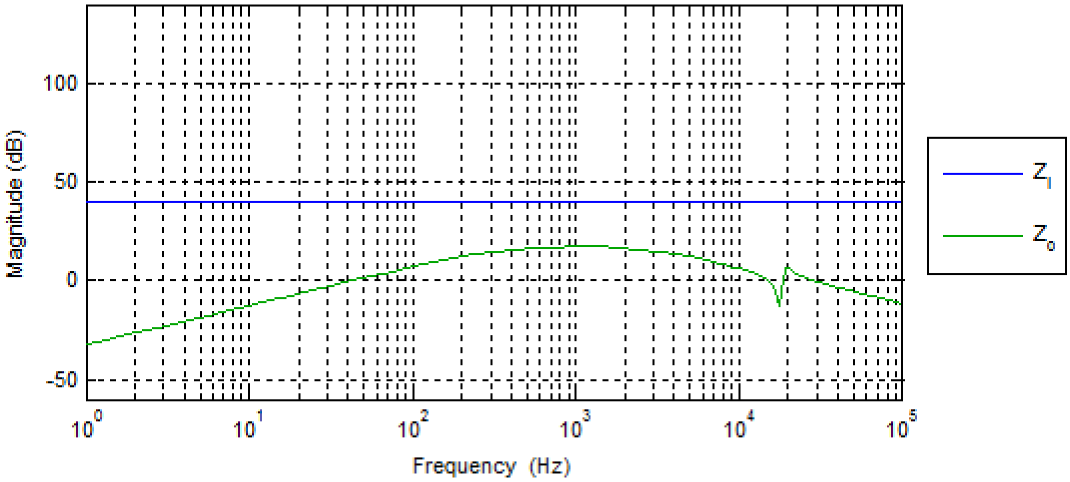

Fig. 3.23. Impedance comparison with P=-1.25 kW.

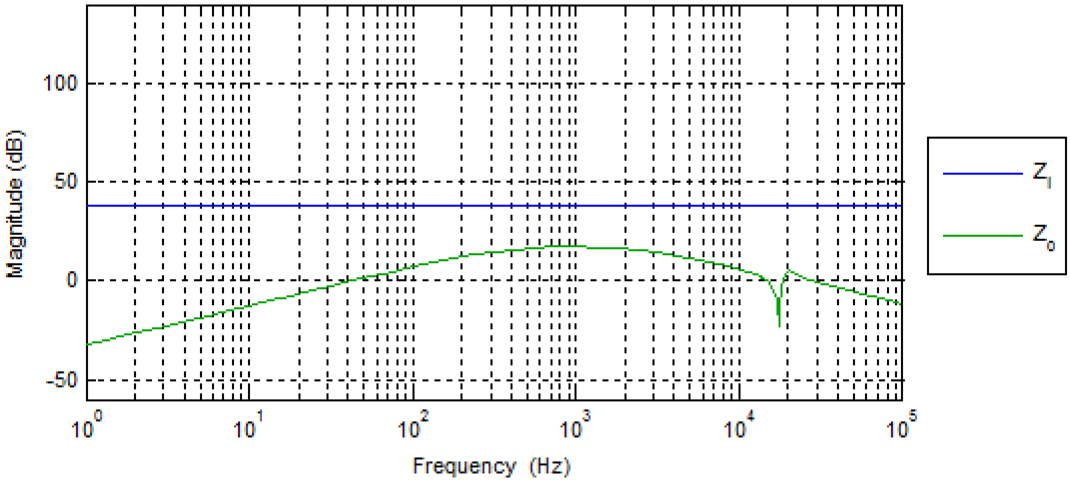

Fig. 3.24. Impedance comparison with P=-1.5 kW.

Consequently, the designed BBCOF with output filter satisfies the Middlebrook criterion for power values from 1.5 to -1.5 kW. For 0 W, the CPL input impedance is infinite, so the comparison has been graphically represented for -1 W, with no loss of validity. Results show that the magnitude of the resonance peak near 22 kHz varies depending on the power. The worst cases occur for negative power values. This means that during step-down mode, part of the ripple in the output voltage will be amplified, and thus will be higher than calculated in chapter 2. As previously mentioned, this problem will be addressed in section 4.3.

3.6 Implementation

The BBCOF with design values in Table 2.II is implemented as shown in Fig. 3.25. The load is left unconnected, since different loads will be simulated. The input current and output voltage are sensed, and the high-side and low-side gating signals are received from the control.

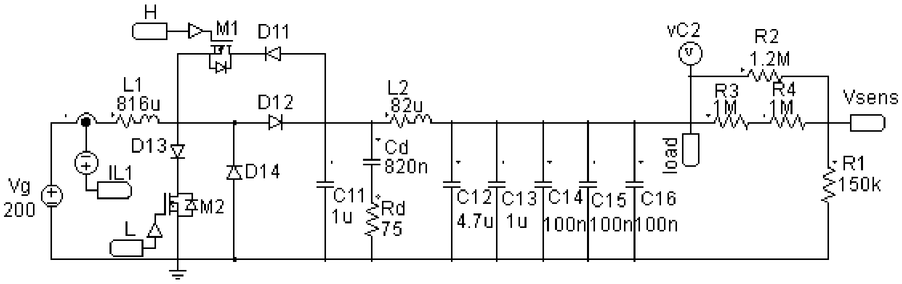

Fig. 3.25. Implementation of the 1.5 kW BBCOF.

The output voltage controller is represented in differentiating two parts. The first part is the voltage error calculation. The sensed voltage is scaled to obtain the 1/110 gain, and subtracted from the voltage reference, which is adjusted by means of the R25 potentiometer. As the control circuit has a unipolar excitation of 5 V, the error voltage is centred at 2.5 V. The second part is the PI controller with additional pole itself, as designed previously and also centred 2.5 V.

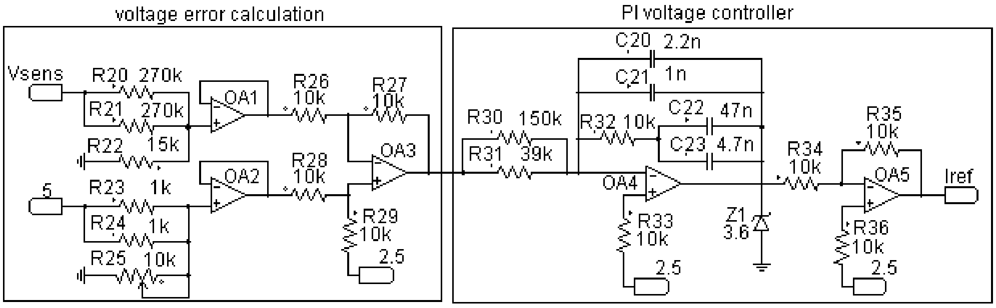

Fig. 3.26. Implementation of the output voltage controller for the BBCOF.

The current reference obtained from the PI with additional pole control is subtracted to the sensed input current of the BBCOF. The result is the sliding surface, which is compared to the hysteresis margins. The upper hysteresis margin can be adjusted by means of R43 potentiometer, while the lower one can be adjusted with R47. The results of the comparisons are introduced in an S-R flip-flop, and the gating signals for the converter are obtained.

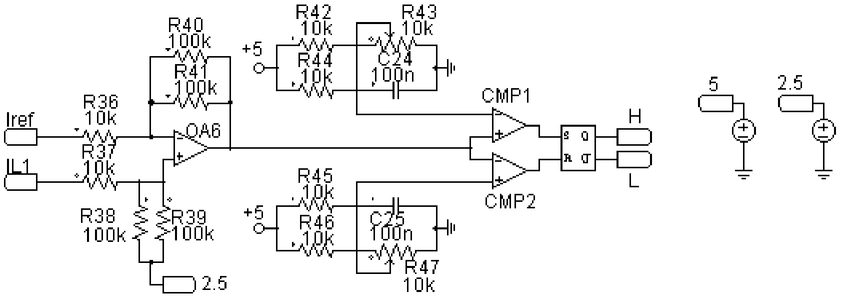

Fig. 3.27. Implementation of the current controller for the BBCOF.

3.7 Simulation results

3.7.1 Simulation with a resistive load

The first simulation consist on connecting a resistive load to the BBCOF with sliding-mode control for the input current and PI control for the output voltage. As a resistive load four lamps have been used as shown in Fig. 3.28. When lighted, the lamps have a resistance of 102 Ω.

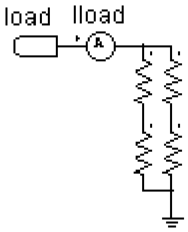

Fig. 3.28. Connection of the four lamps to obtain a 1.2 kW resistive load.

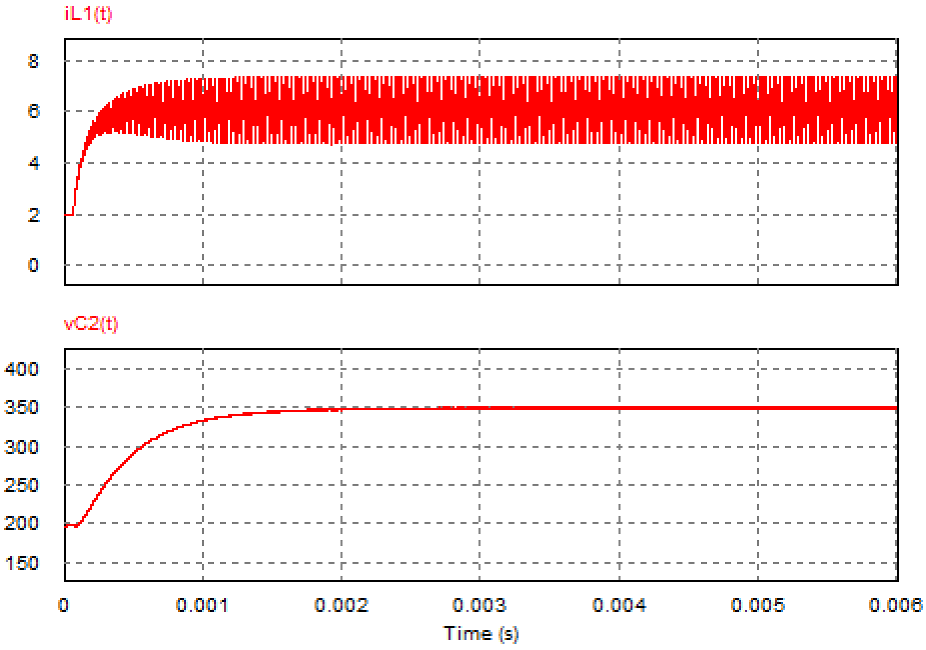

Fig. 3.29. Input current and output voltage waveforms of the BBCOF with a resistive load.

As it can be observed in Fig. 3.29, a sliding motion appears in the input current of the BBCOF after the start-up of the converter. The input current is then regulated by means of the sliding-mode control to match the current reference coming from the output voltage control loop. Once the sliding motion starts, the output voltage starts to increase until it is regulated to the specified voltage of 350 V.

3.7.2 Bidirectional simulation

A bidirectional experiment is proposed here in order to observe the response of the BBCOF and its control both in step-up and down operations, and also during transitions. The experiment consists on connecting two sources to the BBCOF as shown in Fig. 3.30, one at the input, V_g, and one at the output, I_{aux}. For this simulation, the adopted values of the resistors are R_i=36 Ω and R_{load}=108 Ω. The input voltage source has a fixed value of V_g=200 V. The value output current source varies with time, and determines the operating mode of the BBCOF. If the value of the current source is lower than the current flowing through the resistances, the BBCOF will be operating in step-up mode. Otherwise, the current source will be injecting more current to the BBCOF, and thus the converter will be operating in step-down mode. The I_{aux} current profile and the obtained results are reproduced in Fig. 3.31. During the first 30 s, the value of the I_{aux} source is lower than the current consumption of R_{load}, and the BBCOF is delivering power to the load, as can be deduced from the positive value of the input current. For the next 4 s the I_{aux} current constantly increases, making the BBCOF change its operating mode to step-down mode. At t=80 s the I_{aux} source decreases until reaching the exact value of current that the R_{load} consumes, and therefore the BBCOF provides no power. It can be observed that during transitions there is a variation in the output voltage of the BBCOF. The magnitude of these variations is acceptable from the point of view of a load drive.

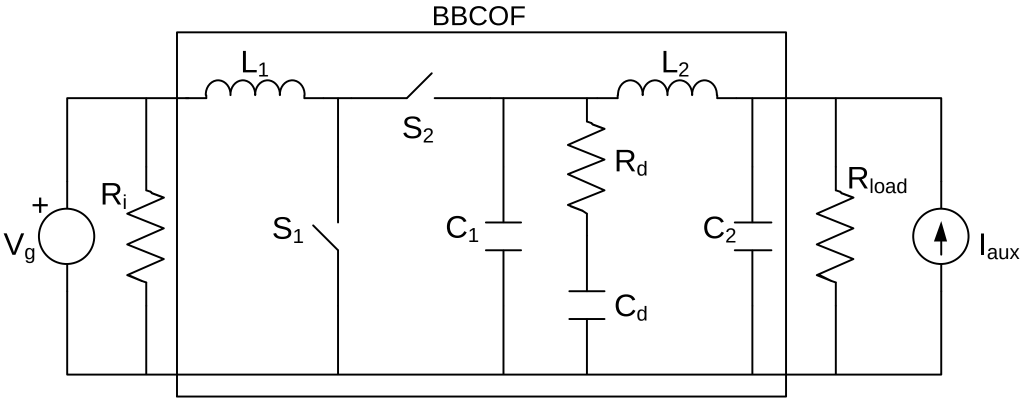

Fig. 3.30. Schematic of the proposed bidirectional experiment.

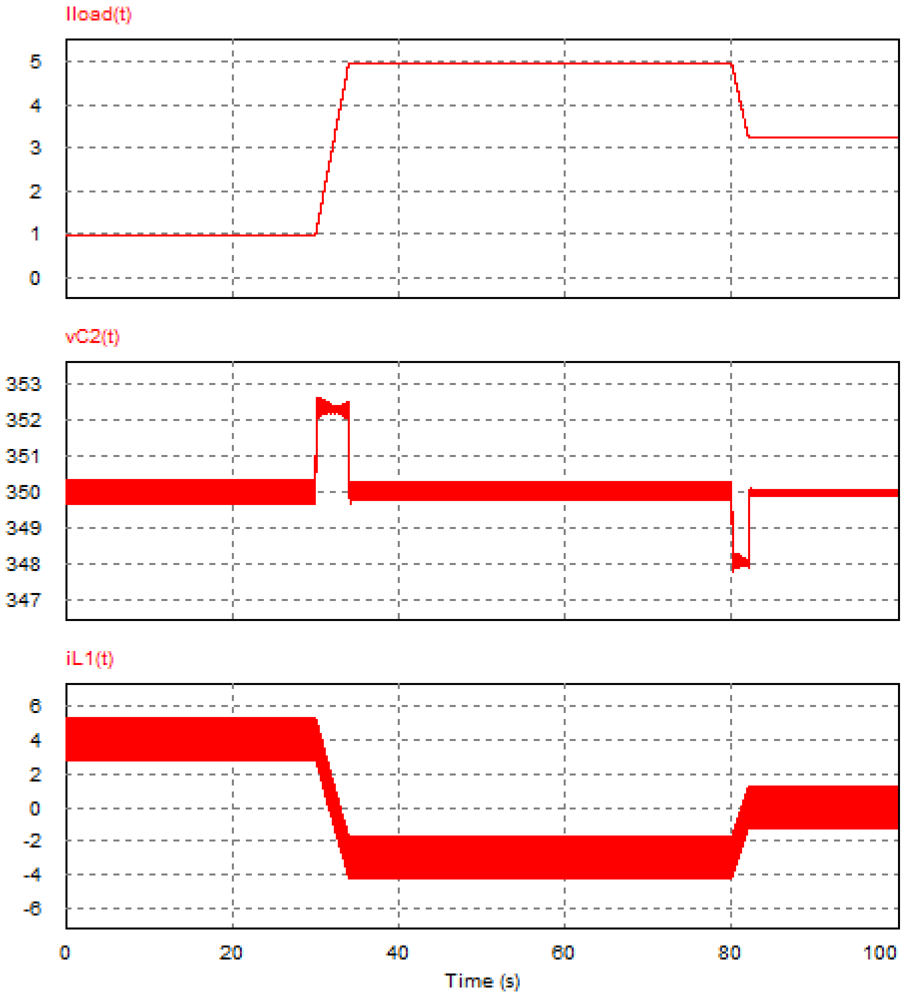

Fig. 3.31. Current profile, output voltage and input current for the bidirectional simulation.

3.7.3 Bidirectional simulation with a CPL

The objective of this simulation is to evaluate the stability of the BBCOF with a sliding-mode controller when the BBCOF is loaded with a CPL, and thus verify the analysis previously presented in this chapter. The model of the CPL load is depicted in Fig. 3.32.

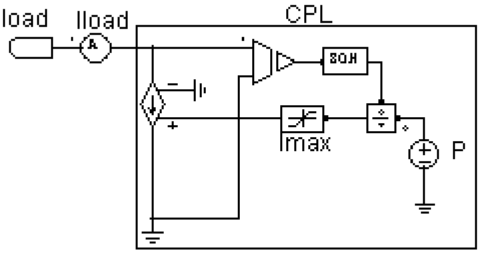

Fig. 3.32. Model of the CPL load model used for simulation.

The power rating of the CPL has a time-varying profile, in order to study the system stability during step-up and step-down mode, as well as the transitions. First, a slow transition from the PI voltage controller point of view is performed. The results are represented in Fig. 3.33. The power of the CPL corresponds to the *Pload(t)* signal. First, the power of the CPL is 1.5 kW, so the BBCOF is operating in step-up mode. When the sliding motion of the input current begins, the output voltage starts to increase until reaching the set-point of 350 V. At instant t=10 ms, the power of the CPL starts to constantly decrease. As the load current of the BBCOF is continuously changing, the output voltage controller is not capable of regulating the voltage to the set-point until a fixed value for the power of the CPL is reached again, causing an overvoltage of 3 V. At t=60 ms a CPL power of -1.5 kW is fixed, and thus the BBCOF is operating in the step-down mode, recovering energy from the load. The output voltage of the BBCOF decreases and reaches the set-point value. Therefore, the sliding-mode-controlled BBCOF with a CPL load has been proven to be stable for step-up and step-down operations, and also during transitions.

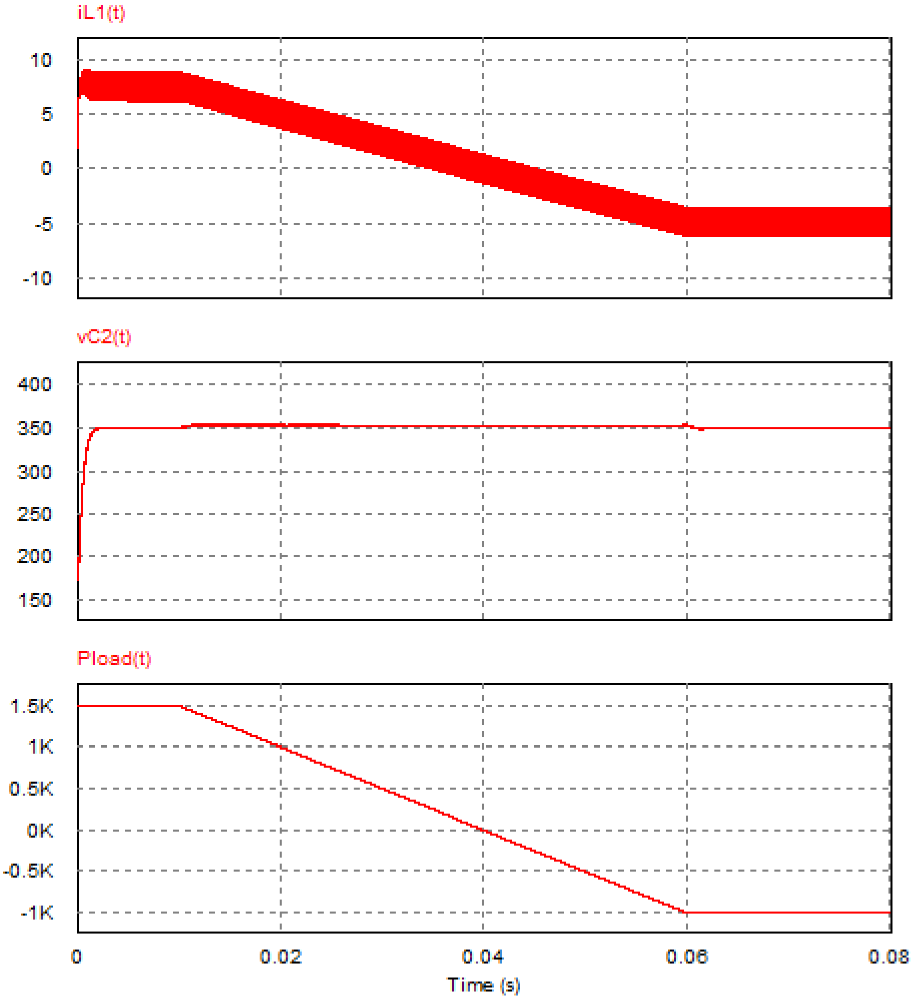

Fig. 3.33. Input current and output voltage waveforms of the BBCOF with a slow time-varying CPL.

Fig. 3.34 shows the result of applying a fast time-varying CPL to the BBCOF. The start-up at a fixed power of 1.5 kW is exactly the same that in the previous simulation. However, when the fast power transient occurs, there appears a current overshoot, since the load variation is faster than the PI controller. The voltage overshoot is higher than 150 V. However, this fast transition is not achievable in the EV application that the BBCOF has been designed for. Consequently, no voltage overshots are expected in the final system. Even in the case this overshot occurred, the converter would suffer no damage since it has been designed with 600-V rated components, as stated in section 2.3.4.

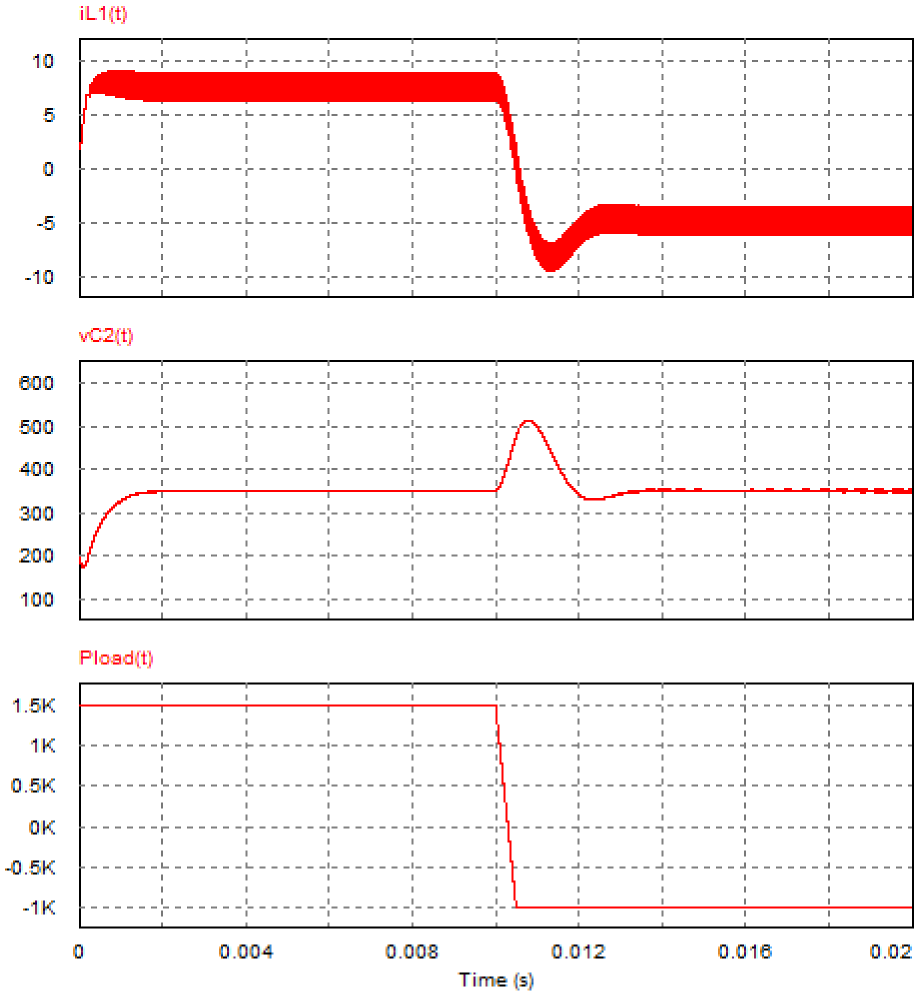

Fig. 3.34. Input current and output voltage waveforms of the BBCOF with a fast time-varying CPL.

3.8 Experimental results

3.8.1 Bidirectional experiment

The bidirectional simulation of section 3.7.2 has been reproduced experimentally to validate the results. The input resistance R_i is implemented with three lamps in parallel of 108 Ω each one, whereas the load resistance R_{load} is composed of two legs of lamps, in which each leg has two lamps connected in series. A DC source in current control mode is used as the I_{aux} source, and its profile is entered manually repeating the defined for simulation in Fig. 3.31. The obtained waveforms are shown in Fig. 3.35, and it is possible to observe that, the input current

UNIVERSITAT ROVIRA I VIRGILI
DESIGN AND CONTROL OF A BIDIRECTIONAL DC/DC CONVERTER FOR AN ELECTRIC VEHICLE APPLICATION.
Laura Albiol Rendillo
Dipòsit Legal: T 1361-2015

of the BBCOF is comparable to the obtained by simulation, while the output voltage is regulated at the set-point voltage.

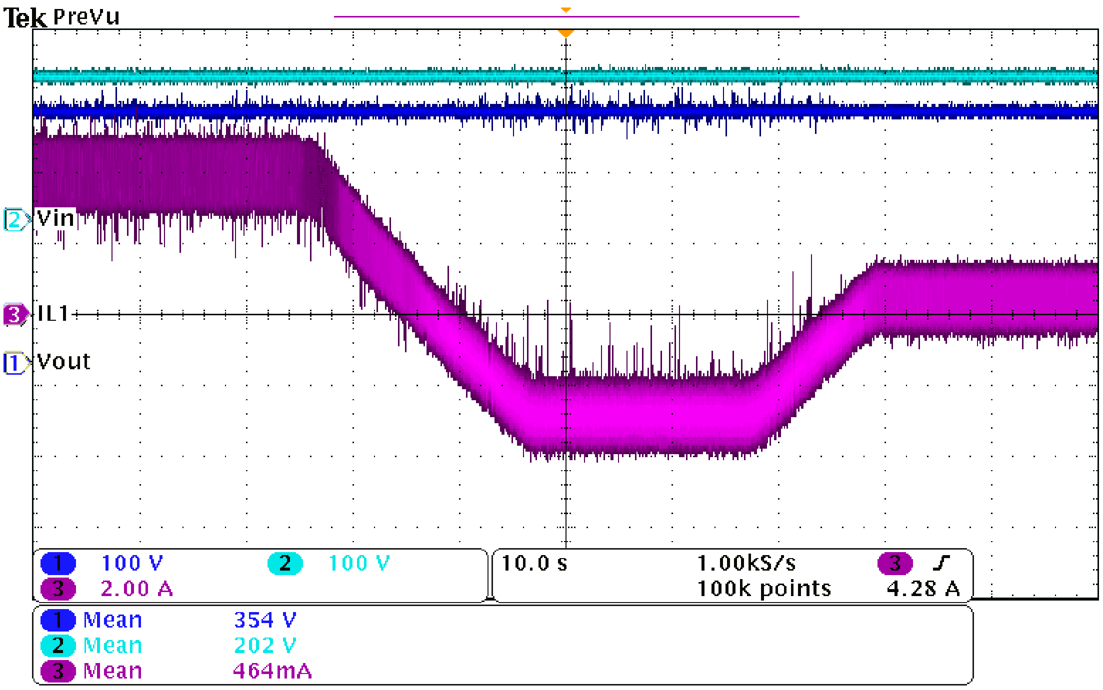

Fig. 3.35. Output voltage, input voltage and input current waveforms of the BBCOF under a bidirectional current profile.

3.9 Conclusions

This chapter presents sliding-mode control as a feasible option to control of the proposed BBCOF for EV applications. After obtaining the bilinear description of the converter, the stability of the BBCOF under sliding-mode control is demonstrated, provided that the RC snubber of chapter 3 is included. Furthermore, the circuit for the analogue sliding-mode controller has been designed.

The small-signal transfer functions of the converter under sliding-mode control are extracted. The output voltage to current reference expression has been used to analytically design the PI voltage controller, and the analogue implementation of this controller has also been described. The output voltage to output current transfer function has been used to calculate the output impedance of the BBCOF. This output impedance has been compared to the input impedance of the CPL for different power ratings, and from this study it has been drawn that the system accomplishes the Middlebrook criterion.

Both the simulation and the experimental results corroborate the validity of the theoretical analysis, and sliding-mode control is proven as an effective and robust method to control the BBCOF.

4 Interleaving

4.1 Why is interleaving necessary?

The EV market is progressively demanding more powerful powertrains, in order to offer to the driver enhanced driveability, equal or even better than ICE vehicles. Regarding the DC/DC converter, this means higher power capability. So as to maintain a reasonable converter efficiency and power density, the solution is to use several DC/DC converters, and thus share the current among them. Depending on the connection between the converters, it is possible to distinguish [74]:

- **Paralleled Converters:** the converters are connected in parallel, which allows current sharing. The commutation of the switching elements of all the converters is synchronous.
- **Interleaved Converters:** the converters are also connected in parallel, but the gating signals of the switching elements are shifted over equal fractions of a switching period.

The mere fact of dividing the power rating between several converters yields several advantages [75], such as:

- Reduced power rating of the switching elements, as current will be shared between the N converters
- Improved dynamic performance and controllability, since the reactive elements have smaller values than those of a unique full-power converter.
- Fault-tolerant capability, since the DC/DC system can continue operating, at reduced power, in case of a converter failure.

Moreover, interleaved converters show ripple reduction due to harmonic compensation or even cancellation. Fig. 4.1 shows the ripple of the input current of a BBCOF considering N interleaved converters, where N ranges from 1 (no interleaving) to 5. The current ripple value has been normalized to the maximum current ripple, which corresponds to N=1 and a duty cycle of 0.5. From this representation, one can conclude that the ripple is drastically reduced by interleaving several converters. This is a key point for an automotive DC/DC converter, as stated in section 1.2. For example, the ripple with one converter is approximately an order of magnitude higher than with three interleaved converters. This phenomenon also occurs in the output voltage of the BBCOFs, where in addition the output capacitor sees a higher ripple frequency, which benefits the filtering properties. Therefore, the interleaving strategy offers several possibilities to redesign the converter: maintain the component values and reduce the switching frequency in order to reduce the switching losses, maintain the switching frequency and thus reduce the size of the reactive elements, or maintain the switching frequency and the component values in order to have reduced ripple.

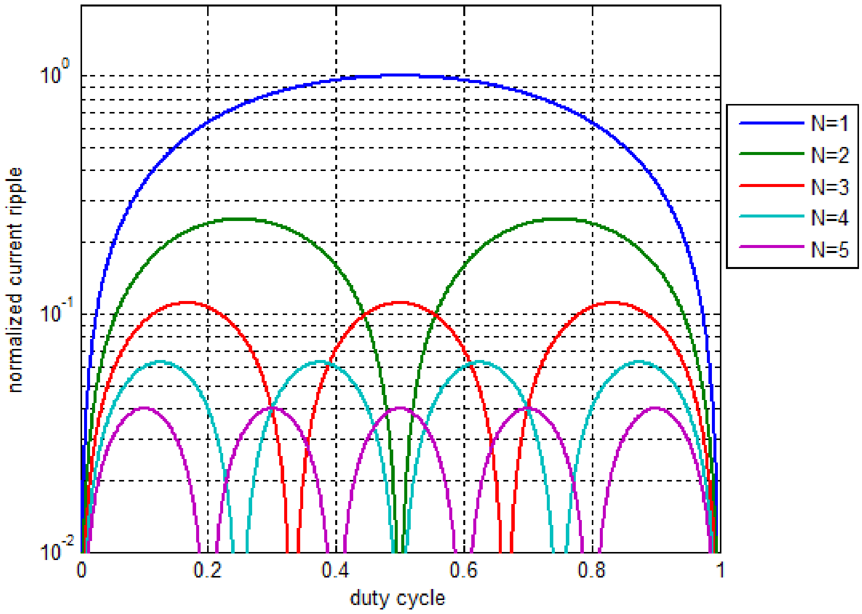

Fig. 4.1. Normalized current ripple versus duty cycle.

The main drawback of both paralleled and interleaved converters is that non-ideal converters will show small differences in the values of their components, and thus they will be unbalanced. Some control techniques could address this issue, but are out of the scope of this thesis.

4.2 Ring-configuration interleaving of BBCOFs

The analysis, design and implementation of sliding-mode control have been already studied in the literature for boost converters [76-79]. For instance, in [76] two multiple-device boost converters are interleaved, and used in a fuel-cell hybrid electric vehicle. In this thesis, the ring-configuration methodology proposed in [80] is applied. The ring configuration consists on generating the current reference for one DC/DC converter from the current of the previous converter, with all the converters connected in parallel. The advantage of ring configuration over other configurations is that it does not require an external synchronizing signal.

In this thesis, a sliding regime is induced in the current of all the input inductors (L_1) of the BBCOFs, connected in parallel, as shown in Fig. 4.2. In [80] it is suggested to create the current reference for the converter from the sum of the reference from the PI voltage regulator *h(t)* and the current from the previous BBCOF. However, in this thesis the current reference for each BBCOF is obtained superimposing the reference from the PI voltage regulator *h(t)* with only the AC component of the current from the previous BBCOF.

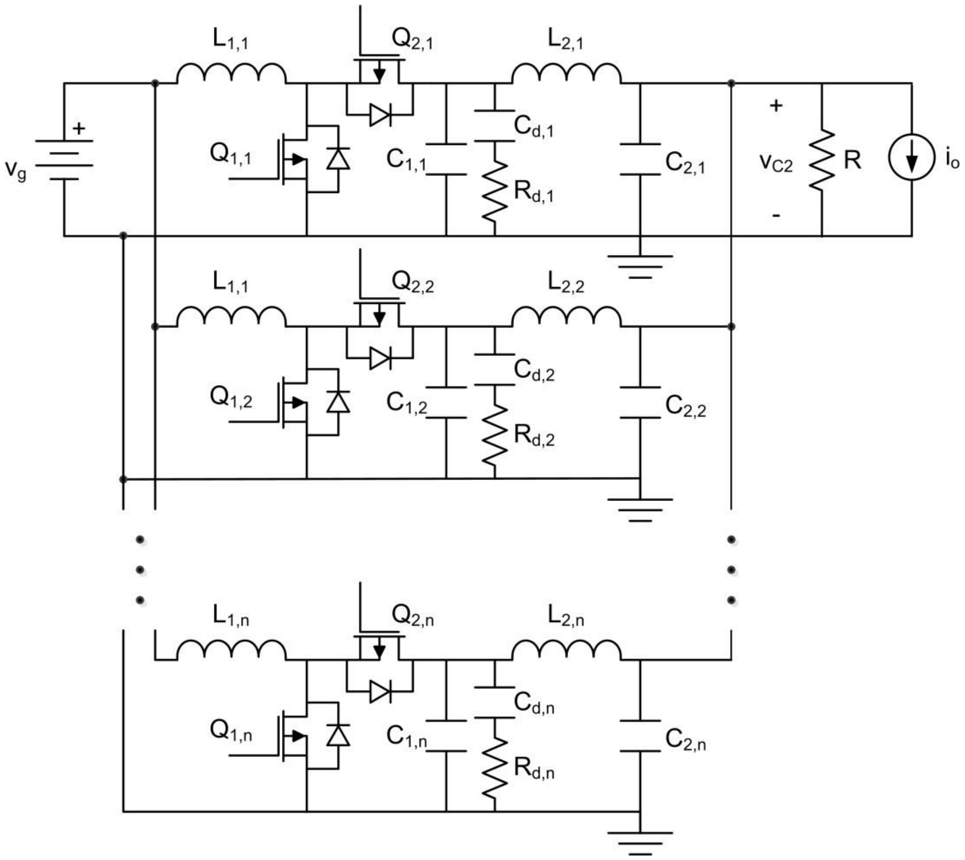

Fig. 4.2. Connection of n interleaved BBCOF.

4.2.1 Current reference composition

The described current reference composition is made by means of the analogue circuit depicted in Fig. 4.3.

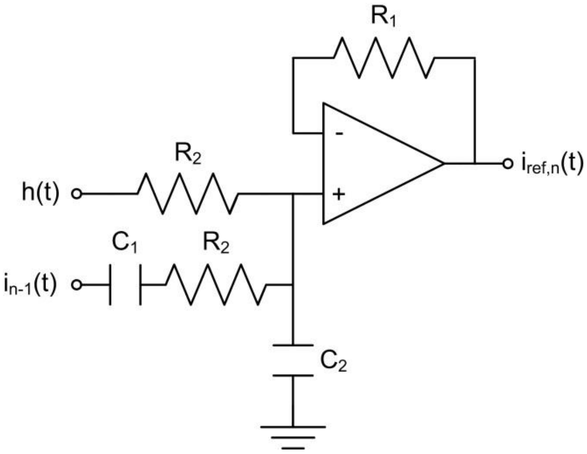

Fig. 4.3. Analogue circuit that generates the current reference $i_{ref}(t)$ for each converter.

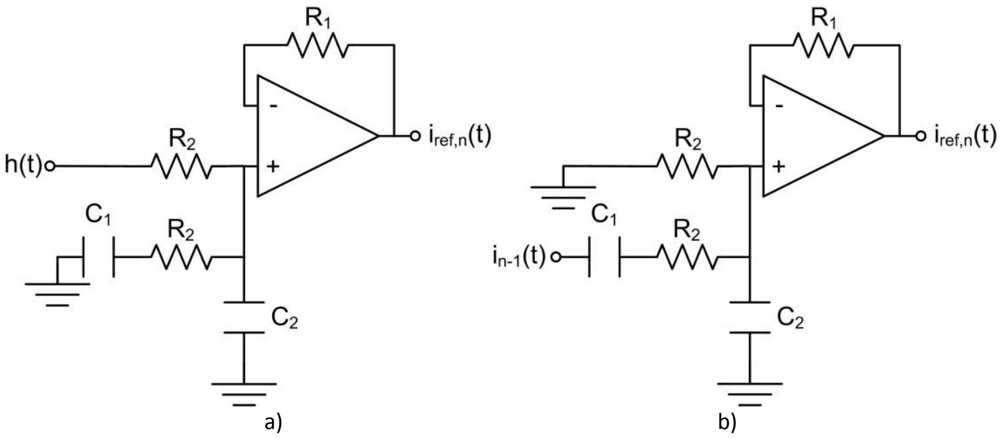

Fig. 4.4. Analysis of the circuit in Fig. 4.3 by superposition: a) considering the reference input h(t), and b) considering the previous phase current $i_{n-1}(t)$.

The circuit in Fig. 4.3 can be analysed by considering the superposition of the two inputs, i.e. h(t) and $i_{n-1}(t)$. Considering h(t) and making $i_{n-1}(t)$ null as in Fig. 4.4.a, the input-output transfer function is

$$\frac{i_{ref,n}(s)}{h(s)}=\frac{C_1R_2s+1}{C_1C_2R_2{}^2s^2+(2C_1+C_2)R_2s+1} \tag{4.1}$$

Otherwise, considering $i_{n-1}(t)$ and making h(t) null, which corresponds to the circuit in Fig. 4.4, the resulting transfer function is

$$\frac{i_{ref,n}(s)}{i_{n-1}(s)}=\frac{C_1R_2s}{C_1C_2R_2{}^2s^2+(2C_1+C_2)R_2s+1} \tag{4.2}$$

Capacitor C_2 is included to deliver additional delay to the system. As its value is in the order of hundreds of picofarads, its effects occur at high frequencies, and therefore can be omitted in this analysis. Thus, the transfer functions (4.1) and (4.2) can be approximated by

$$\frac{i_{ref,n}(s)}{h(s)}\simeq\frac{C_1R_2s+1}{2C_1R_2s+1}=\frac{\tau s+1}{2\tau s+1} \tag{4.3}$$

$$\frac{i_{ref,n}(s)}{i_{n-1}(s)}\simeq\frac{C_1R_2s}{2C_1R_2s+1}=\frac{\tau s}{2\tau s+1}, \tag{4.4}$$

where

$$\tau=C_1R_2 \tag{4.5}$$

4.2.2 Sliding surface calculation for the ring-configuration interleaving

Bearing in mind the transfer functions previously obtained and assuming ideal surface switching, the system with *n* interleaved BBCOFs is depicted in Fig. 4.5. The current reference for the first converter is indeed the sum of the reference from the PI voltage regulator h(t) and the ripple of the current from the n BBCOF. The input current of the first BBCOF is sensed and subtracted to the current reference, obtaining the sliding surface signal $s_1(s)$. Note that a block for the gain of the current sensor, k_{sens}, has been introduced in the model. For the stability analysis, ideal commutation is considered, and then gating signal $u_1(s)$ is obtained. The block BBCOF is described by the equations of the converter.

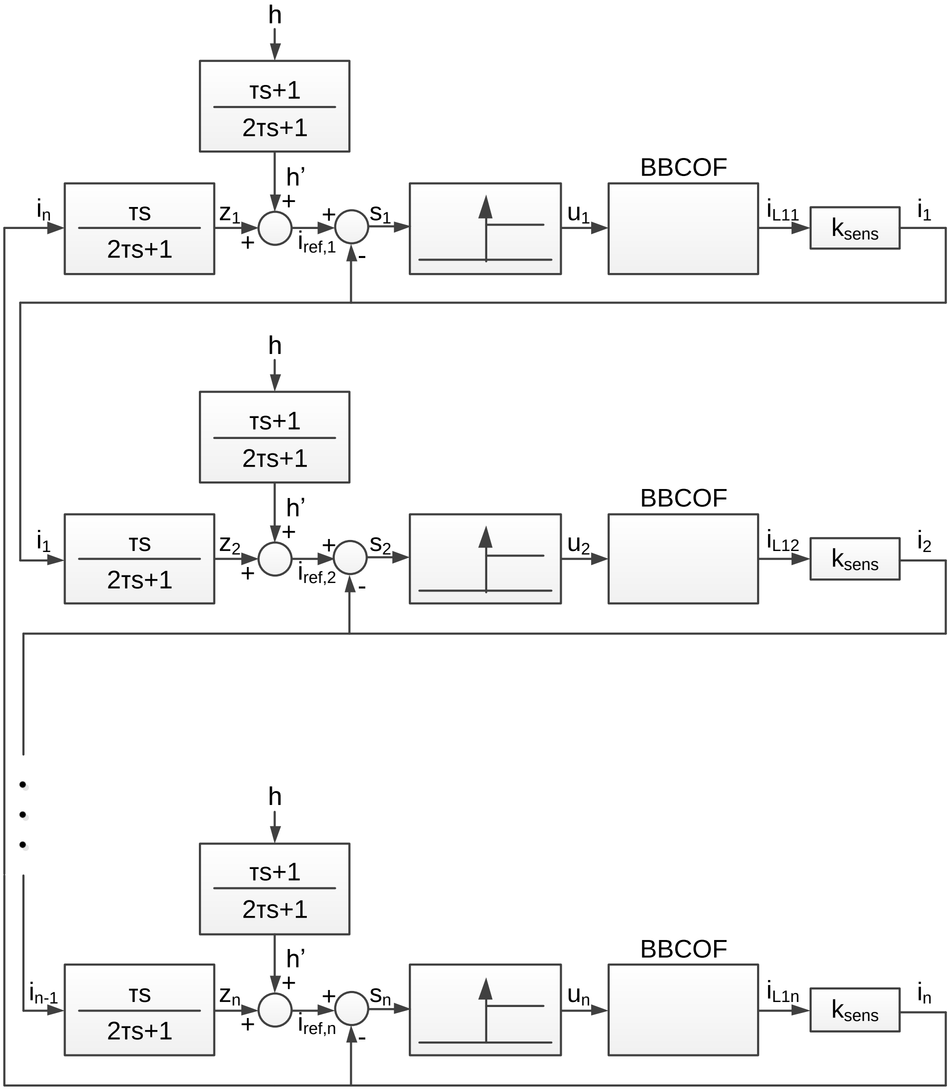

Fig. 4.5. Model of the system with n interleaved BBCOFs.

With no loss of generality, the transfer function $i_{ref,n}(s)/h(s)$ has been considered part of the outer control stage, i.e. the output voltage control loop. As a result, the model of the system presented in Fig. 4.5 is simplified as shown in Fig. 4.6.

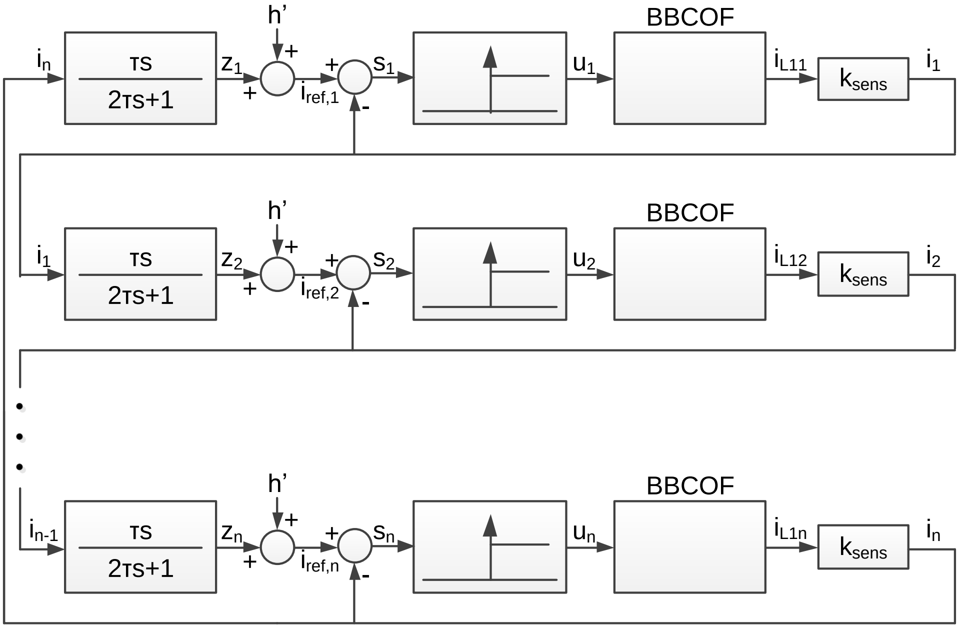

Fig. 4.6. Simplified model of the n interleaved BBCOFs.

The sliding surface is

$$s_j(t)=z_j(t)+h^{'}(t)-k_{sens}i_{L1,j}(t)=0 \tag{4.6}$$

As h'(t) is a slow-dynamics signal coming from the PI voltage controller, it can be regarded as constant. Therefore, the time derivative of the sliding surface is

$$\frac{d}{dt}s_j(t)=\frac{d}{dt}z_j(t)-k_{sens}\frac{d}{dt}i_{L1,j}(t) \tag{4.7}$$

where the signal $z_j(t)$ can be described in the frequency domain as

$$z_j(s)=\frac{\tau s}{2\tau s+1}k_{sens}i_{L1,j-1}(s) \tag{4.8}$$

The previous equation can be rearranged as

$$sz_j(s)=\frac{1}{2}\left[k_{sens}si_{L1,j-1}(s)-\frac{1}{\tau}z_j(s)\right], \tag{4.9}$$

and then, by doing the inverse Laplace transform, the expression for the time derivative of the signal $z_j(t)$ is obtained

$$\frac{d}{dt}z_j(t)=\frac{1}{2}\left[k_{sens}\frac{d}{dt}i_{L1,j-1}(t)-\frac{1}{\tau}z_j(t)\right] \tag{4.10}$$

Evaluating (4.10) in (4.7)

$$\frac{d}{dt}s_j(t)=\frac{1}{2}k_{sens}\frac{d}{dt}i_{L1,j-1}(t)-\frac{1}{2\tau}z_j(t)-k_{sens}\frac{d}{dt}i_{L1,j}(t) \tag{4.11}$$

4.2.3 Reachability conditions

Once the sliding surface of the system has been obtained, it is necessary to determine the reachability conditions, or domains of attraction to the sliding regime. It is essential to ensure that these conditions will be satisfied to guarantee that the sliding motion will take place. The sliding motion is reachable if the following condition is accomplished

$$s_j(t)\cdot\frac{d}{dt}s_j(t)<0 \tag{4.12}$$

In case the sliding surface of the j converter $s_j(t)$ is positive, the time derivative of the sliding surface has to be negative. Therefore, the derivative surface in (4.11) now accomplishes

$$\frac{d}{dt}s_j(t)=\frac{1}{2}k_{sens}\frac{d}{dt}i_{L1,j-1}(t)-\frac{1}{2\tau}z_j(t)-k_{sens}\frac{d}{dt}i_{L1,j}(t)<0 \tag{4.13}$$

Considering ideal commutation, with a positive sliding surface the control signal of this converter, $u_j(t)$, will be equal to 1. Evaluating (4.21) in (4.13), the first reachability condition is extracted

$$\frac{d}{dt}s_j(t)=\frac{1}{2}\frac{k_{sens}}{L_{1,j-1}}\left[v_g(t)-R_{L1,j-1}i_{L1,j-1}(t)\right]-\frac{1}{2\tau}z_j(t)-\frac{k_{sens}}{L_{1,j}}\left[v_g(t)-R_{L1,j}i_{L1,j}(t)\right]<0 \tag{4.14}$$

Assuming that the value of the input inductor is equal over all the converters

$$L_{1,\mathrm{j}}=L_1,\quad j=1,\ldots,n \tag{4.15}$$

the condition for the time derivative of the sliding surface is simplified

$$\frac{d}{dt}s_j(t)=-\frac{1}{2\tau}z_j(t)+\frac{k_{sens}}{L_1}\left[R_{L1}i_{L1,j}(t)-\frac{1}{2}v_g(t)-\frac{1}{2}R_{L1,j-1}i_{L1,j-1}\right]<0 \tag{4.16}$$

Neglecting the resistive losses, a simplified reachability condition can be obtained

$$\frac{d}{dt}s_j(t)=\frac{-1}{2}\left(\frac{k_{sens}}{L_1}v_g(t)+\frac{1}{\tau}z_j(t)\right)<0, \tag{4.17}$$

which depends on the gain of the current sensor, the inductance of L_1, the input voltage, the time constant τ and the input current ripple of the previous converter. Otherwise, for a negative value of the sliding surface, its time derivative has to be positive

$$\frac{d}{dt}s_j(t)=\frac{1}{2}k_{sens}\frac{d}{dt}i_{L1,j-1}(t)-\frac{1}{2\tau}z_j(t)-k_{sens}\frac{d}{dt}i_{L1,j}(t)>0 \tag{4.18}$$

Still considering ideal commutation, the signal $u_j(t)$ will be 0 in this case, and therefore a second reachability condition is obtained

$$\begin{aligned}\frac{d}{dt}s_j(t)=&\frac{1}{2}\frac{k_{sens}}{L_{1,j-1}}\left[v_g(t)-v_{C1,j-1}(t)-R_{L1,j-1}i_{L1,j-1}(t)\right]-\frac{1}{2\tau}z_j(t)-\\&-\frac{k_{sens}}{L_{1,j}}\left[v_g(t)-v_{C1,j}(t)-R_{L1,j}i_{L1,j}(t)\right]>0\end{aligned} \tag{4.19}$$

UNIVERSITAT ROVIRA I VIRGILI
DESIGN AND CONTROL OF A BIDIRECTIONAL DC/DC CONVERTER FOR AN ELECTRIC VEHICLE APPLICATION.
Laura Albiol Rendillo
Dipòsit Legal: T 1361-2015

Neglecting again the parasitic resistances and considering (4.15), the condition in (4.19) can be rewritten as

$$\frac{d}{dt}s_j(t)=\frac{-1}{2}\frac{k_{sens}}{L_1}v_g(t)-\frac{1}{2}\frac{k_{sens}}{L_1}v_{C1,j-1}(t)-\frac{1}{2\tau}z_j(t)+\frac{k_{sens}}{L_1}v_{C1,j}(t)>0 \tag{4.20}$$

The second reachability condition also depends on the current ripple from the previous converter, the time constant τ, the gain of the current sensor, the inductance of L_1, the input voltage and the voltage of capacitor C_1.

4.2.4 Steady state calculation

Note from Fig. 4.2 that the C_{2j} capacitors are connected in parallel, so the output voltage is the same for every converter, and thus a unique output voltage control loop is necessary. Therefore, considering the resistive losses of the inductors, the state variable expressions for any of the BBCOFs are

$$\frac{d}{dt}i_{L1,j}(t)=U_j \tag{4.21}$$

$$\frac{d}{dt}i_{L2,j}(t)=\frac{1}{L_{2,j}}\left[v_{C1,j}(t)-v_{C2,j}(t)-R_{L2,j}i_{L2,j}(t)\right] \tag{4.22}$$

$$\frac{d}{dt}v_{C1,j}(t)=\frac{1}{C_{1,j}}\left[\frac{v_{Cd,j}(t)}{R_{d,j}}-\frac{v_{C1,j}(t)}{R_{d,j}}+i_{L1,j}(t)\left(1-u_j(t)\right)-i_{L2,j}(t)\right] \tag{4.23}$$

$$\frac{d}{dt}v_{Cd,j}(t)=\frac{1}{C_{d,j}}\left[\frac{v_{C1,j}(t)}{R_{d,j}}-\frac{v_{Cd,j}(t)}{R_{d,j}}\right] \tag{4.24}$$

$$\frac{d}{dt}v_{C2}(t)=\frac{1}{\sum_{j=1}^{n}C_{2,j}}\left[i_o(t)-\frac{v_{C2}(t)}{R}+\sum_{j=1}^{n}i_{L2,j}(t)\right], \tag{4.25}$$

where U_j are the discontinuous control actions, as defined in

$$U_j=\frac{1}{L_{1,j}}\left[v_g(t)-v_{C1,j}(t)\left(1-u_j(t)\right)-R_{L1,j}i_{L1,j}(t)\right] \tag{4.26}$$

If the capacitance value is considered to be the same for all C_2 capacitors

$$C_{2,j}=C_2,\quad j=1,\ldots,n, \tag{4.27}$$

the output voltage can be expressed as

$$\frac{d}{dt}v_{C2}(t)=\frac{1}{nC_2}\left[i_o(t)-\frac{v_{C2}(t)}{R}+\sum_{j=1}^{n}i_{L2,j}(t)\right] \tag{4.28}$$

The equivalent control method consists on determining the values of the controls that make null the time derivative of the sliding surface in (4.11). These values for the controls are called equivalent controls

$$\frac{d}{dt}s_j(t)=\frac{1}{2}k_{sens}U_{j-1,eq}(t)-\frac{1}{2\tau}z_j(t)-k_{sens}U_{j,eq}(t)=0 \tag{4.29}$$

The expression for the variable $z_j(t)$ can be isolated from (4.6)

$$z_j(t)=k_{sens}i_{L1,j}(t)-h^{'}(t) \tag{4.30}$$

Using (4.30) in (4.29), the derivative of the sliding surface is

$$\frac{d}{dt}s_j(t)=\frac{1}{2}k_{sens}U_{j-1,eq}(t)-\frac{1}{2\tau}k_{sens}i_{L1,j}(t)+\frac{1}{2\tau}h^{'}(t)-k_{sens}U_{j,eq}(t)=0 \tag{4.31}$$

Considering balanced converters where

$$U_{j-1,eq}(t)=U_{j,eq}(t)=U_{eq}(t), \tag{4.32}$$

the expression in (4.31) can be simplified as

$$\frac{d}{dt}s_j(t)=-\frac{1}{2\tau}k_{sens}i_{L1,j}(t)+\frac{1}{2\tau}h^{'}(t)-\frac{1}{2}k_{sens}U_{j,eq}(t)=0 \tag{4.33}$$

Consequently, the expression obtained for the equivalent control is

$$U_{j,eq}(t)=\frac{1}{\tau}\left(\frac{1}{k_{sens}}h^{'}(t)-i_{L1,j}(t)\right) \tag{4.34}$$

In matrix form, the equivalent controls are

$$\underbrace{\begin{pmatrix}\frac{d}{dt}i_{L1,1}(t)\\ \frac{d}{dt}i_{L1,2}(t)\\ \vdots \\ \frac{d}{dt}i_{L1,\mathrm{n}}(t)\end{pmatrix}}_{U}=\frac{1}{\tau}\left[\underbrace{\begin{pmatrix}-1 & 0 & \cdots & 0\\ 0 & -1 & \cdots & 0\\ \vdots & \vdots & \ddots & \vdots\\ 0 & 0 & \cdots & -1\end{pmatrix}}_{Q}\begin{pmatrix}i_{L1,1}(t)\\ i_{L1,2}(t)\\ \vdots\\ i_{L1,\mathrm{n}}(t)\end{pmatrix}+\begin{pmatrix}h^{'}(t)/k_{sens}\\ h^{'}(t)/k_{sens}\\ \vdots\\ h^{'}(t)/k_{sens}\end{pmatrix}\right] \tag{4.35}$$

Since the determinant of matrix Q is not null

$$|Q|=(-1)^n, \tag{4.36}$$

there exists a unique steady state solution. At steady state, the equivalent control is zero

$$U_{j,eq,ss}(t)=0, \tag{4.37}$$

so the input current deduced from (4.34) is

$$i_{L1,j,ss}(t)=\frac{1}{k_{sens}}h'_{ss}(t), \tag{4.38}$$

where the subscript *ss* denotes the steady state condition. It can be observed that the current in the input inductor is equal to the reference value divided by the current sensor gain, as expected.

4.2.5 Stability of the steady state solution

The next step is to determine whether the found steady state solution is stable. Then, from the auxiliary variable

$$\bar{i}_j(t)=i_{L1,j}(t)-i_{L1,j,ss}(t), \tag{4.39}$$

the following positive definite Lyapunov function is defined

$$V(t)=\sum_{j=1}^{n}\left|\bar{i}_j(t)\right|=\sum_{j=1}^{n}\left(\bar{i}_j(t)\cdot sign\left(\bar{i}_j(t)\right)\right), \tag{4.40}$$

From the system (4.35), the time derivative of this Lyapunov function is

$$\frac{d}{dt}V(t)=\frac{-1}{\tau}\sum_{j=1}^{n}\left(\bar{i}_j\cdot sign\left(\bar{i}_j\right)\right)=\frac{-1}{\tau}\sum_{j=1}^{n}\left|\bar{i}_j\right| \tag{4.41}$$

Since τ is positive, the time derivative of the Lyapunov function is negative definite, and thus the system is stable.

4.3 C_2 impedance-oriented design

Returning to the study of the output impedance of section 3.5, it is desirable that the resonance peak is found under 0 dB in order to attenuate its effects. The adjustment of this peak has been performed with the design of the C_2 capacitor, considering the interleaved system. If a single converter were considered, the value of this capacitor would be much larger, deprecating the size and volume characteristics of the BBCOF. The incremental output impedance of n interleaved BBCOFs, deduced from (4.21)-(4.25), is

$$\frac{d}{dt}s_j(t)=\frac{-1}{2}\frac{k_{sens}}{L_1}v_g(t)-\frac{1}{2}\frac{k_{sens}}{L_1}v_{C1,j-1}(t)-\frac{1}{2\tau}z_j(t)+\frac{k_{sens}}{L_1}v_{C1,j}(t)>0 \tag{4.42}$$

Effectively, the frequency response of the output impedance expression for the interleaved system presents a gain of 1/3 with respect to the single BBCOF system. This effect, shown in Fig. 4.7, occurs since the three output impedances of each converter have been paralleled.

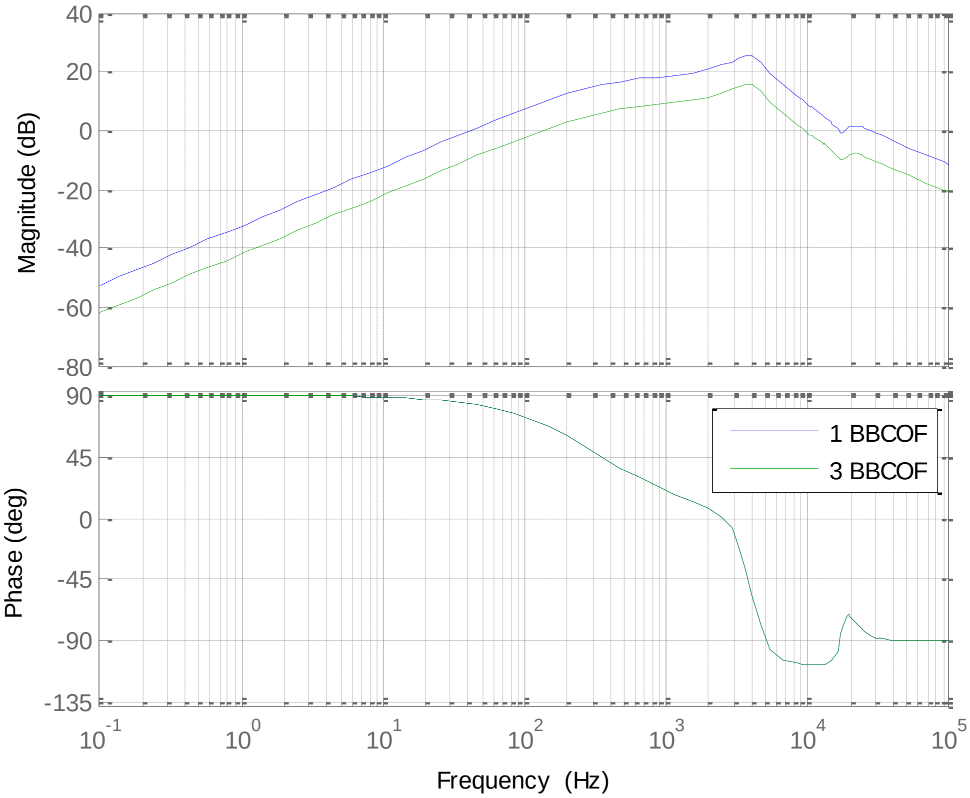

Fig. 4.7. Comparison of the incremental output impedance of the system without and with interleaving.

The incremental output impedance of the three paralleled BBCOF with different values for the C_2 capacitor has been represented in Fig. 4.8. As it can be observed, capacitances below 1 µF are unacceptable, since the peak would be over 0 dB. For slightly bigger capacitances, the gain of the first resonant peak is too high. This is an undesirable effect, since it means that the system would become more susceptible to current variations in the output of the BBCOFs. Consequently, only values higher than 6 µF will be considered for C_2 capacitor. Finally, a value of C_2=6.2 µF is chosen, and in order to guarantee that the C_2/C_1 ratio is greater than 5, the value of the first capacitor is set as C_1=1 µF. With these values, the obtained output impedance frequency response is represented in Fig. 4.9. As it can be observed, the resonance peak has a magnitude below 0 dB, and consequently it is attenuated. This attenuation is especially important, since the resonance frequency is in the vicinity of the switching frequency of the PMSM drive.

UNIVERSITAT ROVIRA I VIRGILI
DESIGN AND CONTROL OF A BIDIRECTIONAL DC/DC CONVERTER FOR AN ELECTRIC VEHICLE APPLICATION.
Laura Albiol Rendillo
Dipòsit Legal: T 1361-2015

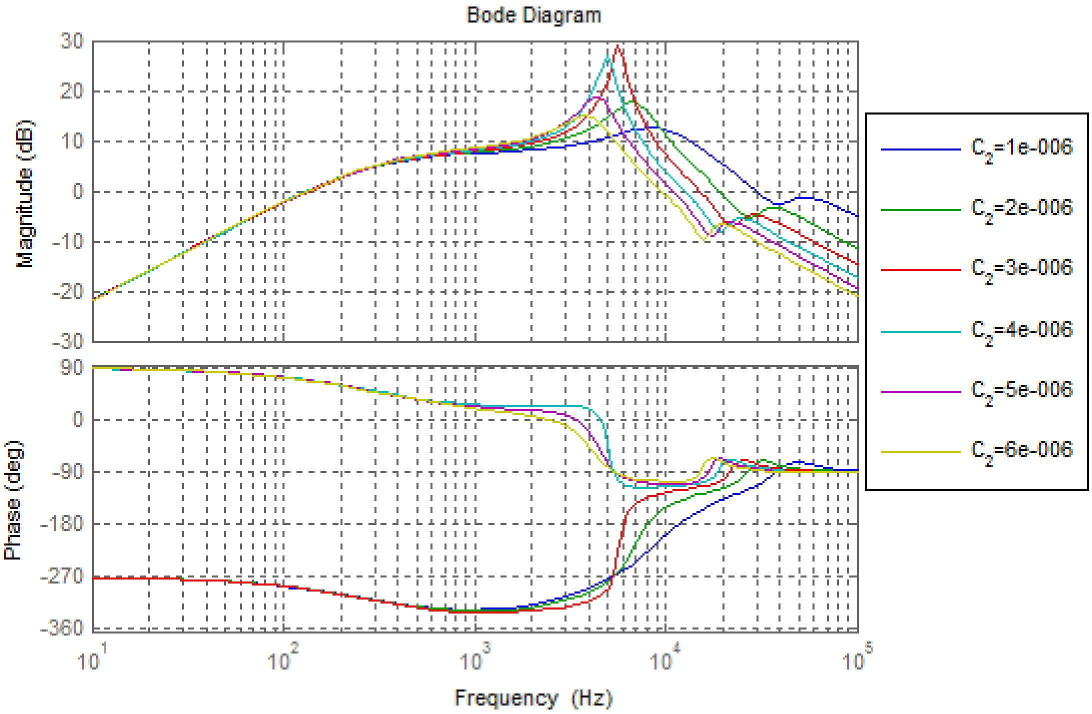

Fig. 4.8. Study of the incremental output impedance for different values of C_2.

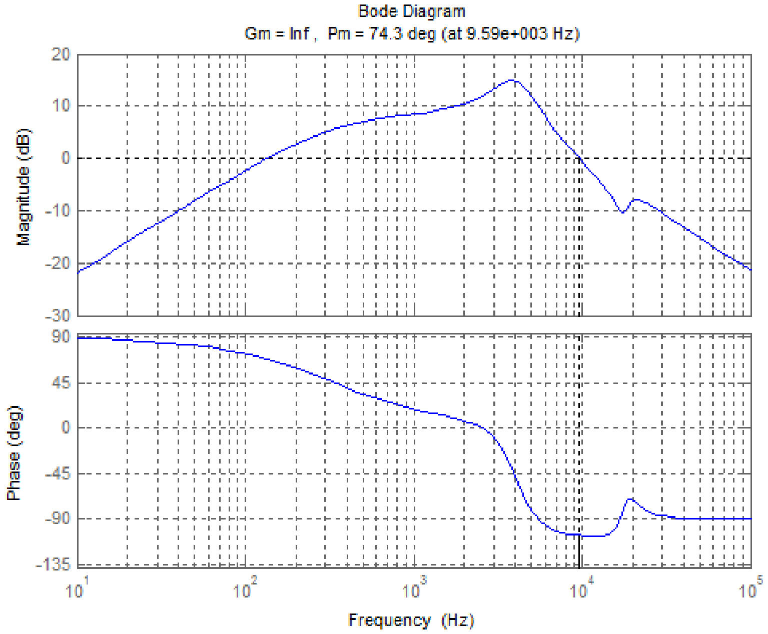

Fig. 4.9. Incremental output impedance of the three interleaved BBCOFs, with the final design of C2=6.2 μF.

4.4 Middlebrook criterion verification

The components of the BBCOFs have already been designed following ripple criterion for the input inductor L_1, impedance criterion for output capacitor C_2, and a sizing ratio with respect to L_1 and C_2 has been applied to L_2 and C_1, respectively. The final step to verify this design is to verify whether the Middlebrook criterion is accomplished, i.e. the input impedance of the motor drive is higher than the output impedance of the interleaved BBCOFs, or not.

Consequently, it is necessary to determine the input impedance of the PMSM drive. In [52] the incremental input admittance of a PMSM drive is described as

$$\frac{\Delta I_{dc}}{\Delta V_{dc}}=\frac{as^2+bs+c}{J\left(V_{dc}{}^*\right)^2\left(s^2L_s+s\left(R_s+k_{Ip}\right)+k_{Ii}\right)}, \tag{4.43}$$

where the *a*, *b* and *c* parameters correspond to

$$a=JL_s\left(1.5I_q{}^*V_q{}^*-I_{dc}{}^*V_{dc}{}^*\right) \tag{4.44}$$

$$b=J\left(1.5V_q{}^*\left(I_{dc}{}^*R_s+V_q{}^*\right)-I_{dc}{}^*V_{dc}{}^*\left(R_s+k_{Ip}\right)\right) \tag{4.45}$$

$$c=\left(2.25I_q{}^*\lambda_f{}^2P^2V_q{}^*-I_{dc}{}^*V_{dc}{}^*Jk_{Ii}\right), \tag{4.46}$$

where $V_{dc}{}^*$ and $I_{dc}{}^*$ are the voltage and current of the DC bus between the BBCOF and the drive at steady state, $V_q{}^*$ and $I_q{}^*$ are the q-axis voltage and current at steady state, R_s and L_s are the stator resistance and inductance of the PMSM, J is its rotor inertia, P is the number of pole pairs, and k_{Ip} and k_{Ii} are the proportional and integral gains of the PMSM current controller.

The PMSM is modelled by means of the following equations

$$T_e=1.5P\lambda_f I_q \tag{4.47}$$

$$\left(Js+B\right)\omega_r=T_e-T_L \tag{4.48}$$

$$V_q=\left(R_s+sL_s\right)I_q+\left(\lambda_f+L_sI_d\right)P\omega_r, \tag{4.49}$$

where T_e is the electromagnetic torque generated by the PMSM, T_L is the load torque and B is its viscous friction. Besides, the model of a lossless inverter is given by

$$V_{dc}I_{dc}=T_e\omega_r, \tag{4.50}$$

Taking into account these expressions, and the machine and controller characteristics, it is possible to evaluate the input admittance transfer function. To obtain the steady state value of the q-axis current, (4.47) and (4.48) are evaluated when *s* tends to zero

$$I_q{}^*=\lim_{s\to 0}\frac{\left(Js+B\right)\omega_r+T_L}{1.5P\lambda_f}=\frac{B\omega_r+T_L}{1.5P\lambda_f} \tag{4.51}$$

As surpassing the base speed is not considered, flux-weakening operation will not take place, and consequently the d-axis current of the PMSM I_d will be null

$$I_d{}^*=0 \tag{4.52}$$

Therefore, the q-axis voltage can be obtained from (4.49), and evaluated at steady state by calculating the limit when *s* tends to zero

$$V_q^* = \lim_{s\to 0}\left[\left(R_s + sL_s\right)I_q + \left(\lambda_f + L_s I_d\right)P\omega_r\right] = R_s I_q^* + \lambda_f P\omega_r \tag{4.53}$$

Moreover, the current of the DC bus between the BBCOF and the PMSM drive at steady state can be derived from (4.47) and (4.50), and its expression is

$$I_{dc}^* = \frac{1.5P\lambda_f I_q^* \omega_r}{V_{dc}} \tag{4.54}$$

Replacing (4.51), (4.53) and (4.54) in (4.43), the incremental input admittance is obtained as a function of the triplet of variables that determine the operating point: the DC bus voltage V_{dc}, the rotor speed ω_r and the load torque T_L. The characteristics of the PMSM drive are detailed in Table 4.I. Therefore, the incremental input admittance transfer function for the described PMSM drive is

$$\frac{\Delta I_{dc}}{\Delta V_{dc}} = \frac{0.1515151515}{V_{dc}^3}\frac{num(s)}{0.01929500000s^2 + 251.2770000s + 494}, \tag{4.55}$$

where the numerator of the transfer function is

$$\begin{aligned} num(s) = {} & 0.071720849s^2V_{dc}T_L^2 + 0.014344170s^2V_{dc}\omega_r T_L + 0.00071720849s^2V_{dc}\omega_r^2 + \\ & + 8.7539540s\omega_r T_L^2 + 17.294246s\omega_r^2 T_L + 4.7466973sT_L^2V_{dc} - \\ & - 1640.6225sT_L\omega_r V_{dc} + 1.6418850s\omega_r^3 - 149.14466s\omega_r^2V_{dc} + 1277T_L^2V_{dc} - \\ & - 737.56839T_L\omega_r V_{dc} - 86.526839\omega_r^2V_{dc} \end{aligned} \tag{4.56}$$

Table 4.I. Characteristics of the PMSM drive.

stator resistance R_s	1.277 Ω
stator inductance L_s	19.295 mH
electrical constant k_e	223 V_{pk}/krp
torque constant k_t	1.8442 N·m/A_{pk}
rotor inertia J	0.0066 kg·m^2
rotor viscous friction B	0.1 N·m·s
proportional gain of the PI speed controller $k_{\omega p}$	0.0
integral gain of the PI speed controller $k_{\omega i}$	1
proportional gain of the PI current controller k_{Ip}	250
proportional gain of the PI current controller k_{Ii}	494

As it is unfeasible to compare the output impedance of the BBCOF with the input admittance of the PMSM for any possible operating point, the driving profile of figure Fig. 4.10 has been established, and this comparison will be done for the most representative points, which are marked in the image. A negative load torque means that energy is being recovered from the load, and consequently the BBCOF is in step-down mode.

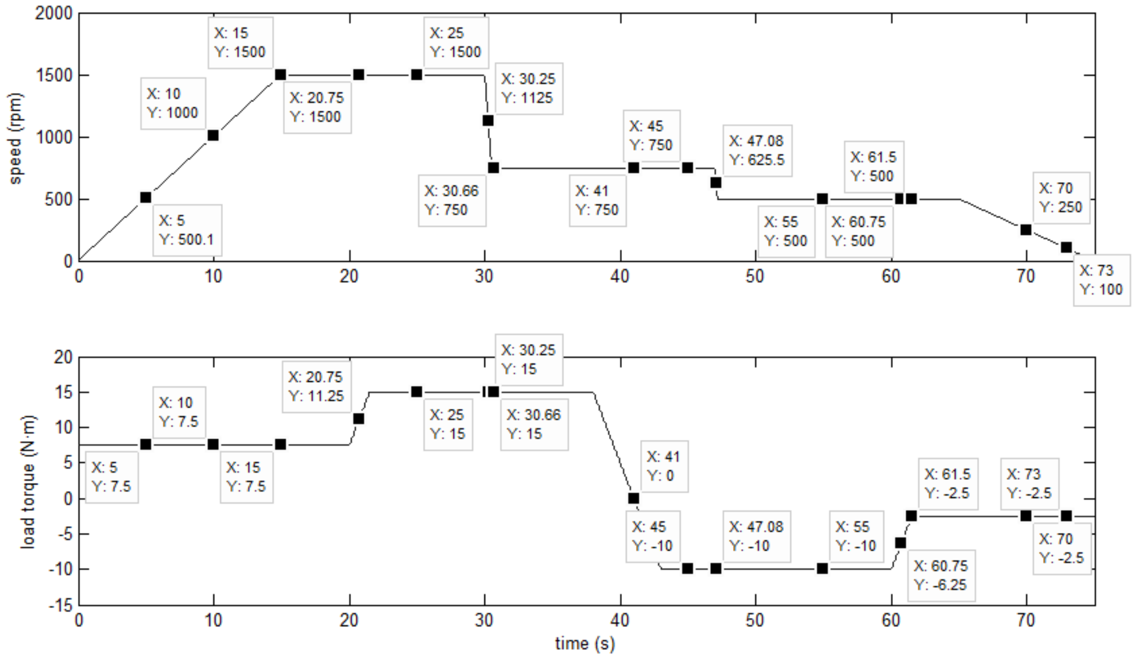

Fig. 4.10. Driving profile for the PMSM with marked operating points.

Next, the magnitude comparison of the output impedance of the BBCOF and the input impedance of the PMSM are compared for all the operating points previously shown in Fig. 4.11, and are presented from Fig. 4.11 to Fig. 4.25.

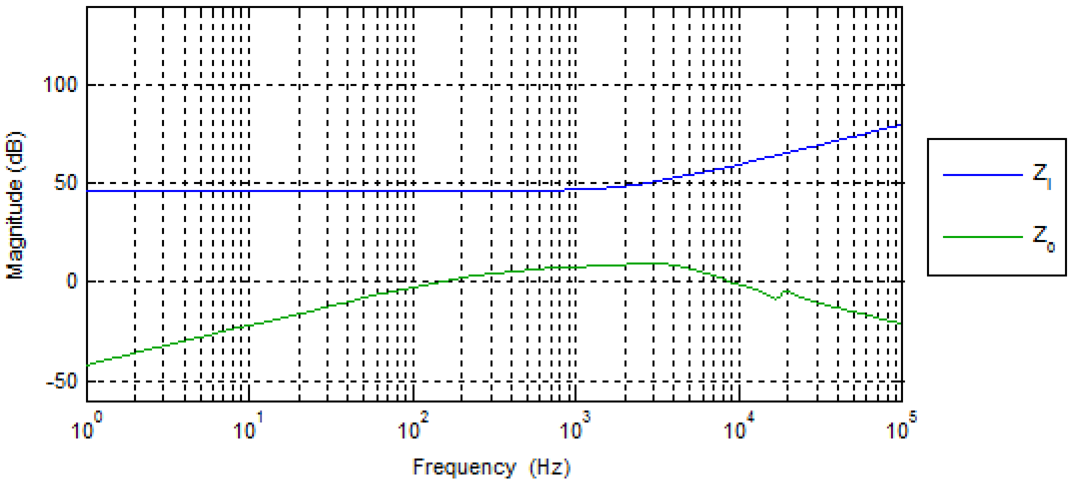

Fig. 4.11. Impedance comparison with ω=500 rpm, T_L=7.5 N·m.

UNIVERSITAT ROVIRA I VIRGILI
DESIGN AND CONTROL OF A BIDIRECTIONAL DC/DC CONVERTER FOR AN ELECTRIC VEHICLE APPLICATION.
Laura Albiol Rendillo
Dipòsit Legal: T 1361-2015

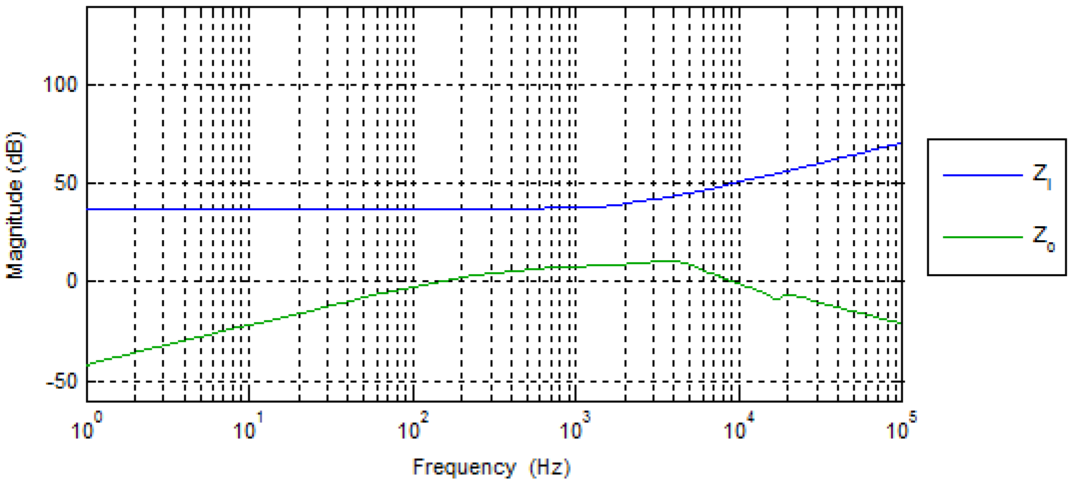

Fig. 4.12. Impedance comparison with ω=1000 rpm, T_L=7.5 N·m.

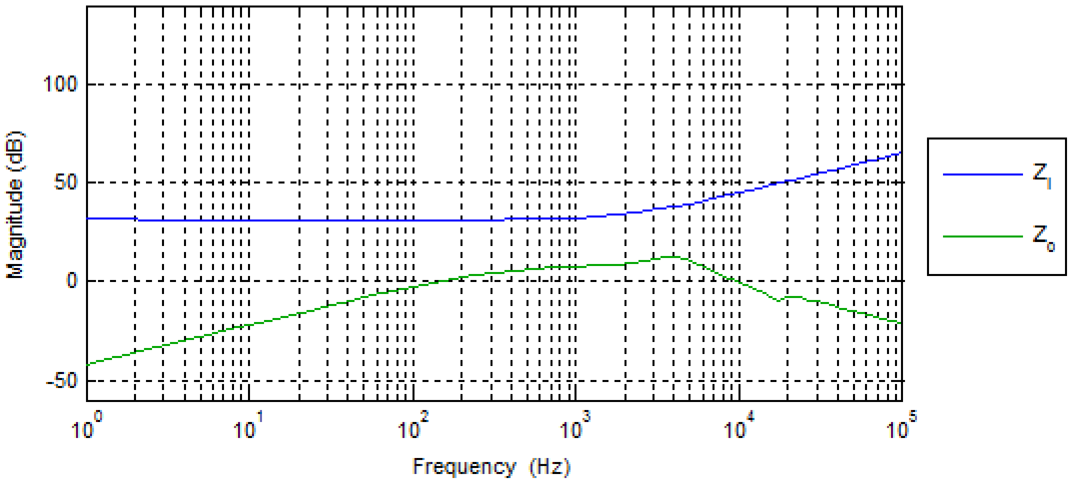

Fig. 4.13. Impedance comparison with ω=1500 rpm, T_L=7.5 N·m.

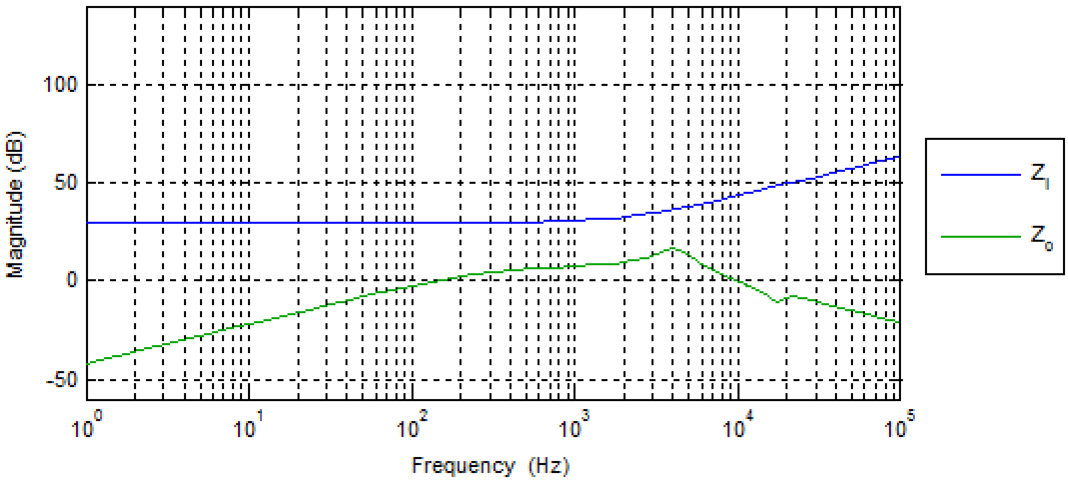

Fig. 4.14. Impedance comparison with ω=1500 rpm, T_L=11.25 N·m.

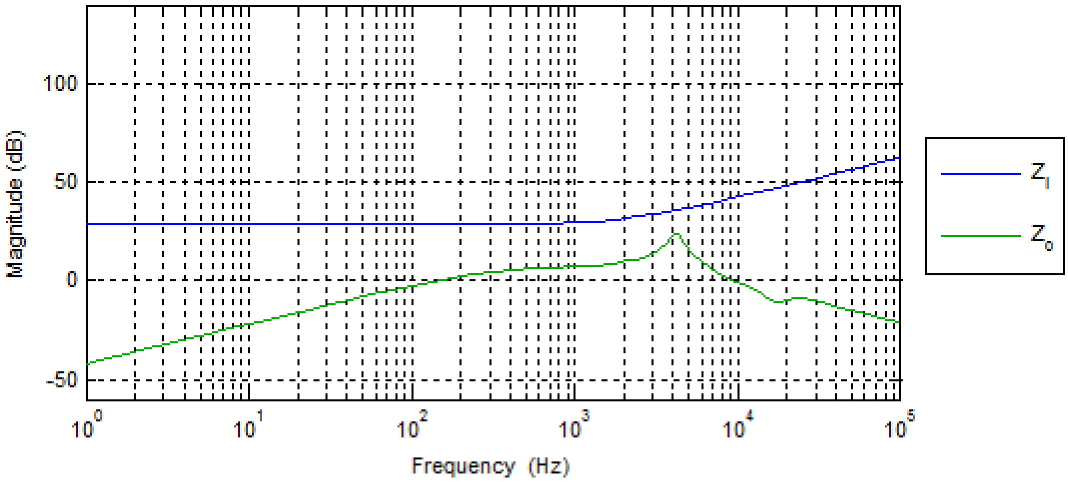

Fig. 4.15. Impedance comparison with ω=1500 rpm, T_L=15 N·m.

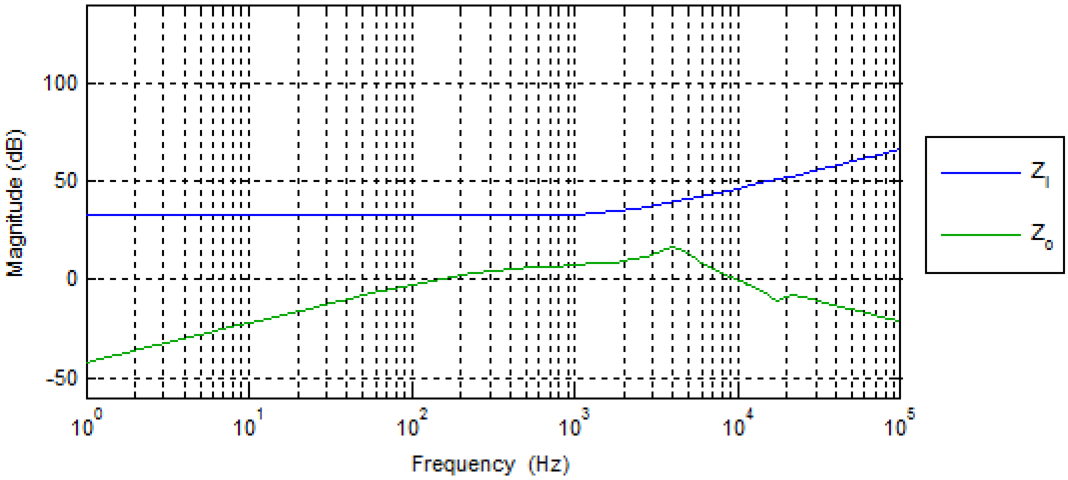

Fig. 4.16. Impedance comparison with ω=1125 rpm, T_L=15 N·m.

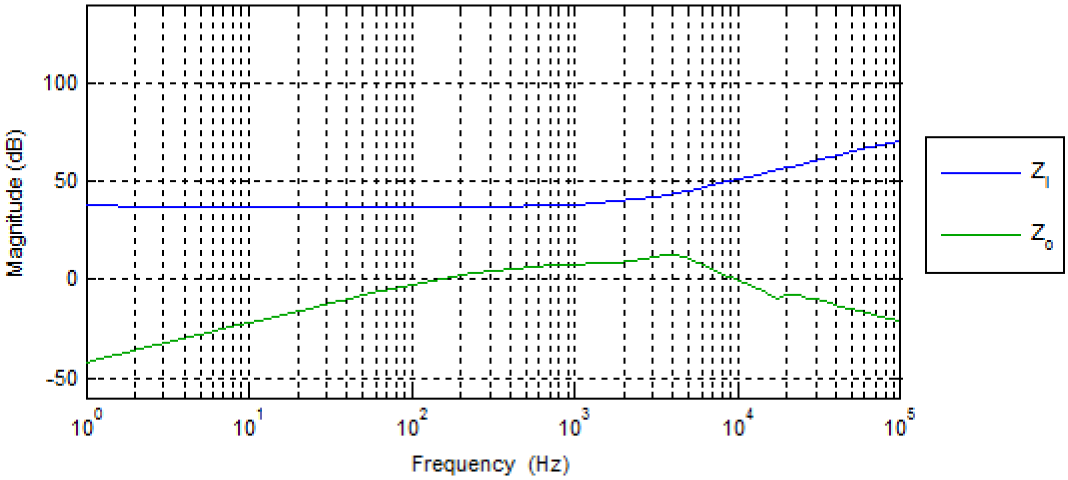

Fig. 4.17. Impedance comparison with ω=750 rpm, T_L=15 N·m.

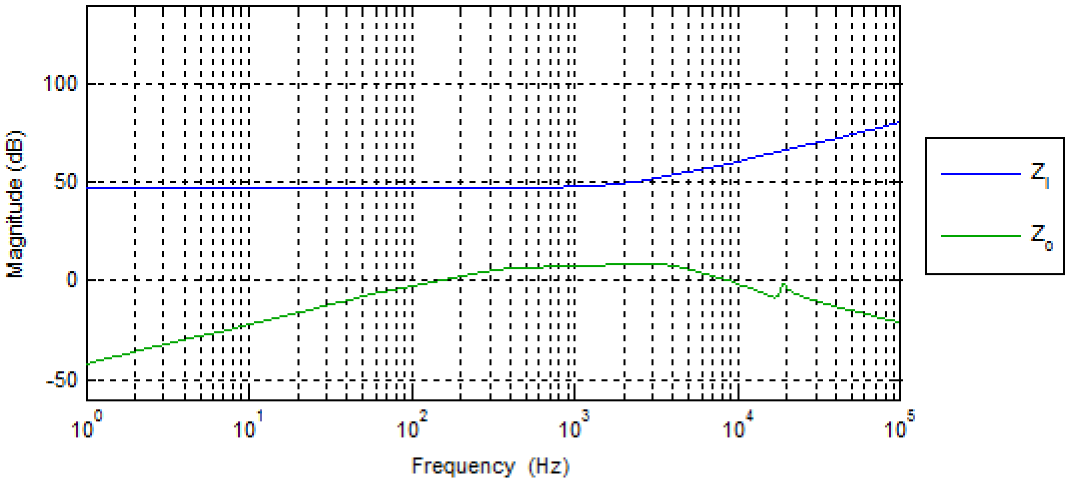

Fig. 4.18. Impedance comparison with ω=750 rpm, T_L=0 N·m.

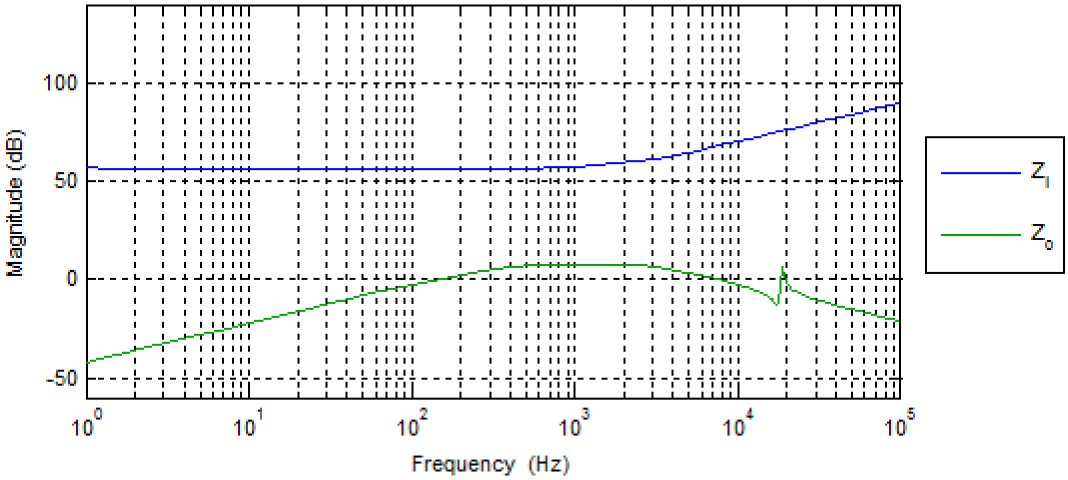

Fig. 4.19. Impedance comparison with ω=750 rpm, T_L=-10 N·m.

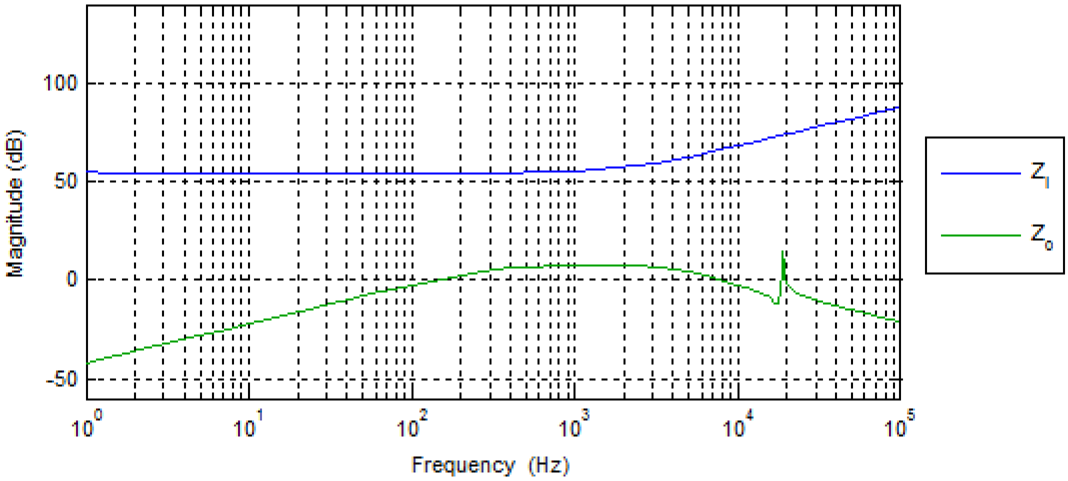

Fig. 4.20. Impedance comparison with ω=625 rpm, T_L=-10 N·m.

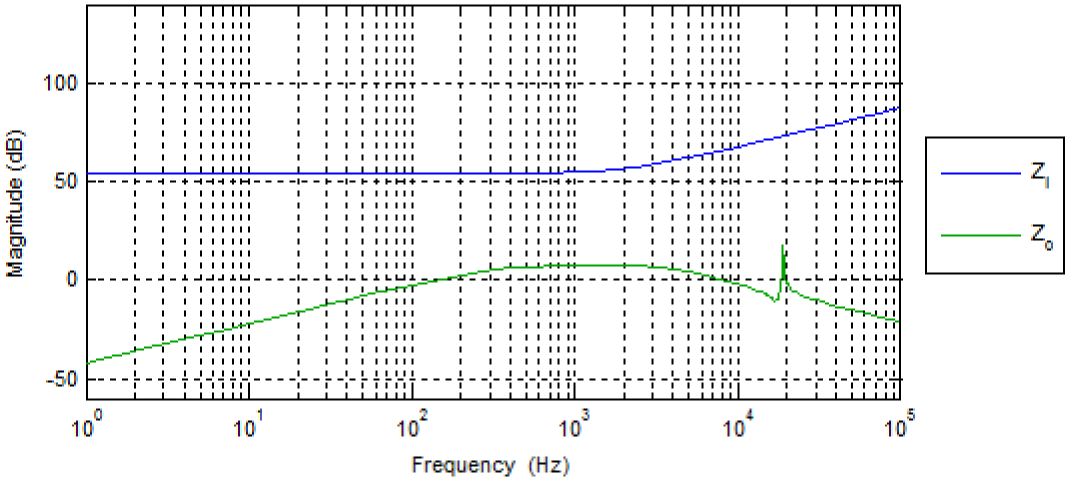

Fig. 4.21. Impedance comparison with ω=500 rpm, T_L=-10 N·m.

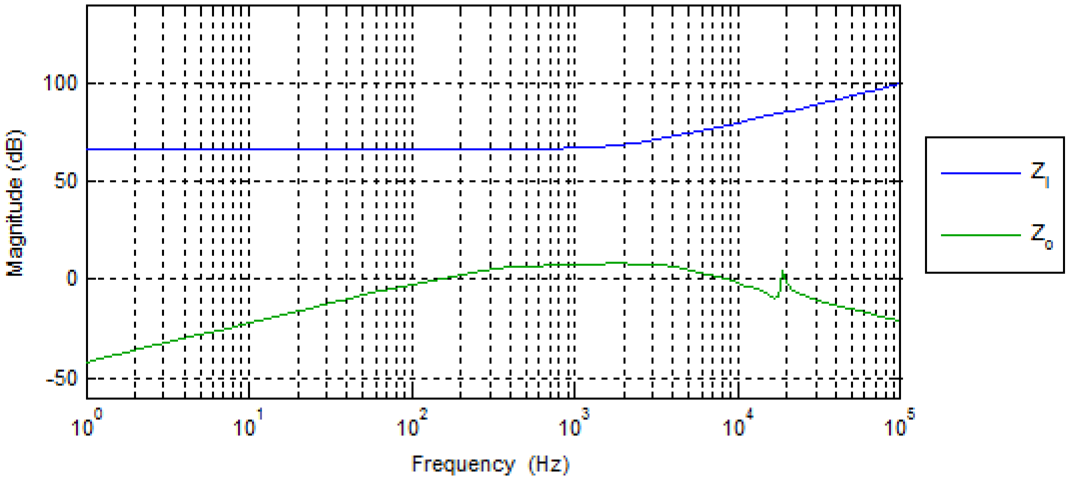

Fig. 4.22. Impedance comparison with ω=500 rpm, T_L=-6.25 N·m.

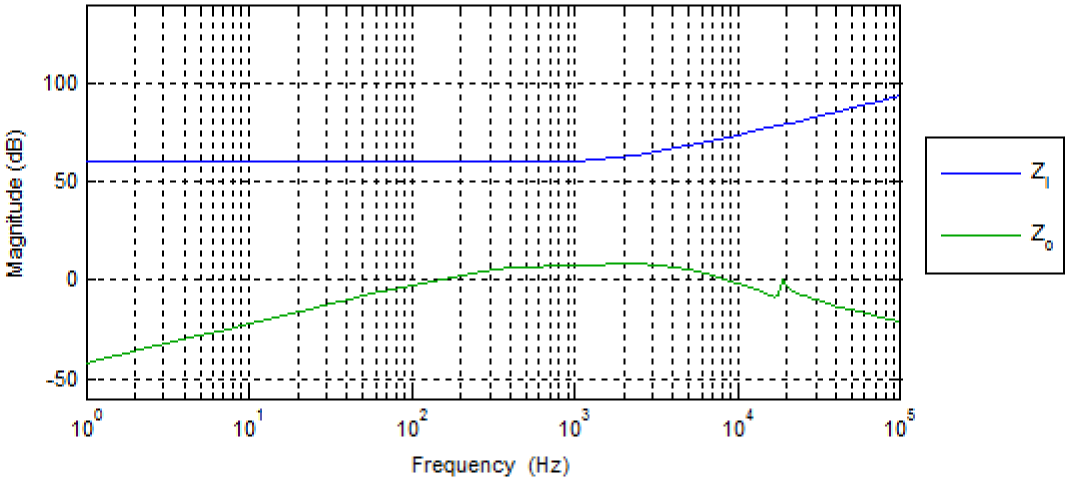

Fig. 4.23. Impedance comparison with ω=500 rpm, T_L=-2.5 N·m.

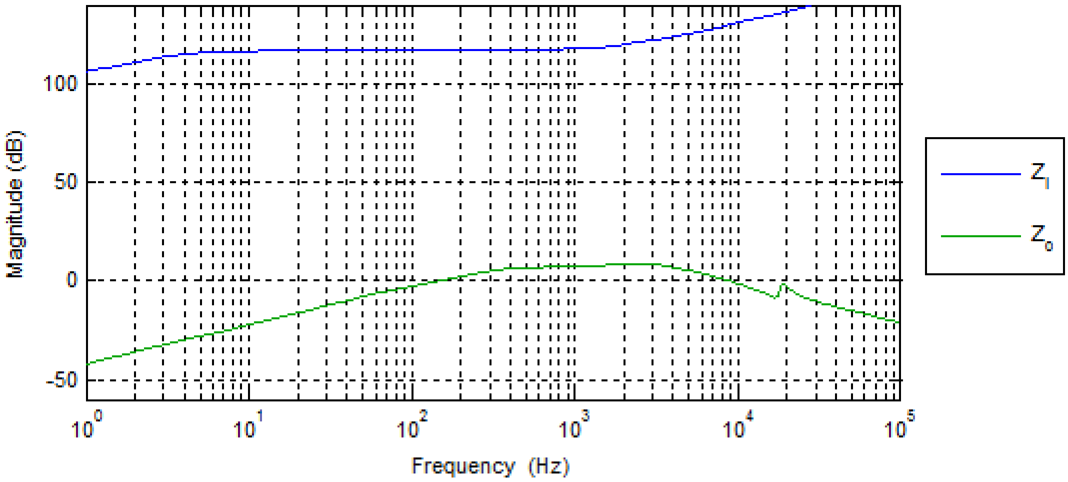

Fig. 4.24. Impedance comparison with ω=250 rpm, T_L=-2.5 N·m.

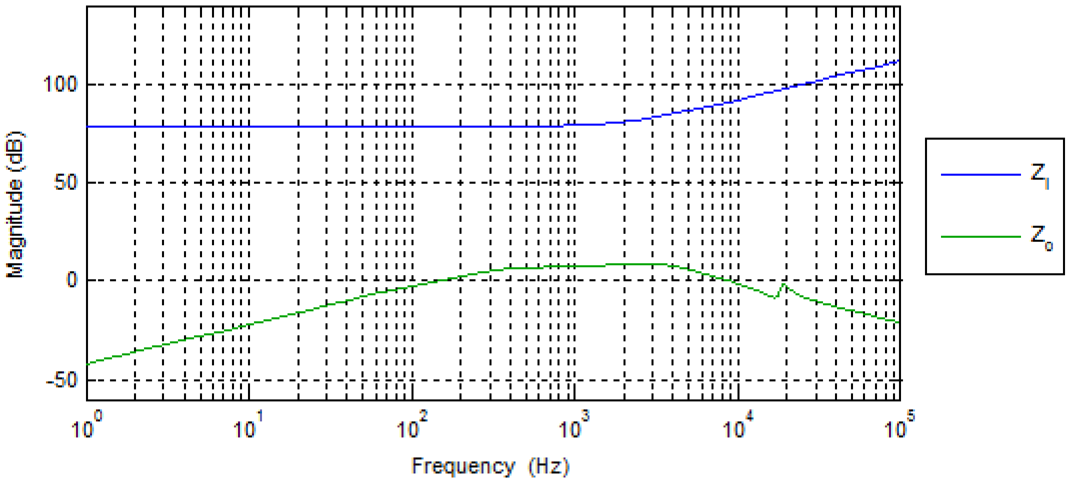

Fig. 4.25. Impedance comparison with ω=100 rpm, T_L=-2.5 N·m.

From the study of the magnitude representation of the output impedance of the BBCOF and the input impedance of the PMSM drive, it is possible to observe that for all the operating points the following condition is true

$$|Z_o| \ll |Z_i|, \tag{4.57}$$

and thus the Middlebrook criterion is accomplished. Furthermore, the results for the selected operating points can be extended to the whole driving profile, and ensure that the designed system is stable. However, it can be noticed that the operating point at which the modulus of the two impedances is closer coincides with the step-up operation of the BBCOF at nominal conditions. This fact is in good agreement with the stability analysis of chapter 2, as stability problems raised during step-up operation, and the CPL equivalent resistance value decreases and is nearer to the aggregate resistance value when the power increases.

4.5 Implementation of the ring-configuration interleaving

The interleaved system presented in this thesis consists of three BBCOF with the characteristics of Table 2.II, connected as depicted in Fig. 4.26. The 200 V voltage source is the same for all the BBCOFs, as well as the load. Note that the voltage is sensed by means of two voltage dividers, one in the power circuit, with resistances R1 to R4, and the other one in the control circuit of Fig. 4.27, with resistances R40 to R42. The voltage gain obtained with this design is 1/110. Then, the output voltage reference value, which can be adjusted by means of R45 potentiometer, is subtracted to the sensed voltage with the 1/110 gain. The control circuit is unipolar and fed with 5 V. Consequently, a null voltage error has to be centred at 2.5 V, so this voltage is added with the operational amplifier (OA) OA3, the same used to calculate the voltage error. This resulting voltage is the input of the PI with additional pole controller, and its output is the current reference. The current reference in a regenerative braking event is limited with the Z1 zener, in order to avoid voltage overshoots when changing from step-up to step-down operation.

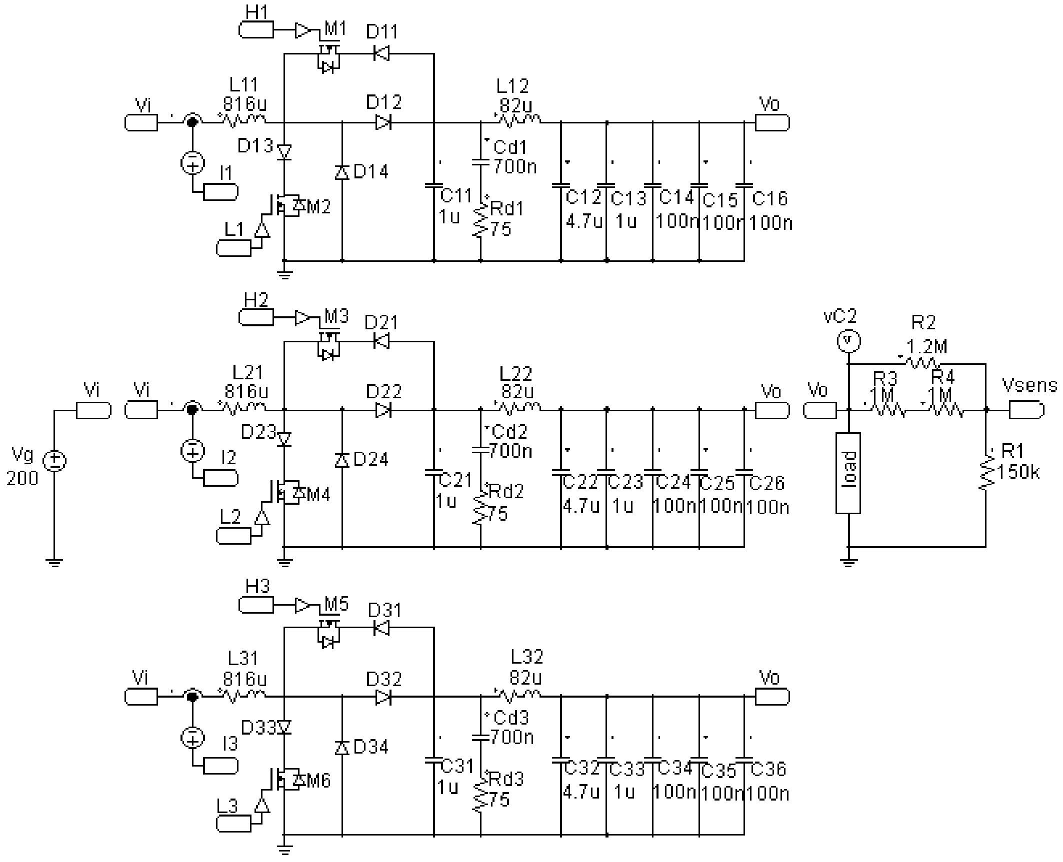

Fig. 4.26. Schematic of the three interleaved BBCOFs.

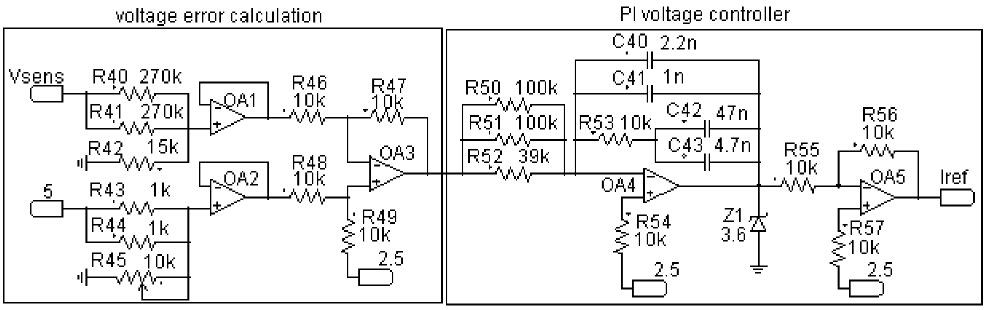

Fig. 4.27. Output voltage controller of the three BBCOFs.

The ring sliding-mode controller is represented in Fig. 4.28. As aforementioned, to obtain the hysteresis margins for one converter the continuous part of the current reference is added to the AC part of the current of the previous converter. This value is used as the high margin value. The difference between the high and the low margin is determined by the threshold voltage of the diode. The sensed current of the converter is compared to these hysteresis margins, and an SR flip-flop is used to obtain the gating signals for the MOSFETs.

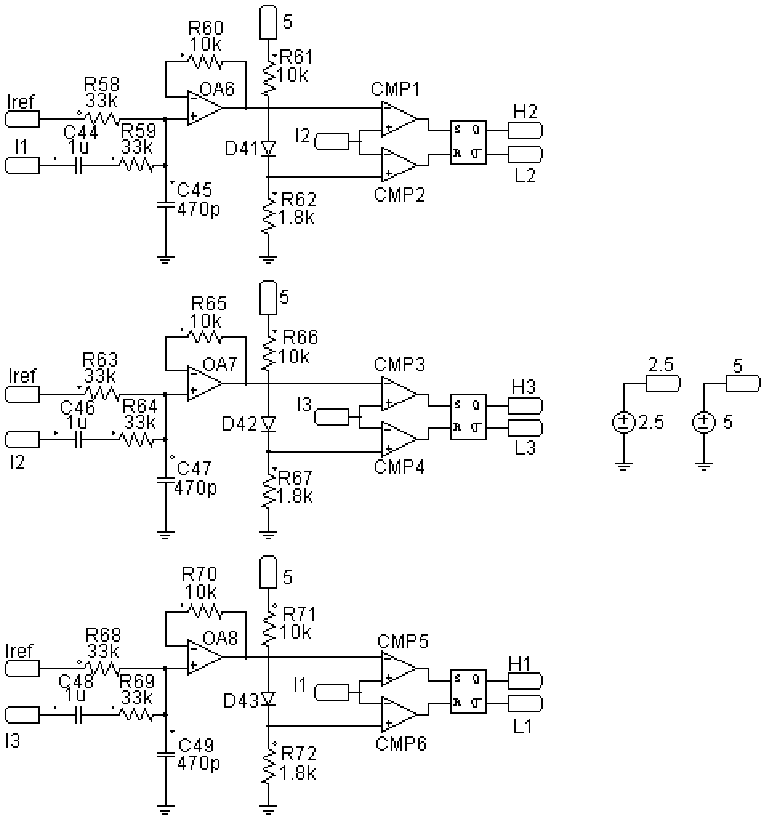

Fig. 4.28. Ring configuration of sliding-mode controller for three BBCOFs.

4.5.1 Verification of the reachability conditions

Once the circuits for voltage and current control of the interleaved BBCOFs have been designed, it is time to verify that the reachability conditions are satisfied during the system start-up, and thus the sliding regime eventually starts. The first reachability condition, (4.17), can be rewritten to obtain the condition for the input voltage as follows

$$v_g(t) > -\frac{L_1}{k_{sens}}\frac{1}{\tau}z_j(t) \tag{4.58}$$

As the control circuit has an unipolar supply of 5 V, the value of the signal $z_j(t)$ will be comprised between 0 and 5V. Therefore, for the worst case, corresponding to $z_j(t)=0$ V, the input voltage of the converter has to accomplish

$$v_g(t) > 0 \tag{4.59}$$

As the input voltage of the converter will be always positive, the first reachability condition is accomplished. The second reachability condition depends on the voltage of the C_1 capacitor of the converter itself and of the previous converter. These voltages might have slight variations, but the following approximation can be done

$$v_{C1,j-1}(t) \simeq v_{C1,j}(t), \tag{4.60}$$

and then the condition is simplified to

$$\frac{d}{dt}s_j(t) = \frac{-1}{2}\frac{k_{sens}}{L_1}v_g(t) + \frac{1}{2}\frac{k_{sens}}{L_1}v_{C1,j}(t) - \frac{1}{2\tau}z_j(t) > 0 \tag{4.61}$$

Therefore, there will be an attraction to the sliding domain when the value of the C_1 capacitor satisfies the following inequality

$$v_{C1,j}(t) > \frac{L_1}{k_{sens}\tau}z_j(t) + v_g(t) \tag{4.62}$$

At the worst case for this condition, the value of the current ripple signal will be $z_j(t)=5$ V. Then, considering the design values of the converter and the controller, the previous expression can be evaluated as

$$v_{C1,j}(t) > v_g(t) + 1.34\,V \tag{4.63}$$

Consequently, when the voltage of the capacitor reaches a value over $v_g(t)$ plus 1.34 V, the dynamics of the system will be attracted to the sliding surface, as depicted previously in Fig. 3.3.

4.6 Simulation results

In order to validate that the system previously described and analysed effectively work in interleaving, the system described in section 4.3 has been simulated with a resistive load in PSIM. In chapter 5 the interleaved converters are simulated with the powertrain setup, and experimental results are also obtained.

The load for this resistive-load simulation is a parallel connection of six legs, where each leg has two lamps connected in series. The lamps have an approximate resistance of 102 Ω once turned on. The disposition of the lamps, together with the second voltage divider to sense the output voltage, is represented in Fig. 4.29.

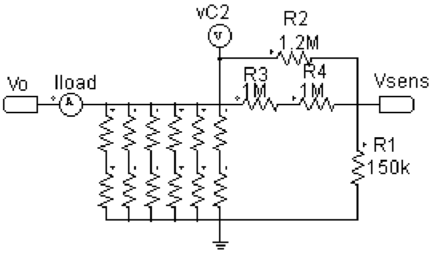

Fig. 4.29. Lamps with sensing stage for interleaving simulation.

The waveforms of the output voltage and the input currents of the BBCOFs are represented in Fig. 4.30. The output voltage is regulated at 350 V, and a transient the sliding motion appears in the currents of the converters. Fig. 4.31 is a close-up of this start-up, where the attraction to the sliding domain and the eventual displacement of the currents can be observed.

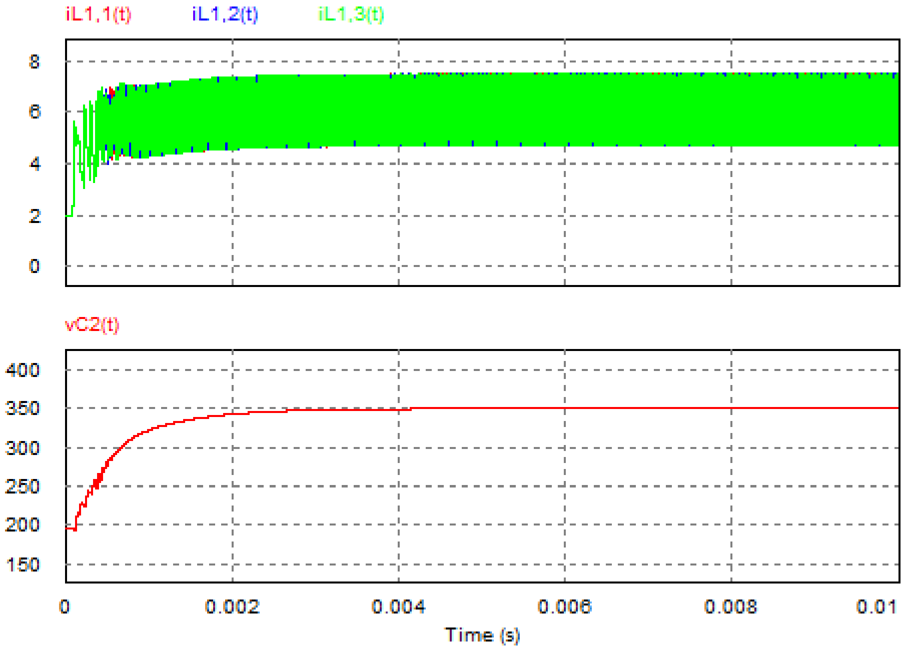

Fig. 4.30. Output voltage and input currents of three interleaved BBCOFs simulated with PSIM.

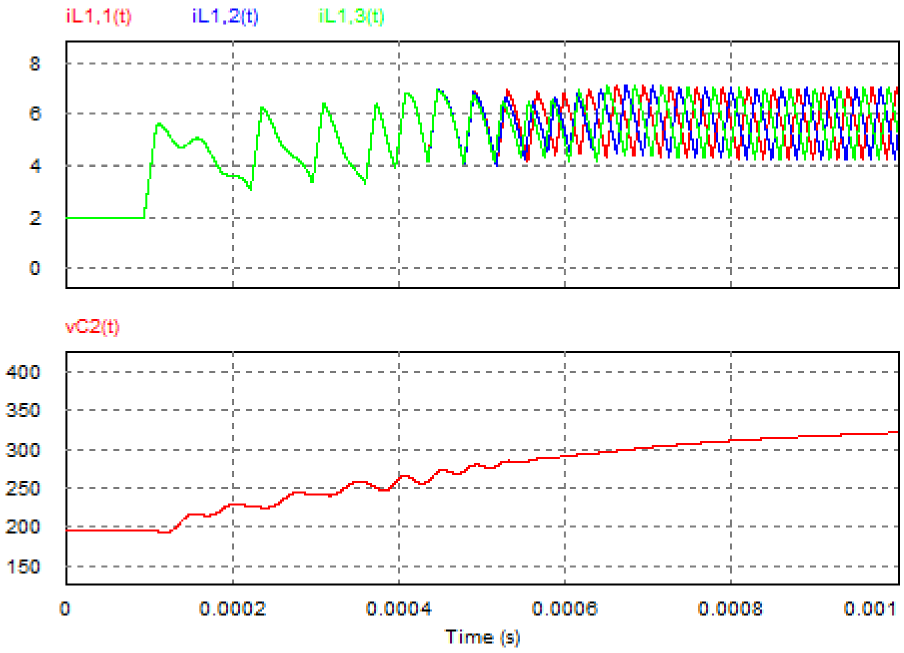

Fig. 4.31. Start-up transient of the three interleaved BBCOFs.

The mean and ripple values at steady state have been represented in Fig. 4.32. The mean value of the output voltage is 350.19 V, and the peak ripple is 6.36 mV, which supposes a 0.0018 %. Note that the ripple has been strongly reduced by interleaving respect to the results of chapter 2. The mean value of the input current is 6.12 A. As the input voltage of the converters is 200 V, the power consumed by each converter is 1.224 kW. The hysteresis margins have been adjusted to obtain a switching frequency of 40 kHz at steady state, and then the current peak ripple is 1.37 A, approximately the same that in chapter 2.

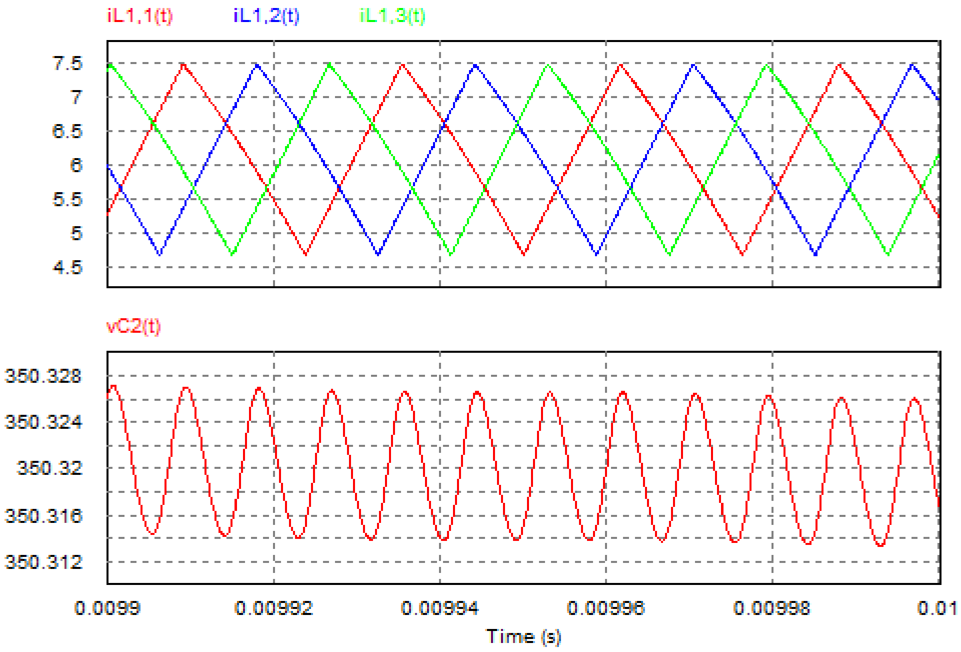

Fig. 4.32. Output voltage and input current ripples at steady state.

4.7 Experimental results

The experiment has been performed with the same system parameters used in the previous section, i.e. three interleaved BBCOFs with twelve lamps connected as defined in Fig. 4.29. The obtained waveforms of the output voltage and input currents are reproduced in Fig. 4.33. The three converters are working in interleaving, but in contrast to the simulation results, the average current has different values for each converter. The difference comes from the irregularity of component values and the wires used for connection. These small unbalancing prevents the interleaving system to fully cancel the third harmonic in the output, and thus the resulting output ripple is considerably higher (94.37 mV) than the 6.36 mV of the simulation results. On average, each converter consumes 1.259 kW. There is a difference of 35 W between the simulation and experimental results, which is due to the losses.

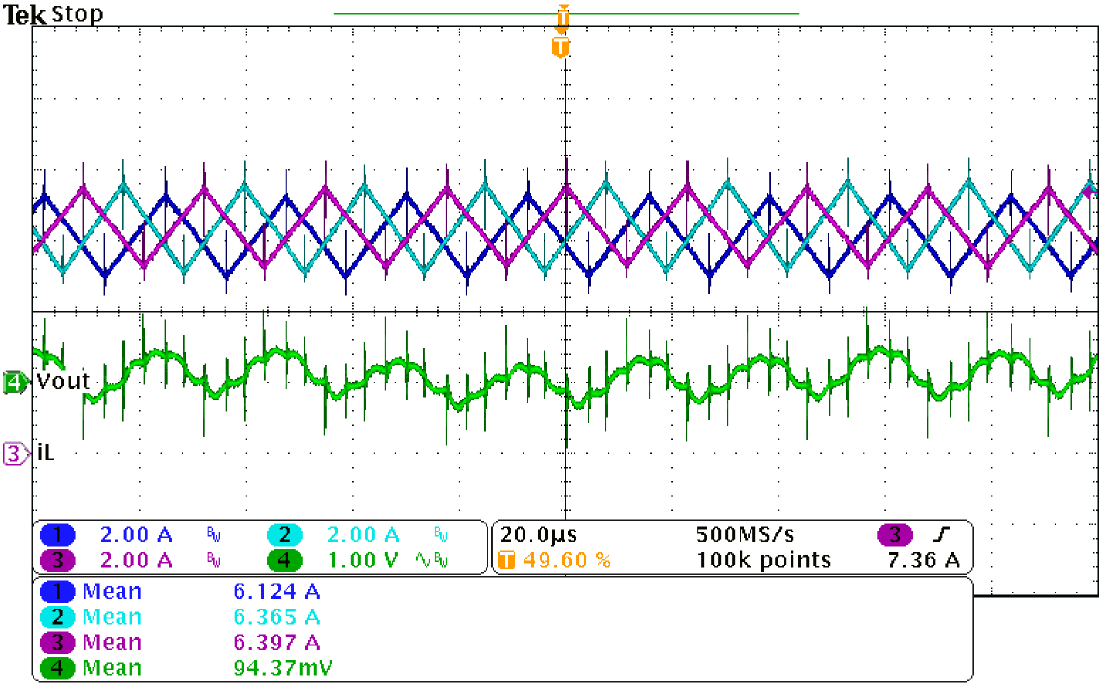

Fig. 4.33. Waveforms of the output voltage and input currents for the interleaved system obtained experimentally.

4.8 Conclusions

At the start of the chapter, interleaving is presented as a solution to effectively increase the power rating of the system by connecting several converters in parallel, apart from offering enhanced switching ripple features. A ring configuration is chosen, analysed and demonstrated to be stable for the BBCOF with the RC snubber.

The capacitors of the BBCOF have been designed for a system of three interleaved converters of 1.5 kW each one. The specification is to have the resonance peak below 0 dB. With this design of BBCOF, the output impedance of the converter has been compared to the input impedance of the PMSM drive. As the input impedance of the motor drive is greater than the output impedance of the BCCOF for any frequency, the Middlebrook criterion is accomplished. Consequently, the connection of the PMSM drive does not cause instability to the BBCOF.

UNIVERSITAT ROVIRA I VIRGILI
DESIGN AND CONTROL OF A BIDIRECTIONAL DC/DC CONVERTER FOR AN ELECTRIC VEHICLE APPLICATION.
Laura Albiol Rendillo
Dipòsit Legal: T 1361-2015

Finally, an analogue circuit performing the analogue interleaved control has been proposed, simulated and experimentally tested. Results show the correct operation of the system, and verify the power ratio increase and ripple reduction that lead to the adoption of the ring-configuration interleaving for BBCOF.

5 EV traction system emulation

5.1 System description

The 4.5 kW platform that emulates the powertrain of an electric vehicle is represented in Fig. 5.1. The traction part of the system is fed with a DC source, with a nominal value of 200 V. This voltage is elevated to 350 V by means of a DC/DC system, which is composed of three BBCOFs in interleaving configuration and their respective control, as seen in Chapter 4. The traction motor is a PMSM, model LSRPM100L, controlled by the Unidrive SP2202 inverter. The traction motor is mechanically coupled to the machine that emulates the load of the traction motor, a PMSM model LSR90SL. Consequently, this load machine has to be able to absorb energy during most part of the operation, but also to deliver energy in case of regenerative braking, or even downhill climbing. The bidirectional power flow is allowed by means of the back-to-back connection of the two Unidrive SP1405 inverters. During motoring operation, the load motor controlled by its inverter (Unidrive SP1405 #1) forces a resistant torque to the traction motor. The inverter is fed from the three-phase electric power, and the voltage is rectified by Unidrive SP1405 #2 inverter. Otherwise, during regenerative braking the load motor forces a torque with the same direction that the torque generated by traction motor, and this provokes the energy recovery. The voltage in the phases of the load motor is rectified by Unidrive SP1405 #1, and later inverted respecting the frequency and phase of the three-phase electric power supply with Unidrive SP1405 #2. The regenerative inductances absorb the voltage differences between the PWM output of Unidrive SP1405 #2 and the sinusoidal voltage in the three-phase power supply [81]. A switching frequency filter and an EMC filter have also been included.

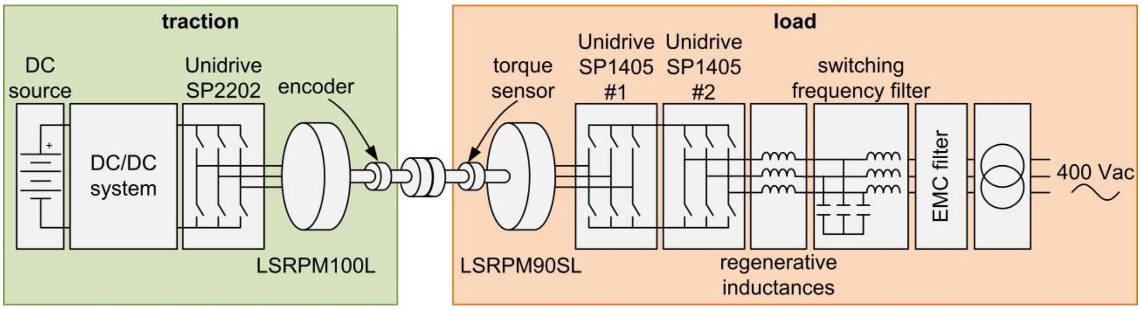

Fig. 5.1. 4.5 kW platform for experimental purposes.

5.2 Simulink model

5.2.1 Description of the system model

The EV traction system emulation previously described has been modelled with Simulink. The general view of this model is reproduced in Fig. 5.2. In the model it is possible to distinguish the traction and the load drives, as well as the driving profile references, a visualization interface and three blocks to convert the mechanical torque to electrical torque and vice-versa.

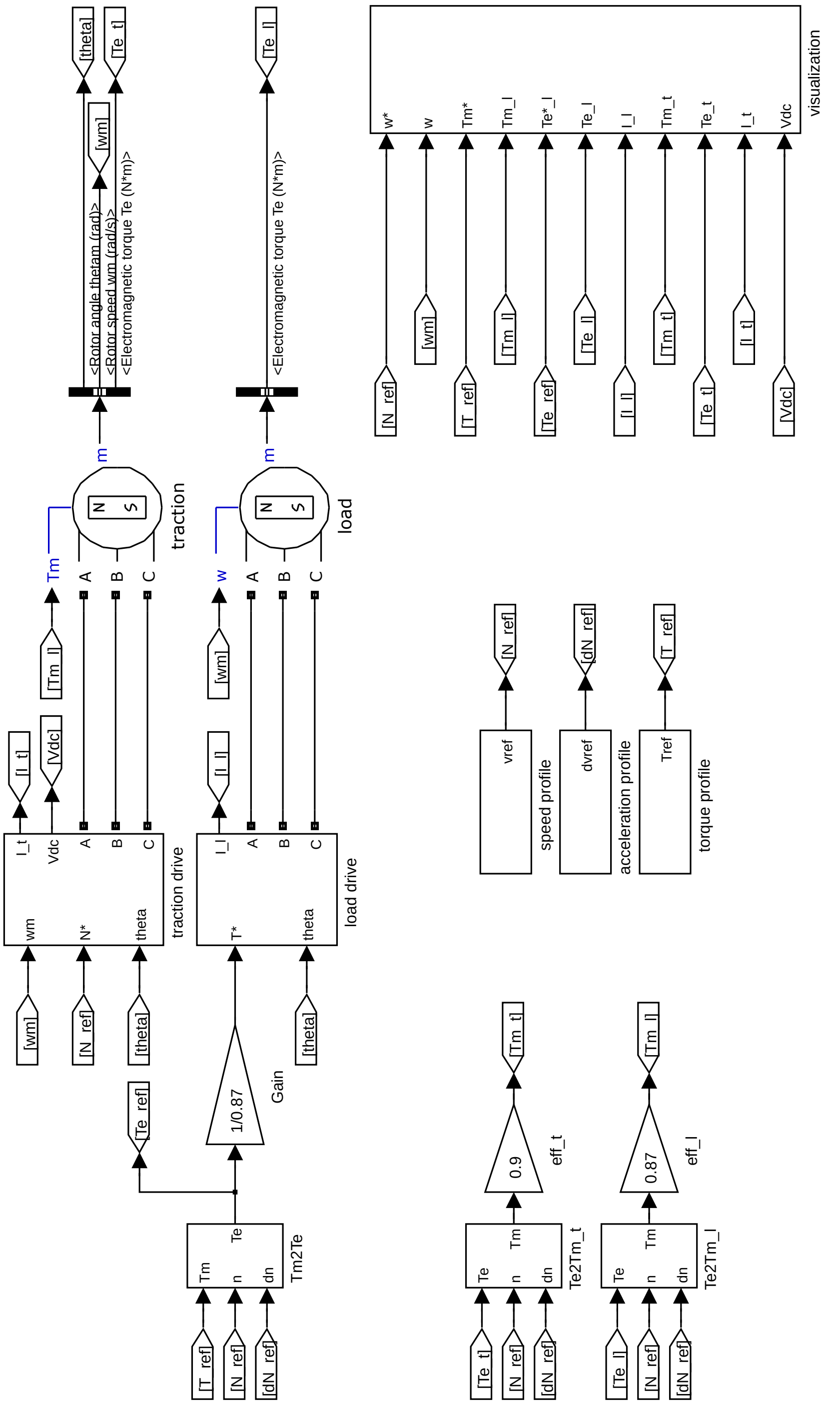

Fig. 5.2. View of the complete model of the EV traction system in Simulink.

In order to clarify the model explanation, the hierarchy of the most relevant subsystems that constitute the EV traction system model is detailed in Table 5.I., and a Hierarchy Reference (HR) is assigned.

Table 5.I. Hierarchy of the Simulink model.

HR	subsystem
1	traction drive
1.1	traction motor control
1.2	traction inverter
1.2.1	DC/DC stage
1.2.1.1	BBCOF
1.2.1.2	ring SMC
1.2.1.2.1	hyst
1.2.1.2.2	SMC
2	load drive
2.1	load inverter

The traction drive in Fig. 5.3 (HR 1) includes the traction inverter and its control. The traction motor control (HR 1.1) is a two-loop cascaded control, as shown in Fig. 5.4. The outer loop is a speed controller, whereas the input loop is a vector torque controller. The vector torque controller generates the gate signals for the traction inverter.

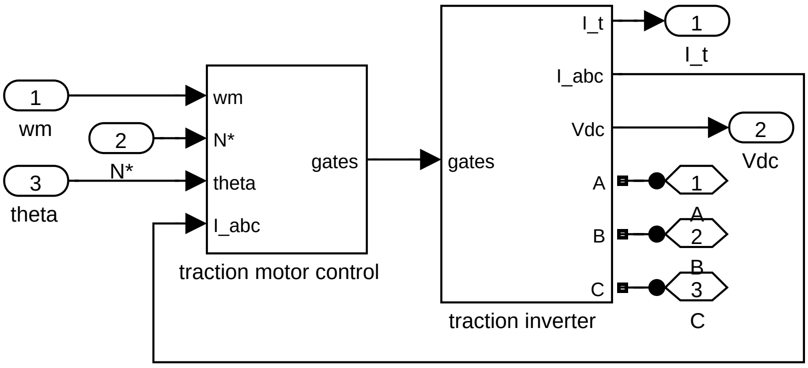

Fig. 5.3. Traction drive subsystem (HR 1).

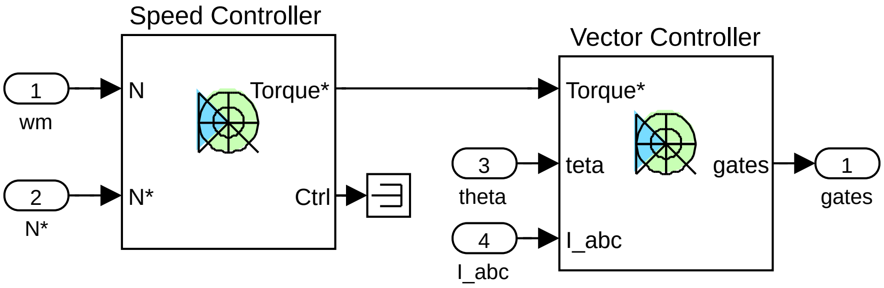

Fig. 5.4. Traction motor control subsystem (HR 1.1).

The traction inverter (HR 1.2) depicted in Fig. 5.5 contains the DC source, the DC/DC stage and the inverter. The rest of the blocks are measuring elements for the current in the phases of the motor and the filtered current of the DC bus.

UNIVERSITAT ROVIRA I VIRGILI
DESIGN AND CONTROL OF A BIDIRECTIONAL DC/DC CONVERTER FOR AN ELECTRIC VEHICLE APPLICATION.
Laura Albiol Rendillo
Dipòsit Legal: T 1361-2015

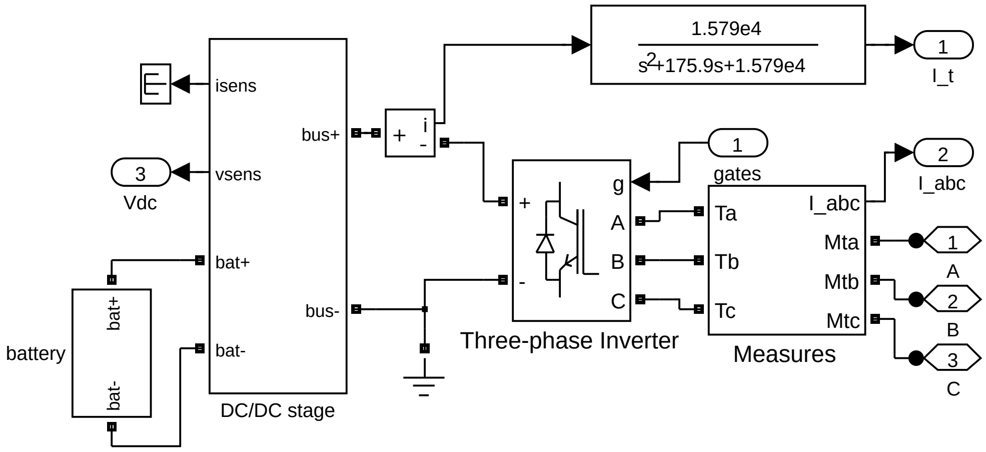

Fig. 5.5. Traction inverter subsystem (HR 1.2).

The so called DC/DC stage (HR 1.2.1) corresponds to the system proposed in chapter 4, i.e. three interleaved BBCOFs with ring-configuration sliding-mode control, as it can be appreciated in Fig. 5.6. The ring-configuration sliding-mode control generates the gating signals for the converters. The input of the converters is the DC source, and the output is the DC bus, where the load inverter is connected. The input current is sensed for each BBCOF, and sent to the sliding-mode controller. As the three BBCOFs are parallel-connected at their output, the output voltage is sensed only in the first BBCOF, the other ones are sent to terminator elements.

The implementation of the BBCOF subsystem (HR 1.2.1.1) with Simulink has been performed as reproduced in Fig. 5.7. The parasitic inductor resistances have been included in the simulation, as well as the characteristics of the MOSFETs and diodes provided by the manufacturers.

The ring SMC subsystem (HR 1.2.1.2) receives the sensed input current of each converter and the current reference from the output voltage control loop. The ring-configuration sliding-mode control is then divided in two types of subsystems. The function of the first one, hyst, is to calculate the hysteresis margins for the sliding-mode control of one converter from the sensed current of the previous converter and the current reference from the output voltage loop. The second one, SMC, generates the gating signals for each BBCOF from the sensed input current of that inverted and the calculated hysteresis margins.

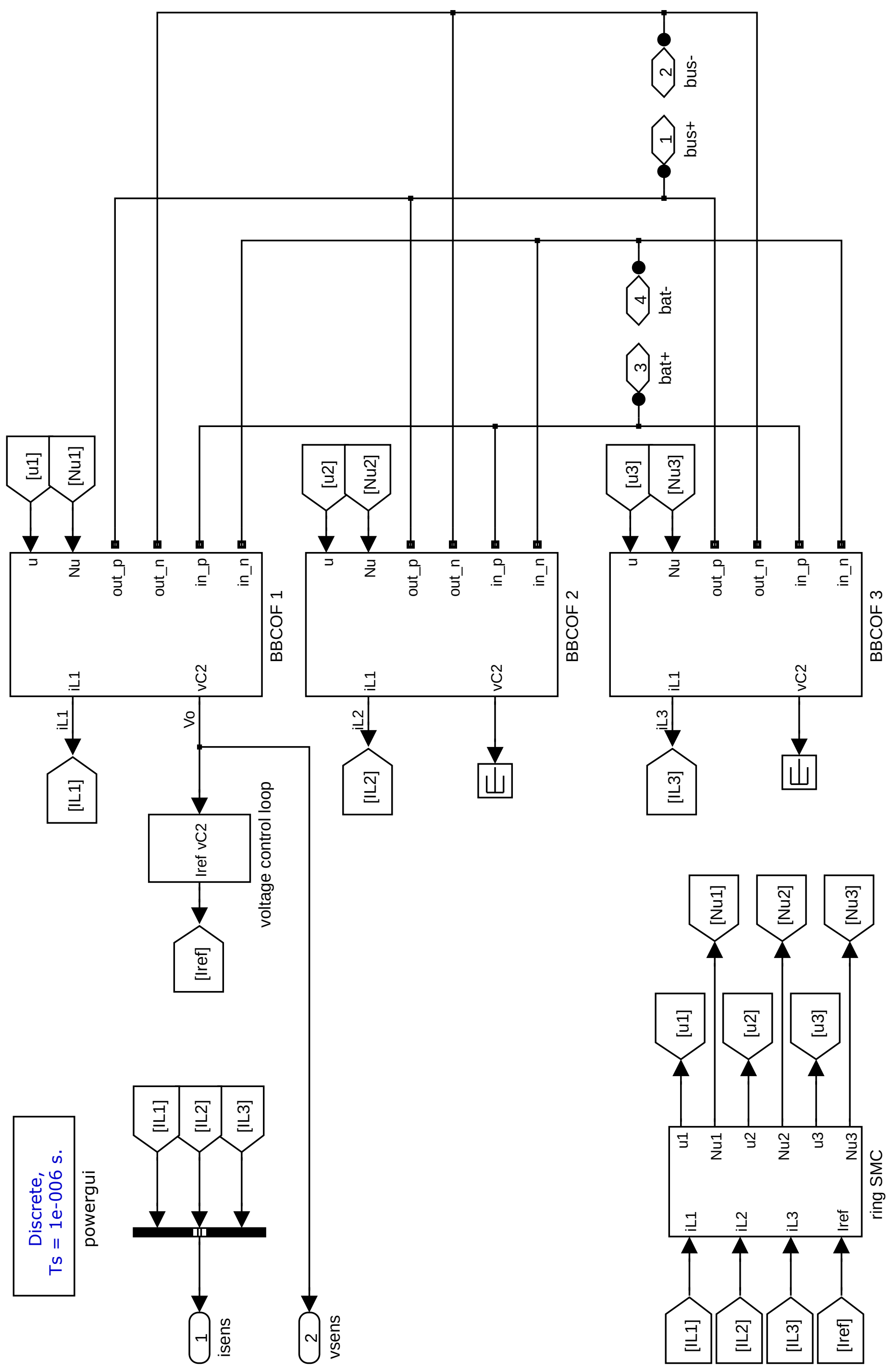

Fig. 5.6. DC/DC stage subsystem (HR 1.2.1).

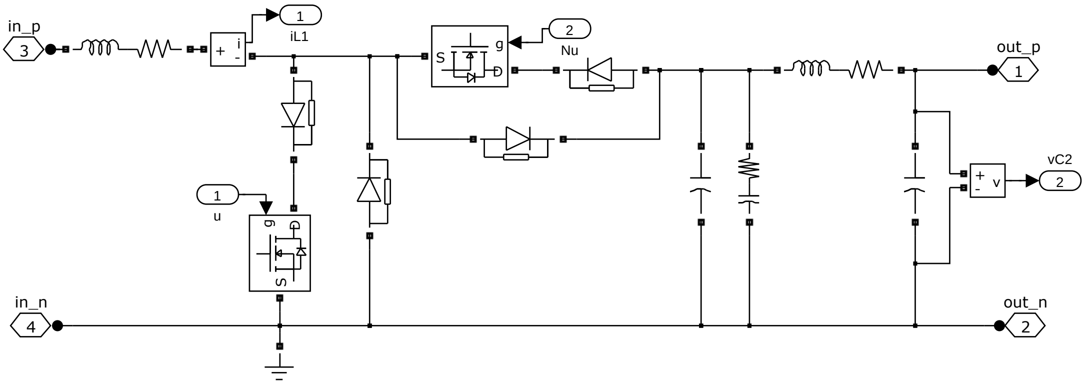

Fig. 5.7. BBCOF subsystem (HR 1.2.1.1).

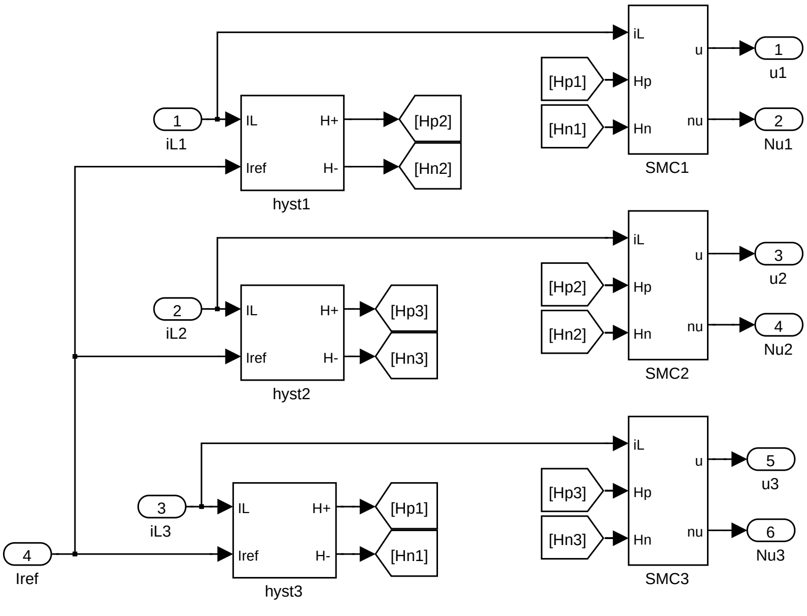

Fig. 5.8. Ring SMC subsystem (HR 1.2.1.2).

The hysteresis limits for the sliding mode controllers are obtained in the hyst subsystems (HR 1.2.1.2.1), represented in Fig. 5.9. The sensed current and the reference current are summed and then a 0.5 gain is applied, as in the analogue circuit proposed in chapter 4. A saturation block is introduced to consider the voltage limitation introduced by the 5 V unipolar excitation. The result is the high hysteresis margin. The low margin is obtained by subtracting a fixed value to the high margin, so that this value will determine the switching frequency at steady state.

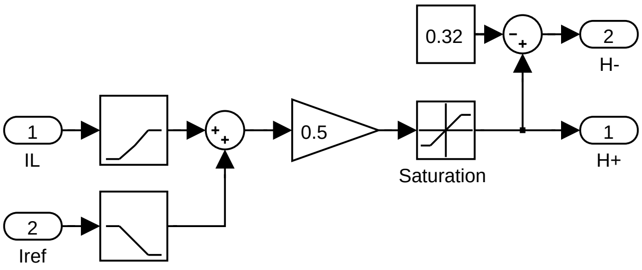

Fig. 5.9. Hyst subsystem (HR 1.2.1.2.1).

The block SMC (HR 1.2.1.2.2) performs the hysteretic switching, according to the received sensed current and the hysteresis margins, as seen in Fig. 5.10. An SR flip-flop is used as a memory element to generate the gating signals for the MOSFETs of the converters.

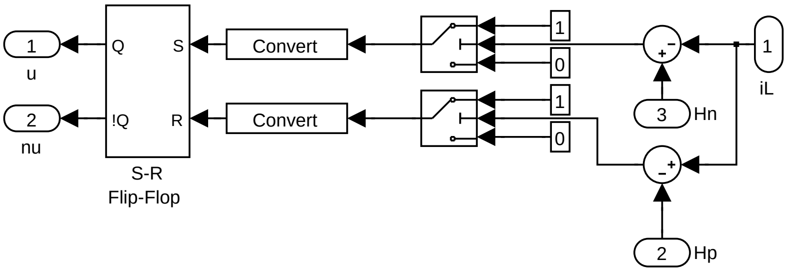

Fig. 5.10. SMC subsystem (HR 1.2.1.2.2).

The load drive (HR 2) only has a torque control loop, performed by means of a vector controller. The subsystem, represented in Fig. 5.11, contains this vector controller and the load inverter.

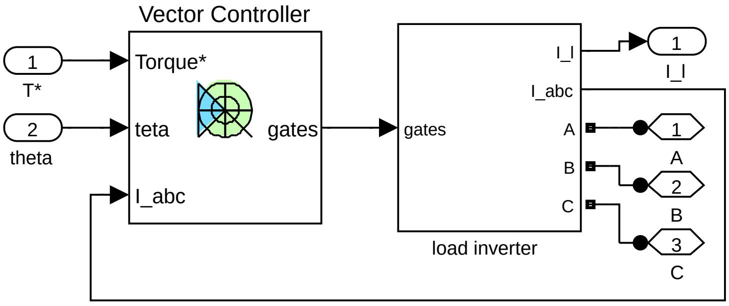

Fig. 5.11. Load drive subsystem (HR 2).

The load inverter (HR 2.1) has been simulated by a three-phase inverter connected to a DC source. This DC voltage source corresponds to the DC bus between the two back-to-back converters of the load part of the system. As this voltage is well regulated, simulating the grid-connected inverter is not relevant from the studied system point of view, and the power-absorption capability has been reproduced by connecting a resistor in parallel with the DC source, as shown in Fig. 5.12.

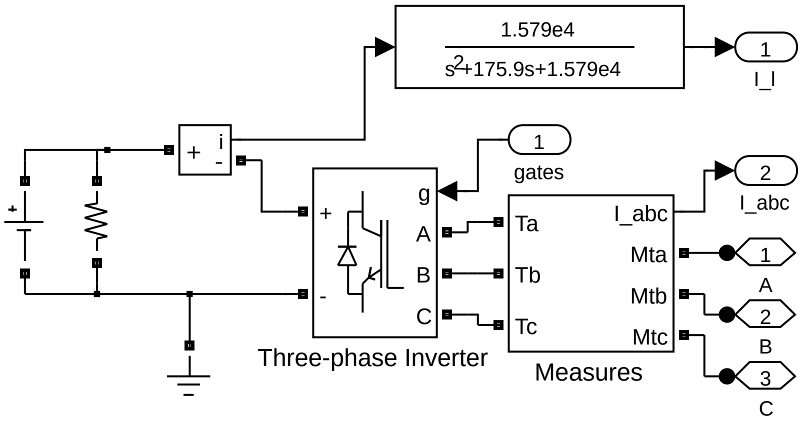

Fig. 5.12. Load inverter subsystem (HR 2.1).

5.2.2 Simulation results

For the simulation, the driving profile shown in Fig. 5.13 has been considered. This profile has been designed in order to include both traction and regenerative braking operations within a limited amount of time. The simulation is time and memory consuming as the simulated converters are not averaged but circuital models are used, and longer profiles could not be applied.

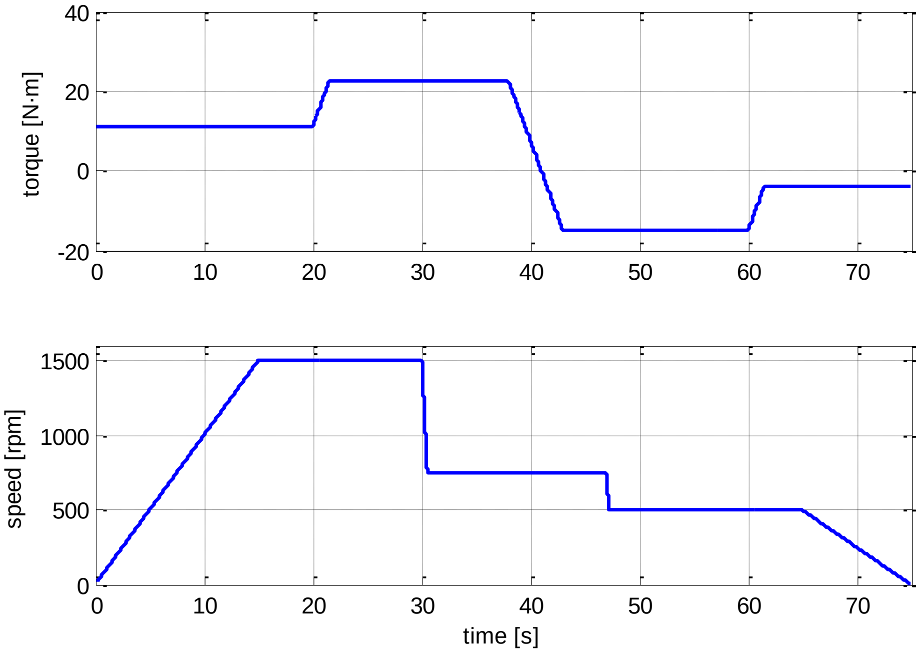

Fig. 5.13. Torque and speed profile for the load and traction motor, respectively.

As it can be seen from the chosen driving profile, the motor starts from standstill and constantly accelerates until reaching a steady speed of 1500 rpm. During all this time the applied torque is constant. Once the motor has been rotating at 1500 rpm for several seconds, the load torque is doubled, requiring a considerable increase of delivered power. At instant t=30 s the speed is rapidly reduced, and 10.5 s later the load becomes negative, and so regenerative braking should occur. During this period of energy recovery the reference speed is decreased again. Finally a null load torque is applied, and shortly later the speed is constantly decreased until reaching standstill again.

The current values of mechanical torque and speed obtained by simulation are shown in Fig. 5.14 and Fig. 5.15, respectively. It can be appreciated that both the torque and the speed closely follow their reference, and thus the speed control for the traction motor and the torque control for both the traction and load motor has been correctly modelled.

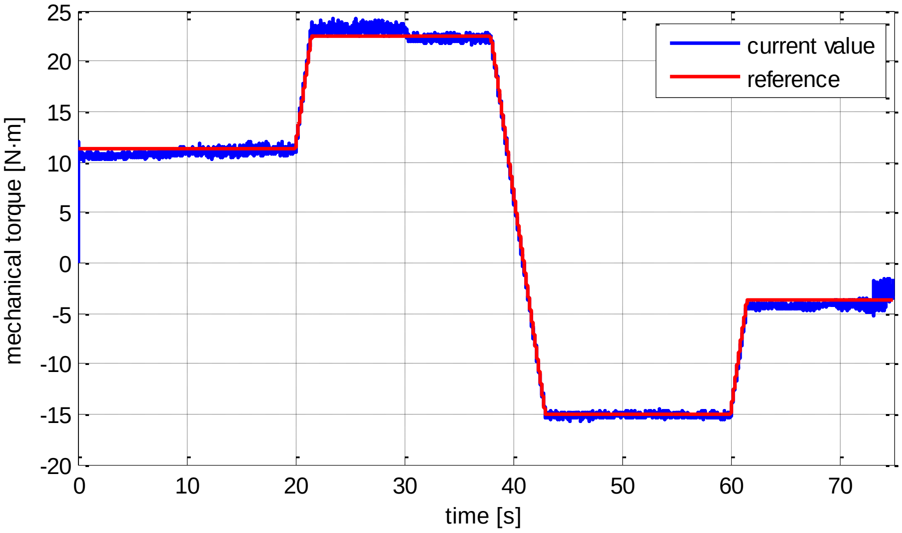

Fig. 5.14. Reference and real mechanical torque obtained by simulation.

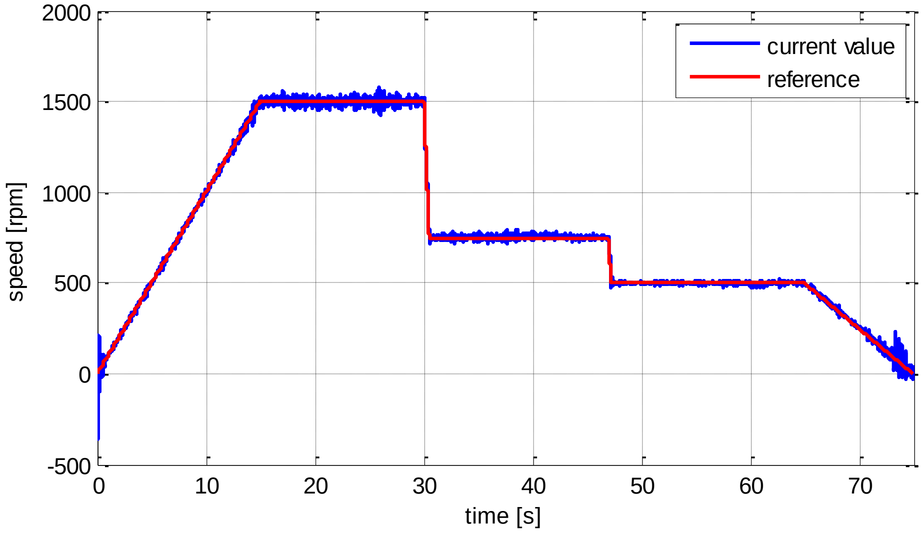

Fig. 5.15. Reference and real speed obtained by simulation.

Fig. 5.16 reproduces the current drawn by the traction motor during the driving profile, or equivalently, the current supplied by the BBCOFs. Note that during regenerative braking the current is negative. This means that energy is being recovered from the traction motor and transferred to the DC source by the BBCOFs. Therefore, these results validate the correct operation of the designed converters under sliding-mode control working in interleaving. Moreover, it can be observed in Fig. 5.17 that the ripple in the DC bus is maintained low during the whole driving profile.

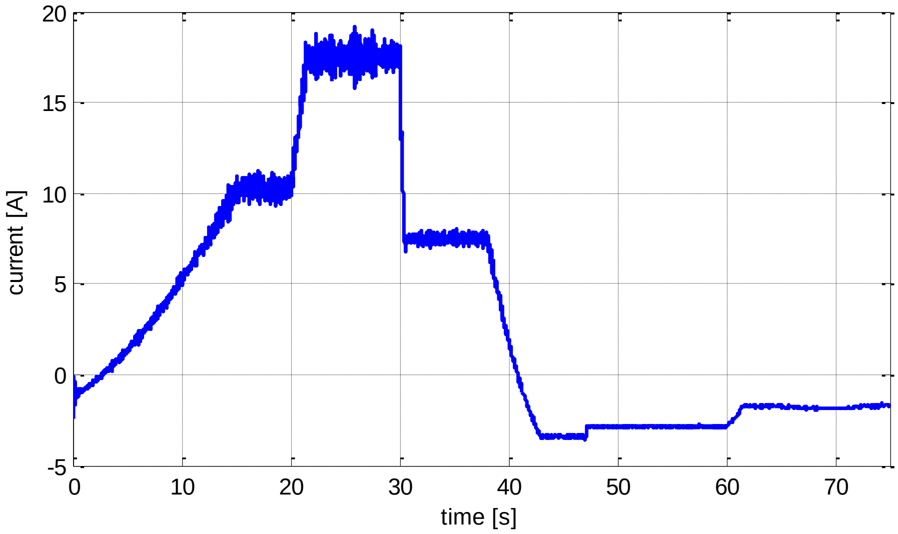

Fig. 5.16. Current consumed by the traction motor obtained by simulation.

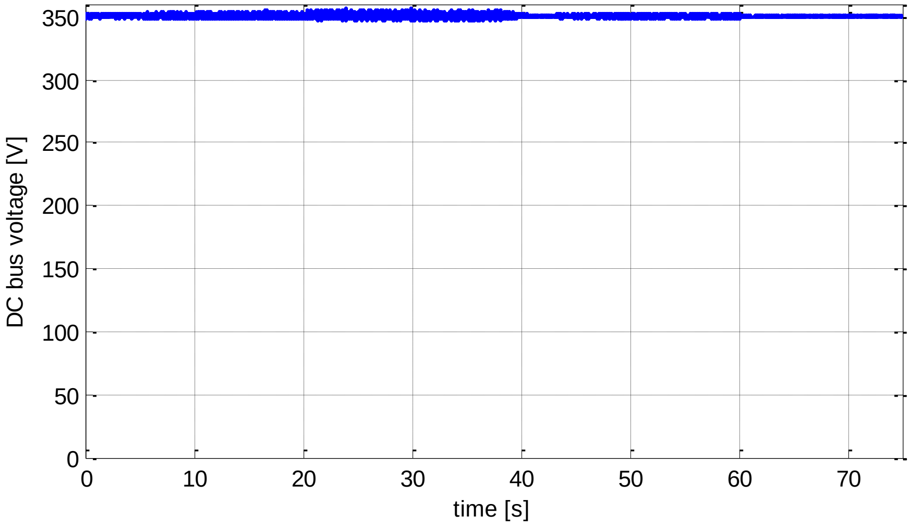

Fig. 5.17. DC bus voltage obtained by simulation.

5.3 Experimental EV traction system emulation

5.3.1 Description of the set-up

In order to test the design of the BBCOFs and their interleaved SMC, the system described in section 5.1 is used. As the DC input element used is not a battery but a DC source, it is necessary to introduce an electronic load to the system in order to absorb the recovered energy during the regenerative braking, as depicted in Fig. 5.18. Then, the adopted solution consists on connecting an electronic load (in this case an EA-EL 9750-75 HP) in parallel with a DC voltage source (Delta Elektronika SM 300-20), named DC source 1 in the figure. The DC source is set to work in current control mode, so it delivers power both to the BBCOFs and the electronic load. When regenerative braking occurs, the recovered current is injected to the electronic load, and hence the DC source delivers no power to the BBCOF and less power to the electronic load. The DC source is protected with a diode to ensure that it is not damaged.

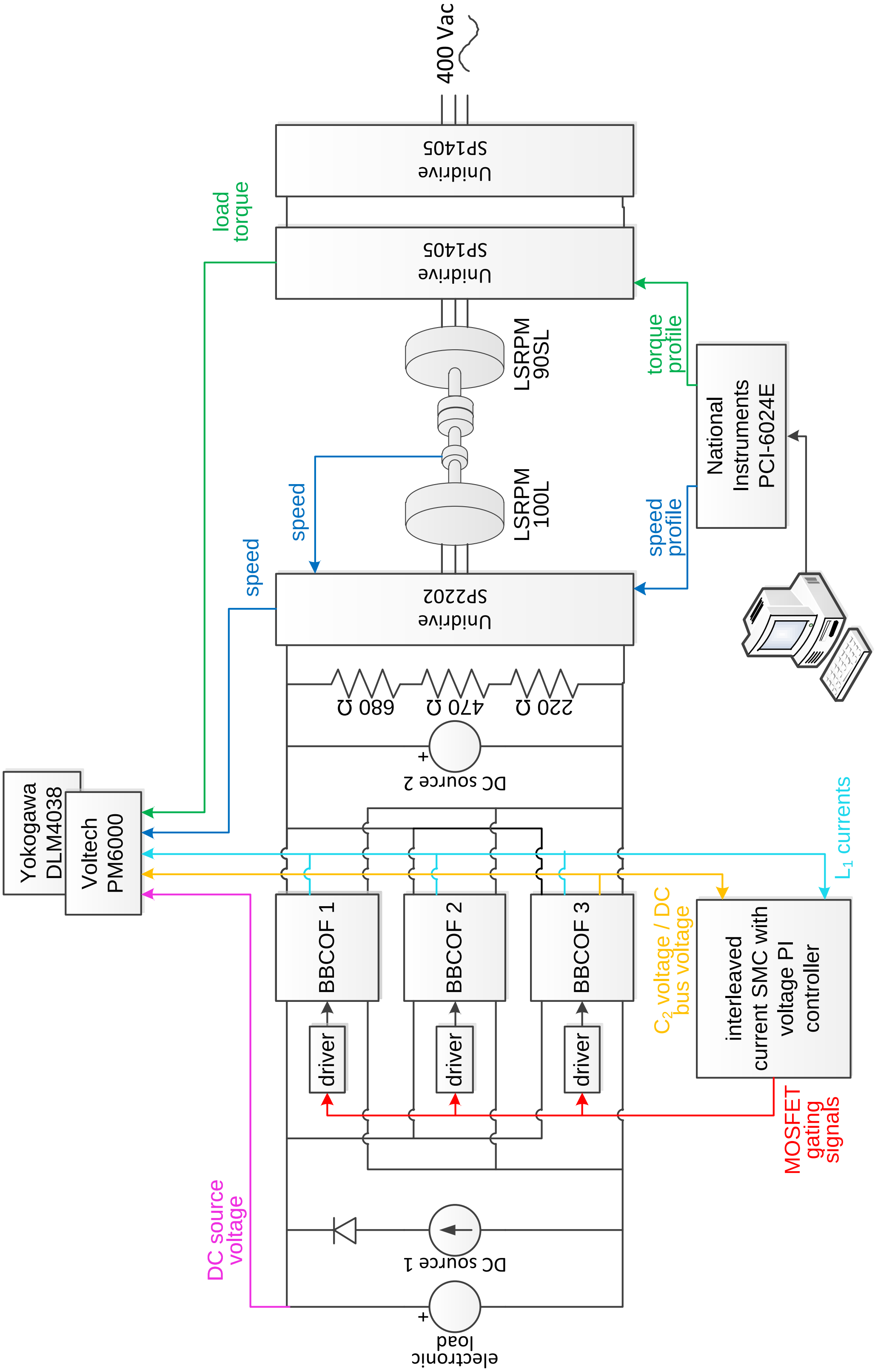

Fig. 5.18. Set-up of the experimental traction system emulator.

The three BBCOFs are connected in parallel, as shown in Fig. 5.19. The sensed input currents from all the converters and the sensed C_2 voltage from one of them are sent to the control board seen in Fig. 5.20, which performs the PI voltage control and the interleaved sliding-mode

UNIVERSITAT ROVIRA I VIRGILI
DESIGN AND CONTROL OF A BIDIRECTIONAL DC/DC CONVERTER FOR AN ELECTRIC VEHICLE APPLICATION.
Laura Albiol Rendillo
Dipòsit Legal: T 1361-2015

current control. As a result, the gating signals for the MOSFETs are obtained and sent to their corresponding IR2110 driver.

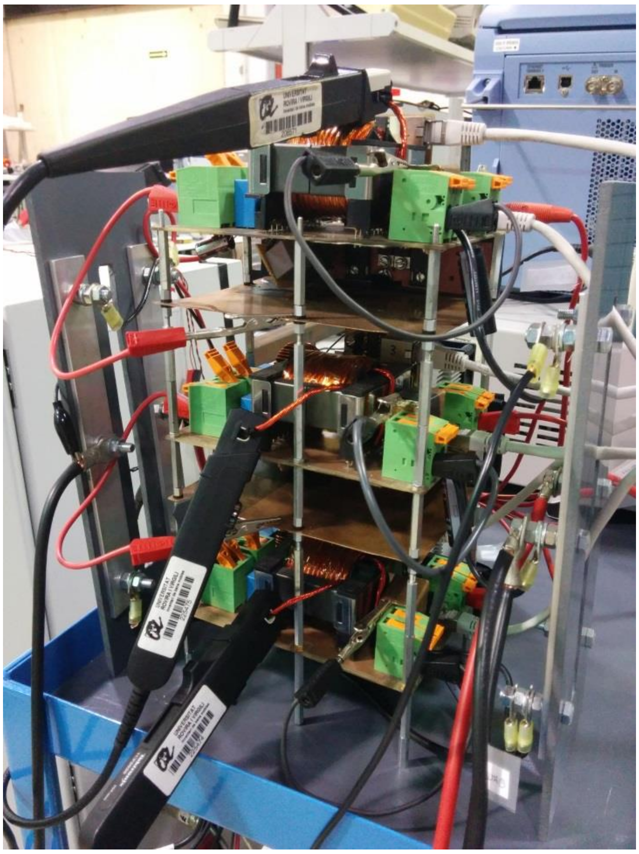

Fig. 5.19. Detailed view of the three BBCOFs connected in parallel with the current probes used for the oscilloscope results.

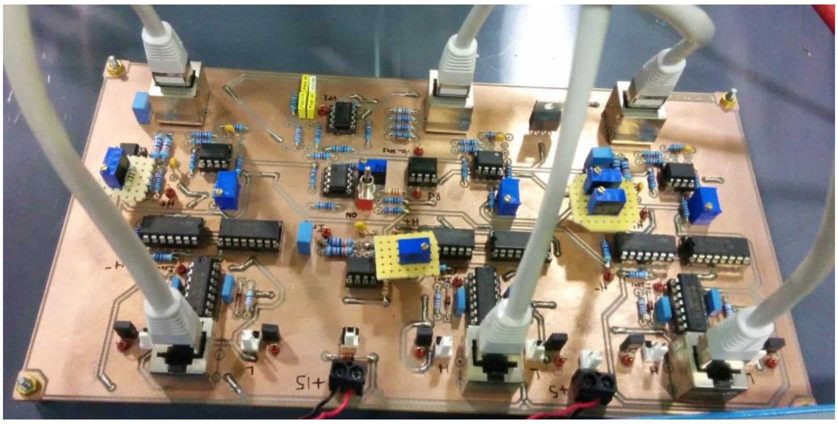

Fig. 5.20. Detailed view of the control board.

As shown in Fig. 5.1, two PMSM are mechanically coupled. The first one, LSRPM100L, is a 4.5 kW machine that is part of the EV emulator powertrain. The other one, LSRPM90SL, is a 3 kW machine that sets a determinate load to the traction motor. Therefore, the load motor has a torque control, which regulates the load torque applied to the traction motor. The traction motor has an outer speed loop control and an inner torque loop. Thus, it is necessary to establish references for the load torque and the speed of the whole powertrain. These references are provided by means of two profiles created with Matlab/Simulink and sent to the inverters using a PCI-6024E Texas Instruments digital acquisition board. The speed is sensed by means of an encoder and sent to the inverter.

Fig. 5.21. Detailed view of the two mechanically coupled PMSMs.

The inverter for the traction machine is a Unidrive SP2202. As it is an industrial inverter, it has an undervoltage relay protection. In this case, it means that if the voltage is lower than 280 V the inverter is inactive, and so no load is applied to the BBCOFs. Consequently, it is not possible to start the system without providing a bus voltage above this value. The solution has been connecting a second DC source (an Amrel SPS800X13-K02D), named DC source 2, configured to work in voltage control mode and feed 340 V, a voltage rating that is 10 V below the desired DC bus voltage. As a consequence, this source will only deliver power when the BBCOFs are not operating. Once they have started up, the voltage in the bus is higher than the configured current rating, and thus no current circulates. The three inverters with their filters and protections are mounted in the steel enclosure shown in Fig. 5.22.

Moreover, a resistive load has been connected in parallel to the inverter, which ensures that the BBCOFs are not unloaded in case of inverter failure and disconnecton. A total resistance of 1.37 kΩ is inserted with the series connection of 680, 470 and 220 Ω resistors. The DC bus has a regulated voltage of 350 V, so the resistors provide an additional power consumption of 90 W to the system, once the system has started up.

Both the Voltech PM6000 power analyser and the Yokogawa DLM4038 oscilloscope are used to register the most relevant signals of the system, which are the DC source voltage, the DC bus voltage (which is the voltage in the C_2 capacitors of the BBCOFs), the input currents of the BBCOFs, the speed of the PMSMs and the torque of the load PMSM. Both the torque and the speed are read from the analogue outputs available in the inverters, and scaled appropriately in the measuring devices, namely the power analyser and the oscilloscope.

UNIVERSITAT ROVIRA I VIRGILI
DESIGN AND CONTROL OF A BIDIRECTIONAL DC/DC CONVERTER FOR AN ELECTRIC VEHICLE APPLICATION.
Laura Albiol Rendillo
Dipòsit Legal: T 1361-2015

Fig. 5.22. Steel enclosure with the inverters, filters and protections.

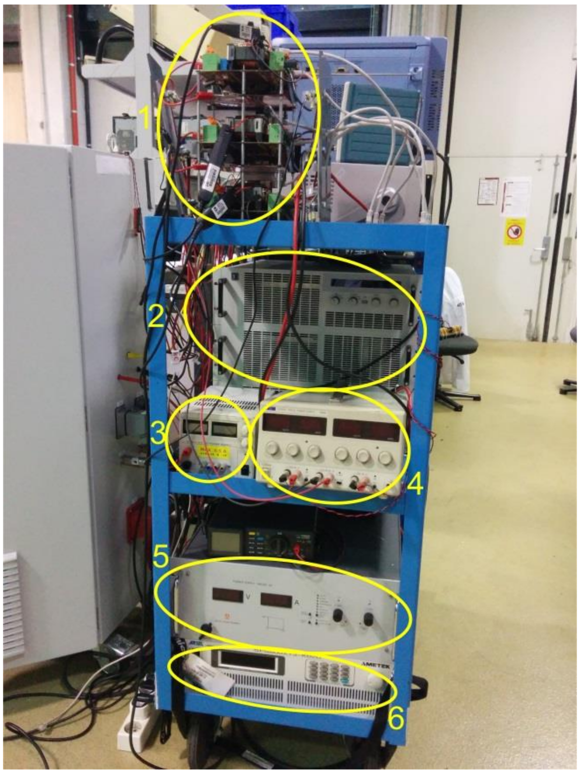

Fig. 5.23. Front view of the cart containing the three BBCOFs (1), the electronic load (2), a DC source for the cooling fans (3), a DC source for the control board (4), the DC source 1 (5) and the DC source 2 (6).

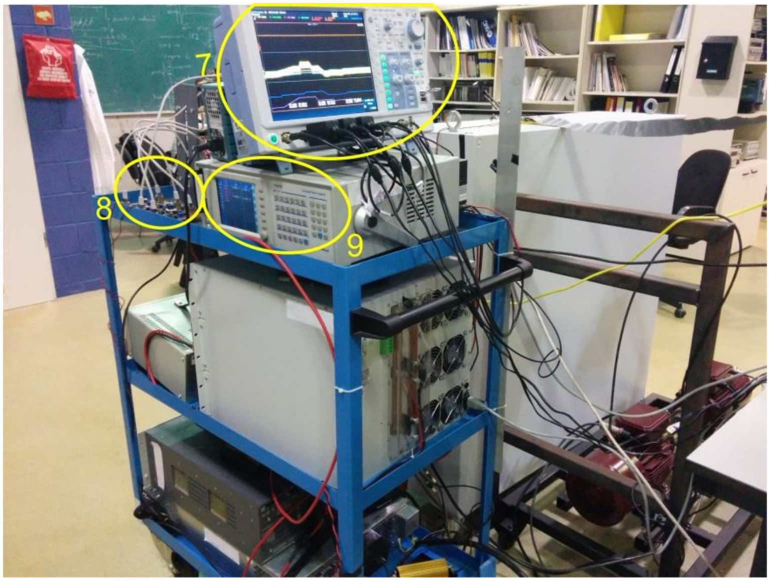

Fig. 5.24. Side view of the cart with the oscilloscope (7), the control board (8) and the power analyser (9).

5.3.2 Dynamic profile experiment

The first experiment to test the feasibility of sliding-mode control for the EV powertrain is to apply the same dynamic profile that was used for simulation purposes, shown in Fig. 5.13. The profile is sent by the acquisition board to the analogue inputs of the inverters, which have a voltage range of 0 to 10 V. The maximum value of 10 V corresponds to 1500 rpm in the case of the reference speed, and to 35.6 N·m for the torque reference. Therefore, in order not to work in one extreme of the voltage range, the reference speed has been limited slightly below. Fig. 5.25 shows the sensed value of the load torque and the speed of the EV powertrain emulator. It can be observed that the load motor follows the reference torque profile, as well as the traction motor follows the speed profile.

The current consumption of each BBCOF has been sensed and reproduced in Fig. 5.26. Note that the current waveform reproduces the product of the torque per the speed waveform. As no field weakening is performed, the power of the motor is directly proportional to the current consumed by the drive. Alike the results of the interleaving experiment, the current is not equally divided between the three BBCOF due to the slight differences in the components values and length of the cables. These results prove the bidirectional operation of the BBCOF with sliding-mode control. When the load torque is negative, the load machine is operating as a motor and the traction one as a generator. Then the current flowing through the BBCOF is negative, so regenerative braking is occurring.

UNIVERSITAT ROVIRA I VIRGILI
DESIGN AND CONTROL OF A BIDIRECTIONAL DC/DC CONVERTER FOR AN ELECTRIC VEHICLE APPLICATION.
Laura Albiol Rendillo
Dipòsit Legal: T 1361-2015

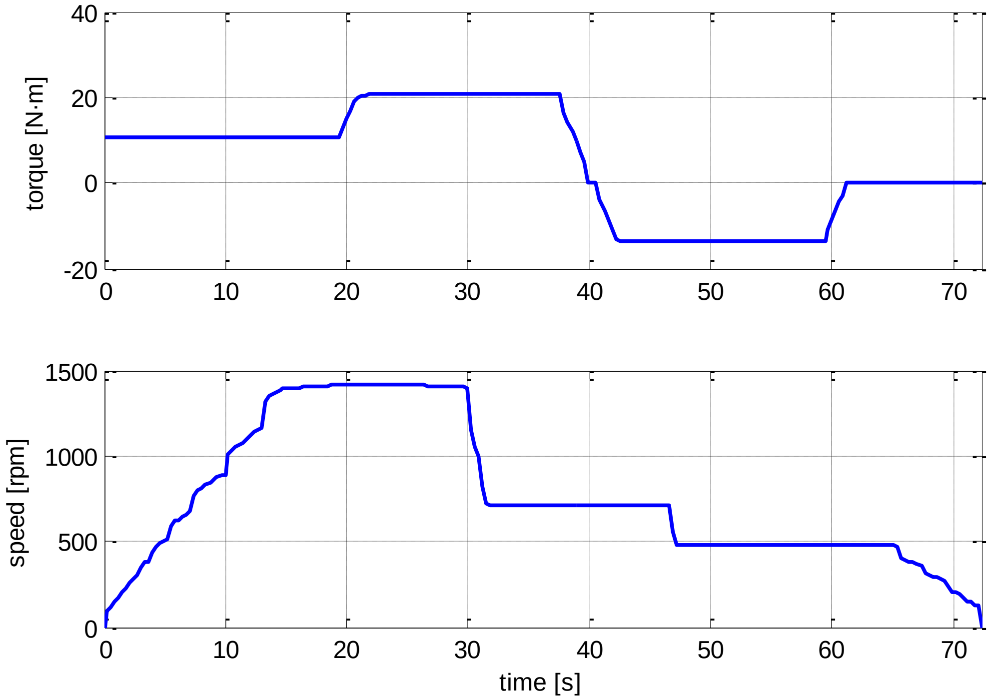

Fig. 5.25. Sensed torque and speed of the EV emulator.

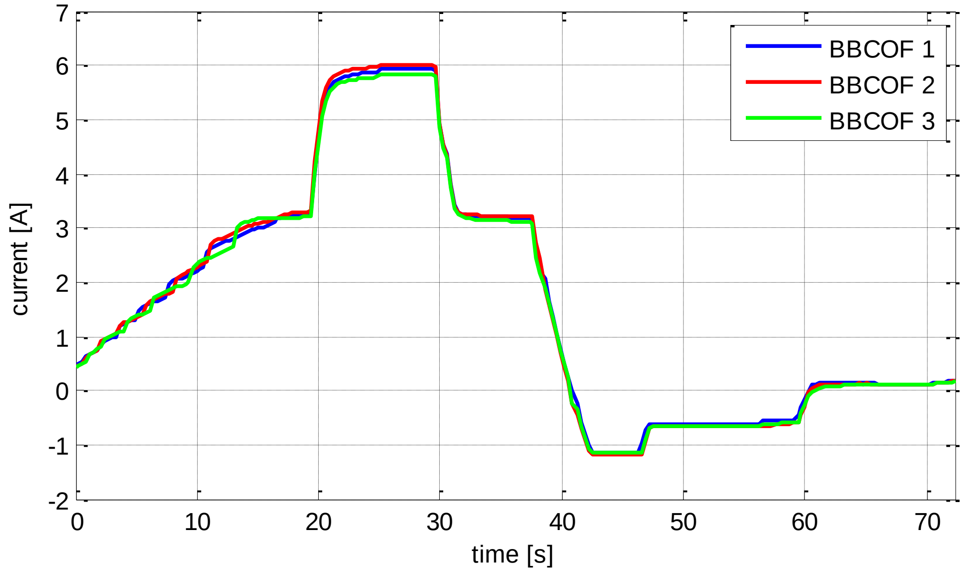

Fig. 5.26. Sensed currents of the three BBCOF.

During the whole driving profile the input DC source feeds the BBCOFs with 200 V, and the output voltage is regulated to the set-point, as shown in Fig. 5.27.

The power of the system is studied by means of the signals registered with the power analyser, and represented in Fig. 5.28. Specifically, electrical power is registered at the input of the BBCOFs and at the DC bus (i.e. the output of the BBCOFs), and the mechanical power of the traction motor is also registered. Moreover, the mechanical power is added to the electrical power dissipated in the aggregate resistances of the DC bus, so that the efficiency of the inverter can be evaluated. It can be observed that during the step-up mode the power at the

UNIVERSITAT ROVIRA I VIRGILI
DESIGN AND CONTROL OF A BIDIRECTIONAL DC/DC CONVERTER FOR AN ELECTRIC VEHICLE APPLICATION.
Laura Albiol Rendillo
Dipòsit Legal: T 1361-2015

input of the BBCOFs is higher than at the DC bus, except for the instant when the motor stops accelerating. Conversely, during step-down mode the power at the DC bus exceeds the power at the input of the BBCOF. The power of the motor, calculated as the product of the sensed torque and speed, is slightly lower than the power of the DC bus but in the instant when the motor abruptly decelerates. Although the efficiency of the BBCOFs and the inverter will be numerically evaluated by means of the static experiments, it can be appreciated that both converter systems have a good performance.

The power of the system is studied by means of the signals registered with the power analyser, and represented in Fig. 5.28. Specifically, electrical power is registered at the input of the BBCOFs and at the DC bus (i.e. the output of the BBCOFs), and the mechanical power of the traction motor is also registered. Moreover, the mechanical power is added to the electrical power dissipated in the aggregate resistances of the DC bus, so that the efficiency of the inverter can be evaluated. It can be observed that during the step-up mode the power at the input of the BBCOFs is higher than at the DC bus, except for the instant when the motor stops accelerating. Conversely, during step-down mode the power at the DC bus exceeds the power at the input of the BBCOF. The power of the motor, calculated as the product of the sensed torque and speed, is slightly lower than the power of the DC bus but in the instant when the motor abruptly decelerates. Although the efficiency of the BBCOFs and the inverter will be numerically evaluated by means of the static experiments, it can be appreciated that both converter systems have a good performance.

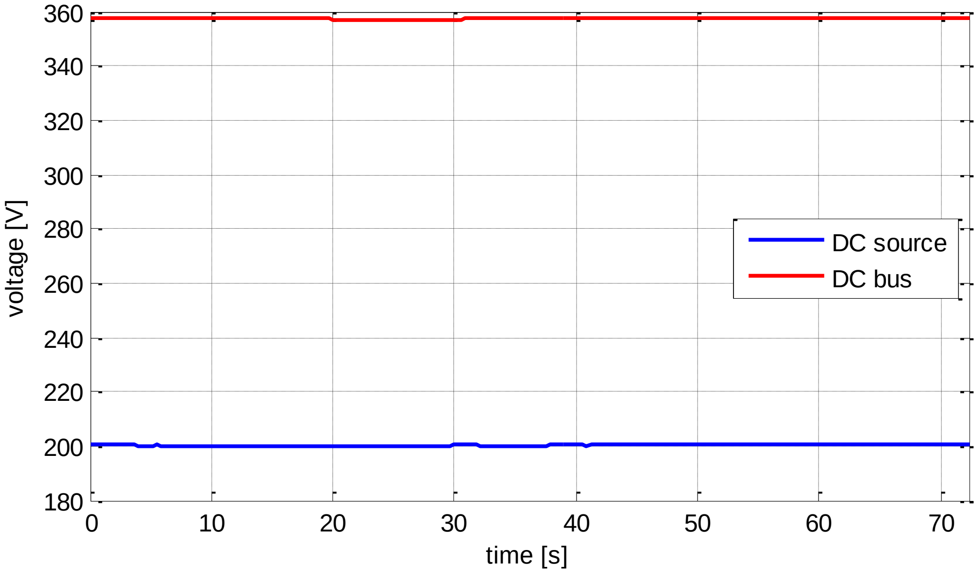

Fig. 5.27. Input and output voltage of the three BBCOFs.

UNIVERSITAT ROVIRA I VIRGILI
DESIGN AND CONTROL OF A BIDIRECTIONAL DC/DC CONVERTER FOR AN ELECTRIC VEHICLE APPLICATION.
Laura Albiol Rendillo
Dipòsit Legal: T 1361-2015

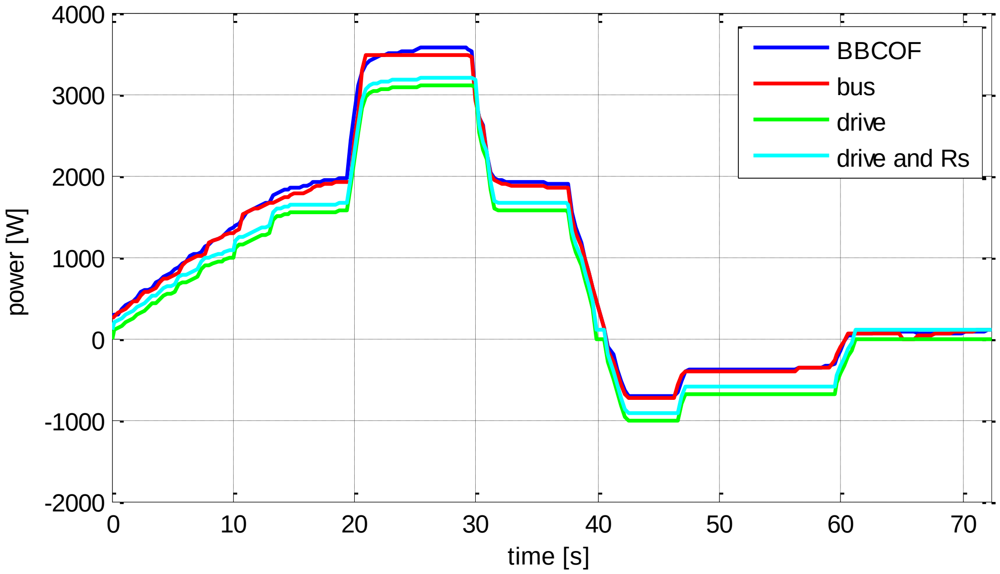

Fig. 5.28. Power at the input of the BBCOFs, at the DC bus, at the motor drive and at the motor drive plus the aggregate resistances.

The results of the dynamic experiment are summarised with the capture of the oscilloscope in Fig. 5.29. The top window shows the voltage both at the input of the BBCOF (in red) and at the DC bus (in orange). The window in the middle contains the input currents of the three BBCOFs, which are superimposed, the current at the DC bus with a cyan-coloured line, and also the current supplied by DC source 1 in an orange line, calculated as the sum of the input currents of the BBCOFs. Finally, the bottom window contains the mechanical variables of the system, namely the speed (in purple) and torque (in blue) of the traction motor. These magnitudes are obtained from the inverters, and thus their value is normalised to 10 V.

5.3.3 Step-up static experiment

The objective of the step-up static experiment is to evaluate the efficiency of the interleaved BBCOFs. The speed of the traction motor is set to 1400 rpm, and the torque of the load motor to 21 N·m. The motor is operated in these conditions for 15 minutes, in order not to have temperature drifting, and then the power at different parts of the system is represented in Fig. 5.30. From this data, the efficiency of the BBCOFs and the inverter are calculated. The former is the division of the DC bus by the DC source power, whereas the latter is the division of the drive and the aggregate resistances by the DC bus power. The results reproduced in Fig. 5.31 show an average of 97.9% efficiency for the BBCOFs and 92.9% for the inverter. The achieved efficiency for the BBCOF meets the high efficiency criterion for automotive DC/DC converters, outlined in the introduction of this thesis.

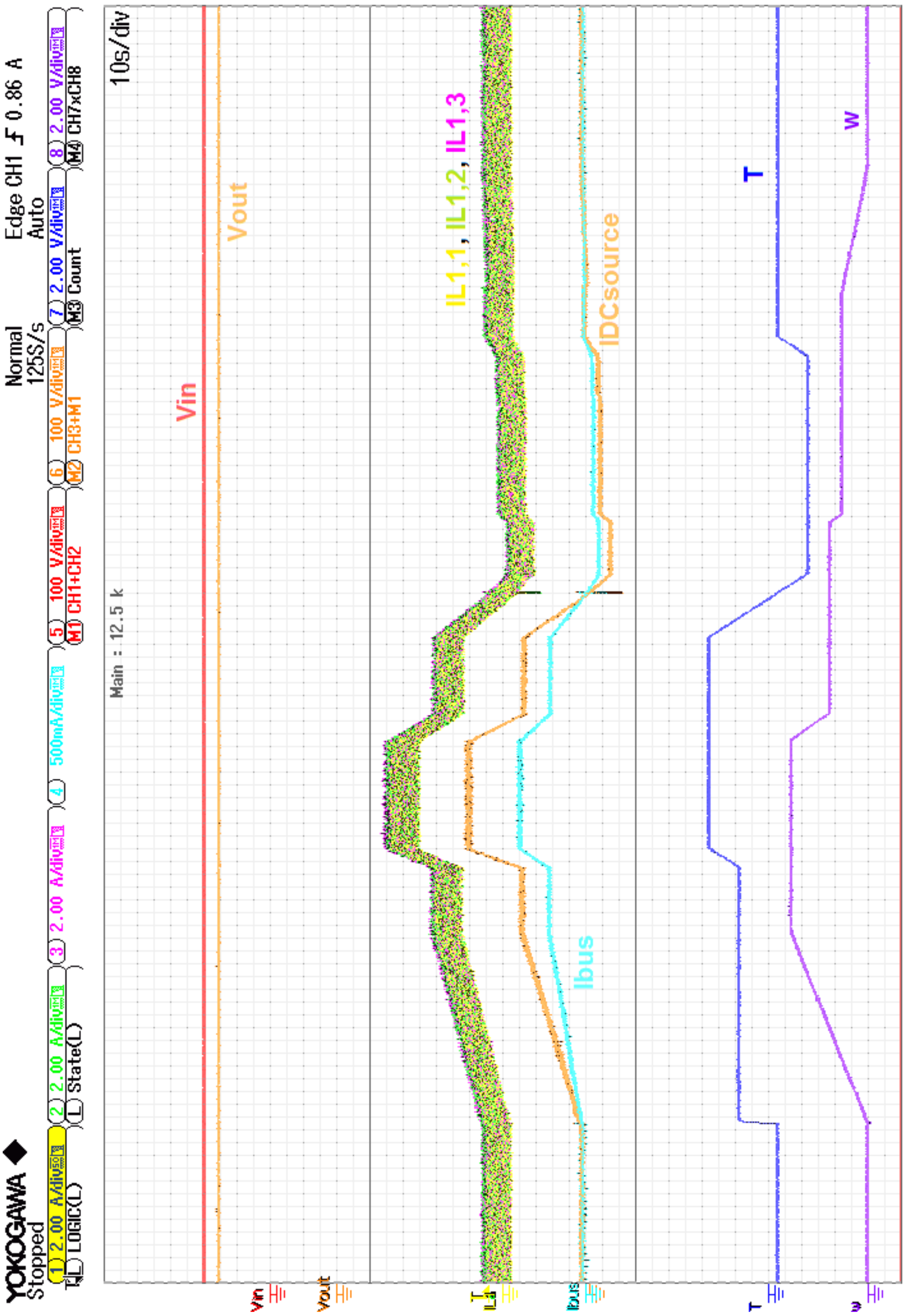

Fig. 5.29. Results of the dynamic profile experiment obtained with the oscilloscope.

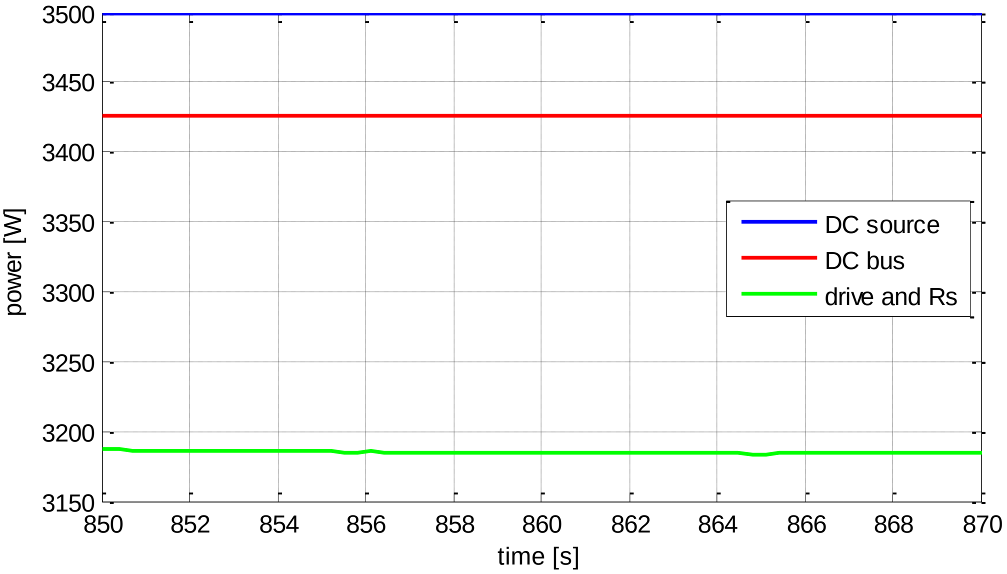

Fig. 5.30. Power at the DC source, DC bus and drive with power dissipated in the aggregate resistances during the step-up experiment.

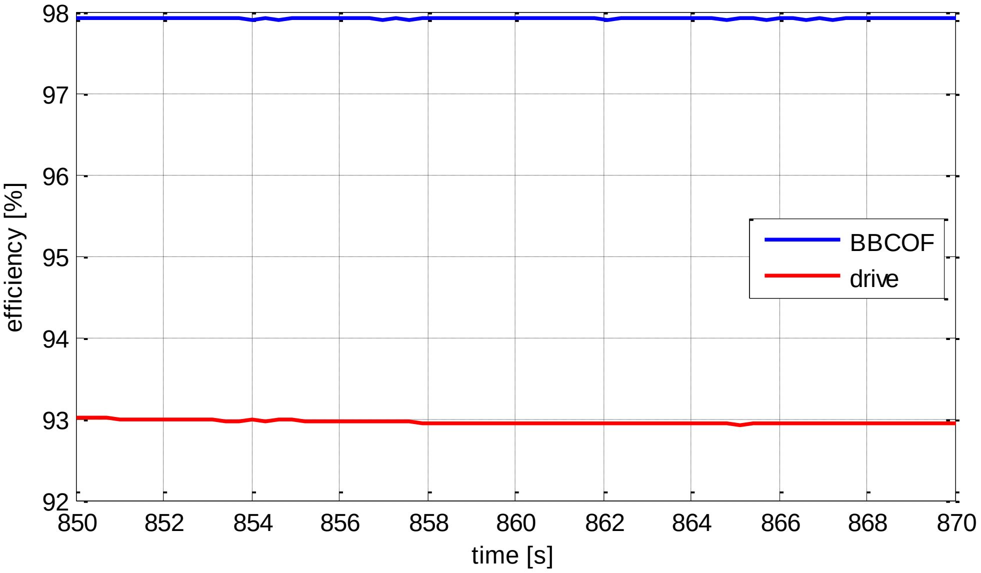

Fig. 5.31. Efficiency of the BBCOFs and motor drive during static step-up operation.

5.3.4 Step-down static experiment

For the step-down static experiment, the speed reference is maintained at 1400 rpm, whilst the load torque is set to -13.75 N·m. The motor is operated also for 15 minutes, and the measured power is referred in Fig. 5.32. From these power measurements, the efficiency of the BBCOFs and the inverter is inferred, and represented in Fig. 5.33. The efficiency of the BBCOFs is reduced to 97%, but still is a good efficiency rating. Moreover, as the powertrain is usually operating in the step-up mode, obtaining a high efficiency of the step-down mode is not critical. The efficiency of the inverter is also reduced to 86.4%.

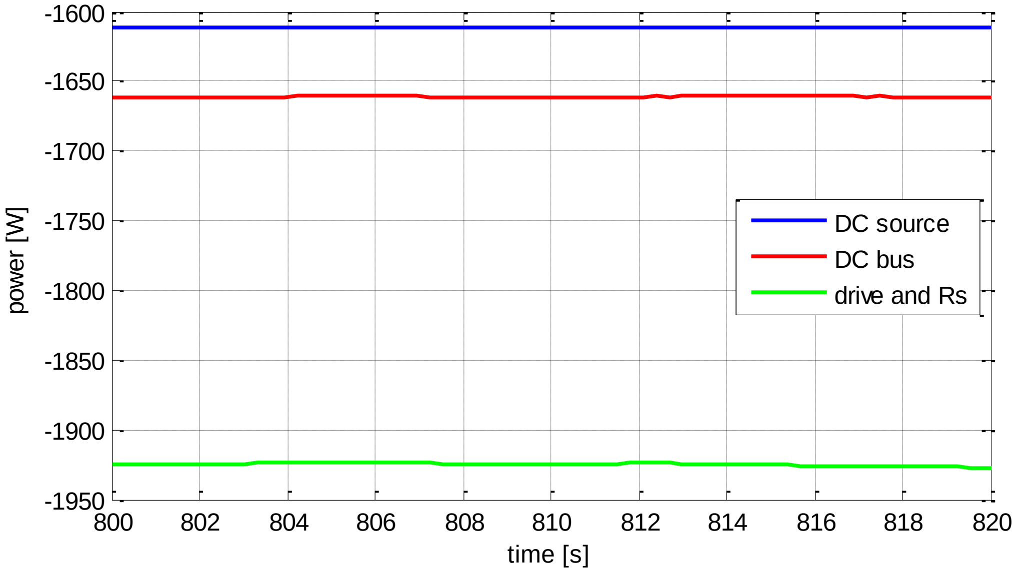

Fig. 5.32. Power at the DC source, DC bus and drive with power dissipated in the aggregate resistances during the step-down experiment.

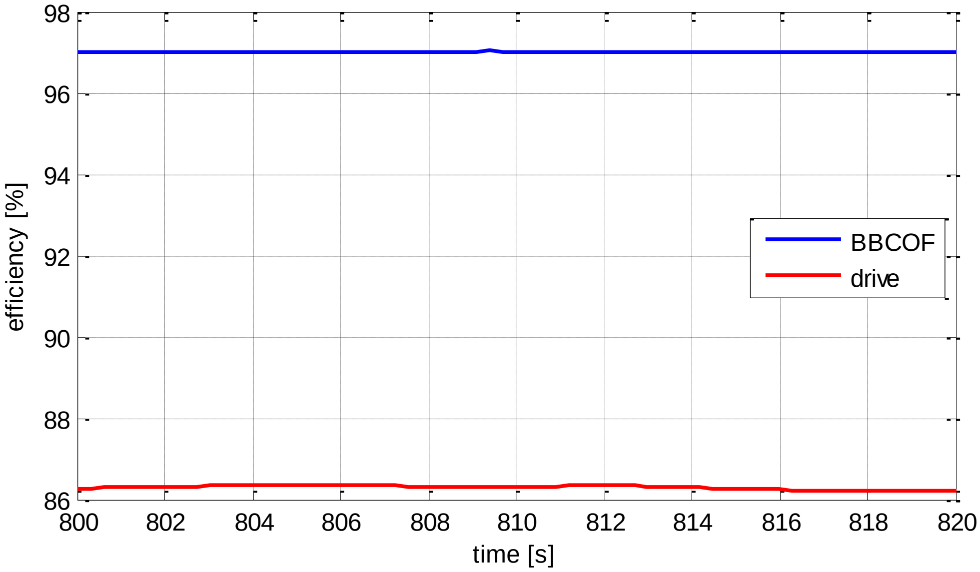

Fig. 5.33. Efficiency of the BBCOFs and motor drive during static step-down operation.

5.4 Conclusions

The objective of the EV powertrain emulator is to have a platform that permits testing the proposed solution of BBCOF with ring-configuration sliding-mode controller with a realistic driving profile. In this chapter, the characteristics of the EV powertrain emulator are set and described.

Next, a Matlab/Simulink model has been obtained. This model enables the verification of the complete system under a driving profile before connecting the real platform. Besides, it is a

UNIVERSITAT ROVIRA I VIRGILI
DESIGN AND CONTROL OF A BIDIRECTIONAL DC/DC CONVERTER FOR AN ELECTRIC VEHICLE APPLICATION.
Laura Albiol Rendillo
Dipòsit Legal: T 1361-2015

tool that allows the user to test possible system modifications before implementation, as results are in good agreement with those obtained experimentally. Furthermore, experimental results validate that the BBCOF with ring-configuration sliding-mode control is a feasible solution for the DC/DC system of an EV powertrain.

6 Digital control of the BBCOF

6.1 Introduction

The inherent advantages of digital devices such as high noise immunity, absence of ageing effects, ability to implement complex control algorithms and flexibility in changing controller parameters have contributed to establishing digital control strategies as a real and feasible alternative to the classical analogue control techniques applied to switching converters regulation [82]. Another advantage of digital devices is the communication ability that allows them to interface other digital systems as in the battery control system of an electric vehicle.

Recently in [83-86] the discrete-time sliding-mode approach [44] was used to design and implement PWM digital controllers based on sliding-mode theory. In those works, it was proven that this methodology can be shown as a natural way of implementing fixed-frequency sliding-mode-based controllers. Although the digital control of BBCOF is expected to be studied as part of a future work, some promising simulation results have been obtained after applying the discrete-time sliding mode theory to digitally implement the previous analogue sliding-mode controllers of the BBCOF, and are shown in this thesis due to their interest. Moreover, besides the inherent advantages of digital controllers, the use of PWM digital controllers to regulate switching power converters facilitates their operation in interleaving. The study outlined in this chapter is based on the PhD thesis of Adrià Marcos-Pastor [87], who has collaborated with the following analysis.

6.2 Design of the digital current-control loop

In order to design the digital control for the BBCOF, the first step is to obtain the discrete-time model of the BBCOF by means of the Euler method following [87], expressed as

$$x(k+1)= F\tau x(k)+E\tau+Hx(k)+G, \tag{6.1}$$

where

$$H=I+A_2T, \tag{6.2}$$

$$F=A_1-A_2, \tag{6.3}$$

$$G=B_2T, \tag{6.4}$$

$$E=B_1-B_2 \tag{6.5}$$

The matrices A_1, A_2, B_1 and B2 correspond to the averaged model matrices of the BBCOF, annotated in Table 3.I, I is the identity matrix, T is the switching period and τ in the conduction time of Q1 MOSFET. Following the procedure described in [83], the discrete sliding surface is defined as

$$s(k)=i_{L1}(k)-i_{ref} \tag{6.6}$$

The objective of the discrete-time sliding-mode control is that in the following sampling period the current flowing through L_1 reaches the reference current value, thus implying

$$s(k+1)=i_{L1}(k+1)-i_{ref}=0 \tag{6.7}$$

From (6.1) the value for $i_{L1}(k+1)$ is extracted, and substituted in (6.7). Then, isolating τ the action control that guarantees the current reference is achieved in the next period is obtained

$$\tau_{eq}=\frac{L_1\left(i_{ref}-i_{L1}(k)\right)+T\left(v_{C1}(k)-v_g(k)\right)}{v_{C1}(k)} \tag{6.8}$$

In order to validate this approach, the digitally current-controlled system is simulated and compared to its analogue equivalent, both loaded with a resistance. Then, the obtained control action (6.8) is implemented by means of arithmetical blocks in PSIM as shown in Fig. 6.1, and PWM modulation is performed. i_{L1} current and v_{C1} voltage are sampled with ZOH blocks.

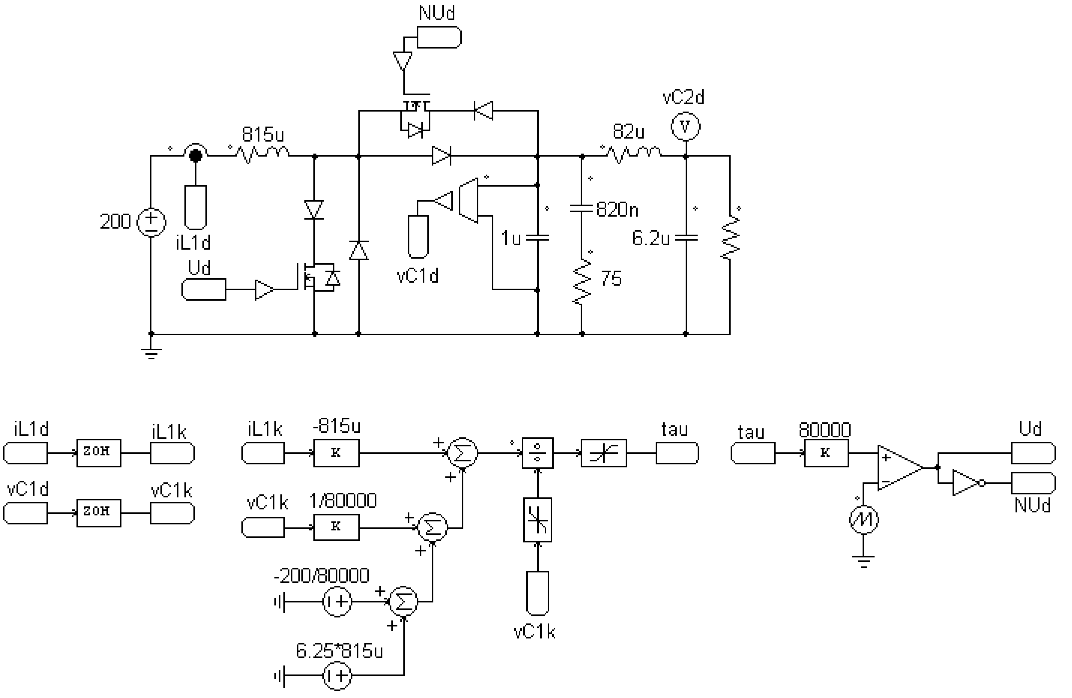

Fig. 6.1. Schematic of the current digital control of the BBCOF.

The current digital control of the BBCOF has been simulated and compared to the analogue sliding-mode control of Fig. 6.2. The results reproduced in Fig. 6.3 show that the digital and the analogue dynamics are comparable and thus the digital control obtained by the application of discrete-time sliding-mode theory to the discrete-time model of the BBCOF obtained through the Euler's Method. In the represented waveforms, letter 'a' denotes the analogue control, and 'd' the digital control.

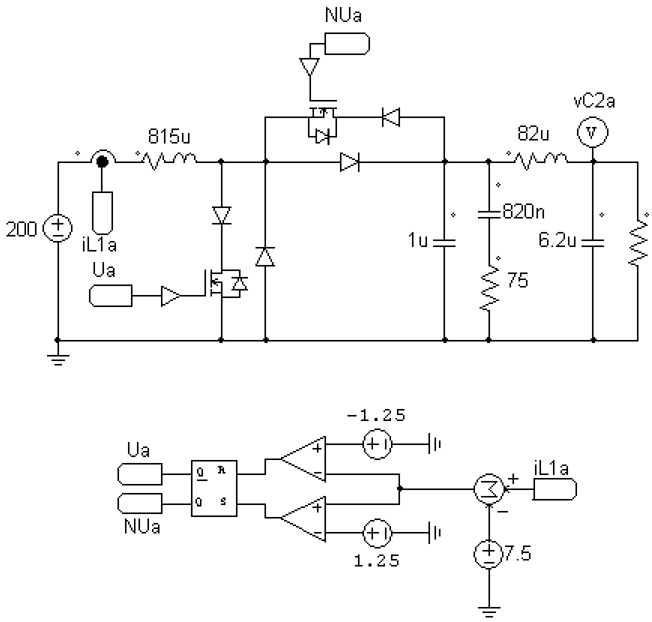

Fig. 6.2. Schematic of the current analogue control of the BBCOF.

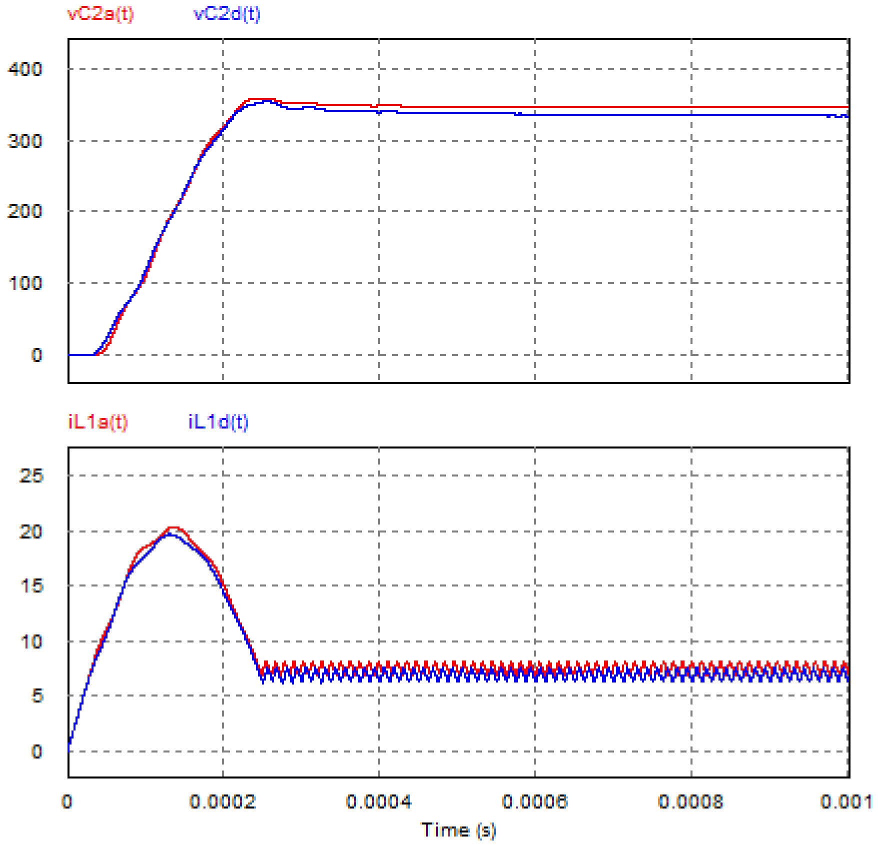

Fig. 6.3. Comparison between the digital and analogue current control for the BBCOF.

6.3 Design of the digital voltage-control loop

As it can be observed in the simulation results of the previous section, the current of the BBCOF is effectively regulated by the digital sliding-mode control, and its dynamics is really close to the dynamics of the analogously controlled BBCOF. Therefore, a second voltage discrete control loop is designed according to the digital redesign approach procedure [82]. As the current-control surface now has a variable current reference

$$s(k)=i_{L1}(k)-i_{ref}(k-1)=0\,, \tag{6.9}$$

a time delay of one period is added to the current reference to output voltage transfer function $\tilde{v}_{C2}(s)/\tilde{i}_{ref}(s)$ of the continuous system. Then, following the same procedure of section 3.4, a new PI controller with an additional pole is designed to obtain a phase margin of 50°. From this controller, the equivalent digital controller obtained by means of the bilinear transform is

$$G_c(z)=\frac{0.03838+0.001471z^{-1}-0.03691z^{2}}{1-1.412z^{-1}+0.4118z^{-2}} \tag{6.10}$$

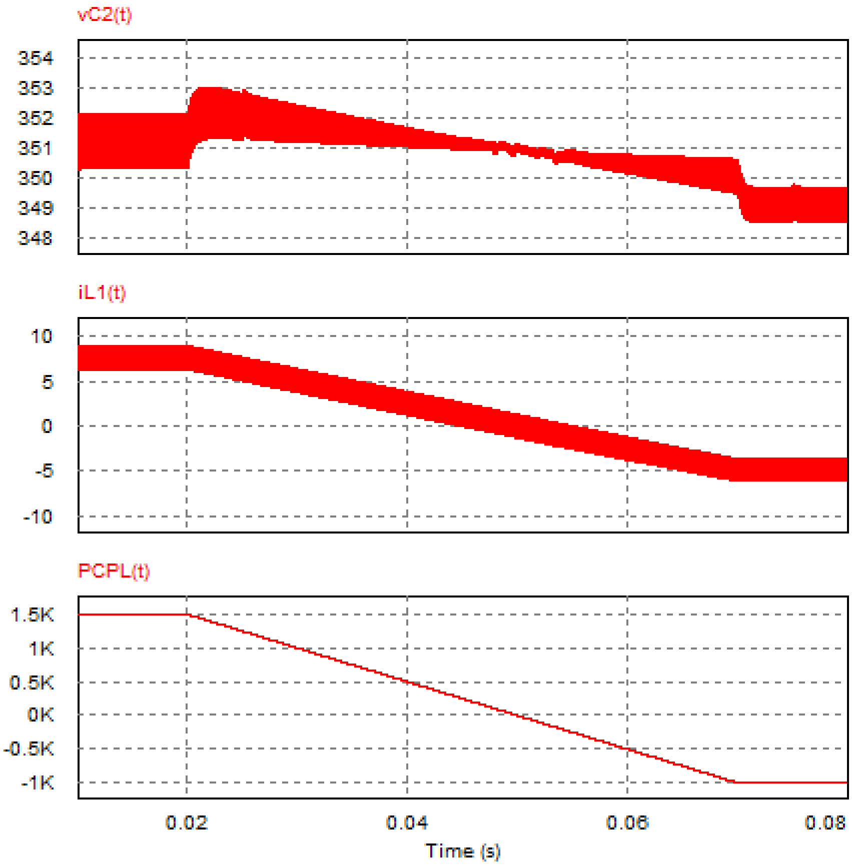

Fig. 6.4. Simulation results of the two-loop digital control of the BBCOF.

The simulated results presented in Fig. 6.4 show that the digital implementation of the sliding-mode control has a similar dynamic behaviour to the analogue one and also maintains its seamless bidirectional characteristics when the load is a CPL.

6.4 Interleaved connection of BBCOF with digital control

Since this digital control relies on PWM modulation, the interleaving connection of the three BBCOF is straightforward. The system has been simulated with a time-varying CPL, and results are reproduced in Fig. 6.5. It can be appreciated that the interleaved system with the two-loop digital controller

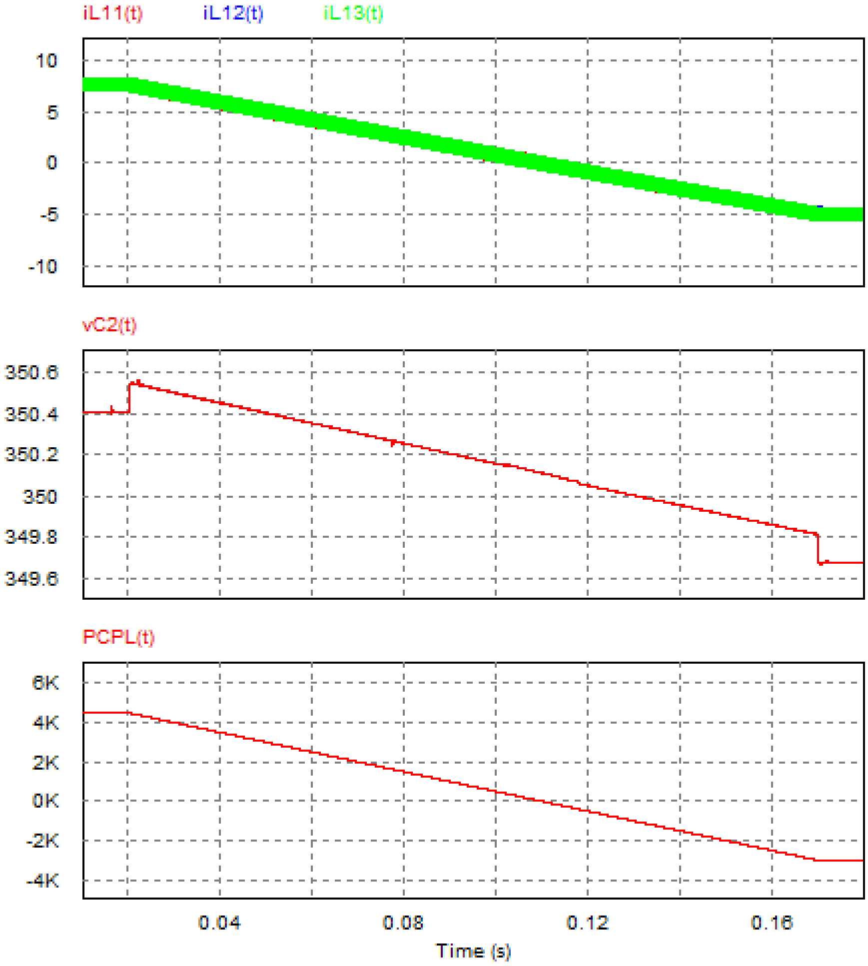

Fig. 6.5. Simulation results of the interleaving of three BBCOF with the two-loop digital control.

6.5 Conclusions

The simulated results show the feasibility and good behaviour of the discrete-time version of the seamless analogue control based on sliding-mode theory. The interleaved connection of three BBCOF converters also shows similar simulation results to the analogue version when it is connected to a CPL. However, the procedure to operate the converters in interleaving is easier.

The detailed study of the stability of the current discrete control is left as a future work of interest, as well as the connection to the motor drive and the experimental implementation.

7 Conclusions and future work

In this thesis the design, analysis, control and implementation of a bidirectional DC/DC converter for an EV powertrain are proposed, and later with a 4.5 kW prototype. The development of this solution comprises the analysis and design of the chosen BBCOF topology, the design and implementation of a sliding-mode current control for the BBCOF, the addition of a PI control to regulate the output voltage, the adoption of interleaving to increase the power rating of the system and testing the solution both with a real emulation platform and its Matlab/Simulink model.

Concerning the load of the converter, which is the motor drive system, it has to be taken into account that it can behave as a CPL, which have an unstabilising effect due to their negative incremental impedance. Therefore the stability of the BBCOF with the model of a CPL has been verified, provided that an RC snubber is included in the design. Then the selected topology is confirmed as an appropriate candidate for the EV powertrain application, and a 1.5 kW prototype is designed.

Sliding-mode control has been proven to be a robust technique in front of system uncertainties. In this case, it is shown that regenerative operation is allowed with no need to change the control method, and not even determining whether the BBCOF is operating in step-up or step-down mode. The small-signal transfer functions of the BBCOF under sliding-mode control have been extracted, and the PI controller to regulate the output voltage has been designed accordingly. An analogue implementation of the current sliding-mode and voltage PI control is developed, simulated and experimentally tested.

In order to obtain a 4.5 kW system from the 1.5 kW designed BBCOF, three converters have been interleaved. Due to the variable switching frequency of the sliding-mode control, a ring configuration strategy has been used in order to achieve the interleaved behaviour of the converter. The current control is still a sliding mode control, where the reference is the sum of the AC component of the current of the previous converter plus the DC component of the output of the PI controller. The result is a system of the desired power-rating with reduced ripple in comparison to the individual converters. Simulation and experimental results corroborate the theoretical study of this solution.

Finally, the specifications for a 4.5 kW EV powertrain emulator have been defined. This EV powertrain is composed of a PMSM drive for traction mechanically coupled to a load PMSM. The load motor is fed with two back-to-back inverters, so as to extract and supply energy to the AC grid. Then, the model of the entire system has been obtained with Matlab/Simulink. This model proves to be a useful tool to test system modifications before its real

UNIVERSITAT ROVIRA I VIRGILI
DESIGN AND CONTROL OF A BIDIRECTIONAL DC/DC CONVERTER FOR AN ELECTRIC VEHICLE APPLICATION.
Laura Albiol Rendillo
Dipòsit Legal: T 1361-2015

implementation. The EV powertrain emulator is run under a realistic driving profile, and results show the stability and regenerative braking capability, as the simulation results of the Matlab/Simulink do. Consequently, the proposed system can be fairly considered as an appropriate solution for the EV powertrain, with the added value of a unique control of the DC/DC converter for both traction and regenerative braking modes.

During this thesis, many ideas on how to continue with the present work have arisen. The first and more obvious is to increase the power rating of the system from 4.5 kW to a value over 100 kW, which corresponds to the power of a standard EV. An in-depth study should be done, but basically the solution depends on both increasing the number of BBCOF and increasing the maximum power delivered by each of them. At this point, the construction of the passive elements to minimize the weight and volume of the system should be considered. By connecting more converters in parallel the ripple would be reduced, and so would be the inductors and capacitors. Consequently, it would be possible to increase the power per converter ratio. The subsequent design could be tested before implementation by means of the developed Matlab/Simulink model.

A second future work that deserves further attention is the digital implementation of the sliding-mode control for the BBCOF. Digital sliding-mode control has recently drawn the interest of researchers in power electronics. In [88] the implementation of a sliding-mode control for an inverter is presented, whereas [89] discusses about a hybrid digital-analogue control for a photovoltaic boost converter. A two-loop digital sliding-mode control for DC/DC converters is first introduced in [90], and further developed with a PWM strategy in [83], where the sliding-mode approach is derived to obtain PWM-controlled system. With this digital implementation, sliding-mode control operates at a fixed frequency, eliminating its main drawback. Therefore, it would be interesting to apply the same procedure to obtain a discrete-time PWM control based on sliding-mode control. Another advantageous feature of the digital implementation to be considered is the simplicity of the interleaved system, since it consists on phase-shifting the control signals. Preliminary simulation results of this future work have also been presented in this thesis.

Moreover, a digital management of the DC/DC system enables the connection and disconnection of individual BBCOF in order to supply the required power at every instant, as well as modifying the DC bus voltage rating online in order to maximise the efficiency of the system.

The modularity provided by interleaving several BBCOF modules makes it possible to achieve a fault-tolerant system. In case of failure of one of the modules, it could be disconnected while the rest continue operating. Therefore the EV could continue its way with reduced power and a warning for the driver. This failure management would also be more practical if it were digitally implemented.

Last but not least, the electromagnetic interferences (EMI) generated by the BBCOFs should be evaluated and the design should be adapted to accomplish the EMI regulation concerning EV, i.e. SAE J-1113.

UNIVERSITAT ROVIRA I VIRGILI
DESIGN AND CONTROL OF A BIDIRECTIONAL DC/DC CONVERTER FOR AN ELECTRIC VEHICLE APPLICATION.
Laura Albiol Rendillo
Dipòsit Legal: T 1361-2015

8 Appendix

This appendix contains the equations that, due to their excessive dimensions, have not been included in their corresponding chapter.

8.1 Stability under sliding-mode control

The constant current reference to output voltage transfer function from section 3.2.1 is

$$
\begin{aligned}
\frac{V_{C_2}(s)}{K(s)} = {} & \Big(R^2\,\big(2\,k\,R_{L_1} - V_g\big)\,\big(R\,\mathrm{I}_o\,R_{L_2} - R\,V_{C_2} - R_{L_2}\,V_{C_2}\big)\Big)\Big/\Big(\Big(R^3\,\mathrm{I}_o^2\,C_1\,C_2\,C_d\,L_2\,R_d\,R_{L_2}^2 \\
& - 2\,R^3\,\mathrm{I}_o\,C_1\,C_2\,C_d\,L_2\,R_d\,R_{L_2}\,V_{C_2} - 2\,R^2\,\mathrm{I}_o\,C_1\,C_2\,C_d\,L_2\,R_d\,R_{L_2}^2\,V_{C_2} + R^3\,C_1\,C_2\,C_d\,L_2\,R_d\,V_{C_2}^2 \\
& + 2\,R^2\,C_1\,C_2\,C_d\,L_2\,R_d\,R_{L_2}\,V_{C_2}^2 + R\,C_1\,C_2\,C_d\,L_2\,R_d\,R_{L_2}^2\,V_{C_2}^2\Big)\,s^4 + \Big(R^3\,\mathrm{I}_o^2\,C_1\,C_2\,C_d\,R_d\,R_{L_2}^3 \\
& - 2\,R^3\,\mathrm{I}_o\,C_1\,C_2\,C_d\,R_d\,R_{L_2}^2\,V_{C_2} - 2\,R^2\,\mathrm{I}_o\,C_1\,C_2\,C_d\,R_d\,R_{L_2}^3\,V_{C_2} - R^3\,k^2\,C_2\,C_d\,L_2\,R_d\,R_{L_1} + R^3 \\
& \mathrm{I}_o^2\,C_1\,C_2\,L_2\,R_{L_2}^2 + R^3\,\mathrm{I}_o^2\,C_2\,C_d\,L_2\,R_{L_2}^2 + R^3\,C_1\,C_2\,C_d\,R_d\,R_{L_2}\,V_{C_2}^2 + R^2\,\mathrm{I}_o^2\,C_1\,C_d\,L_2\,R_d\,R_{L_2}^2 \\
& + 2\,R^2\,C_1\,C_2\,C_d\,R_d\,R_{L_2}^2\,V_{C_2}^2 + R\,C_1\,C_2\,C_d\,R_d\,R_{L_2}^3\,V_{C_2}^2 + R^3\,k\,C_2\,C_d\,L_2\,R_d\,V_g \\
& - 2\,R^3\,\mathrm{I}_o\,C_1\,C_2\,L_2\,R_{L_2}\,V_{C_2} - 2\,R^3\,\mathrm{I}_o\,C_2\,C_d\,L_2\,R_{L_2}\,V_{C_2} - 2\,R^2\,\mathrm{I}_o\,C_1\,C_2\,L_2\,R_{L_2}^2\,V_{C_2} \\
& - 2\,R^2\,\mathrm{I}_o\,C_1\,C_d\,L_2\,R_d\,R_{L_2}\,V_{C_2} - 2\,R^2\,\mathrm{I}_o\,C_2\,C_d\,L_2\,R_{L_2}^2\,V_{C_2} - 2\,R\,\mathrm{I}_o\,C_1\,C_d\,L_2\,R_d\,R_{L_2}^2\,V_{C_2} + R^3\,C_1\,C_2\,L_2 \\
& V_{C_2}^2 + R^3\,C_2\,C_d\,L_2\,V_{C_2}^2 + 2\,R^2\,C_1\,C_2\,L_2\,R_{L_2}\,V_{C_2}^2 + R^2\,C_1\,C_d\,L_2\,R_d\,V_{C_2}^2 + 2\,R^2\,C_2\,C_d\,L_2\,R_{L_2}\,V_{C_2}^2 \\
& + R\,C_1\,C_2\,L_2\,R_{L_2}^2\,V_{C_2}^2 + 2\,R\,C_1\,C_d\,L_2\,R_d\,R_{L_2}\,V_{C_2}^2 + R\,C_2\,C_d\,L_2\,R_{L_2}^2\,V_{C_2}^2 + C_1\,C_d\,L_2\,R_d\,R_{L_2}^2\,V_{C_2}^2\Big)\,s^3 \\
& + \Big(-R^3\,k^2\,C_2\,C_d\,R_d\,R_{L_1}\,R_{L_2} + R^3\,\mathrm{I}_o^2\,C_1\,C_2\,R_{L_2}^3 + R^3\,\mathrm{I}_o^2\,C_1\,C_d\,R_d\,R_{L_2}^2 + R^3\,\mathrm{I}_o^2\,C_2\,C_d\,R_d\,R_{L_2}^2 + R^3 \\
& \mathrm{I}_o^2\,C_2\,C_d\,R_{L_2}^3 + R^2\,\mathrm{I}_o^2\,C_1\,C_d\,R_d\,R_{L_2}^3 + R^3\,k\,C_2\,C_d\,R_d\,R_{L_2}\,V_g - 2\,R^3\,\mathrm{I}_o\,C_1\,C_2\,R_{L_2}^2\,V_{C_2} \\
& - 2\,R^3\,\mathrm{I}_o\,C_1\,C_d\,R_d\,R_{L_2}\,V_{C_2} - 2\,R^3\,\mathrm{I}_o\,C_2\,C_d\,R_d\,R_{L_2}\,V_{C_2} - 2\,R^3\,\mathrm{I}_o\,C_2\,C_d\,R_{L_2}^2\,V_{C_2} - 2\,R^2\,\mathrm{I}_o\,C_1\,C_2 \\
& R_{L_2}^3\,V_{C_2} - 4\,R^2\,\mathrm{I}_o\,C_1\,C_d\,R_d\,R_{L_2}^2\,V_{C_2} - 2\,R^2\,\mathrm{I}_o\,C_2\,C_d\,R_d\,R_{L_2}^2\,V_{C_2} - 2\,R^2\,\mathrm{I}_o\,C_2\,C_d\,R_{L_2}^3\,V_{C_2} \\
& - 2\,R\,\mathrm{I}_o\,C_1\,C_d\,R_d\,R_{L_2}^3\,V_{C_2} - R^3\,k^2\,C_2\,L_2\,R_{L_1} + R^3\,C_1\,C_2\,R_{L_2}\,V_{C_2}^2 + R^3\,C_1\,C_d\,R_d\,V_{C_2}^2 + R^3\,C_2\,C_d\,R_d \\
& V_{C_2}^2 + R^3\,C_2\,C_d\,R_{L_2}\,V_{C_2}^2 - R^2\,k^2\,C_d\,L_2\,R_d\,R_{L_1} + R^2\,\mathrm{I}_o^2\,C_1\,L_2\,R_{L_2}^2 + R^2\,\mathrm{I}_o^2\,C_d\,L_2\,R_{L_2}^2 + 2\,R^2\,C_1\,C_2\,R_{L_2}^2 \\
& V_{C_2}^2 + 3\,R^2\,C_1\,C_d\,R_d\,R_{L_2}\,V_{C_2}^2 + 2\,R^2\,C_2\,C_d\,R_d\,R_{L_2}\,V_{C_2}^2 + 2\,R^2\,C_2\,C_d\,R_{L_2}^2\,V_{C_2}^2 + R\,C_1\,C_2\,R_{L_2}^3\,V_{C_2}^2 \\
& + 3\,R\,C_1\,C_d\,R_d\,R_{L_2}^2\,V_{C_2}^2 + R\,C_2\,C_d\,R_d\,R_{L_2}^2\,V_{C_2}^2 + R\,C_2\,C_d\,R_{L_2}^3\,V_{C_2}^2 + C_1\,C_d\,R_d\,R_{L_2}^3\,V_{C_2}^2 \\
& + R^3\,k\,C_2\,L_2\,V_g + R^2\,k\,C_d\,L_2\,R_d\,V_g - 2\,R^2\,\mathrm{I}_o\,C_1\,L_2\,R_{L_2}\,V_{C_2} - 2\,R^2\,\mathrm{I}_o\,C_d\,L_2\,R_{L_2}\,V_{C_2} - 2\,R\,\mathrm{I}_o\,C_1\,L_2
\end{aligned}
\tag{8.1}
$$

UNIVERSITAT ROVIRA I VIRGILI
DESIGN AND CONTROL OF A BIDIRECTIONAL DC/DC CONVERTER FOR AN ELECTRIC VEHICLE APPLICATION.
Laura Albiol Rendillo
Dipòsit Legal: T 1361-2015

$$
\begin{aligned}
&R_{L_2}^2 V_{C_2} - 2 R \mathrm{I}_o C_d L_2 R_{L_2}^2 V_{C_2} + R^2 C_1 L_2 V_{C_2}^2 + R^2 C_d L_2 V_{C_2}^2 + 2 R C_1 L_2 R_{L_2} V_{C_2}^2 + 2 R C_d L_2 R_{L_2} \\
&V_{C_2}^2 + C_1 L_2 R_{L_2}^2 V_{C_2}^2 + C_d L_2 R_{L_2}^2 V_{C_2}^2 \Big) s^2 + \Big(-R^3 k^2 C_2 R_{L_1} R_{L_2} - R^3 k^2 C_d R_d R_{L_1} + R^3 \mathrm{I}_o^2 C_1 R_{L_2}^2 \\
&+ R^3 \mathrm{I}_o^2 C_2 R_{L_2}^2 + R^3 \mathrm{I}_o^2 C_d R_{L_2}^2 - R^2 k^2 C_d R_d R_{L_1} R_{L_2} + R^2 \mathrm{I}_o^2 C_1 R_{L_2}^3 + R^2 \mathrm{I}_o^2 C_d R_d R_{L_2}^2 + R^2 \mathrm{I}_o^2 C_d R_{L_2}^3 \\
&+ R^3 k C_2 R_{L_2} V_g + R^3 k C_d R_d V_g - 2 R^3 \mathrm{I}_o C_1 R_{L_2} V_{C_2} - 2 R^3 \mathrm{I}_o C_2 R_{L_2} V_{C_2} - 2 R^3 \mathrm{I}_o C_d R_{L_2} V_{C_2} \\
&+ R^2 k C_d R_d R_{L_2} V_g - 4 R^2 \mathrm{I}_o C_1 R_{L_2}^2 V_{C_2} - 2 R^2 \mathrm{I}_o C_2 R_{L_2}^2 V_{C_2} - 2 R^2 \mathrm{I}_o C_d R_d R_{L_2} V_{C_2} - 4 R^2 \mathrm{I}_o C_d \\
&R_{L_2}^2 V_{C_2} - 2 R \mathrm{I}_o C_1 R_{L_2}^3 V_{C_2} - 2 R \mathrm{I}_o C_d R_d R_{L_2}^2 V_{C_2} - 2 R \mathrm{I}_o C_d R_{L_2}^3 V_{C_2} + R^3 C_1 V_{C_2}^2 + R^3 C_2 V_{C_2}^2 \\
&+ R^3 C_d V_{C_2}^2 - R^2 k^2 L_2 R_{L_1} + 3 R^2 C_1 R_{L_2} V_{C_2}^2 + 2 R^2 C_2 R_{L_2} V_{C_2}^2 + R^2 C_d R_d V_{C_2}^2 + 3 R^2 C_d R_{L_2} V_{C_2}^2 \\
&+ 3 R C_1 R_{L_2}^2 V_{C_2}^2 + R C_2 R_{L_2}^2 V_{C_2}^2 + 2 R C_d R_d R_{L_2} V_{C_2}^2 + 3 R C_d R_{L_2}^2 V_{C_2}^2 + C_1 R_{L_2}^3 V_{C_2}^2 + C_d R_d R_{L_2}^2 \\
&V_{C_2}^2 + C_d R_{L_2}^3 V_{C_2}^2 + R^2 k L_2 V_g \Big) s + \mathrm{I}_o^2 R^2 R_{L_2}^2 - R^3 R_{L_1} k^2 - R^2 R_{L_1} R_{L_2} k^2 - 2 \mathrm{I}_o R^2 R_{L_2} V_{C_2} - 2 \mathrm{I}_o R \\
&R_{L_2}^2 V_{C_2} + R^3 V_g k + R^2 R_{L_2} V_g k + R^2 V_{C_2}^2 + 2 R R_{L_2} V_{C_2}^2 + R_{L_2}^2 V_{C_2}^2 \Big)
\end{aligned}
$$

8.2 Small-signal analysis expression

The following equation is the nonlinear expression between the converter inputs, i.e. voltage input, output current and current reference, and the output voltage. It is obtained by combining (3.60)-(3.67) as explained in section 3.3.

$$
\begin{aligned}
&\frac{1}{R}\Bigg(L_2 \left(\frac{\mathrm{d}^4}{\mathrm{d}t^4} v_{C2}(t)\right) C_2 R + R_{L2} \left(\frac{\mathrm{d}^3}{\mathrm{d}t^3} v_{C2}(t)\right) C_2 R - L_2 \left(\frac{\mathrm{d}^3}{\mathrm{d}t^3} i_o(t)\right) R - R_{L2} \left(\frac{\mathrm{d}^2}{\mathrm{d}t^2} i_o(t)\right) R \\
&+ L_2 \left(\frac{\mathrm{d}^3}{\mathrm{d}t^3} v_{C2}(t)\right) + \left(\frac{\mathrm{d}^2}{\mathrm{d}t^2} v_{C2}(t)\right) R + R_{L2} \left(\frac{\mathrm{d}^2}{\mathrm{d}t^2} v_{C2}(t)\right)\Bigg) = -\Bigg(-2 C_1 C_2 i_o(t) \left(\frac{\mathrm{d}}{\mathrm{d}t} v_{C2}(t)\right)^2 \\
&R_{L2}^3 - 2 C_2 C_d i_o(t) \left(\frac{\mathrm{d}}{\mathrm{d}t} v_{C2}(t)\right)^2 R^2 R_{L2}^3 + 2 C_2 C_d L_2 \left(\frac{\mathrm{d}}{\mathrm{d}t} v_{C2}(t)\right)^3 R R_{L2}^2 \\
&+ 2 C_2 C_d v_{C2}(t) \left(\frac{\mathrm{d}}{\mathrm{d}t} v_{C2}(t)\right)^2 R R_{L2}^3 - 2 C_d L_2 i_o(t) \left(\frac{\mathrm{d}}{\mathrm{d}t} v_{C2}(t)\right)^2 R R_{L2}^2 \\
&- 2 C_d v_{C2}(t)\, i_o(t) \left(\frac{\mathrm{d}}{\mathrm{d}t} v_{C2}(t)\right) R R_{L2}^3 + C_2^2 C_d \left(\frac{\mathrm{d}}{\mathrm{d}t} v_{C2}(t)\right)^3 R^2 R_{L2}^2 R_d + 3 C_d \\
&L_2^2 \left(\frac{\mathrm{d}}{\mathrm{d}t} i_o(t)\right)^2 \left(\frac{\mathrm{d}}{\mathrm{d}t} v_{C2}(t)\right) R^2 R_d + C_d i_o(t)^2 \left(\frac{\mathrm{d}}{\mathrm{d}t} v_{C2}(t)\right) R^2 R_{L2}^2 R_d - 3 C_d \\
&L_2^2 \left(\frac{\mathrm{d}}{\mathrm{d}t} i_o(t)\right) \left(\frac{\mathrm{d}}{\mathrm{d}t} v_{C2}(t)\right)^2 R R_d + 2 C_d L_2 v_{C2}(t) \left(\frac{\mathrm{d}}{\mathrm{d}t} v_{C2}(t)\right)^2 R R_d \\
&+ 2 C_d L_2 v_{C2}(t) \left(\frac{\mathrm{d}}{\mathrm{d}t} v_{C2}(t)\right)^2 R_{L2} R_d - i_{ref}(t)^2 R^3 R_{L1} \left(\frac{\mathrm{d}}{\mathrm{d}t} v_{C2}(t)\right) R_d C_d \\
&+ i_{ref}(t)\, R^3 v_g(t) \left(\frac{\mathrm{d}}{\mathrm{d}t} v_{C2}(t)\right) R_d C_d - C_d v_{C2}(t)^2 \left(\frac{\mathrm{d}}{\mathrm{d}t} i_o(t)\right) R R_{L2}^2 R_d \\
&- C_d v_g(t)\, v_{C2}(t) \left(\frac{\mathrm{d}}{\mathrm{d}t} i_{ref}(t)\right) R^3 R_d - C_d v_{C2}(t) \left(\frac{\mathrm{d}}{\mathrm{d}t} v_g(t)\right) i_{ref}(t)\, R^3 R_d \\
&+ C_d L_1 v_{C2}(t) \left(\frac{\mathrm{d}}{\mathrm{d}t} i_{ref}(t)\right)^2 R^3 R_d + 2 C_d v_{C2}(t)^2 \left(\frac{\mathrm{d}}{\mathrm{d}t} v_{C2}(t)\right) R R_{L2} R_d - C_d i_o(t)^2 \left(\frac{\mathrm{d}}{\mathrm{d}t} i_o(t)\right) \\
&R_{L2}^2 R_d + 2 C_d L_2 v_{C2}(t) \left(\frac{\mathrm{d}}{\mathrm{d}t} i_o(t)\right)^2 R^3 R_d - 2 C_d v_{C2}(t)^2 \left(\frac{\mathrm{d}}{\mathrm{d}t} i_o(t)\right) R^2 R_{L2} R_d \\
&+ 2 C_d v_{C2}(t)\, i_o(t) \left(\frac{\mathrm{d}}{\mathrm{d}t} i_o(t)\right) R^3 R_{L2}^2 + 2 C_d v_{C2}(t)\, i_o(t) \left(\frac{\mathrm{d}}{\mathrm{d}t} i_o(t)\right) R^2 R_{L2}^3 - 3 C_d
\end{aligned}
\tag{8.2}
$$

$$L_2^2 \left(\frac{\mathrm{d}}{\mathrm{d}t}\, i_o(t) \right) \left(\frac{\mathrm{d}}{\mathrm{d}t}\, v_{C2}(t) \right)^2 R\, R_{L2} - 4\, C_2\, L_2\, i_o(t) \left(\frac{\mathrm{d}}{\mathrm{d}t}\, v_{C2}(t) \right)^2 R^2\, R_{L2}$$

$$+ 2\, C_1\, C_2\, L_2 \left(\frac{\mathrm{d}}{\mathrm{d}t}\, v_{C2}(t) \right)^3 R^2\, R_{L2} + 2\, C_1\, C_2\, v_{C2}(t) \left(\frac{\mathrm{d}}{\mathrm{d}t}\, v_{C2}(t) \right)^2 R^3\, R_{L2}$$

$$+ 4\, C_1\, C_2\, v_{C2}(t) \left(\frac{\mathrm{d}}{\mathrm{d}t}\, v_{C2}(t) \right)^2 R^2\, R_{L2}^2 - 2\, C_1\, L_2\, i_o(t) \left(\frac{\mathrm{d}}{\mathrm{d}t}\, i_o(t) \right)^2 R^3\, R_{L2}^2 + v_{C2}(t)^3\, R^2$$

$$+ 2\, C_2\, C_d\, L_2 \left(\frac{\mathrm{d}}{\mathrm{d}t}\, v_{C2}(t) \right)^3 R^2\, R_{L2} + 2\, C_2\, C_d\, v_{C2}(t) \left(\frac{\mathrm{d}}{\mathrm{d}t}\, v_{C2}(t) \right)^2 R^3\, R_{L2}$$

$$+ 4\, C_2\, C_d\, v_{C2}(t) \left(\frac{\mathrm{d}}{\mathrm{d}t}\, v_{C2}(t) \right)^2 R^2\, R_{L2}^2 - 2\, C_d\, L_2\, v_{C2}(t) \left(\frac{\mathrm{d}}{\mathrm{d}t}\, i_o(t) \right) \left(\frac{\mathrm{d}}{\mathrm{d}t}\, v_{C2}(t) \right) R^3$$

$$- 2\, C_d\, L_2\, i_o(t) \left(\frac{\mathrm{d}}{\mathrm{d}t}\, v_{C2}(t) \right)^2 R^2\, R_{L2} - 2\, C_d\, v_{C2}(t)\, i_o(t) \left(\frac{\mathrm{d}}{\mathrm{d}t}\, v_{C2}(t) \right) R^3\, R_{L2}$$

$$- 4\, C_d\, v_{C2}(t)\, i_o(t) \left(\frac{\mathrm{d}}{\mathrm{d}t}\, v_{C2}(t) \right) R^2\, R_{L2}^2 + 4\, C_d\, L_2\, v_{C2}(t) \left(\frac{\mathrm{d}}{\mathrm{d}t}\, v_{C2}(t) \right)^2 R\, R_{L2} - C_1$$

$$C_2^2 \left(\frac{\mathrm{d}}{\mathrm{d}t}\, i_o(t) \right) \left(\frac{\mathrm{d}}{\mathrm{d}t}\, v_{C2}(t) \right)^2 R^3\, R_{L2}^3 - 2\, C_1\, L_2\, i_o(t) \left(\frac{\mathrm{d}}{\mathrm{d}t}\, v_{C2}(t) \right)^2 R\, R_{L2}^2$$

$$+ 4\, C_1\, L_2\, v_{C2}(t) \left(\frac{\mathrm{d}}{\mathrm{d}t}\, v_{C2}(t) \right)^2 R\, R_{L2} + 2\, C_1\, C_2\, v_{C2}(t) \left(\frac{\mathrm{d}}{\mathrm{d}t}\, v_{C2}(t) \right)^2 R\, R_{L2}^3$$

$$- 2\, C_1\, v_{C2}(t)\, i_o(t) \left(\frac{\mathrm{d}}{\mathrm{d}t}\, v_{C2}(t) \right) R^3\, R_{L2} - 4\, C_1\, v_{C2}(t)\, i_o(t) \left(\frac{\mathrm{d}}{\mathrm{d}t}\, v_{C2}(t) \right) R^2\, R_{L2}^2 - 2$$

$$C_2^2\, L_2 \left(\frac{\mathrm{d}}{\mathrm{d}t}\, i_o(t) \right) \left(\frac{\mathrm{d}}{\mathrm{d}t}\, v_{C2}(t) \right)^2 R^3\, R_{L2} - 2\, C_2\, C_d\, i_o(t) \left(\frac{\mathrm{d}}{\mathrm{d}t}\, v_{C2}(t) \right)^2 R^3\, R_{L2}^2$$

$$- C_2\, v_g(t) \left(\frac{\mathrm{d}}{\mathrm{d}t}\, v_{C2}(t) \right) i_{ref}(t)\, R^3\, R_{L2} + 2\, C_1\, C_2\, L_2 \left(\frac{\mathrm{d}}{\mathrm{d}t}\, v_{C2}(t) \right)^3 R\, R_{L2}^2 - 3\, C_1$$

$$L_2^2 \left(\frac{\mathrm{d}}{\mathrm{d}t}\, i_o(t) \right) \left(\frac{\mathrm{d}}{\mathrm{d}t}\, v_{C2}(t) \right)^2 R\, R_{L2} - C_d\, L_2\, v_{C2}(t)^2 \left(\frac{\mathrm{d}^2}{\mathrm{d}t^2}\, i_o(t) \right) R^3 - C_2^2\, L_2^2\, i_o(t) \left(\frac{\mathrm{d}^2}{\mathrm{d}t^2}\, v_{C2}(t) \right)^2 R^3 + C_2^3$$

$$L_2^2 \left(\frac{\mathrm{d}^2}{\mathrm{d}t^2}\, v_{C2}(t) \right)^2 \left(\frac{\mathrm{d}}{\mathrm{d}t}\, v_{C2}(t) \right) R^3 + C_1\, C_2^2\, L_2^3 \left(\frac{\mathrm{d}^2}{\mathrm{d}t^2}\, v_{C2}(t) \right)^3 R^2 - C_d\, L_2^3 \left(\frac{\mathrm{d}}{\mathrm{d}t}\, i_o(t) \right)^2 \left(\frac{\mathrm{d}^2}{\mathrm{d}t^2}\, i_o(t) \right) R^3$$

$$- C_d\, L_2^2 \left(\frac{\mathrm{d}}{\mathrm{d}t}\, i_o(t) \right)^3 R^3\, R_{L2} - C_d\, i_o(t)^2 \left(\frac{\mathrm{d}}{\mathrm{d}t}\, i_o(t) \right) R^3\, R_{L2}^3 - C_d\, v_{C2}(t)^2 \left(\frac{\mathrm{d}}{\mathrm{d}t}\, i_o(t) \right) R^3\, R_{L2}$$

$$- 2\, C_d\, v_{C2}(t)^2 \left(\frac{\mathrm{d}}{\mathrm{d}t}\, i_o(t) \right) R^2\, R_{L2}^2 - C_d\, v_{C2}(t)^2 \left(\frac{\mathrm{d}}{\mathrm{d}t}\, i_o(t) \right) R\, R_{L2}^3 + 2\, L_2\, i_o(t)^2 \left(\frac{\mathrm{d}}{\mathrm{d}t}\, v_{C2}(t) \right) R^2\, R_{L2}$$

$$- 2\, L_2\, v_{C2}(t)\, i_o(t) \left(\frac{\mathrm{d}}{\mathrm{d}t}\, v_{C2}(t) \right) R^2 + C_1\, i_o(t)^2 \left(\frac{\mathrm{d}}{\mathrm{d}t}\, v_{C2}(t) \right) R^3\, R_{L2}^2 + C_2$$

$$L_2^2 \left(\frac{\mathrm{d}}{\mathrm{d}t}\, i_o(t) \right)^2 \left(\frac{\mathrm{d}}{\mathrm{d}t}\, v_{C2}(t) \right) R^3 + C_2^2\, C_d \left(\frac{\mathrm{d}}{\mathrm{d}t}\, v_{C2}(t) \right)^3 R^3\, R_{L2}^2 + C_d\, L_2^2 \left(\frac{\mathrm{d}}{\mathrm{d}t}\, i_o(t) \right)^2 \left(\frac{\mathrm{d}}{\mathrm{d}t}\, v_{C2}(t) \right) R^3$$

$$+ C_d\, i_o(t)^2 \left(\frac{\mathrm{d}}{\mathrm{d}t}\, v_{C2}(t) \right) R^3\, R_{L2}^2 - 2\, C_d\, L_2^2 \left(\frac{\mathrm{d}}{\mathrm{d}t}\, i_o(t) \right) \left(\frac{\mathrm{d}}{\mathrm{d}t}\, v_{C2}(t) \right)^2 R^2$$

$$+ 2\, C_d\, L_2\, v_{C2}(t) \left(\frac{\mathrm{d}}{\mathrm{d}t}\, v_{C2}(t) \right)^2 R^2 - 4\, v_{C2}(t)^2\, i_o(t)\, R^2\, R_{L2} + 3\, v_{C2}(t)\, i_o(t)^2\, R^2\, R_{L2}^2 - 3\, v_{C2}(t)^2\, i_o(t)\, R\, R_{L2}^2$$

$$+ C_2\, L_2^2 \left(\frac{\mathrm{d}}{\mathrm{d}t}\, v_{C2}(t) \right)^3 R + C_1\, L_2^2 \left(\frac{\mathrm{d}}{\mathrm{d}t}\, v_{C2}(t) \right)^3 R_{L2} + C_1\, v_{C2}(t)^2 \left(\frac{\mathrm{d}}{\mathrm{d}t}\, v_{C2}(t) \right) R_{L2}^3$$

$$+ v_{C2}(t)\, i_{ref}(t)^2\, R^3\, R_{L1} + 2\, L_2\, v_{C2}(t)^2 \left(\frac{\mathrm{d}}{\mathrm{d}t}\, v_{C2}(t) \right) R + 2\, L_2\, v_{C2}(t)^2 \left(\frac{\mathrm{d}}{\mathrm{d}t}\, v_{C2}(t) \right) R_{L2} + C_d$$

$$L_2^2 \left(\frac{\mathrm{d}}{\mathrm{d}t}\, v_{C2}(t) \right)^3 R_d + C_d\, L_2^2 \left(\frac{\mathrm{d}}{\mathrm{d}t}\, v_{C2}(t) \right)^3 R_{L2} + C_d\, v_{C2}(t)^2 \left(\frac{\mathrm{d}}{\mathrm{d}t}\, v_{C2}(t) \right) R_{L2}^3 + C_1\, L_2^2 \left(\frac{\mathrm{d}}{\mathrm{d}t}\, v_{C2}(t) \right)^3 R$$

$$+ C_1\, v_{C2}(t)^2 \left(\frac{\mathrm{d}}{\mathrm{d}t}\, v_{C2}(t) \right) R^3 + C_2\, v_{C2}(t)^2 \left(\frac{\mathrm{d}}{\mathrm{d}t}\, v_{C2}(t) \right) R^3 - L_2^2\, i_o(t) \left(\frac{\mathrm{d}}{\mathrm{d}t}\, i_o(t) \right)^2 R^3 +$$

$$C_2^3 \left(\frac{\mathrm{d}}{\mathrm{d}t}\, v_{C2}(t) \right)^3 R^3\, R_{L2}^2 + C_d\, L_2^2 \left(\frac{\mathrm{d}}{\mathrm{d}t}\, v_{C2}(t) \right)^3 R + C_d\, v_{C2}(t)^2 \left(\frac{\mathrm{d}}{\mathrm{d}t}\, v_{C2}(t) \right) R^3 -$$

$$L_2^2\, i_o(t) \left(\frac{\mathrm{d}}{\mathrm{d}t}\, v_{C2}(t) \right)^2 R + L_2^2\, v_{C2}(t) \left(\frac{\mathrm{d}}{\mathrm{d}t}\, i_o(t) \right)^2 R^2 - 2\, L_2\, v_{C2}(t)^2 \left(\frac{\mathrm{d}}{\mathrm{d}t}\, i_o(t) \right) R^2 + 2\, v_{C2}(t)\, i_o(t)^2\, R^3\, R_{L2}$$

UNIVERSITAT ROVIRA I VIRGILI
DESIGN AND CONTROL OF A BIDIRECTIONAL DC/DC CONVERTER FOR AN ELECTRIC VEHICLE APPLICATION.
Laura Albiol Rendillo
Dipòsit Legal: T 1361-2015

$$+ C_1 L_2^3 \left(\frac{d^2}{dt^2} v_{C2}(t) \right) \left(\frac{d}{dt} v_{C2}(t) \right)^2 + C_d L_2^3 \left(\frac{d^2}{dt^2} v_{C2}(t) \right) \left(\frac{d}{dt} v_{C2}(t) \right)^2 - v_g(t)\, v_{C2}(t)\, i_{ref}(t)\, R^3$$

$$+ 2\, C_2 C_d \left(\frac{d}{dt} v_{C2}(t) \right) i_{ref}(t) \left(\frac{d}{dt} i_{ref}(t) \right) R^3 R_{L1} R_{L2} R_d$$

$$- i_{ref}(t)\, R^3 \left(\frac{d}{dt} i_{ref}(t) \right) L_1 R_{L2} \left(\frac{d^2}{dt^2} v_{C2}(t) \right) C_2 R_d C_d$$

$$- i_{ref}(t)\, R^3 \left(\frac{d}{dt} i_{ref}(t) \right) L_1 L_2 \left(\frac{d^3}{dt^3} v_{C2}(t) \right) C_2 R_d C_d$$

$$- 4\, C_2 C_d L_2 i_o(t) \left(\frac{d^2}{dt^2} v_{C2}(t) \right) \left(\frac{d}{dt} v_{C2}(t) \right) R^2 R_{L2} R_d$$

$$+ 4\, C_2 C_d L_2 v_{C2}(t) \left(\frac{d^2}{dt^2} v_{C2}(t) \right) \left(\frac{d}{dt} v_{C2}(t) \right) R\, R_{L2} R_d - 4$$

$$C_2^2 C_d L_2 \left(\frac{d}{dt} i_o(t) \right) \left(\frac{d^2}{dt^2} v_{C2}(t) \right) \left(\frac{d}{dt} v_{C2}(t) \right) R^3 R_{L2} R_d$$

$$+ 4\, C_2 C_d L_2 i_o(t) \left(\frac{d}{dt} i_o(t) \right) \left(\frac{d^2}{dt^2} v_{C2}(t) \right) R^3 R_{L2} R_d$$

$$- 4\, C_2 C_d L_2 v_{C2}(t) \left(\frac{d}{dt} i_o(t) \right) \left(\frac{d^2}{dt^2} v_{C2}(t) \right) R^2 R_{L2} R_d$$

$$+ C_2 C_d L_1 L_2 \left(\frac{d^2}{dt^2} v_{C2}(t) \right) \left(\frac{d^2}{dt^2} i_{ref}(t) \right) i_{ref}(t)\, R^3 R_d$$

$$+ C_2 C_d L_1 \left(\frac{d}{dt} v_{C2}(t) \right) \left(\frac{d^2}{dt^2} i_{ref}(t) \right) i_{ref}(t)\, R^3 R_{L2} R_d$$

$$+ 2\, C_2 C_d L_2 \left(\frac{d^2}{dt^2} v_{C2}(t) \right) i_{ref}(t) \left(\frac{d}{dt} i_{ref}(t) \right) R^3 R_{L1} R_d + 2\, C_1 C_2 L_2^2 v_{C2}(t) \left(\frac{d^2}{dt^2} v_{C2}(t) \right)^2 R^2 - 2\, C_1$$

$$L_2^2 v_{C2}(t) \left(\frac{d}{dt} i_o(t) \right) \left(\frac{d^2}{dt^2} v_{C2}(t) \right) R^2 - 2\, C_1 C_2 L_2^3 \left(\frac{d}{dt} i_o(t) \right) \left(\frac{d^2}{dt^2} v_{C2}(t) \right)^2 R^2 - 2\, C_2^2$$

$$L_2^2 \left(\frac{d}{dt} i_o(t) \right) \left(\frac{d^2}{dt^2} v_{C2}(t) \right) \left(\frac{d}{dt} v_{C2}(t) \right) R^3 + 2\, C_d L_2 v_{C2}(t)^2 \left(\frac{d^2}{dt^2} v_{C2}(t) \right) R\, R_{L2} + C_2^3 C_d$$

$$L_2^2 \left(\frac{d^2}{dt^2} v_{C2}(t) \right)^3 R^3 R_{L2} + C_2^3 C_d \left(\frac{d^2}{dt^2} v_{C2}(t) \right) \left(\frac{d}{dt} v_{C2}(t) \right)^2 R^3 R_{L2}^3 + C_2 C_d i_o(t)^2 \left(\frac{d^2}{dt^2} v_{C2}(t) \right) R^3 R_{L2}^3$$

$$- 4\, C_1 L_2 v_{C2}(t) \left(\frac{d}{dt} i_o(t) \right) \left(\frac{d}{dt} v_{C2}(t) \right) R\, R_{L2}^2 - 6\, C_1 L_2 v_{C2}(t) \left(\frac{d}{dt} i_o(t) \right) \left(\frac{d}{dt} v_{C2}(t) \right) R^2 R_{L2}$$

$$- 2\, C_1 C_2 L_2 \left(\frac{d}{dt} i_o(t) \right) \left(\frac{d}{dt} v_{C2}(t) \right)^2 R^3 R_{L2} + 4\, C_1 L_2 i_o(t) \left(\frac{d}{dt} i_o(t) \right) \left(\frac{d}{dt} v_{C2}(t) \right) R^2 R_{L2}^2$$

$$+ 4\, C_2 L_2 i_o(t) \left(\frac{d}{dt} i_o(t) \right) \left(\frac{d}{dt} v_{C2}(t) \right) R^3 R_{L2} + C_2 L_1 \left(\frac{d}{dt} v_{C2}(t) \right) i_{ref}(t) \left(\frac{d}{dt} i_{ref}(t) \right) R^3 R_{L2}$$

$$+ 2\, C_1 L_2 i_o(t) \left(\frac{d}{dt} i_o(t) \right) \left(\frac{d}{dt} v_{C2}(t) \right) R^3 R_{L2} - 4\, C_2 L_2 v_{C2}(t) \left(\frac{d}{dt} i_o(t) \right) \left(\frac{d}{dt} v_{C2}(t) \right) R^2 R_{L2}$$

$$+ 2\, C_2 C_d L_2 \left(\frac{d}{dt} i_o(t) \right)^2 \left(\frac{d}{dt} v_{C2}(t) \right) R^3 R_{L2}^2 + 2\, C_2 C_d i_o(t) \left(\frac{d}{dt} i_o(t) \right) \left(\frac{d}{dt} v_{C2}(t) \right) R^3 R_{L2}^3$$

$$- 4\, C_2 C_d L_2 \left(\frac{d}{dt} i_o(t) \right) \left(\frac{d}{dt} v_{C2}(t) \right)^2 R^2 R_{L2}^2 - 2\, C_2 C_d v_{C2}(t) \left(\frac{d}{dt} i_o(t) \right) \left(\frac{d}{dt} v_{C2}(t) \right) R^3 R_{L2}^2$$

$$- 2\, C_2 C_d v_{C2}(t) \left(\frac{d}{dt} i_o(t) \right) \left(\frac{d}{dt} v_{C2}(t) \right) R^2 R_{L2}^3 + 4\, C_d L_2 i_o(t) \left(\frac{d}{dt} i_o(t) \right) \left(\frac{d}{dt} v_{C2}(t) \right) R^2 R_{L2}^2$$

$$- 4\, C_d L_2 v_{C2}(t) \left(\frac{d}{dt} i_o(t) \right) \left(\frac{d}{dt} v_{C2}(t) \right) R\, R_{L2}^2 - C_2^2 C_d \left(\frac{d}{dt} i_o(t) \right) \left(\frac{d}{dt} v_{C2}(t) \right)^2 R^3 R_{L2}^2 R_d$$

$$- 2\, C_d L_2 i_o(t) \left(\frac{d}{dt} i_o(t) \right)^2 R^3 R_{L2} R_d + 2\, C_d L_2 v_{C2}(t) \left(\frac{d}{dt} i_o(t) \right)^2 R^2 R_{L2} R_d$$

$$+ 2\, C_d v_{C2}(t)\, i_o(t) \left(\frac{d}{dt} i_o(t) \right) R^3 R_{L2} R_d + 2\, C_d v_{C2}(t)\, i_o(t) \left(\frac{d}{dt} i_o(t) \right) R^2 R_{L2}^2 R_d$$

$$+ 2\, C_d v_{C2}(t)\, i_{ref}(t) \left(\frac{d}{dt} i_{ref}(t) \right) R^3 R_{L1} R_d + C_d L_2 v_g(t) \left(\frac{d}{dt} i_o(t) \right) \left(\frac{d}{dt} i_{ref}(t) \right) R^3 R_d$$

$$+ C_d\, v_g(t)\, i_o(t) \left(\frac{\mathrm{d}}{\mathrm{d}t}\, i_{ref}(t)\right) R^3 R_{L2} R_d - C_d L_2\, v_g(t) \left(\frac{\mathrm{d}}{\mathrm{d}t}\, v_{C2}(t)\right) \left(\frac{\mathrm{d}}{\mathrm{d}t}\, i_{ref}(t)\right) R^2 R_d$$

$$- C_d\, v_g(t)\, v_{C2}(t) \left(\frac{\mathrm{d}}{\mathrm{d}t}\, i_{ref}(t)\right) R^2 R_{L2} R_d + C_d L_2 \left(\frac{\mathrm{d}}{\mathrm{d}t}\, i_o(t)\right) \left(\frac{\mathrm{d}}{\mathrm{d}t}\, v_g(t)\right) i_{ref}(t)\, R^3 R_d$$

$$+ C_d\, i_o(t) \left(\frac{\mathrm{d}}{\mathrm{d}t}\, v_g(t)\right) i_{ref}(t)\, R^3 R_{L2} R_d - C_d L_2 \left(\frac{\mathrm{d}}{\mathrm{d}t}\, v_{C2}(t)\right) \left(\frac{\mathrm{d}}{\mathrm{d}t}\, v_g(t)\right) i_{ref}(t)\, R^2 R_d$$

$$- C_d\, v_{C2}(t) \left(\frac{\mathrm{d}}{\mathrm{d}t}\, v_g(t)\right) i_{ref}(t)\, R^2 R_{L2} R_d - C_d L_1 L_2 \left(\frac{\mathrm{d}}{\mathrm{d}t}\, i_o(t)\right) \left(\frac{\mathrm{d}}{\mathrm{d}t}\, i_{ref}(t)\right)^2 R^3 R_d$$

$$- C_d L_1\, i_o(t) \left(\frac{\mathrm{d}}{\mathrm{d}t}\, i_{ref}(t)\right)^2 R^3 R_{L2} R_d + C_d L_1 L_2 \left(\frac{\mathrm{d}}{\mathrm{d}t}\, v_{C2}(t)\right) \left(\frac{\mathrm{d}}{\mathrm{d}t}\, i_{ref}(t)\right)^2 R^2 R_d$$

$$+ C_d L_1\, v_{C2}(t) \left(\frac{\mathrm{d}}{\mathrm{d}t}\, i_{ref}(t)\right)^2 R^2 R_{L2} R_d - 2\, C_2 C_d L_2 \left(\frac{\mathrm{d}}{\mathrm{d}t}\, i_o(t)\right) \left(\frac{\mathrm{d}}{\mathrm{d}t}\, v_{C2}(t)\right)^2 R^3 R_{L2}$$

$$+ 2\, C_d L_2\, i_o(t) \left(\frac{\mathrm{d}}{\mathrm{d}t}\, i_o(t)\right) \left(\frac{\mathrm{d}}{\mathrm{d}t}\, v_{C2}(t)\right) R^3 R_{L2} - 6\, C_d L_2\, v_{C2}(t) \left(\frac{\mathrm{d}}{\mathrm{d}t}\, i_o(t)\right) \left(\frac{\mathrm{d}}{\mathrm{d}t}\, v_{C2}(t)\right) R^2 R_{L2}$$

$$+ 2\, C_1 C_2 L_2 \left(\frac{\mathrm{d}}{\mathrm{d}t}\, i_o(t)\right)^2 \left(\frac{\mathrm{d}}{\mathrm{d}t}\, v_{C2}(t)\right) R^3 R_{L2}^2 + 2\, C_1 C_2\, i_o(t) \left(\frac{\mathrm{d}}{\mathrm{d}t}\, i_o(t)\right) \left(\frac{\mathrm{d}}{\mathrm{d}t}\, v_{C2}(t)\right) R^3 R_{L2}^3$$

$$- 4\, C_1 C_2 L_2 \left(\frac{\mathrm{d}}{\mathrm{d}t}\, i_o(t)\right) \left(\frac{\mathrm{d}}{\mathrm{d}t}\, v_{C2}(t)\right)^2 R^2 R_{L2}^2 - 2\, C_1 C_2\, v_{C2}(t) \left(\frac{\mathrm{d}}{\mathrm{d}t}\, i_o(t)\right) \left(\frac{\mathrm{d}}{\mathrm{d}t}\, v_{C2}(t)\right) R^3 R_{L2}^2$$

$$- 2\, C_1 C_2\, v_{C2}(t) \left(\frac{\mathrm{d}}{\mathrm{d}t}\, i_o(t)\right) \left(\frac{\mathrm{d}}{\mathrm{d}t}\, v_{C2}(t)\right) R^2 R_{L2}^3 + i_{ref}(t)\, R^2\, v_g(t)\, R_{L2} \left(\frac{\mathrm{d}}{\mathrm{d}t}\, v_{C2}(t)\right) R_d C_d$$

$$+ i_{ref}(t)^2 R^3 R_{L1} R_{L2} \left(\frac{\mathrm{d}}{\mathrm{d}t}\, i_o(t)\right) R_d C_d - i_{ref}(t)\, R^3\, v_g(t)\, R_{L2} \left(\frac{\mathrm{d}}{\mathrm{d}t}\, i_o(t)\right) R_d C_d$$

$$- i_{ref}(t)\, R^3 \left(\frac{\mathrm{d}}{\mathrm{d}t}\, i_{ref}(t)\right) L_1 \left(\frac{\mathrm{d}}{\mathrm{d}t}\, v_{C2}(t)\right) R_d C_d - i_{ref}(t)^2 R^2 R_{L1} R_{L2} \left(\frac{\mathrm{d}}{\mathrm{d}t}\, v_{C2}(t)\right) R_d C_d$$

$$- 2\, C_2 C_d\, i_o(t) \left(\frac{\mathrm{d}}{\mathrm{d}t}\, v_{C2}(t)\right)^2 R^2 R_{L2}^2 R_d + 2\, C_2 C_d L_2 \left(\frac{\mathrm{d}}{\mathrm{d}t}\, v_{C2}(t)\right)^3 R\, R_{L2} R_d$$

$$+ 2\, C_2 C_d\, v_{C2}(t) \left(\frac{\mathrm{d}}{\mathrm{d}t}\, v_{C2}(t)\right)^2 R^2 R_{L2} R_d + 2\, C_2 C_d\, v_{C2}(t) \left(\frac{\mathrm{d}}{\mathrm{d}t}\, v_{C2}(t)\right)^2 R\, R_{L2}^2 R_d$$

$$- 4\, C_d L_2\, v_{C2}(t) \left(\frac{\mathrm{d}}{\mathrm{d}t}\, i_o(t)\right) \left(\frac{\mathrm{d}}{\mathrm{d}t}\, v_{C2}(t)\right) R^2 R_d - 2\, C_d L_2\, i_o(t) \left(\frac{\mathrm{d}}{\mathrm{d}t}\, v_{C2}(t)\right)^2 R\, R_{L2} R_d$$

$$- 2\, C_d\, v_{C2}(t)\, i_o(t) \left(\frac{\mathrm{d}}{\mathrm{d}t}\, v_{C2}(t)\right) R^2 R_{L2} R_d - 2\, C_d\, v_{C2}(t)\, i_o(t) \left(\frac{\mathrm{d}}{\mathrm{d}t}\, v_{C2}(t)\right) R\, R_{L2}^2 R_d - 2\, C_1$$

$$L_2^2\, v_{C2}(t) \left(\frac{\mathrm{d}^2}{\mathrm{d}t^2}\, i_o(t)\right) \left(\frac{\mathrm{d}}{\mathrm{d}t}\, v_{C2}(t)\right) R\, R_{L2} - 2\, C_1 C_2 L_2^2\, i_o(t) \left(\frac{\mathrm{d}^2}{\mathrm{d}t^2}\, v_{C2}(t)\right)^2 R^2 R_{L2} + 2\, C_1$$

$$L_2^2\, i_o(t) \left(\frac{\mathrm{d}}{\mathrm{d}t}\, i_o(t)\right) \left(\frac{\mathrm{d}^2}{\mathrm{d}t^2}\, v_{C2}(t)\right) R^2 R_{L2} - 2\, C_1 L_2^2\, i_o(t) \left(\frac{\mathrm{d}^2}{\mathrm{d}t^2}\, v_{C2}(t)\right) \left(\frac{\mathrm{d}}{\mathrm{d}t}\, v_{C2}(t)\right) R\, R_{L2}$$

$$- 2\, C_1 L_2\, v_{C2}(t)\, i_o(t) \left(\frac{\mathrm{d}^2}{\mathrm{d}t^2}\, v_{C2}(t)\right) R^2 R_{L2} + 3\, C_1 C_2 L_2^2 \left(\frac{\mathrm{d}}{\mathrm{d}t}\, i_o(t)\right)^2 \left(\frac{\mathrm{d}^2}{\mathrm{d}t^2}\, v_{C2}(t)\right) R^3 R_{L2} + 2\, C_1 C_2^2$$

$$L_2^2 \left(\frac{\mathrm{d}^3}{\mathrm{d}t^3}\, v_{C2}(t)\right) \left(\frac{\mathrm{d}}{\mathrm{d}t}\, v_{C2}(t)\right)^2 R^2 R_{L2} + 5\, C_2^2 C_d L_2^2 \left(\frac{\mathrm{d}^2}{\mathrm{d}t^2}\, v_{C2}(t)\right)^2 \left(\frac{\mathrm{d}}{\mathrm{d}t}\, v_{C2}(t)\right) R^2 R_{L2} + 5$$

$$C_2^2 C_d L_2 \left(\frac{\mathrm{d}^2}{\mathrm{d}t^2}\, v_{C2}(t)\right) \left(\frac{\mathrm{d}}{\mathrm{d}t}\, v_{C2}(t)\right)^2 R^2 R_{L2}^2 - 2\, C_2 C_d L_2^2\, i_o(t) \left(\frac{\mathrm{d}^2}{\mathrm{d}t^2}\, v_{C2}(t)\right)^2 R^2 R_{L2} + 2\, C_2 C_d$$

$$L_2^2\, v_{C2}(t) \left(\frac{\mathrm{d}^2}{\mathrm{d}t^2}\, v_{C2}(t)\right)^2 R\, R_{L2} + 5\, C_2 C_d L_2^2 \left(\frac{\mathrm{d}^2}{\mathrm{d}t^2}\, v_{C2}(t)\right) \left(\frac{\mathrm{d}}{\mathrm{d}t}\, v_{C2}(t)\right)^2 R\, R_{L2}$$

$$+ C_1 C_2 L_2\, i_o(t)^2 \left(\frac{\mathrm{d}^3}{\mathrm{d}t^3}\, v_{C2}(t)\right) R^3 R_{L2}^2 - C_1 C_2^2 L_2 \left(\frac{\mathrm{d}^2}{\mathrm{d}t^2}\, i_o(t)\right) \left(\frac{\mathrm{d}}{\mathrm{d}t}\, v_{C2}(t)\right)^2 R^3 R_{L2}^2$$

$$- 2\, C_2 C_d\, v_{C2}(t)\, i_o(t) \left(\frac{\mathrm{d}^2}{\mathrm{d}t^2}\, v_{C2}(t)\right) R^3 R_{L2}^2 - 2\, C_2 C_d\, v_{C2}(t)\, i_o(t) \left(\frac{\mathrm{d}^2}{\mathrm{d}t^2}\, v_{C2}(t)\right) R^2 R_{L2}^3 +$$

$$C_2^3 C_d L_2 \left(\frac{\mathrm{d}^3}{\mathrm{d}t^3}\, v_{C2}(t)\right) \left(\frac{\mathrm{d}}{\mathrm{d}t}\, v_{C2}(t)\right)^2 R^3 R_{L2}^2 - 2\, C_2^2 C_d L_2^3 \left(\frac{\mathrm{d}}{\mathrm{d}t}\, i_o(t)\right) \left(\frac{\mathrm{d}^3}{\mathrm{d}t^3}\, v_{C2}(t)\right) \left(\frac{\mathrm{d}^2}{\mathrm{d}t^2}\, v_{C2}(t)\right) R^3$$

$$+ 2\, C_2^2 C_d L_2^3 \left(\frac{\mathrm{d}^3}{\mathrm{d}t^3}\, v_{C2}(t)\right) \left(\frac{\mathrm{d}^2}{\mathrm{d}t^2}\, v_{C2}(t)\right) \left(\frac{\mathrm{d}}{\mathrm{d}t}\, v_{C2}(t)\right) R^2 + 2\, C_2^2 C_d$$

UNIVERSITAT ROVIRA I VIRGILI
DESIGN AND CONTROL OF A BIDIRECTIONAL DC/DC CONVERTER FOR AN ELECTRIC VEHICLE APPLICATION.
Laura Albiol Rendillo
Dipòsit Legal: T 1361-2015

$$L_2^2 v_{C2}(t) \left(\frac{\mathrm{d}^3}{\mathrm{d}t^3} v_{C2}(t) \right) \left(\frac{\mathrm{d}^2}{\mathrm{d}t^2} v_{C2}(t) \right) R^3 + 2 C_2^2 C_d L_2^2 \left(\frac{\mathrm{d}^3}{\mathrm{d}t^3} v_{C2}(t) \right) \left(\frac{\mathrm{d}}{\mathrm{d}t} v_{C2}(t) \right)^2 R^2 R_{L2}$$

$$+ C_2 C_d L_2 i_o(t)^2 \left(\frac{\mathrm{d}^3}{\mathrm{d}t^3} v_{C2}(t) \right) R^3 R_{L2}^2 - 2 C_2 C_d L_2^3 \left(\frac{\mathrm{d}}{\mathrm{d}t} i_o(t) \right) \left(\frac{\mathrm{d}^3}{\mathrm{d}t^3} v_{C2}(t) \right) \left(\frac{\mathrm{d}}{\mathrm{d}t} v_{C2}(t) \right) R^2$$

$$- 2 C_2 C_d L_2^2 v_{C2}(t) \left(\frac{\mathrm{d}}{\mathrm{d}t} i_o(t) \right) \left(\frac{\mathrm{d}^3}{\mathrm{d}t^3} v_{C2}(t) \right) R^3 + 2 C_2 C_d L_2^2 v_{C2}(t) \left(\frac{\mathrm{d}^3}{\mathrm{d}t^3} v_{C2}(t) \right) \left(\frac{\mathrm{d}}{\mathrm{d}t} v_{C2}(t) \right) R^2$$

$$+ 2 C_2 C_d L_2 v_{C2}(t)^2 \left(\frac{\mathrm{d}^3}{\mathrm{d}t^3} v_{C2}(t) \right) R^2 R_{L2} + 2 C_1 C_2^2 L_2 v_{C2}(t) \left(\frac{\mathrm{d}^2}{\mathrm{d}t^2} v_{C2}(t) \right)^2 R^2 R_{L2}^2 + 2 C_1 C_2$$

$$L_2^2 v_{C2}(t) \left(\frac{\mathrm{d}^3}{\mathrm{d}t^3} v_{C2}(t) \right) \left(\frac{\mathrm{d}}{\mathrm{d}t} v_{C2}(t) \right) R^2 + 2 C_1 C_2^2 L_2 \left(\frac{\mathrm{d}^2}{\mathrm{d}t^2} v_{C2}(t) \right) \left(\frac{\mathrm{d}}{\mathrm{d}t} v_{C2}(t) \right)^2 R^3 R_{L2} - 2 C_1 C_2$$

$$L_2^2 \left(\frac{\mathrm{d}}{\mathrm{d}t} i_o(t) \right) \left(\frac{\mathrm{d}^2}{\mathrm{d}t^2} v_{C2}(t) \right) \left(\frac{\mathrm{d}}{\mathrm{d}t} v_{C2}(t) \right) R^3 + 2 C_1 C_2 L_2 v_{C2}(t) \left(\frac{\mathrm{d}^2}{\mathrm{d}t^2} v_{C2}(t) \right) \left(\frac{\mathrm{d}}{\mathrm{d}t} v_{C2}(t) \right) R^3$$

$$+ C_2 L_1 L_2 \left(\frac{\mathrm{d}^2}{\mathrm{d}t^2} v_{C2}(t) \right) i_{ref}(t) \left(\frac{\mathrm{d}}{\mathrm{d}t} i_{ref}(t) \right) R^3 + 2 C_d L_2^2 i_o(t) \left(\frac{\mathrm{d}}{\mathrm{d}t} i_o(t) \right) \left(\frac{\mathrm{d}^2}{\mathrm{d}t^2} v_{C2}(t) \right) R^2 R_{L2} - 2 C_d$$

$$L_2^2 v_{C2}(t) \left(\frac{\mathrm{d}}{\mathrm{d}t} i_o(t) \right) \left(\frac{\mathrm{d}^2}{\mathrm{d}t^2} v_{C2}(t) \right) R R_{L2} - 2 C_d L_2^2 i_o(t) \left(\frac{\mathrm{d}^2}{\mathrm{d}t^2} v_{C2}(t) \right) \left(\frac{\mathrm{d}}{\mathrm{d}t} v_{C2}(t) \right) R R_{L2}$$

$$- 2 C_d L_2 v_{C2}(t) i_o(t) \left(\frac{\mathrm{d}^2}{\mathrm{d}t^2} v_{C2}(t) \right) R^2 R_{L2} - 2 C_d L_2 v_{C2}(t) i_o(t) \left(\frac{\mathrm{d}^2}{\mathrm{d}t^2} v_{C2}(t) \right) R R_{L2}^2 + 2$$

$$C_2^3 C_d L_2 \left(\frac{\mathrm{d}^2}{\mathrm{d}t^2} v_{C2}(t) \right)^2 \left(\frac{\mathrm{d}}{\mathrm{d}t} v_{C2}(t) \right) R^3 R_{L2}^2 - 2 C_2^2 C_d L_2 i_o(t) \left(\frac{\mathrm{d}^2}{\mathrm{d}t^2} v_{C2}(t) \right)^2 R^3 R_{L2}^2 - 2$$

$$C_2^2 C_d i_o(t) \left(\frac{\mathrm{d}^2}{\mathrm{d}t^2} v_{C2}(t) \right) \left(\frac{\mathrm{d}}{\mathrm{d}t} v_{C2}(t) \right) R^3 R_{L2}^3 + 2 C_2^2 C_d L_2 v_{C2}(t) \left(\frac{\mathrm{d}^2}{\mathrm{d}t^2} v_{C2}(t) \right)^2 R^3 R_{L2} + 2$$

$$C_2^2 C_d L_2 v_{C2}(t) \left(\frac{\mathrm{d}^2}{\mathrm{d}t^2} v_{C2}(t) \right)^2 R^2 R_{L2}^2 + 2 C_2^2 C_d v_{C2}(t) \left(\frac{\mathrm{d}^2}{\mathrm{d}t^2} v_{C2}(t) \right) \left(\frac{\mathrm{d}}{\mathrm{d}t} v_{C2}(t) \right) R^3 R_{L2}^2 + 2$$

$$C_2^2 C_d v_{C2}(t) \left(\frac{\mathrm{d}^2}{\mathrm{d}t^2} v_{C2}(t) \right) \left(\frac{\mathrm{d}}{\mathrm{d}t} v_{C2}(t) \right) R^2 R_{L2}^3 - C_2^2 C_d L_2 \left(\frac{\mathrm{d}^2}{\mathrm{d}t^2} i_o(t) \right) \left(\frac{\mathrm{d}}{\mathrm{d}t} v_{C2}(t) \right)^2 R^3 R_{L2}^2 + 2 C_2 C_d$$

$$L_2^3 \left(\frac{\mathrm{d}}{\mathrm{d}t} i_o(t) \right) \left(\frac{\mathrm{d}^2}{\mathrm{d}t^2} i_o(t) \right) \left(\frac{\mathrm{d}^2}{\mathrm{d}t^2} v_{C2}(t) \right) R^3 - 2 C_2 C_d L_2^3 \left(\frac{\mathrm{d}^2}{\mathrm{d}t^2} i_o(t) \right) \left(\frac{\mathrm{d}^2}{\mathrm{d}t^2} v_{C2}(t) \right) \left(\frac{\mathrm{d}}{\mathrm{d}t} v_{C2}(t) \right) R^2$$

$$- 2 C_2 C_d L_2^2 v_{C2}(t) \left(\frac{\mathrm{d}^2}{\mathrm{d}t^2} i_o(t) \right) \left(\frac{\mathrm{d}^2}{\mathrm{d}t^2} v_{C2}(t) \right) R^3 - 2 C_2 C_d L_2^2 \left(\frac{\mathrm{d}^2}{\mathrm{d}t^2} i_o(t) \right) \left(\frac{\mathrm{d}}{\mathrm{d}t} v_{C2}(t) \right)^2 R^2 R_{L2}$$

$$- 2 C_d L_2^2 i_o(t) \left(\frac{\mathrm{d}}{\mathrm{d}t} i_o(t) \right) \left(\frac{\mathrm{d}^2}{\mathrm{d}t^2} i_o(t) \right) R^3 R_{L2} + 2 C_d L_2^2 v_{C2}(t) \left(\frac{\mathrm{d}}{\mathrm{d}t} i_o(t) \right) \left(\frac{\mathrm{d}^2}{\mathrm{d}t^2} i_o(t) \right) R^2 R_{L2} + 2 C_d$$

$$L_2^2 i_o(t) \left(\frac{\mathrm{d}^2}{\mathrm{d}t^2} i_o(t) \right) \left(\frac{\mathrm{d}}{\mathrm{d}t} v_{C2}(t) \right) R^2 R_{L2} + C_2 C_d L_2 v_{C2}(t)^2 \left(\frac{\mathrm{d}^3}{\mathrm{d}t^3} v_{C2}(t) \right) R R_{L2}^2 - 2 C_1 C_2$$

$$L_2^2 \left(\frac{\mathrm{d}^2}{\mathrm{d}t^2} i_o(t) \right) \left(\frac{\mathrm{d}}{\mathrm{d}t} v_{C2}(t) \right)^2 R^2 R_{L2} - 4 C_2^2 L_2 i_o(t) \left(\frac{\mathrm{d}^2}{\mathrm{d}t^2} v_{C2}(t) \right) \left(\frac{\mathrm{d}}{\mathrm{d}t} v_{C2}(t) \right) R^3 R_{L2} + C_1$$

$$C_2^3 L_2 \left(\frac{\mathrm{d}^3}{\mathrm{d}t^3} v_{C2}(t) \right) \left(\frac{\mathrm{d}}{\mathrm{d}t} v_{C2}(t) \right)^2 R^3 R_{L2}^2 + 2 C_1 L_2^2 v_{C2}(t) \left(\frac{\mathrm{d}}{\mathrm{d}t} i_o(t) \right) \left(\frac{\mathrm{d}^2}{\mathrm{d}t^2} i_o(t) \right) R^2 R_{L2} + 2 C_1$$

$$C_2^2 v_{C2}(t) \left(\frac{\mathrm{d}^2}{\mathrm{d}t^2} v_{C2}(t) \right) \left(\frac{\mathrm{d}}{\mathrm{d}t} v_{C2}(t) \right) R^3 R_{L2}^2 + 2 C_1 C_2^2 v_{C2}(t) \left(\frac{\mathrm{d}^2}{\mathrm{d}t^2} v_{C2}(t) \right) \left(\frac{\mathrm{d}}{\mathrm{d}t} v_{C2}(t) \right) R^2 R_{L2}^3 + 2 C_1$$

$$C_2^2 L_2 v_{C2}(t) \left(\frac{\mathrm{d}^2}{\mathrm{d}t^2} v_{C2}(t) \right)^2 R^3 R_{L2} - 2 C_1 C_2 v_{C2}(t) i_o(t) \left(\frac{\mathrm{d}^2}{\mathrm{d}t^2} v_{C2}(t) \right) R^3 R_{L2}^2 - 2 C_1 C_2^2$$

$$L_2^3 \left(\frac{\mathrm{d}}{\mathrm{d}t} i_o(t) \right) \left(\frac{\mathrm{d}^3}{\mathrm{d}t^3} v_{C2}(t) \right) \left(\frac{\mathrm{d}^2}{\mathrm{d}t^2} v_{C2}(t) \right) R^3 + 2 C_1 C_2^2$$

$$L_2^3 \left(\frac{\mathrm{d}^3}{\mathrm{d}t^3} v_{C2}(t) \right) \left(\frac{\mathrm{d}^2}{\mathrm{d}t^2} v_{C2}(t) \right) \left(\frac{\mathrm{d}}{\mathrm{d}t} v_{C2}(t) \right) R^2 + 2 C_1 C_2^2 L_2^2 v_{C2}(t) \left(\frac{\mathrm{d}^3}{\mathrm{d}t^3} v_{C2}(t) \right) \left(\frac{\mathrm{d}^2}{\mathrm{d}t^2} v_{C2}(t) \right) R^3$$

$$+ 4 C_2^2 L_2 v_{C2}(t) \left(\frac{\mathrm{d}^2}{\mathrm{d}t^2} v_{C2}(t) \right) \left(\frac{\mathrm{d}}{\mathrm{d}t} v_{C2}(t) \right) R^2 R_{L2} - 4 C_2 L_2 v_{C2}(t) i_o(t) \left(\frac{\mathrm{d}^2}{\mathrm{d}t^2} v_{C2}(t) \right) R^2 R_{L2}$$

$$+ 2 C_1 C_2 L_2^2 v_{C2}(t) \left(\frac{\mathrm{d}^2}{\mathrm{d}t^2} v_{C2}(t) \right)^2 R R_{L2} - 2 C_1 L_2^2 v_{C2}(t) \left(\frac{\mathrm{d}}{\mathrm{d}t} i_o(t) \right) \left(\frac{\mathrm{d}^2}{\mathrm{d}t^2} v_{C2}(t) \right) R R_{L2}$$

$$- 2 C_1 L_2 v_{C2}(t) i_o(t) \left(\frac{\mathrm{d}^2}{\mathrm{d}t^2} v_{C2}(t) \right) R R_{L2}^2 + 5 C_1 C_2^2 L_2^2 \left(\frac{\mathrm{d}^2}{\mathrm{d}t^2} v_{C2}(t) \right)^2 \left(\frac{\mathrm{d}}{\mathrm{d}t} v_{C2}(t) \right) R^2 R_{L2} + 5 C_1 C_2$$

$$L_2^2 \left(\frac{\mathrm{d}^2}{\mathrm{d}t^2} v_{C2}(t) \right) \left(\frac{\mathrm{d}}{\mathrm{d}t} v_{C2}(t) \right)^2 R\, R_{L2} + 2\, C_d L_2 v_{C2}(t)\, i_o(t) \left(\frac{\mathrm{d}^2}{\mathrm{d}t^2} i_o(t) \right) R^3 R_{L2}$$

$$+ 2\, C_d L_2 v_{C2}(t)\, i_o(t) \left(\frac{\mathrm{d}^2}{\mathrm{d}t^2} i_o(t) \right) R^2 R_{L2}^2 - 2\, C_d L_2^2 v_{C2}(t) \left(\frac{\mathrm{d}^2}{\mathrm{d}t^2} i_o(t) \right) \left(\frac{\mathrm{d}}{\mathrm{d}t} v_{C2}(t) \right) R\, R_{L2} - 3\, C_2^2 C_d$$

$$L_2^2 \left(\frac{\mathrm{d}}{\mathrm{d}t} i_o(t) \right) \left(\frac{\mathrm{d}^2}{\mathrm{d}t^2} v_{C2}(t) \right)^2 R^3 R_{L2} + 3\, C_2 C_d L_2^2 \left(\frac{\mathrm{d}}{\mathrm{d}t} i_o(t) \right)^2 \left(\frac{\mathrm{d}^2}{\mathrm{d}t^2} v_{C2}(t) \right) R^3 R_{L2} - 2\, C_1 C_2$$

$$L_2^3 \left(\frac{\mathrm{d}^2}{\mathrm{d}t^2} i_o(t) \right) \left(\frac{\mathrm{d}^2}{\mathrm{d}t^2} v_{C2}(t) \right) \left(\frac{\mathrm{d}}{\mathrm{d}t} v_{C2}(t) \right) R^2 - 2\, C_1 C_2 L_2^2 v_{C2}(t) \left(\frac{\mathrm{d}^2}{\mathrm{d}t^2} i_o(t) \right) \left(\frac{\mathrm{d}^2}{\mathrm{d}t^2} v_{C2}(t) \right) R^3$$

$$- 2\, C_1 L_2^2 i_o(t) \left(\frac{\mathrm{d}}{\mathrm{d}t} i_o(t) \right) \left(\frac{\mathrm{d}^2}{\mathrm{d}t^2} i_o(t) \right) R^3 R_{L2} + 2\, C_1 L_2^2 i_o(t) \left(\frac{\mathrm{d}^2}{\mathrm{d}t^2} i_o(t) \right) \left(\frac{\mathrm{d}}{\mathrm{d}t} v_{C2}(t) \right) R^2 R_{L2}$$

$$+ 2\, C_1 L_2 v_{C2}(t)\, i_o(t) \left(\frac{\mathrm{d}^2}{\mathrm{d}t^2} i_o(t) \right) R^3 R_{L2} + 2\, C_1 L_2 v_{C2}(t)\, i_o(t) \left(\frac{\mathrm{d}^2}{\mathrm{d}t^2} i_o(t) \right) R^2 R_{L2}^2 - 3\, C_1 C_2^2$$

$$L_2^2 \left(\frac{\mathrm{d}}{\mathrm{d}t} i_o(t) \right) \left(\frac{\mathrm{d}^2}{\mathrm{d}t^2} v_{C2}(t) \right)^2 R^3 R_{L2} - 3\, C_2^2 C_d L_2^2 \left(\frac{\mathrm{d}}{\mathrm{d}t} i_o(t) \right) \left(\frac{\mathrm{d}^2}{\mathrm{d}t^2} v_{C2}(t) \right)^2 R^3 R_d + 2$$

$$C_2^2 C_d L_2 v_{C2}(t) \left(\frac{\mathrm{d}^2}{\mathrm{d}t^2} v_{C2}(t) \right)^2 R^3 R_d + 3\, C_2 C_d L_2^2 \left(\frac{\mathrm{d}}{\mathrm{d}t} i_o(t) \right)^2 \left(\frac{\mathrm{d}^2}{\mathrm{d}t^2} v_{C2}(t) \right) R^3 R_d$$

$$+ C_2 C_d i_o(t)^2 \left(\frac{\mathrm{d}^2}{\mathrm{d}t^2} v_{C2}(t) \right) R^3 R_{L2}^2 R_d + 2\, C_2 C_d v_{C2}(t)^2 \left(\frac{\mathrm{d}^2}{\mathrm{d}t^2} v_{C2}(t) \right) R^2 R_{L2} R_d$$

$$+ C_2 C_d v_{C2}(t)^2 \left(\frac{\mathrm{d}^2}{\mathrm{d}t^2} v_{C2}(t) \right) R\, R_{L2}^2 R_d + C_d L_1 v_{C2}(t) \left(\frac{\mathrm{d}^2}{\mathrm{d}t^2} i_{ref}(t) \right) i_{ref}(t)\, R^3 R_d + 2$$

$$C_2^2 C_d L_2 \left(\frac{\mathrm{d}^2}{\mathrm{d}t^2} v_{C2}(t) \right) \left(\frac{\mathrm{d}}{\mathrm{d}t} v_{C2}(t) \right)^2 R^3 R_{L2} - 2\, C_2 C_d L_2^2 \left(\frac{\mathrm{d}}{\mathrm{d}t} i_o(t) \right) \left(\frac{\mathrm{d}^2}{\mathrm{d}t^2} v_{C2}(t) \right) \left(\frac{\mathrm{d}}{\mathrm{d}t} v_{C2}(t) \right) R^3$$

$$+ 2\, C_2 C_d L_2 v_{C2}(t) \left(\frac{\mathrm{d}^2}{\mathrm{d}t^2} v_{C2}(t) \right) \left(\frac{\mathrm{d}}{\mathrm{d}t} v_{C2}(t) \right) R^3 + 2\, C_1 C_2^3 L_2 \left(\frac{\mathrm{d}^2}{\mathrm{d}t^2} v_{C2}(t) \right)^2 \left(\frac{\mathrm{d}}{\mathrm{d}t} v_{C2}(t) \right) R^3 R_{L2}^2$$

$$- 2\, C_1 C_2^2 i_o(t) \left(\frac{\mathrm{d}^2}{\mathrm{d}t^2} v_{C2}(t) \right) \left(\frac{\mathrm{d}}{\mathrm{d}t} v_{C2}(t) \right) R^3 R_{L2}^3 + 5\, C_1 C_2^2 L_2 \left(\frac{\mathrm{d}^2}{\mathrm{d}t^2} v_{C2}(t) \right) \left(\frac{\mathrm{d}}{\mathrm{d}t} v_{C2}(t) \right)^2 R^2 R_{L2}^2$$

$$+ 2\, C_1 C_2 L_2 v_{C2}(t)^2 \left(\frac{\mathrm{d}^3}{\mathrm{d}t^3} v_{C2}(t) \right) R^2 R_{L2} + C_1 C_2 L_2 v_{C2}(t)^2 \left(\frac{\mathrm{d}^3}{\mathrm{d}t^3} v_{C2}(t) \right) R\, R_{L2}^2 - 2\, C_1$$

$$C_2^2 L_2 i_o(t) \left(\frac{\mathrm{d}^2}{\mathrm{d}t^2} v_{C2}(t) \right)^2 R^3 R_{L2}^2 - 2\, C_1 C_2 v_{C2}(t)\, i_o(t) \left(\frac{\mathrm{d}^2}{\mathrm{d}t^2} v_{C2}(t) \right) R^2 R_{L2}^3 - 2\, C_1 C_2$$

$$L_2^3 \left(\frac{\mathrm{d}}{\mathrm{d}t} i_o(t) \right) \left(\frac{\mathrm{d}^3}{\mathrm{d}t^3} v_{C2}(t) \right) \left(\frac{\mathrm{d}}{\mathrm{d}t} v_{C2}(t) \right) R^2 - 2\, C_1 C_2 L_2^2 v_{C2}(t) \left(\frac{\mathrm{d}}{\mathrm{d}t} i_o(t) \right) \left(\frac{\mathrm{d}^3}{\mathrm{d}t^3} v_{C2}(t) \right) R^3$$

$$+ 2\, C_1 C_2 L_2^3 \left(\frac{\mathrm{d}}{\mathrm{d}t} i_o(t) \right) \left(\frac{\mathrm{d}^2}{\mathrm{d}t^2} i_o(t) \right) \left(\frac{\mathrm{d}^2}{\mathrm{d}t^2} v_{C2}(t) \right) R^3 + i_{ref}(t)^2 R^3 R_{L1} L_2 \left(\frac{\mathrm{d}^2}{\mathrm{d}t^2} i_o(t) \right) R_d C_d$$

$$- i_{ref}(t)\, R^3 v_g(t)\, L_2 \left(\frac{\mathrm{d}^2}{\mathrm{d}t^2} i_o(t) \right) R_d C_d - i_{ref}(t)^2 R^2 R_{L1} L_2 \left(\frac{\mathrm{d}^2}{\mathrm{d}t^2} v_{C2}(t) \right) R_d C_d$$

$$+ i_{ref}(t)\, R^2 v_g(t)\, L_2 \left(\frac{\mathrm{d}^2}{\mathrm{d}t^2} v_{C2}(t) \right) R_d C_d + 3\, C_2^2 C_d L_2^2 \left(\frac{\mathrm{d}^2}{\mathrm{d}t^2} v_{C2}(t) \right)^2 \left(\frac{\mathrm{d}}{\mathrm{d}t} v_{C2}(t) \right) R^2 R_d + 3\, C_2 C_d$$

$$L_2^2 \left(\frac{\mathrm{d}^2}{\mathrm{d}t^2} v_{C2}(t) \right) \left(\frac{\mathrm{d}}{\mathrm{d}t} v_{C2}(t) \right)^2 R\, R_d + C_2^3 C_d \left(\frac{\mathrm{d}^2}{\mathrm{d}t^2} v_{C2}(t) \right) \left(\frac{\mathrm{d}}{\mathrm{d}t} v_{C2}(t) \right)^2 R^3 R_{L2}^2 R_d - C_d$$

$$L_2^3 \left(\frac{\mathrm{d}^2}{\mathrm{d}t^2} i_o(t) \right) \left(\frac{\mathrm{d}}{\mathrm{d}t} v_{C2}(t) \right)^2 R + C_1 L_2 v_{C2}(t)^2 \left(\frac{\mathrm{d}^2}{\mathrm{d}t^2} v_{C2}(t) \right) R^2 - C_1 L_2^3 \left(\frac{\mathrm{d}^2}{\mathrm{d}t^2} i_o(t) \right) \left(\frac{\mathrm{d}}{\mathrm{d}t} v_{C2}(t) \right)^2 R$$

$$+ C_1 L_2^3 \left(\frac{\mathrm{d}}{\mathrm{d}t} i_o(t) \right)^2 \left(\frac{\mathrm{d}^2}{\mathrm{d}t^2} v_{C2}(t) \right) R^2 + C_2^2 C_d L_2^3 \left(\frac{\mathrm{d}^2}{\mathrm{d}t^2} v_{C2}(t) \right)^3 R^2 + C_d$$

$$L_2^3 \left(\frac{\mathrm{d}}{\mathrm{d}t} i_o(t) \right)^2 \left(\frac{\mathrm{d}^2}{\mathrm{d}t^2} v_{C2}(t) \right) R^2 + C_d L_2 v_{C2}(t)^2 \left(\frac{\mathrm{d}^2}{\mathrm{d}t^2} v_{C2}(t) \right) R^2 + C_d L_2 v_{C2}(t)^2 \left(\frac{\mathrm{d}^2}{\mathrm{d}t^2} v_{C2}(t) \right) R_{L2}^2 +$$

$$C_2^2 L_2^2 v_{C2}(t) \left(\frac{\mathrm{d}^2}{\mathrm{d}t^2} v_{C2}(t) \right)^2 R^2 + 2\, C_2 L_2 v_{C2}(t)^2 \left(\frac{\mathrm{d}^2}{\mathrm{d}t^2} v_{C2}(t) \right) R^2 + C_1 L_2 v_{C2}(t)^2 \left(\frac{\mathrm{d}^2}{\mathrm{d}t^2} v_{C2}(t) \right) R_{L2}^2 + 2$$

$$C_2^2 L_2^2 \left(\frac{\mathrm{d}^2}{\mathrm{d}t^2} v_{C2}(t) \right) \left(\frac{\mathrm{d}}{\mathrm{d}t} v_{C2}(t) \right)^2 R^2 - C_1 L_2 v_{C2}(t)^2 \left(\frac{\mathrm{d}^2}{\mathrm{d}t^2} i_o(t) \right) R^3 - C_1$$

$$L_2^3 \left(\frac{\mathrm{d}}{\mathrm{d}t} i_o(t) \right)^2 \left(\frac{\mathrm{d}^2}{\mathrm{d}t^2} i_o(t) \right) R^3 - 2\, C_2 C_d v_{C2}(t) \left(\frac{\mathrm{d}}{\mathrm{d}t} i_o(t) \right) \left(\frac{\mathrm{d}}{\mathrm{d}t} v_{C2}(t) \right) R^2 R_{L2}^2 R_d$$

$$-2\,C_d L_2 \left(\frac{\mathrm{d}}{\mathrm{d}t}\, i_o(t)\right) i_{ref}(t) \left(\frac{\mathrm{d}}{\mathrm{d}t}\, i_{ref}(t)\right) R^3 R_{L1} R_d - 2\,C_d\, i_o(t)\, i_{ref}(t) \left(\frac{\mathrm{d}}{\mathrm{d}t}\, i_{ref}(t)\right) R^3 R_{L1} R_{L2} R_d$$

$$+2\,C_d L_2 \left(\frac{\mathrm{d}}{\mathrm{d}t}\, v_{C2}(t)\right) i_{ref}(t) \left(\frac{\mathrm{d}}{\mathrm{d}t}\, i_{ref}(t)\right) R^2 R_{L1} R_d + 2\,C_d\, v_{C2}(t)\, i_{ref}(t) \left(\frac{\mathrm{d}}{\mathrm{d}t}\, i_{ref}(t)\right) R^2 R_{L1} R_{L2} R_d$$

$$-i_{ref}(t)\, R^2 \left(\frac{\mathrm{d}}{\mathrm{d}t}\, i_{ref}(t)\right) L_1 R_{L2} \left(\frac{\mathrm{d}}{\mathrm{d}t}\, v_{C2}(t)\right) R_d C_d + i_{ref}(t)\, R^3 \left(\frac{\mathrm{d}}{\mathrm{d}t}\, i_{ref}(t)\right) L_1 R_{L2} \left(\frac{\mathrm{d}}{\mathrm{d}t}\, i_o(t)\right) R_d C_d$$

$$-C_2 C_d\, v_g(t) \left(\frac{\mathrm{d}}{\mathrm{d}t}\, v_{C2}(t)\right) \left(\frac{\mathrm{d}}{\mathrm{d}t}\, i_{ref}(t)\right) R^3 R_{L2} R_d - C_2 C_d \left(\frac{\mathrm{d}}{\mathrm{d}t}\, v_{C2}(t)\right) \left(\frac{\mathrm{d}}{\mathrm{d}t}\, v_g(t)\right) i_{ref}(t)\, R^3 R_{L2} R_d$$

$$+C_2 C_d L_1 \left(\frac{\mathrm{d}}{\mathrm{d}t}\, v_{C2}(t)\right) \left(\frac{\mathrm{d}}{\mathrm{d}t}\, i_{ref}(t)\right)^2 R^3 R_{L2} R_d + 4\,C_d L_2\, i_o(t) \left(\frac{\mathrm{d}}{\mathrm{d}t}\, i_o(t)\right) \left(\frac{\mathrm{d}}{\mathrm{d}t}\, v_{C2}(t)\right) R^2 R_{L2} R_d$$

$$-4\,C_d L_2\, v_{C2}(t) \left(\frac{\mathrm{d}}{\mathrm{d}t}\, i_o(t)\right) \left(\frac{\mathrm{d}}{\mathrm{d}t}\, v_{C2}(t)\right) R\, R_{L2} R_d - 4\,C_2 C_d L_2 \left(\frac{\mathrm{d}}{\mathrm{d}t}\, i_o(t)\right) \left(\frac{\mathrm{d}}{\mathrm{d}t}\, v_{C2}(t)\right)^2 R^2 R_{L2} R_d$$

$$+2\,C_2 C_d L_2 \left(\frac{\mathrm{d}}{\mathrm{d}t}\, i_o(t)\right)^2 \left(\frac{\mathrm{d}}{\mathrm{d}t}\, v_{C2}(t)\right) R^3 R_{L2} R_d + 2\,C_2 C_d\, i_o(t) \left(\frac{\mathrm{d}}{\mathrm{d}t}\, i_o(t)\right) \left(\frac{\mathrm{d}}{\mathrm{d}t}\, v_{C2}(t)\right) R^3 R_{L2}^2 R_d$$

$$-2\,C_2 C_d\, v_{C2}(t) \left(\frac{\mathrm{d}}{\mathrm{d}t}\, i_o(t)\right) \left(\frac{\mathrm{d}}{\mathrm{d}t}\, v_{C2}(t)\right) R^3 R_{L2} R_d + 2\,C_2 C_d L_2\, i_o(t) \left(\frac{\mathrm{d}^2}{\mathrm{d}t^2}\, i_o(t)\right) \left(\frac{\mathrm{d}}{\mathrm{d}t}\, v_{C2}(t)\right) R^3 R_{L2}^2$$

$$-2\,C_2^2 C_d L_2^2 \left(\frac{\mathrm{d}^2}{\mathrm{d}t^2}\, i_o(t)\right) \left(\frac{\mathrm{d}^2}{\mathrm{d}t^2}\, v_{C2}(t)\right) \left(\frac{\mathrm{d}}{\mathrm{d}t}\, v_{C2}(t)\right) R^3 R_{L2} - 8\,C_1 C_2$$

$$L_2^2 \left(\frac{\mathrm{d}}{\mathrm{d}t}\, i_o(t)\right) \left(\frac{\mathrm{d}^2}{\mathrm{d}t^2}\, v_{C2}(t)\right) \left(\frac{\mathrm{d}}{\mathrm{d}t}\, v_{C2}(t)\right) R^2 R_{L2} - 2\,C_2^2 C_d L_2\, i_o(t) \left(\frac{\mathrm{d}^3}{\mathrm{d}t^3}\, v_{C2}(t)\right) \left(\frac{\mathrm{d}}{\mathrm{d}t}\, v_{C2}(t)\right) R^3 R_{L2}^2$$

$$+2\,C_1 C_2 L_2^2\, i_o(t) \left(\frac{\mathrm{d}}{\mathrm{d}t}\, i_o(t)\right) \left(\frac{\mathrm{d}^3}{\mathrm{d}t^3}\, v_{C2}(t)\right) R^3 R_{L2} + 2\,C_2 C_d$$

$$L_2^2 \left(\frac{\mathrm{d}}{\mathrm{d}t}\, i_o(t)\right) \left(\frac{\mathrm{d}^2}{\mathrm{d}t^2}\, i_o(t)\right) \left(\frac{\mathrm{d}}{\mathrm{d}t}\, v_{C2}(t)\right) R^3 R_{L2} - 2\,C_1 C_2^2$$

$$L_2^2 \left(\frac{\mathrm{d}}{\mathrm{d}t}\, i_o(t)\right) \left(\frac{\mathrm{d}^3}{\mathrm{d}t^3}\, v_{C2}(t)\right) \left(\frac{\mathrm{d}}{\mathrm{d}t}\, v_{C2}(t)\right) R^3 R_{L2} - 2\,C_1 C_2 L_2\, v_{C2}(t) \left(\frac{\mathrm{d}^2}{\mathrm{d}t^2}\, i_o(t)\right) \left(\frac{\mathrm{d}}{\mathrm{d}t}\, v_{C2}(t)\right) R^3 R_{L2}$$

$$+2\,C_2^2 C_d L_2\, v_{C2}(t) \left(\frac{\mathrm{d}^3}{\mathrm{d}t^3}\, v_{C2}(t)\right) \left(\frac{\mathrm{d}}{\mathrm{d}t}\, v_{C2}(t)\right) R^2 R_{L2}^2 + 4\,C_2 C_d L_2\, i_o(t) \left(\frac{\mathrm{d}}{\mathrm{d}t}\, i_o(t)\right) \left(\frac{\mathrm{d}^2}{\mathrm{d}t^2}\, v_{C2}(t)\right) R^3$$

$$R_{L2}^2 - 2\,C_2 C_d L_2\, v_{C2}(t) \left(\frac{\mathrm{d}^2}{\mathrm{d}t^2}\, i_o(t)\right) \left(\frac{\mathrm{d}}{\mathrm{d}t}\, v_{C2}(t)\right) R^2 R_{L2}^2$$

$$-2\,C_1 C_2 L_2\, v_{C2}(t) \left(\frac{\mathrm{d}^2}{\mathrm{d}t^2}\, i_o(t)\right) \left(\frac{\mathrm{d}}{\mathrm{d}t}\, v_{C2}(t)\right) R^2 R_{L2}^2 + 4\,C_1 C_2 L_2\, i_o(t) \left(\frac{\mathrm{d}}{\mathrm{d}t}\, i_o(t)\right) \left(\frac{\mathrm{d}^2}{\mathrm{d}t^2}\, v_{C2}(t)\right) R^3$$

$$R_{L2}^2 - 8\,C_2 C_d L_2^2 \left(\frac{\mathrm{d}}{\mathrm{d}t}\, i_o(t)\right) \left(\frac{\mathrm{d}^2}{\mathrm{d}t^2}\, v_{C2}(t)\right) \left(\frac{\mathrm{d}}{\mathrm{d}t}\, v_{C2}(t)\right) R^2 R_{L2}$$

$$-2\,C_2 C_d L_2\, v_{C2}(t)\, i_o(t) \left(\frac{\mathrm{d}^3}{\mathrm{d}t^3}\, v_{C2}(t)\right) R^3 R_{L2} - 6\,C_1 C_2 L_2\, i_o(t) \left(\frac{\mathrm{d}^2}{\mathrm{d}t^2}\, v_{C2}(t)\right) \left(\frac{\mathrm{d}}{\mathrm{d}t}\, v_{C2}(t)\right) R^2 R_{L2}^2 - 4$$

$$C_2^2 C_d L_2 \left(\frac{\mathrm{d}}{\mathrm{d}t}\, i_o(t)\right) \left(\frac{\mathrm{d}^2}{\mathrm{d}t^2}\, v_{C2}(t)\right) \left(\frac{\mathrm{d}}{\mathrm{d}t}\, v_{C2}(t)\right) R^3 R_{L2}^2 + 2$$

$$C_2^2 C_d L_2\, v_{C2}(t) \left(\frac{\mathrm{d}^3}{\mathrm{d}t^3}\, v_{C2}(t)\right) \left(\frac{\mathrm{d}}{\mathrm{d}t}\, v_{C2}(t)\right) R^3 R_{L2} - 2\,C_2^2 C_d$$

$$L_2^2 \left(\frac{\mathrm{d}}{\mathrm{d}t}\, i_o(t)\right) \left(\frac{\mathrm{d}^3}{\mathrm{d}t^3}\, v_{C2}(t)\right) \left(\frac{\mathrm{d}}{\mathrm{d}t}\, v_{C2}(t)\right) R^3 R_{L2} + 2\,C_2 C_d L_2^2\, i_o(t) \left(\frac{\mathrm{d}^2}{\mathrm{d}t^2}\, i_o(t)\right) \left(\frac{\mathrm{d}^2}{\mathrm{d}t^2}\, v_{C2}(t)\right) R^3 R_{L2}$$

$$-2\,C_1 C_2 L_2\, v_{C2}(t)\, i_o(t) \left(\frac{\mathrm{d}^3}{\mathrm{d}t^3}\, v_{C2}(t)\right) R^3 R_{L2} - 2\,C_1 C_2 L_2\, v_{C2}(t)\, i_o(t) \left(\frac{\mathrm{d}^3}{\mathrm{d}t^3}\, v_{C2}(t)\right) R^2 R_{L2}^2$$

$$+2\,C_1 C_2 L_2\, i_o(t) \left(\frac{\mathrm{d}^2}{\mathrm{d}t^2}\, i_o(t)\right) \left(\frac{\mathrm{d}}{\mathrm{d}t}\, v_{C2}(t)\right) R^3 R_{L2}^2 + 2\,C_1 C_2 L_2^2\, i_o(t) \left(\frac{\mathrm{d}^2}{\mathrm{d}t^2}\, i_o(t)\right) \left(\frac{\mathrm{d}^2}{\mathrm{d}t^2}\, v_{C2}(t)\right) R^3 R_{L2}$$

$$-2\,C_2 C_d L_2\, v_{C2}(t)\, i_o(t) \left(\frac{\mathrm{d}^3}{\mathrm{d}t^3}\, v_{C2}(t)\right) R^2 R_{L2}^2 - 2\,C_2^2 C_d L_2^2\, i_o(t) \left(\frac{\mathrm{d}^3}{\mathrm{d}t^3}\, v_{C2}(t)\right) \left(\frac{\mathrm{d}^2}{\mathrm{d}t^2}\, v_{C2}(t)\right) R^3 R_{L2}$$

$$-2\,C_2 C_d L_2\, v_{C2}(t) \left(\frac{\mathrm{d}^2}{\mathrm{d}t^2}\, i_o(t)\right) \left(\frac{\mathrm{d}}{\mathrm{d}t}\, v_{C2}(t)\right) R^3 R_{L2} + 2\,C_2 C_d$$

$$L_2^2\, i_o(t) \left(\frac{\mathrm{d}}{\mathrm{d}t}\, i_o(t)\right) \left(\frac{\mathrm{d}^3}{\mathrm{d}t^3}\, v_{C2}(t)\right) R^3 R_{L2} + 2\,C_2^3 C_d L_2^2 \left(\frac{\mathrm{d}^3}{\mathrm{d}t^3}\, v_{C2}(t)\right) \left(\frac{\mathrm{d}^2}{\mathrm{d}t^2}\, v_{C2}(t)\right) \left(\frac{\mathrm{d}}{\mathrm{d}t}\, v_{C2}(t)\right) R^3 R_{L2}$$

$$+ 2\, C_1\, C_2^2\, L_2\, v_{C2}(t) \left(\frac{\mathrm{d}^3}{\mathrm{d}t^3}\, v_{C2}(t)\right) \left(\frac{\mathrm{d}}{\mathrm{d}t}\, v_{C2}(t)\right) R^3\, R_{L2} + 2\, C_1\, C_2$$

$$L_2^2 \left(\frac{\mathrm{d}}{\mathrm{d}t}\, i_o(t)\right) \left(\frac{\mathrm{d}^2}{\mathrm{d}t^2}\, i_o(t)\right) \left(\frac{\mathrm{d}}{\mathrm{d}t}\, v_{C2}(t)\right) R^3\, R_{L2} - 2\, C_2\, C_d\, L_2^2\, v_{C2}(t) \left(\frac{\mathrm{d}}{\mathrm{d}t}\, i_o(t)\right) \left(\frac{\mathrm{d}^3}{\mathrm{d}t^3}\, v_{C2}(t)\right) R^2\, R_{L2}$$

$$+ 2\, C_1\, C_2^2\, L_2\, v_{C2}(t) \left(\frac{\mathrm{d}^3}{\mathrm{d}t^3}\, v_{C2}(t)\right) \left(\frac{\mathrm{d}}{\mathrm{d}t}\, v_{C2}(t)\right) R^2\, R_{L2}^2 + 2\, C_2\, C_d$$

$$L_2^2\, v_{C2}(t) \left(\frac{\mathrm{d}^3}{\mathrm{d}t^3}\, v_{C2}(t)\right) \left(\frac{\mathrm{d}}{\mathrm{d}t}\, v_{C2}(t)\right) R\, R_{L2} + 2\, C_1\, C_2\, L_2^2\, v_{C2}(t) \left(\frac{\mathrm{d}^3}{\mathrm{d}t^3}\, v_{C2}(t)\right) \left(\frac{\mathrm{d}}{\mathrm{d}t}\, v_{C2}(t)\right) R\, R_{L2}$$

$$- 2\, C_1\, C_2\, L_2\, i_o(t) \left(\frac{\mathrm{d}^2}{\mathrm{d}t^2}\, v_{C2}(t)\right) \left(\frac{\mathrm{d}}{\mathrm{d}t}\, v_{C2}(t)\right) R^3\, R_{L2} - 2\, C_2\, C_d$$

$$L_2^2\, v_{C2}(t) \left(\frac{\mathrm{d}^2}{\mathrm{d}t^2}\, i_o(t)\right) \left(\frac{\mathrm{d}^2}{\mathrm{d}t^2}\, v_{C2}(t)\right) R^2\, R_{L2} + 8\, C_2\, C_d\, L_2\, v_{C2}(t) \left(\frac{\mathrm{d}^2}{\mathrm{d}t^2}\, v_{C2}(t)\right) \left(\frac{\mathrm{d}}{\mathrm{d}t}\, v_{C2}(t)\right) R^2\, R_{L2}$$

$$- 2\, C_1\, C_2^2\, L_2^2 \left(\frac{\mathrm{d}^2}{\mathrm{d}t^2}\, i_o(t)\right) \left(\frac{\mathrm{d}^2}{\mathrm{d}t^2}\, v_{C2}(t)\right) \left(\frac{\mathrm{d}}{\mathrm{d}t}\, v_{C2}(t)\right) R^3\, R_{L2} + 2\, C_2^2\, C_d$$

$$L_2^2\, v_{C2}(t) \left(\frac{\mathrm{d}^3}{\mathrm{d}t^3}\, v_{C2}(t)\right) \left(\frac{\mathrm{d}^2}{\mathrm{d}t^2}\, v_{C2}(t)\right) R^2\, R_{L2} - 2\, C_1\, C_2\, L_2^2\, v_{C2}(t) \left(\frac{\mathrm{d}}{\mathrm{d}t}\, i_o(t)\right) \left(\frac{\mathrm{d}^3}{\mathrm{d}t^3}\, v_{C2}(t)\right) R^2\, R_{L2}$$

$$- 6\, C_2\, C_d\, L_2\, i_o(t) \left(\frac{\mathrm{d}^2}{\mathrm{d}t^2}\, v_{C2}(t)\right) \left(\frac{\mathrm{d}}{\mathrm{d}t}\, v_{C2}(t)\right) R^2\, R_{L2}^2 - 2\, C_1\, C_2$$

$$L_2^2\, v_{C2}(t) \left(\frac{\mathrm{d}^2}{\mathrm{d}t^2}\, i_o(t)\right) \left(\frac{\mathrm{d}^2}{\mathrm{d}t^2}\, v_{C2}(t)\right) R^2\, R_{L2} - 2\, C_2\, C_d\, L_2\, i_o(t) \left(\frac{\mathrm{d}^2}{\mathrm{d}t^2}\, v_{C2}(t)\right) \left(\frac{\mathrm{d}}{\mathrm{d}t}\, v_{C2}(t)\right) R^3\, R_{L2}$$

$$- 4\, C_1\, C_2\, L_2\, v_{C2}(t) \left(\frac{\mathrm{d}}{\mathrm{d}t}\, i_o(t)\right) \left(\frac{\mathrm{d}^2}{\mathrm{d}t^2}\, v_{C2}(t)\right) R^2\, R_{L2}^2 - 2\, C_1\, C_2^2\, L_2\, i_o(t) \left(\frac{\mathrm{d}^3}{\mathrm{d}t^3}\, v_{C2}(t)\right) \left(\frac{\mathrm{d}}{\mathrm{d}t}\, v_{C2}(t)\right) R^3$$

$$R_{L2}^2 - 2\, C_1\, C_2\, L_2^2\, i_o(t) \left(\frac{\mathrm{d}^3}{\mathrm{d}t^3}\, v_{C2}(t)\right) \left(\frac{\mathrm{d}}{\mathrm{d}t}\, v_{C2}(t)\right) R^2\, R_{L2} - 2\, C_2\, C_d$$

$$L_2^2\, i_o(t) \left(\frac{\mathrm{d}^3}{\mathrm{d}t^3}\, v_{C2}(t)\right) \left(\frac{\mathrm{d}}{\mathrm{d}t}\, v_{C2}(t)\right) R^2\, R_{L2} + 6\, C_2\, C_d\, L_2\, v_{C2}(t) \left(\frac{\mathrm{d}^2}{\mathrm{d}t^2}\, v_{C2}(t)\right) \left(\frac{\mathrm{d}}{\mathrm{d}t}\, v_{C2}(t)\right) R\, R_{L2}^2$$

$$- 4\, C_2\, C_d\, L_2\, v_{C2}(t) \left(\frac{\mathrm{d}}{\mathrm{d}t}\, i_o(t)\right) \left(\frac{\mathrm{d}^2}{\mathrm{d}t^2}\, v_{C2}(t)\right) R^3\, R_{L2} - 4\, C_2\, C_d\, L_2\, v_{C2}(t) \left(\frac{\mathrm{d}}{\mathrm{d}t}\, i_o(t)\right) \left(\frac{\mathrm{d}^2}{\mathrm{d}t^2}\, v_{C2}(t)\right) R^2$$

$$R_{L2}^2 - C_d\, L_1\, L_2 \left(\frac{\mathrm{d}}{\mathrm{d}t}\, i_o(t)\right) \left(\frac{\mathrm{d}^2}{\mathrm{d}t^2}\, i_{ref}(t)\right) i_{ref}(t)\, R^3\, R_d - C_d\, L_1\, i_o(t) \left(\frac{\mathrm{d}^2}{\mathrm{d}t^2}\, i_{ref}(t)\right) i_{ref}(t)\, R^3\, R_{L2}\, R_d$$

$$+ C_d\, L_1\, L_2 \left(\frac{\mathrm{d}}{\mathrm{d}t}\, v_{C2}(t)\right) \left(\frac{\mathrm{d}^2}{\mathrm{d}t^2}\, i_{ref}(t)\right) i_{ref}(t)\, R^2\, R_d + C_d\, L_1\, v_{C2}(t) \left(\frac{\mathrm{d}^2}{\mathrm{d}t^2}\, i_{ref}(t)\right) i_{ref}(t)\, R^2\, R_{L2}\, R_d$$

$$- i_{ref}(t)^2\, R^3\, R_{L1}\, R_{L2} \left(\frac{\mathrm{d}^2}{\mathrm{d}t^2}\, v_{C2}(t)\right) C_2\, R_d\, C_d - i_{ref}(t)^2\, R^3\, R_{L1}\, L_2 \left(\frac{\mathrm{d}^3}{\mathrm{d}t^3}\, v_{C2}(t)\right) C_2\, R_d\, C_d$$

$$- i_{ref}(t)\, R^2 \left(\frac{\mathrm{d}}{\mathrm{d}t}\, i_{ref}(t)\right) L_1\, L_2 \left(\frac{\mathrm{d}^2}{\mathrm{d}t^2}\, v_{C2}(t)\right) R_d\, C_d + i_{ref}(t)\, R^3\, v_g(t)\, L_2 \left(\frac{\mathrm{d}^3}{\mathrm{d}t^3}\, v_{C2}(t)\right) C_2\, R_d\, C_d$$

$$+ i_{ref}(t)\, R^3\, v_g(t)\, R_{L2} \left(\frac{\mathrm{d}^2}{\mathrm{d}t^2}\, v_{C2}(t)\right) C_2\, R_d\, C_d + i_{ref}(t)\, R^3 \left(\frac{\mathrm{d}}{\mathrm{d}t}\, i_{ref}(t)\right) L_1\, L_2 \left(\frac{\mathrm{d}^2}{\mathrm{d}t^2}\, i_o(t)\right) R_d\, C_d$$

$$- C_2\, C_d\, L_2\, v_g(t) \left(\frac{\mathrm{d}^2}{\mathrm{d}t^2}\, v_{C2}(t)\right) \left(\frac{\mathrm{d}}{\mathrm{d}t}\, i_{ref}(t)\right) R^3\, R_d - C_2\, C_d\, L_2 \left(\frac{\mathrm{d}^2}{\mathrm{d}t^2}\, v_{C2}(t)\right) \left(\frac{\mathrm{d}}{\mathrm{d}t}\, v_g(t)\right) i_{ref}(t)\, R^3\, R_d$$

$$+ C_2\, C_d\, L_1\, L_2 \left(\frac{\mathrm{d}^2}{\mathrm{d}t^2}\, v_{C2}(t)\right) \left(\frac{\mathrm{d}}{\mathrm{d}t}\, i_{ref}(t)\right)^2 R^3\, R_d - 4\, C_1$$

$$C_2^2\, L_2 \left(\frac{\mathrm{d}}{\mathrm{d}t}\, i_o(t)\right) \left(\frac{\mathrm{d}^2}{\mathrm{d}t^2}\, v_{C2}(t)\right) \left(\frac{\mathrm{d}}{\mathrm{d}t}\, v_{C2}(t)\right) R^3\, R_{L2}^2$$

$$- 4\, C_1\, C_2\, L_2\, v_{C2}(t) \left(\frac{\mathrm{d}}{\mathrm{d}t}\, i_o(t)\right) \left(\frac{\mathrm{d}^2}{\mathrm{d}t^2}\, v_{C2}(t)\right) R^3\, R_{L2}$$

$$+ 8\, C_1\, C_2\, L_2\, v_{C2}(t) \left(\frac{\mathrm{d}^2}{\mathrm{d}t^2}\, v_{C2}(t)\right) \left(\frac{\mathrm{d}}{\mathrm{d}t}\, v_{C2}(t)\right) R^2\, R_{L2} + 2\, C_1\, C_2^3$$

$$L_2^2 \left(\frac{\mathrm{d}^3}{\mathrm{d}t^3}\, v_{C2}(t)\right) \left(\frac{\mathrm{d}^2}{\mathrm{d}t^2}\, v_{C2}(t)\right) \left(\frac{\mathrm{d}}{\mathrm{d}t}\, v_{C2}(t)\right) R^3\, R_{L2} - 2\, C_1\, C_2^2$$

$$L_2^2\, i_o(t) \left(\frac{\mathrm{d}^3}{\mathrm{d}t^3}\, v_{C2}(t)\right) \left(\frac{\mathrm{d}^2}{\mathrm{d}t^2}\, v_{C2}(t)\right) R^3\, R_{L2} + 2\, C_1\, C_2^2\, L_2^2\, v_{C2}(t) \left(\frac{\mathrm{d}^3}{\mathrm{d}t^3}\, v_{C2}(t)\right) \left(\frac{\mathrm{d}^2}{\mathrm{d}t^2}\, v_{C2}(t)\right) R^2\, R_{L2}$$

UNIVERSITAT ROVIRA I VIRGILI
DESIGN AND CONTROL OF A BIDIRECTIONAL DC/DC CONVERTER FOR AN ELECTRIC VEHICLE APPLICATION.
Laura Albiol Rendillo
Dipòsit Legal: T 1361-2015

$$+6\,C_1\,C_2\,L_2\,v_{C2}(t)\left(\frac{\mathrm{d}^2}{\mathrm{d}t^2}\,v_{C2}(t)\right)\left(\frac{\mathrm{d}}{\mathrm{d}t}\,v_{C2}(t)\right)R\,R_{L2}^2$$

$$+4\,C_2\,C_d\,L_2\,v_{C2}(t)\left(\frac{\mathrm{d}^2}{\mathrm{d}t^2}\,v_{C2}(t)\right)\left(\frac{\mathrm{d}}{\mathrm{d}t}\,v_{C2}(t)\right)R^2\,R_d+2$$

$$C_2^3\,C_d\,L_2\left(\frac{\mathrm{d}^2}{\mathrm{d}t^2}\,v_{C2}(t)\right)^2\left(\frac{\mathrm{d}}{\mathrm{d}t}\,v_{C2}(t)\right)R^3\,R_{L2}\,R_d-2\,C_2^2\,C_d\,L_2\,i_o(t)\left(\frac{\mathrm{d}^2}{\mathrm{d}t^2}\,v_{C2}(t)\right)^2R^3\,R_{L2}\,R_d-2$$

$$C_2^2\,C_d\,i_o(t)\left(\frac{\mathrm{d}^2}{\mathrm{d}t^2}\,v_{C2}(t)\right)\left(\frac{\mathrm{d}}{\mathrm{d}t}\,v_{C2}(t)\right)R^3\,R_{L2}^2\,R_d+4\,C_2^2\,C_d\,L_2\left(\frac{\mathrm{d}^2}{\mathrm{d}t^2}\,v_{C2}(t)\right)\left(\frac{\mathrm{d}}{\mathrm{d}t}\,v_{C2}(t)\right)^2R^2\,R_{L2}\,R_d$$

$$-6\,C_2\,C_d\,L_2^2\left(\frac{\mathrm{d}}{\mathrm{d}t}\,i_o(t)\right)\left(\frac{\mathrm{d}^2}{\mathrm{d}t^2}\,v_{C2}(t)\right)\left(\frac{\mathrm{d}}{\mathrm{d}t}\,v_{C2}(t)\right)R^2\,R_d+2\,C_2^2\,C_d\,L_2\,v_{C2}(t)\left(\frac{\mathrm{d}^2}{\mathrm{d}t^2}\,v_{C2}(t)\right)^2R^2\,R_{L2}\,R_d$$

$$+2\,C_2^2\,C_d\,v_{C2}(t)\left(\frac{\mathrm{d}^2}{\mathrm{d}t^2}\,v_{C2}(t)\right)\left(\frac{\mathrm{d}}{\mathrm{d}t}\,v_{C2}(t)\right)R^3\,R_{L2}\,R_d+2\,C_2^2\,C_d\,v_{C2}(t)\left(\frac{\mathrm{d}^2}{\mathrm{d}t^2}\,v_{C2}(t)\right)\left(\frac{\mathrm{d}}{\mathrm{d}t}\,v_{C2}(t)\right)R^2$$

$$R_{L2}^2\,R_d-4\,C_2\,C_d\,L_2\,v_{C2}(t)\left(\frac{\mathrm{d}}{\mathrm{d}t}\,i_o(t)\right)\left(\frac{\mathrm{d}^2}{\mathrm{d}t^2}\,v_{C2}(t)\right)R^3\,R_d-2\,C_2\,C_d\,v_{C2}(t)\,i_o(t)\left(\frac{\mathrm{d}^2}{\mathrm{d}t^2}\,v_{C2}(t)\right)R^3\,R_{L2}\,R_d$$

$$-2\,C_2\,C_d\,v_{C2}(t)\,i_o(t)\left(\frac{\mathrm{d}^2}{\mathrm{d}t^2}\,v_{C2}(t)\right)R^2\,R_{L2}^2\,R_d-2\,C_d\,L_2^2\,v_{C2}(t)\left(\frac{\mathrm{d}}{\mathrm{d}t}\,i_o(t)\right)\left(\frac{\mathrm{d}^2}{\mathrm{d}t^2}\,v_{C2}(t)\right)R^2+2\,C_1$$

$$L_2^3\left(\frac{\mathrm{d}}{\mathrm{d}t}\,i_o(t)\right)\left(\frac{\mathrm{d}^2}{\mathrm{d}t^2}\,i_o(t)\right)\left(\frac{\mathrm{d}}{\mathrm{d}t}\,v_{C2}(t)\right)R^2-2\,C_2\,L_2^2\,v_{C2}(t)\left(\frac{\mathrm{d}}{\mathrm{d}t}\,i_o(t)\right)\left(\frac{\mathrm{d}^2}{\mathrm{d}t^2}\,v_{C2}(t)\right)R^2$$

$$+2\,C_2\,L_2\,v_{C2}(t)^2\left(\frac{\mathrm{d}^2}{\mathrm{d}t^2}\,v_{C2}(t)\right)R\,R_{L2}+2\,C_1\,L_2^2\,v_{C2}(t)\left(\frac{\mathrm{d}^2}{\mathrm{d}t^2}\,v_{C2}(t)\right)\left(\frac{\mathrm{d}}{\mathrm{d}t}\,v_{C2}(t)\right)R_{L2}$$

$$+2\,C_1\,L_2\,v_{C2}(t)^2\left(\frac{\mathrm{d}^2}{\mathrm{d}t^2}\,v_{C2}(t)\right)R\,R_{L2}-C_1\,L_2\,v_{C2}(t)^2\left(\frac{\mathrm{d}^2}{\mathrm{d}t^2}\,i_o(t)\right)R\,R_{L2}^2+C_1\,L_2\,i_o(t)^2\left(\frac{\mathrm{d}^2}{\mathrm{d}t^2}\,v_{C2}(t)\right)R^2$$

$$R_{L2}^2-C_2\,L_2\,v_g(t)\left(\frac{\mathrm{d}^2}{\mathrm{d}t^2}\,v_{C2}(t)\right)i_{ref}(t)\,R^3-2\,C_2\,L_2\,v_{C2}(t)\,i_o(t)\left(\frac{\mathrm{d}^2}{\mathrm{d}t^2}\,v_{C2}(t)\right)R^3+2\,C_2$$

$$L_2^2\,i_o(t)\left(\frac{\mathrm{d}}{\mathrm{d}t}\,i_o(t)\right)\left(\frac{\mathrm{d}^2}{\mathrm{d}t^2}\,v_{C2}(t)\right)R^3+C_1\,C_2^3\left(\frac{\mathrm{d}^2}{\mathrm{d}t^2}\,v_{C2}(t)\right)\left(\frac{\mathrm{d}}{\mathrm{d}t}\,v_{C2}(t)\right)^2R^3\,R_{L2}^3$$

$$+C_1\,C_2\,v_{C2}(t)^2\left(\frac{\mathrm{d}^2}{\mathrm{d}t^2}\,v_{C2}(t)\right)R^3\,R_{L2}+2\,C_1\,C_2\,v_{C2}(t)^2\left(\frac{\mathrm{d}^2}{\mathrm{d}t^2}\,v_{C2}(t)\right)R^2\,R_{L2}^2+2\,C_2$$

$$L_2^2\,v_{C2}(t)\left(\frac{\mathrm{d}^2}{\mathrm{d}t^2}\,v_{C2}(t)\right)\left(\frac{\mathrm{d}}{\mathrm{d}t}\,v_{C2}(t)\right)R+C_1\,C_2^3\,L_2^3\left(\frac{\mathrm{d}^3}{\mathrm{d}t^3}\,v_{C2}(t)\right)\left(\frac{\mathrm{d}^2}{\mathrm{d}t^2}\,v_{C2}(t)\right)^2R^3-C_1\,C_2^2$$

$$L_2^3\left(\frac{\mathrm{d}^2}{\mathrm{d}t^2}\,i_o(t)\right)\left(\frac{\mathrm{d}^2}{\mathrm{d}t^2}\,v_{C2}(t)\right)^2R^3-C_1\,L_2\,i_o(t)^2\left(\frac{\mathrm{d}^2}{\mathrm{d}t^2}\,i_o(t)\right)R^3\,R_{L2}^2+C_1\,C_2^3\,L_2^2\left(\frac{\mathrm{d}^2}{\mathrm{d}t^2}\,v_{C2}(t)\right)^3R^3\,R_{L2}$$

$$+C_1\,C_2\,L_2\,v_{C2}(t)^2\left(\frac{\mathrm{d}^3}{\mathrm{d}t^3}\,v_{C2}(t)\right)R^3+C_1\,C_2^2\,L_2^2\left(\frac{\mathrm{d}^2}{\mathrm{d}t^2}\,v_{C2}(t)\right)^2\left(\frac{\mathrm{d}}{\mathrm{d}t}\,v_{C2}(t)\right)R^3+2\,C_1\,C_2$$

$$L_2^2\left(\frac{\mathrm{d}^2}{\mathrm{d}t^2}\,v_{C2}(t)\right)\left(\frac{\mathrm{d}}{\mathrm{d}t}\,v_{C2}(t)\right)^2R^2+2\,C_2^2\,L_2\,v_{C2}(t)\left(\frac{\mathrm{d}^2}{\mathrm{d}t^2}\,v_{C2}(t)\right)\left(\frac{\mathrm{d}}{\mathrm{d}t}\,v_{C2}(t)\right)R^3-C_2^2\,C_d$$

$$L_2^3\left(\frac{\mathrm{d}^2}{\mathrm{d}t^2}\,i_o(t)\right)\left(\frac{\mathrm{d}^2}{\mathrm{d}t^2}\,v_{C2}(t)\right)^2R^3-C_d\,L_2\,i_o(t)^2\left(\frac{\mathrm{d}^2}{\mathrm{d}t^2}\,i_o(t)\right)R^3\,R_{L2}^2+2\,C_d$$

$$L_2^3\left(\frac{\mathrm{d}}{\mathrm{d}t}\,i_o(t)\right)\left(\frac{\mathrm{d}^2}{\mathrm{d}t^2}\,i_o(t)\right)\left(\frac{\mathrm{d}}{\mathrm{d}t}\,v_{C2}(t)\right)R^2+2\,C_d\,L_2^2\,v_{C2}(t)\left(\frac{\mathrm{d}}{\mathrm{d}t}\,i_o(t)\right)\left(\frac{\mathrm{d}^2}{\mathrm{d}t^2}\,i_o(t)\right)R^3-2\,C_d$$

$$L_2^2\,v_{C2}(t)\left(\frac{\mathrm{d}^2}{\mathrm{d}t^2}\,i_o(t)\right)\left(\frac{\mathrm{d}}{\mathrm{d}t}\,v_{C2}(t)\right)R^2-2\,C_d\,L_2\,v_{C2}(t)^2\left(\frac{\mathrm{d}^2}{\mathrm{d}t^2}\,i_o(t)\right)R^2\,R_{L2}$$

$$-C_d\,L_2\,v_{C2}(t)^2\left(\frac{\mathrm{d}^2}{\mathrm{d}t^2}\,i_o(t)\right)R\,R_{L2}^2+2\,C_1\,C_2\,L_2^3\left(\frac{\mathrm{d}^2}{\mathrm{d}t^2}\,v_{C2}(t)\right)^2\left(\frac{\mathrm{d}}{\mathrm{d}t}\,v_{C2}(t)\right)R-2\,C_1$$

$$L_2^3\left(\frac{\mathrm{d}}{\mathrm{d}t}\,i_o(t)\right)\left(\frac{\mathrm{d}^2}{\mathrm{d}t^2}\,v_{C2}(t)\right)\left(\frac{\mathrm{d}}{\mathrm{d}t}\,v_{C2}(t)\right)R+2\,C_1\,L_2^2\,v_{C2}(t)\left(\frac{\mathrm{d}^2}{\mathrm{d}t^2}\,v_{C2}(t)\right)\left(\frac{\mathrm{d}}{\mathrm{d}t}\,v_{C2}(t)\right)R+2\,C_1$$

$$L_2^2\,v_{C2}(t)\left(\frac{\mathrm{d}}{\mathrm{d}t}\,i_o(t)\right)\left(\frac{\mathrm{d}^2}{\mathrm{d}t^2}\,i_o(t)\right)R^3-2\,C_1\,L_2^2\,v_{C2}(t)\left(\frac{\mathrm{d}^2}{\mathrm{d}t^2}\,i_o(t)\right)\left(\frac{\mathrm{d}}{\mathrm{d}t}\,v_{C2}(t)\right)R^2+C_1\,C_2$$

$$L_2^3\left(\frac{\mathrm{d}^3}{\mathrm{d}t^3}\,v_{C2}(t)\right)\left(\frac{\mathrm{d}}{\mathrm{d}t}\,v_{C2}(t)\right)^2R+C_1\,C_2\,v_{C2}(t)^2\left(\frac{\mathrm{d}^2}{\mathrm{d}t^2}\,v_{C2}(t)\right)R\,R_{L2}^3$$

$$+2\,C_2\,L_2\,i_o(t)^2\left(\frac{\mathrm{d}^2}{\mathrm{d}t^2}\,v_{C2}(t)\right)R^3\,R_{L2}+C_2\,L_2\left(\frac{\mathrm{d}^2}{\mathrm{d}t^2}\,v_{C2}(t)\right)i_{ref}(t)^2\,R^3\,R_{L1}-2\,C_2\,C_d$$

$$L_2^3 \left(\frac{\mathrm{d}}{\mathrm{d}t}\, i_o(t) \right) \left(\frac{\mathrm{d}^2}{\mathrm{d}t^2}\, v_{C2}(t) \right)^2 R^2 + 2\, C_2\, C_d\, L_2^3 \left(\frac{\mathrm{d}^2}{\mathrm{d}t^2}\, v_{C2}(t) \right)^2 \left(\frac{\mathrm{d}}{\mathrm{d}t}\, v_{C2}(t) \right) R + 2\, C_2\, C_d$$

$$L_2^2\, v_{C2}(t) \left(\frac{\mathrm{d}^2}{\mathrm{d}t^2}\, v_{C2}(t) \right)^2 R^2 + C_d\, L_2\, i_o(t)^2 \left(\frac{\mathrm{d}^2}{\mathrm{d}t^2}\, v_{C2}(t) \right) R^2\, R_{L2}^2 - 2\, C_d$$

$$L_2^3 \left(\frac{\mathrm{d}}{\mathrm{d}t}\, i_o(t) \right) \left(\frac{\mathrm{d}^2}{\mathrm{d}t^2}\, v_{C2}(t) \right) \left(\frac{\mathrm{d}}{\mathrm{d}t}\, v_{C2}(t) \right) R - 4\, C_2\, v_{C2}(t)\; i_o(t) \left(\frac{\mathrm{d}}{\mathrm{d}t}\, v_{C2}(t) \right) R^3\, R_{L2}$$

$$+ 4\, L_2\, v_{C2}(t)\; i_o(t) \left(\frac{\mathrm{d}}{\mathrm{d}t}\, i_o(t) \right) R^2\, R_{L2} - L_1\, L_2 \left(\frac{\mathrm{d}}{\mathrm{d}t}\, i_o(t) \right) i_{ref}(t) \left(\frac{\mathrm{d}}{\mathrm{d}t}\, i_{ref}(t) \right) R^3$$

$$- L_1\, i_o(t)\; i_{ref}(t) \left(\frac{\mathrm{d}}{\mathrm{d}t}\, i_{ref}(t) \right) R^3\, R_{L2} + L_1\, L_2 \left(\frac{\mathrm{d}}{\mathrm{d}t}\, v_{C2}(t) \right) i_{ref}(t) \left(\frac{\mathrm{d}}{\mathrm{d}t}\, i_{ref}(t) \right) R^2$$

$$+ L_1\, v_{C2}(t)\; i_{ref}(t) \left(\frac{\mathrm{d}}{\mathrm{d}t}\, i_{ref}(t) \right) R^2\, R_{L2} + 4\, C_2\, L_2\, v_{C2}(t) \left(\frac{\mathrm{d}}{\mathrm{d}t}\, v_{C2}(t) \right)^2 R\, R_{L2}$$

$$- 4\, L_2\, v_{C2}(t)\; i_o(t) \left(\frac{\mathrm{d}}{\mathrm{d}t}\, v_{C2}(t) \right) R\, R_{L2} + 2\, C_d\, L_2\, v_{C2}(t) \left(\frac{\mathrm{d}}{\mathrm{d}t}\, i_o(t) \right)^2 R^3\, R_{L2}$$

$$+ 2\, C_d\, L_2\, v_{C2}(t) \left(\frac{\mathrm{d}}{\mathrm{d}t}\, i_o(t) \right)^2 R^2\, R_{L2}^2 - 2\, C_2\, L_2\, v_{C2}(t) \left(\frac{\mathrm{d}}{\mathrm{d}t}\, i_o(t) \right) \left(\frac{\mathrm{d}}{\mathrm{d}t}\, v_{C2}(t) \right) R^3 -$$

$$C_2^2\, C_d \left(\frac{\mathrm{d}}{\mathrm{d}t}\, i_o(t) \right) \left(\frac{\mathrm{d}}{\mathrm{d}t}\, v_{C2}(t) \right)^2 R^3\, R_{L2}^3 - 2\, C_d\, L_2\, i_o(t) \left(\frac{\mathrm{d}}{\mathrm{d}t}\, i_o(t) \right)^2 R^3\, R_{L2}^2 + 3\, C_d$$

$$L_2^2 \left(\frac{\mathrm{d}}{\mathrm{d}t}\, i_o(t) \right)^2 \left(\frac{\mathrm{d}}{\mathrm{d}t}\, v_{C2}(t) \right) R^2\, R_{L2} - 2\, C_1\, v_{C2}(t)\; i_o(t) \left(\frac{\mathrm{d}}{\mathrm{d}t}\, v_{C2}(t) \right) R\, R_{L2}^3$$

$$+ 2\, C_1\, L_2\, v_{C2}(t) \left(\frac{\mathrm{d}}{\mathrm{d}t}\, i_o(t) \right)^2 R^3\, R_{L2} + 2\, C_1\, v_{C2}(t)\; i_o(t) \left(\frac{\mathrm{d}}{\mathrm{d}t}\, i_o(t) \right) R^3\, R_{L2}^2$$

$$- 2\, C_1\, L_2\, v_{C2}(t) \left(\frac{\mathrm{d}}{\mathrm{d}t}\, i_o(t) \right) \left(\frac{\mathrm{d}}{\mathrm{d}t}\, v_{C2}(t) \right) R^3 + 2\, C_1\, L_2\, v_{C2}(t) \left(\frac{\mathrm{d}}{\mathrm{d}t}\, i_o(t) \right)^2 R^2\, R_{L2}^2$$

$$+ C_2 \left(\frac{\mathrm{d}}{\mathrm{d}t}\, v_{C2}(t) \right) i_{ref}(t)^2\, R^3\, R_{L1}\, R_{L2} + 2\, C_1\, v_{C2}(t)\; i_o(t) \left(\frac{\mathrm{d}}{\mathrm{d}t}\, i_o(t) \right) R^2\, R_{L2}^3 + 3\, C_1$$

$$L_2^2 \left(\frac{\mathrm{d}}{\mathrm{d}t}\, i_o(t) \right)^2 \left(\frac{\mathrm{d}}{\mathrm{d}t}\, v_{C2}(t) \right) R^2\, R_{L2} - v_{C2}(t)^2\, i_o(t)\; R^3 + 2\, v_{C2}(t)^3\, R\, R_{L2} + L_2^2\, v_{C2}(t) \left(\frac{\mathrm{d}}{\mathrm{d}t}\, v_{C2}(t) \right)^2$$

$$- i_o(t)^3\, R^3\, R_{L2}^2 + C_2\, C_d\, v_{C2}(t)^2 \left(\frac{\mathrm{d}^2}{\mathrm{d}t^2}\, v_{C2}(t) \right) R^3\, R_{L2} + 2\, C_2\, C_d\, v_{C2}(t)^2 \left(\frac{\mathrm{d}^2}{\mathrm{d}t^2}\, v_{C2}(t) \right) R^2\, R_{L2}^2$$

$$+ C_2\, C_d\, v_{C2}(t)^2 \left(\frac{\mathrm{d}^2}{\mathrm{d}t^2}\, v_{C2}(t) \right) R\, R_{L2}^3 + C_2^3\, C_d\, L_2^3 \left(\frac{\mathrm{d}^3}{\mathrm{d}t^3}\, v_{C2}(t) \right) \left(\frac{\mathrm{d}^2}{\mathrm{d}t^2}\, v_{C2}(t) \right)^2 R^3 + C_2\, C_d$$

$$L_2^3 \left(\frac{\mathrm{d}}{\mathrm{d}t}\, i_o(t) \right)^2 \left(\frac{\mathrm{d}^3}{\mathrm{d}t^3}\, v_{C2}(t) \right) R^3 + C_2^3\, C_d\, L_2^2 \left(\frac{\mathrm{d}^2}{\mathrm{d}t^2}\, v_{C2}(t) \right)^3 R^3\, R_d + C_2\, C_d\, v_{C2}(t)^2 \left(\frac{\mathrm{d}^2}{\mathrm{d}t^2}\, v_{C2}(t) \right) R^3\, R_d$$

$$- 2\, C_2\, L_2^2\, i_o(t) \left(\frac{\mathrm{d}^2}{\mathrm{d}t^2}\, v_{C2}(t) \right) \left(\frac{\mathrm{d}}{\mathrm{d}t}\, v_{C2}(t) \right) R^2 + C_2\, C_d\, L_2^3 \left(\frac{\mathrm{d}^3}{\mathrm{d}t^3}\, v_{C2}(t) \right) \left(\frac{\mathrm{d}}{\mathrm{d}t}\, v_{C2}(t) \right)^2 R$$

$$+ C_2\, C_d\, L_2\, v_{C2}(t)^2 \left(\frac{\mathrm{d}^3}{\mathrm{d}t^3}\, v_{C2}(t) \right) R^3 + C_1\, C_2\, i_o(t)^2 \left(\frac{\mathrm{d}^2}{\mathrm{d}t^2}\, v_{C2}(t) \right) R^3\, R_{L2}^3 + C_1\, C_2$$

$$L_2^3 \left(\frac{\mathrm{d}}{\mathrm{d}t}\, i_o(t) \right)^2 \left(\frac{\mathrm{d}^3}{\mathrm{d}t^3}\, v_{C2}(t) \right) R^3 + 2\, C_2^3\, L_2 \left(\frac{\mathrm{d}^2}{\mathrm{d}t^2}\, v_{C2}(t) \right) \left(\frac{\mathrm{d}}{\mathrm{d}t}\, v_{C2}(t) \right)^2 R^3\, R_{L2} + C_2^2\, C_d$$

$$L_2^2 \left(\frac{\mathrm{d}^2}{\mathrm{d}t^2}\, v_{C2}(t) \right)^2 \left(\frac{\mathrm{d}}{\mathrm{d}t}\, v_{C2}(t) \right) R^3 + 2\, C_2\, C_d\, L_2^2 \left(\frac{\mathrm{d}^2}{\mathrm{d}t^2}\, v_{C2}(t) \right) \left(\frac{\mathrm{d}}{\mathrm{d}t}\, v_{C2}(t) \right)^2 R^2 + 2\, C_d$$

$$L_2^2\, v_{C2}(t) \left(\frac{\mathrm{d}^2}{\mathrm{d}t^2}\, v_{C2}(t) \right) \left(\frac{\mathrm{d}}{\mathrm{d}t}\, v_{C2}(t) \right) R + 2\, C_d\, L_2^2\, v_{C2}(t) \left(\frac{\mathrm{d}^2}{\mathrm{d}t^2}\, v_{C2}(t) \right) \left(\frac{\mathrm{d}}{\mathrm{d}t}\, v_{C2}(t) \right) R_{L2}$$

$$- 2\, C_1\, L_2\, v_{C2}(t)^2 \left(\frac{\mathrm{d}^2}{\mathrm{d}t^2}\, i_o(t) \right) R^2\, R_{L2} - 6\, C_2\, v_{C2}(t)\; i_o(t) \left(\frac{\mathrm{d}}{\mathrm{d}t}\, v_{C2}(t) \right) R^2\, R_{L2}^2$$

$$- 2\, C_1\, C_2\, i_o(t) \left(\frac{\mathrm{d}}{\mathrm{d}t}\, v_{C2}(t) \right)^2 R^3\, R_{L2}^2 - 2\, C_1\, L_2\, i_o(t) \left(\frac{\mathrm{d}}{\mathrm{d}t}\, v_{C2}(t) \right)^2 R^2\, R_{L2}$$

$$+ 3\, C_1\, v_{C2}(t)^2 \left(\frac{\mathrm{d}}{\mathrm{d}t}\, v_{C2}(t) \right) R^2\, R_{L2} - 2\, L_2^2\, v_{C2}(t) \left(\frac{\mathrm{d}}{\mathrm{d}t}\, i_o(t) \right) \left(\frac{\mathrm{d}}{\mathrm{d}t}\, v_{C2}(t) \right) R + C_2^2\, C_d \left(\frac{\mathrm{d}}{\mathrm{d}t}\, v_{C2}(t) \right)^3 R^2$$

$$R_{L2}^3 + C_d\, i_o(t)^2 \left(\frac{\mathrm{d}}{\mathrm{d}t}\, v_{C2}(t) \right) R^2\, R_{L2}^3 + 2\, C_d\, L_2\, v_{C2}(t) \left(\frac{\mathrm{d}}{\mathrm{d}t}\, v_{C2}(t) \right)^2 R_{L2}^2 + 2\, C_1\, L_2\, v_{C2}(t) \left(\frac{\mathrm{d}}{\mathrm{d}t}\, v_{C2}(t) \right)^2 R^2$$

$$+ C_1\, C_2^2 \left(\frac{\mathrm{d}}{\mathrm{d}t}\, v_{C2}(t) \right)^3 R^2\, R_{L2}^3 - C_1\, v_{C2}(t)^2 \left(\frac{\mathrm{d}}{\mathrm{d}t}\, i_o(t) \right) R\, R_{L2}^3 + C_1\, i_o(t)^2 \left(\frac{\mathrm{d}}{\mathrm{d}t}\, v_{C2}(t) \right) R^2\, R_{L2}^3$$

$$+ 2 L_2 v_{C2}(t)\, i_o(t) \left(\frac{\mathrm{d}}{\mathrm{d}t} i_o(t)\right) R^3 + L_1 v_{C2}(t)\, i_{ref}(t) \left(\frac{\mathrm{d}}{\mathrm{d}t} i_{ref}(t)\right) R^3 - 3 C_2^2\, i_o(t) \left(\frac{\mathrm{d}}{\mathrm{d}t} v_{C2}(t)\right)^2 R^3 R_{L2}^2$$

$$+ 2 C_2^2 L_2 \left(\frac{\mathrm{d}}{\mathrm{d}t} v_{C2}(t)\right)^3 R^2 R_{L2} - L_2 \left(\frac{\mathrm{d}}{\mathrm{d}t} i_o(t)\right) i_{ref}(t)^2 R^3 R_{L1} - i_o(t)\, i_{ref}(t)^2 R^3 R_{L1} R_{L2}$$

$$+ L_2 \left(\frac{\mathrm{d}}{\mathrm{d}t} v_{C2}(t)\right) i_{ref}(t)^2 R^2 R_{L1} + v_{C2}(t)\, i_{ref}(t)^2 R^2 R_{L1} R_{L2} + 3 C_1 v_{C2}(t)^2 \left(\frac{\mathrm{d}}{\mathrm{d}t} v_{C2}(t)\right) R R_{L2}^2$$

$$- C_1 v_{C2}(t)^2 \left(\frac{\mathrm{d}}{\mathrm{d}t} i_o(t)\right) R^3 R_{L2} - 2 C_1 v_{C2}(t)^2 \left(\frac{\mathrm{d}}{\mathrm{d}t} i_o(t)\right) R^2 R_{L2}^2 + C_1 L_2^2 \left(\frac{\mathrm{d}}{\mathrm{d}t} i_o(t)\right)^2 \left(\frac{\mathrm{d}}{\mathrm{d}t} v_{C2}(t)\right) R^3$$

$$- 2 C_1 L_2^2 \left(\frac{\mathrm{d}}{\mathrm{d}t} i_o(t)\right) \left(\frac{\mathrm{d}}{\mathrm{d}t} v_{C2}(t)\right)^2 R^2 + 3 C_2^2 v_{C2}(t) \left(\frac{\mathrm{d}}{\mathrm{d}t} v_{C2}(t)\right)^2 R^2 R_{L2}^2$$

$$+ 4 C_2 v_{C2}(t)^2 \left(\frac{\mathrm{d}}{\mathrm{d}t} v_{C2}(t)\right) R^2 R_{L2} + 3 C_2 v_{C2}(t)^2 \left(\frac{\mathrm{d}}{\mathrm{d}t} v_{C2}(t)\right) R R_{L2}^2 + 2$$

$$C_2^2 v_{C2}(t) \left(\frac{\mathrm{d}}{\mathrm{d}t} v_{C2}(t)\right)^2 R^3 R_{L2} + 2 C_2 L_2 v_{C2}(t) \left(\frac{\mathrm{d}}{\mathrm{d}t} v_{C2}(t)\right)^2 R^2 - 2 L_2 i_o(t)^2 \left(\frac{\mathrm{d}}{\mathrm{d}t} i_o(t)\right) R^3 R_{L2} + 2$$

$$L_2^2 i_o(t) \left(\frac{\mathrm{d}}{\mathrm{d}t} i_o(t)\right) \left(\frac{\mathrm{d}}{\mathrm{d}t} v_{C2}(t)\right) R^2 + 3 C_2 i_o(t)^2 \left(\frac{\mathrm{d}}{\mathrm{d}t} v_{C2}(t)\right) R^3 R_{L2}^2 + C_d v_{C2}(t)^2 \left(\frac{\mathrm{d}}{\mathrm{d}t} v_{C2}(t)\right) R^2 R_d$$

$$+ C_d v_{C2}(t)^2 \left(\frac{\mathrm{d}}{\mathrm{d}t} v_{C2}(t)\right) R_{L2}^2 R_d - C_d L_2^2 \left(\frac{\mathrm{d}}{\mathrm{d}t} i_o(t)\right)^3 R^3 R_d - C_d v_{C2}(t)^2 \left(\frac{\mathrm{d}}{\mathrm{d}t} i_o(t)\right) R^3 R_d$$

$$- 2 L_2 v_{C2}(t)^2 \left(\frac{\mathrm{d}}{\mathrm{d}t} i_o(t)\right) R R_{L2} + L_2 v_g(t) \left(\frac{\mathrm{d}}{\mathrm{d}t} i_o(t)\right) i_{ref}(t) R^3 + v_g(t)\, i_o(t)\, i_{ref}(t) R^3 R_{L2}$$

$$- L_2 v_g(t) \left(\frac{\mathrm{d}}{\mathrm{d}t} v_{C2}(t)\right) i_{ref}(t) R^2 - v_g(t)\, v_{C2}(t)\, i_{ref}(t) R^2 R_{L2} - 2 C_2 L_2^2 \left(\frac{\mathrm{d}}{\mathrm{d}t} i_o(t)\right) \left(\frac{\mathrm{d}}{\mathrm{d}t} v_{C2}(t)\right)^2 R^2$$

$$+ 2 C_1 L_2 v_{C2}(t) \left(\frac{\mathrm{d}}{\mathrm{d}t} v_{C2}(t)\right)^2 R_{L2}^2 + 3 C_d v_{C2}(t)^2 \left(\frac{\mathrm{d}}{\mathrm{d}t} v_{C2}(t)\right) R^2 R_{L2} + 3 C_d v_{C2}(t)^2 \left(\frac{\mathrm{d}}{\mathrm{d}t} v_{C2}(t)\right) R$$

$$R_{L2}^2 + C_1 C_2^2 \left(\frac{\mathrm{d}}{\mathrm{d}t} v_{C2}(t)\right)^3 R^3 R_{L2}^2 - C_1 i_o(t)^2 \left(\frac{\mathrm{d}}{\mathrm{d}t} i_o(t)\right) R^3 R_{L2}^3 - C_1 L_2^2 \left(\frac{\mathrm{d}}{\mathrm{d}t} i_o(t)\right)^3 R^3 R_{L2} + v_{C2}(t)^3$$

$$R_{L2}^2\Big) \Big/ \Big(R_d C_1 C_d R \Big(L_2 \left(\frac{\mathrm{d}^2}{\mathrm{d}t^2} v_{C2}(t)\right) C_2 R + R_{L2} \left(\frac{\mathrm{d}}{\mathrm{d}t} v_{C2}(t)\right) C_2 R - L_2 \left(\frac{\mathrm{d}}{\mathrm{d}t} i_o(t)\right) R$$

$$- R_{L2} i_o(t) R + L_2 \left(\frac{\mathrm{d}}{\mathrm{d}t} v_{C2}(t)\right) + v_{C2}(t) R + R_{L2} v_{C2}(t)\Big)^2\Big)$$

8.3 Output current to output voltage transfer function

The small-signal output current to output voltage transfer function has been calculated according to the procedure described in section 3.3.1, and the resulting expression is

$$\frac{\tilde{v}_{C2}(s)}{\tilde{i}_o(s)} = \Big(\Big(\Big(R^2 \mathrm{I}_o^2 C_1 C_d L_2 R_{L2}^2 R_d - 2 R^2 \mathrm{I}_o C_1 C_d L_2 R_{L2} R_d V_{C2} - 2 R \mathrm{I}_o C_1 C_d L_2 R_{L2}^2 R_d V_{C2} + R^2 C_1 C_d L_2 R_d \tag{8.3}$$

$$V_{C2}^2 + 2 R C_1 C_d L_2 R_{L2} R_d V_{C2}^2 + C_1 C_d L_2 R_{L2}^2 R_d V_{C2}^2\Big) s^3 + \Big(R^2 \mathrm{I}_o^2 C_1 C_d R_{L2}^3 R_d - 2 R^2 \mathrm{I}_o C_1 C_d R_{L2}^2 R_d V_{C2}$$

$$- 2 R \mathrm{I}_o C_1 C_d R_{L2}^3 R_d V_{C2} + R^2 \mathrm{I}_o^2 C_1 L_2 R_{L2}^2 + R^2 \mathrm{I}_o^2 C_d L_2 R_{L2}^2 - R^2 \mathrm{I}_{ref}^2 C_d L_2 R_{L1} R_d + R^2 C_1 C_d R_{L2} R_d V_{C2}^2$$

$$+ 2 R C_1 C_d R_{L2}^2 R_d V_{C2}^2 + C_1 C_d R_{L2}^3 R_d V_{C2}^2 - 2 R^2 \mathrm{I}_o C_1 L_2 R_{L2} V_{C2} - 2 R^2 \mathrm{I}_o C_d L_2 R_{L2} V_{C2}$$

$$+ R^2 \mathrm{I}_{ref} C_d L_2 R_d V_g - 2 R \mathrm{I}_o C_1 L_2 R_{L2}^2 V_{C2} - 2 R \mathrm{I}_o C_d L_2 R_{L2}^2 V_{C2} + R^2 C_1 L_2 V_{C2}^2 + R^2 C_d L_2 V_{C2}^2$$

$$+ 2 R C_1 L_2 R_{L2} V_{C2}^2 + 2 R C_d L_2 R_{L2} V_{C2}^2 + C_1 L_2 R_{L2}^2 V_{C2}^2 + C_d L_2 R_{L2}^2 V_{C2}^2\Big) s^2 + \Big(R^2 \mathrm{I}_o^2 C_1 R_{L2}^3 + R^2 \mathrm{I}_o^2 C_d$$

$$R_{L2}^3 + R^2 \mathrm{I}_o^2 C_d R_{L2}^2 R_d - R^2 \mathrm{I}_{ref}^2 C_d R_{L1} R_{L2} R_d - 2 R^2 \mathrm{I}_o C_1 R_{L2}^2 V_{C2} - 2 R^2 \mathrm{I}_o C_d R_{L2}^2 V_{C2}$$

$$- 2 R^2 \mathrm{I}_o C_d R_{L2} R_d V_{C2} + R^2 \mathrm{I}_{ref} C_d R_{L2} R_d V_g - 2 R \mathrm{I}_o C_1 R_{L2}^3 V_{C2} - 2 R \mathrm{I}_o C_d R_{L2}^3 V_{C2} - 2 R \mathrm{I}_o C_d R_{L2}^2 R_d V_{C2}$$

$$- R^2 \mathrm{I}_{ref}^2 L_2 R_{L1} + R^2 C_1 R_{L2} V_{C2}^2 + R^2 C_d R_{L2} V_{C2}^2 + R^2 C_d R_d V_{C2}^2 + 2 R C_1 R_{L2}^2 V_{C2}^2 + 2 R C_d R_{L2}^2 V_{C2}^2$$

$$+ 2 R C_d R_{L2} R_d V_{C2}^2 + C_1 R_{L2}^3 V_{C2}^2 + C_d R_{L2}^3 V_{C2}^2 + C_d R_{L2}^2 R_d V_{C2}^2 + R^2 \mathrm{I}_{ref} L_2 V_g\Big) s - R^2 \mathrm{I}_{ref}^2 R_{L1} R_{L2} + R^2$$

$$R_{L2}^2 \mathrm{I}_o^2 - 2 R^2 \mathrm{I}_o R_{L2} V_{C2} + R^2 \mathrm{I}_{ref} V_g R_{L2} - 2 R R_{L2}^2 \mathrm{I}_o V_{C2} + R^2 V_{C2}^2 + 2 R R_{L2} V_{C2}^2 + R_{L2}^2 V_{C2}^2\Big) R\Big) \Big/ \Big(\Big(R^3$$

$$\mathrm{I}_o^2 C_1 C_2 C_d L_2 R_{L2}^2 R_d - 2 R^3 \mathrm{I}_o C_1 C_2 C_d L_2 R_{L2} R_d V_{C2} - 2 R^2 \mathrm{I}_o C_1 C_2 C_d L_2 R_{L2}^2 R_d V_{C2} + R^3 C_1 C_2 C_d L_2 R_d$$

$$V_{C2}^2 + 2 R^2 C_1 C_2 C_d L_2 R_{L2} R_d V_{C2}^2 + R C_1 C_2 C_d L_2 R_{L2}^2 R_d V_{C2}^2\Big) s^4 + \Big(R^3 \mathrm{I}_o^2 C_1 C_2 C_d R_{L2}^3 R_d$$

$$- 2 R^3 \mathrm{I}_o C_1 C_2 C_d R_{L2}^2 R_d V_{C2} - 2 R^2 \mathrm{I}_o C_1 C_2 C_d R_{L2}^3 R_d V_{C2} + R^3 \mathrm{I}_o^2 C_1 C_2 L_2 R_{L2}^2 + R^3 \mathrm{I}_o^2 C_2 C_d L_2 R_{L2}^2 - R^3$$

$$\mathrm{I}_{ref}^2 C_2 C_d L_2 R_{L1} R_d + R^3 C_1 C_2 C_d R_{L2} R_d V_{C2}^2 + R^2 \mathrm{I}_o^2 C_1 C_d L_2 R_{L2}^2 R_d + 2 R^2 C_1 C_2 C_d R_{L2}^2 R_d V_{C2}^2$$

$$+ R C_1 C_2 C_d R_{L2}^3 R_d V_{C2}^2 - 2 R^3 \mathrm{I}_o C_1 C_2 L_2 R_{L2} V_{C2} - 2 R^3 \mathrm{I}_o C_2 C_d L_2 R_{L2} V_{C2} + R^3 \mathrm{I}_{ref} C_2 C_d L_2 R_d V_g$$

$$
\begin{aligned}
&-2 R^2 \mathrm{I}_o C_1 C_2 L_2 R_{L2}^2 V_{C2} - 2 R^2 \mathrm{I}_o C_1 C_d L_2 R_{L2} R_d V_{C2} - 2 R^2 \mathrm{I}_o C_2 C_d L_2 R_{L2}^2 V_{C2} - 2 R \mathrm{I}_o C_1 C_d L_2 \\
&R_{L2}^2 R_d V_{C2} + R^3 C_1 C_2 L_2 V_{C2}^2 + R^3 C_2 C_d L_2 V_{C2}^2 + 2 R^2 C_1 C_2 L_2 R_{L2} V_{C2}^2 + R^2 C_1 C_d L_2 R_d V_{C2}^2 \\
&+2 R^2 C_2 C_d L_2 R_{L2} V_{C2}^2 + R C_1 C_2 L_2 R_{L2}^2 V_{C2}^2 + 2 R C_1 C_d L_2 R_{L2} R_d V_{C2}^2 + R C_2 C_d L_2 R_{L2}^2 V_{C2}^2 + C_1 C_d L_2 \\
&R_{L2}^2 R_d V_{C2}^2) \, s^3 + (R^3 \mathrm{I}_o^2 C_1 C_2 R_{L2}^3 + R^3 \mathrm{I}_o^2 C_1 C_d R_{L2}^2 R_d + R^3 \mathrm{I}_o^2 C_2 C_d R_{L2}^3 + R^3 \mathrm{I}_o^2 C_2 C_d R_{L2}^2 R_d - R^3 \\
&\mathrm{I}_{ref}^2 C_2 C_d R_{L1} R_{L2} R_d + R^2 \mathrm{I}_o^2 C_1 C_d R_{L2}^3 R_d - 2 R^3 \mathrm{I}_o C_1 C_2 R_{L2}^2 V_{C2} - 2 R^3 \mathrm{I}_o C_1 C_d R_{L2} R_d V_{C2} - 2 R^3 \mathrm{I}_o C_2 C_d \\
&R_{L2}^2 V_{C2} - 2 R^3 \mathrm{I}_o C_2 C_d R_{L2} R_d V_{C2} + R^3 \mathrm{I}_{ref} C_2 C_d R_{L2} R_d V_g - 2 R^2 \mathrm{I}_o C_1 C_2 R_{L2}^3 V_{C2} - 4 R^2 \mathrm{I}_o C_1 C_d \\
&R_{L2}^2 R_d V_{C2} - 2 R^2 \mathrm{I}_o C_2 C_d R_{L2}^3 V_{C2} - 2 R^2 \mathrm{I}_o C_2 C_d R_{L2}^2 R_d V_{C2} - 2 R \mathrm{I}_o C_1 C_d R_{L2}^3 R_d V_{C2} - R^3 \mathrm{I}_{ref}^2 C_2 L_2 R_{L1} \\
&+ R^3 C_1 C_2 R_{L2} V_{C2}^2 + R^3 C_1 C_d R_d V_{C2}^2 + R^3 C_2 C_d R_{L2} V_{C2}^2 + R^3 C_2 C_d R_d V_{C2}^2 + R^2 \mathrm{I}_o^2 C_1 L_2 R_{L2}^2 + R^2 \\
&\mathrm{I}_o^2 C_d L_2 R_{L2}^2 - R^2 \mathrm{I}_{ref}^2 C_d L_2 R_{L1} R_d + 2 R^2 C_1 C_2 R_{L2}^2 V_{C2}^2 + 3 R^2 C_1 C_d R_{L2} R_d V_{C2}^2 + 2 R^2 C_2 C_d R_{L2}^2 V_{C2}^2 \\
&+ 2 R^2 C_2 C_d R_{L2} R_d V_{C2}^2 + R C_1 C_2 R_{L2}^3 V_{C2}^2 + 3 R C_1 C_d R_{L2}^2 R_d V_{C2}^2 + R C_2 C_d R_{L2}^3 V_{C2}^2 + R C_2 C_d R_{L2}^2 R_d \\
&V_{C2}^2 + C_1 C_d R_{L2}^3 R_d V_{C2}^2 + R^3 \mathrm{I}_{ref} C_2 L_2 V_g - 2 R^2 \mathrm{I}_o C_1 L_2 R_{L2} V_{C2} - 2 R^2 \mathrm{I}_o C_d L_2 R_{L2} V_{C2} + R^2 \mathrm{I}_{ref} C_d L_2 R_d V_g \\
&- 2 R \mathrm{I}_o C_1 L_2 R_{L2}^2 V_{C2} - 2 R \mathrm{I}_o C_d L_2 R_{L2}^2 V_{C2} + R^2 C_1 L_2 V_{C2}^2 + R^2 C_d L_2 V_{C2}^2 + 2 R C_1 L_2 R_{L2} V_{C2}^2 \\
&+ 2 R C_d L_2 R_{L2} V_{C2}^2 + C_1 L_2 R_{L2}^2 V_{C2}^2 + C_d L_2 R_{L2}^2 V_{C2}^2) \, s^2 + (R^3 \mathrm{I}_o^2 C_1 R_{L2}^2 + R^3 \mathrm{I}_o^2 C_2 R_{L2}^2 + R^3 \mathrm{I}_o^2 C_d R_{L2}^2 \\
&- R^3 \mathrm{I}_{ref}^2 C_2 R_{L1} R_{L2} - R^3 \mathrm{I}_{ref}^2 C_d R_{L1} R_d + R^2 \mathrm{I}_o^2 C_1 R_{L2}^3 + R^2 \mathrm{I}_o^2 C_d R_{L2}^3 + R^2 \mathrm{I}_o^2 C_d R_{L2}^2 R_d - R^2 \mathrm{I}_{ref}^2 C_d R_{L1} R_{L2} R_d \\
&- 2 R^3 \mathrm{I}_o C_1 R_{L2} V_{C2} - 2 R^3 \mathrm{I}_o C_2 R_{L2} V_{C2} - 2 R^3 \mathrm{I}_o C_d R_{L2} V_{C2} + R^3 \mathrm{I}_{ref} C_2 R_{L2} V_g + R^3 \mathrm{I}_{ref} C_d R_d V_g \\
&- 4 R^2 \mathrm{I}_o C_1 R_{L2}^2 V_{C2} - 2 R^2 \mathrm{I}_o C_2 R_{L2}^2 V_{C2} - 4 R^2 \mathrm{I}_o C_d R_{L2}^2 V_{C2} - 2 R^2 \mathrm{I}_o C_d R_{L2} R_d V_{C2} + R^2 \mathrm{I}_{ref} C_d R_{L2} R_d V_g \\
&- 2 R \mathrm{I}_o C_1 R_{L2}^3 V_{C2} - 2 R \mathrm{I}_o C_d R_{L2}^3 V_{C2} - 2 R \mathrm{I}_o C_d R_{L2}^2 R_d V_{C2} + R^3 C_1 V_{C2}^2 + R^3 C_2 V_{C2}^2 + R^3 C_d V_{C2}^2 - R^2 \\
&\mathrm{I}_{ref}^2 L_2 R_{L1} + 3 R^2 C_1 R_{L2} V_{C2}^2 + 2 R^2 C_2 R_{L2} V_{C2}^2 + 3 R^2 C_d R_{L2} V_{C2}^2 + R^2 C_d R_d V_{C2}^2 + 3 R C_1 R_{L2}^2 V_{C2}^2 + R C_2 \\
&R_{L2}^2 V_{C2}^2 + 3 R C_d R_{L2}^2 V_{C2}^2 + 2 R C_d R_{L2} R_d V_{C2}^2 + C_1 R_{L2}^3 V_{C2}^2 + C_d R_{L2}^3 V_{C2}^2 + C_d R_{L2}^2 R_d V_{C2}^2 + R^2 \mathrm{I}_{ref} L_2 V_g) \, s \\
&- R^3 \mathrm{I}_{ref}^2 R_{L1} - R^2 \mathrm{I}_{ref}^2 R_{L1} R_{L2} + R^2 R_{L2}^2 \mathrm{I}_o^2 + R^3 \mathrm{I}_{ref} V_g - 2 R^2 \mathrm{I}_o R_{L2} V_{C2} + R^2 \mathrm{I}_{ref} V_g R_{L2} - 2 R R_{L2}^2 \mathrm{I}_o V_{C2} + R^2 \\
&V_{C2}^2 + 2 R R_{L2} V_{C2}^2 + R_{L2}^2 V_{C2}^2)
\end{aligned}
$$

8.4 Input voltage to output voltage transfer function

The obtained expression for the small-signal input voltage to output voltage transfer function of section 3.3.2 is

$$
\begin{aligned}
\frac{\tilde{v}_{C2}(s)}{\tilde{v}_g(s)} = &-\left(R^2 \mathrm{I}_{ref} (s C_d R_d + 1) (R \mathrm{I}_o R_{L2} - R V_{C2} - R_{L2} V_{C2}) \right) \Big/ \left((R^3 \mathrm{I}_o^2 C_1 C_2 C_d L_2 R_{L2}^2 R_d \right. \\
&- 2 R^3 \mathrm{I}_o C_1 C_2 C_d L_2 R_{L2} R_d V_{C2} - 2 R^2 \mathrm{I}_o C_1 C_2 C_d L_2 R_{L2}^2 R_d V_{C2} + R^3 C_1 C_2 C_d L_2 R_d V_{C2}^2 \\
&+ 2 R^2 C_1 C_2 C_d L_2 R_{L2} R_d V_{C2}^2 + R C_1 C_2 C_d L_2 R_{L2}^2 R_d V_{C2}^2) \, s^4 + (R^3 \mathrm{I}_o^2 C_1 C_2 C_d R_{L2}^3 R_d - 2 R^3 \mathrm{I}_o C_1 C_2 C_d \\
&R_{L2}^2 R_d V_{C2} - 2 R^2 \mathrm{I}_o C_1 C_2 C_d R_{L2}^3 R_d V_{C2} + R^3 \mathrm{I}_o^2 C_1 C_2 L_2 R_{L2}^2 + R^3 \mathrm{I}_o^2 C_2 C_d L_2 R_{L2}^2 - R^3 \mathrm{I}_{ref}^2 C_2 C_d L_2 R_{L1} R_d \\
&+ R^3 C_1 C_2 C_d R_{L2} R_d V_{C2}^2 + R^2 \mathrm{I}_o^2 C_1 C_d L_2 R_{L2}^2 R_d + 2 R^2 C_1 C_2 C_d R_{L2}^2 R_d V_{C2}^2 + R C_1 C_2 C_d R_{L2}^3 R_d V_{C2}^2 \\
&- 2 R^3 \mathrm{I}_o C_1 C_2 L_2 R_{L2} V_{C2} - 2 R^3 \mathrm{I}_o C_2 C_d L_2 R_{L2} V_{C2} + R^3 \mathrm{I}_{ref} C_2 C_d L_2 R_d V_g - 2 R^2 \mathrm{I}_o C_1 C_2 L_2 R_{L2}^2 V_{C2} \\
&- 2 R^2 \mathrm{I}_o C_1 C_d L_2 R_{L2} R_d V_{C2} - 2 R^2 \mathrm{I}_o C_2 C_d L_2 R_{L2}^2 V_{C2} - 2 R \mathrm{I}_o C_1 C_d L_2 R_{L2}^2 R_d V_{C2} + R^3 C_1 C_2 L_2 V_{C2}^2 \\
&+ R^3 C_2 C_d L_2 V_{C2}^2 + 2 R^2 C_1 C_2 L_2 R_{L2} V_{C2}^2 + R^2 C_1 C_d L_2 R_d V_{C2}^2 + 2 R^2 C_2 C_d L_2 R_{L2} V_{C2}^2 + R C_1 C_2 L_2 R_{L2}^2 \\
&V_{C2}^2 + 2 R C_1 C_d L_2 R_{L2} R_d V_{C2}^2 + R C_2 C_d L_2 R_{L2}^2 V_{C2}^2 + C_1 C_d L_2 R_{L2}^2 R_d V_{C2}^2) \, s^3 + (R^3 \mathrm{I}_o^2 C_1 C_2 R_{L2}^3 + R^3 \\
&\mathrm{I}_o^2 C_1 C_d R_{L2}^2 R_d + R^3 \mathrm{I}_o^2 C_2 C_d R_{L2}^3 + R^3 \mathrm{I}_o^2 C_2 C_d R_{L2}^2 R_d - R^3 \mathrm{I}_{ref}^2 C_2 C_d R_{L1} R_{L2} R_d + R^2 \mathrm{I}_o^2 C_1 C_d R_{L2}^3 R_d \\
&- 2 R^3 \mathrm{I}_o C_1 C_2 R_{L2}^2 V_{C2} - 2 R^3 \mathrm{I}_o C_1 C_d R_{L2} R_d V_{C2} - 2 R^3 \mathrm{I}_o C_2 C_d R_{L2}^2 V_{C2} - 2 R^3 \mathrm{I}_o C_2 C_d R_{L2} R_d V_{C2} \\
&+ R^3 \mathrm{I}_{ref} C_2 C_d R_{L2} R_d V_g - 2 R^2 \mathrm{I}_o C_1 C_2 R_{L2}^3 V_{C2} - 4 R^2 \mathrm{I}_o C_1 C_d R_{L2}^2 R_d V_{C2} - 2 R^2 \mathrm{I}_o C_2 C_d R_{L2}^3 V_{C2} \\
&- 2 R^2 \mathrm{I}_o C_2 C_d R_{L2}^2 R_d V_{C2} - 2 R \mathrm{I}_o C_1 C_d R_{L2}^3 R_d V_{C2} - R^3 \mathrm{I}_{ref}^2 C_2 L_2 R_{L1} + R^3 C_1 C_2 R_{L2} V_{C2}^2 + R^3 C_1 C_d R_d \\
&V_{C2}^2 + R^3 C_2 C_d R_{L2} V_{C2}^2 + R^3 C_2 C_d R_d V_{C2}^2 + R^2 \mathrm{I}_o^2 C_1 L_2 R_{L2}^2 + R^2 \mathrm{I}_o^2 C_d L_2 R_{L2}^2 - R^2 \mathrm{I}_{ref}^2 C_d L_2 R_{L1} R_d \\
&+ 2 R^2 C_1 C_2 R_{L2}^2 V_{C2}^2 + 3 R^2 C_1 C_d R_{L2} R_d V_{C2}^2 + 2 R^2 C_2 C_d R_{L2}^2 V_{C2}^2 + 2 R^2 C_2 C_d R_{L2} R_d V_{C2}^2 + R C_1 C_2 R_{L2}^3 \\
&V_{C2}^2 + 3 R C_1 C_d R_{L2}^2 R_d V_{C2}^2 + R C_2 C_d R_{L2}^3 V_{C2}^2 + R C_2 C_d R_{L2}^2 R_d V_{C2}^2 + C_1 C_d R_{L2}^3 R_d V_{C2}^2 + R^3 \mathrm{I}_{ref} C_2 L_2 V_g \\
&- 2 R^2 \mathrm{I}_o C_1 L_2 R_{L2} V_{C2} - 2 R^2 \mathrm{I}_o C_d L_2 R_{L2} V_{C2} + R^2 \mathrm{I}_{ref} C_d L_2 R_d V_g - 2 R \mathrm{I}_o C_1 L_2 R_{L2}^2 V_{C2} - 2 R \mathrm{I}_o C_d L_2 \\
&R_{L2}^2 V_{C2} + R^2 C_1 L_2 V_{C2}^2 + R^2 C_d L_2 V_{C2}^2 + 2 R C_1 L_2 R_{L2} V_{C2}^2 + 2 R C_d L_2 R_{L2} V_{C2}^2 + C_1 L_2 R_{L2}^2 V_{C2}^2 + C_d L_2 \\
&R_{L2}^2 V_{C2}^2) \, s^2 + (R^3 \mathrm{I}_o^2 C_1 R_{L2}^2 + R^3 \mathrm{I}_o^2 C_2 R_{L2}^2 + R^3 \mathrm{I}_o^2 C_d R_{L2}^2 - R^3 \mathrm{I}_{ref}^2 C_2 R_{L1} R_{L2} - R^3 \mathrm{I}_{ref}^2 C_d R_{L1} R_d + R^2 \mathrm{I}_o^2 C_1 \\
&R_{L2}^3 + R^2 \mathrm{I}_o^2 C_d R_{L2}^3 + R^2 \mathrm{I}_o^2 C_d R_{L2}^2 R_d - R^2 \mathrm{I}_{ref}^2 C_d R_{L1} R_{L2} R_d - 2 R^3 \mathrm{I}_o C_1 R_{L2} V_{C2} - 2 R^3 \mathrm{I}_o C_2 R_{L2} V_{C2}
\end{aligned}
\tag{8.4}
$$

$$-2 R^3 I_o C_d R_{L2} V_{C2} + R^3 I_{ref} C_2 R_{L2} V_g + R^3 I_{ref} C_d R_d V_g - 4 R^2 I_o C_1 R_{L2}^2 V_{C2} - 2 R^2 I_o C_2 R_{L2}^2 V_{C2}$$
$$-4 R^2 I_o C_d R_{L2}^2 V_{C2} - 2 R^2 I_o C_d R_{L2} R_d V_{C2} + R^2 I_{ref} C_d R_{L2} R_d V_g - 2 R I_o C_1 R_{L2}^3 V_{C2} - 2 R I_o C_d R_{L2}^3 V_{C2}$$
$$-2 R I_o C_d R_{L2}^2 R_d V_{C2} + R^3 C_1 V_{C2}^2 + R^3 C_2 V_{C2}^2 + R^3 C_d V_{C2}^2 - R^2 I_{ref}^2 L_2 R_{L1} + 3 R^2 C_1 R_{L2} V_{C2}^2$$
$$+2 R^2 C_2 R_{L2} V_{C2}^2 + 3 R^2 C_d R_{L2} V_{C2}^2 + R^2 C_d R_d V_{C2}^2 + 3 R C_1 R_{L2}^2 V_{C2}^2 + R C_2 R_{L2}^2 V_{C2}^2 + 3 R C_d R_{L2}^2 V_{C2}^2$$
$$+2 R C_d R_{L2} R_d V_{C2}^2 + C_1 R_{L2}^3 V_{C2}^2 + C_d R_{L2}^3 V_{C2}^2 + C_d R_{L2}^2 R_d V_{C2}^2 + R^2 I_{ref} L_2 V_g \big) s - R^3 I_{ref}^2 R_{L1} - R^2$$
$$I_{ref}^2 R_{L1} R_{L2} + R^2 R_{L2}^2 I_o^2 + R^3 I_{ref} V_g - 2 R^2 I_o R_{L2} V_{C2} + R^2 I_{ref} V_g R_{L2} - 2 R R_{L2}^2 I_o V_{C2} + R^2 V_{C2}^2 + 2 R R_{L2} V_{C2}^2$$
$$+R_{L2}^2 V_{C2}^2 \big)$$

8.5 Current reference to output voltage transfer function

The small signal current reference to output voltage is obtained as described in section 3.3.3, and its expression is the following

$$\frac{\tilde{v}_{C2}(s)}{\tilde{i}_{ref}(s)} = \big(R^2 \big(C_d L_1 R_d I_{ref} s^2 + \big(2 I_{ref} C_d R_{L1} R_d - C_d R_d V_g + I_{ref} L_1\big) s + 2 R_{L1} I_{ref} - V_g\big) \big(R I_o R_{L2} - R V_{C2} \tag{8.5}$$

$$-R_{L2} V_{C2}\big)\big) \Big/ \Big(\big(R^3 I_o^2 C_1 C_2 C_d L_2 R_{L2}^2 R_d - 2 R^3 I_o C_1 C_2 C_d L_2 R_{L2} R_d V_{C2} - 2 R^2 I_o C_1 C_2 C_d L_2 R_{L2}^2 R_d V_{C2}$$
$$+R^3 C_1 C_2 C_d L_2 R_d V_{C2}^2 + 2 R^2 C_1 C_2 C_d L_2 R_{L2} R_d V_{C2}^2 + R C_1 C_2 C_d L_2 R_{L2}^2 R_d V_{C2}^2\big) s^4 + \big(R^3 I_o^2 C_1 C_2 C_d$$
$$R_{L2}^3 R_d - 2 R^3 I_o C_1 C_2 C_d R_{L2}^2 R_d V_{C2} - 2 R^2 I_o C_1 C_2 C_d R_{L2}^3 R_d V_{C2} + R^3 I_o^2 C_1 C_2 L_2 R_{L2}^2 + R^3 I_o^2 C_2 C_d L_2 R_{L2}^2$$
$$-R^3 I_{ref}^2 C_2 C_d L_2 R_{L1} R_d + R^3 C_1 C_2 C_d R_{L2} R_d V_{C2}^2 + R^2 I_o^2 C_1 C_d L_2 R_{L2}^2 R_d + 2 R^2 C_1 C_2 C_d R_{L2}^2 R_d V_{C2}^2$$
$$+R C_1 C_2 C_d R_{L2}^3 R_d V_{C2}^2 - 2 R^3 I_o C_1 C_2 L_2 R_{L2} V_{C2} - 2 R^3 I_o C_2 C_d L_2 R_{L2} V_{C2} + R^3 I_{ref} C_2 C_d L_2 R_d V_g$$
$$-2 R^2 I_o C_1 C_2 L_2 R_{L2}^2 V_{C2} - 2 R^2 I_o C_1 C_d L_2 R_{L2} R_d V_{C2} - 2 R^2 I_o C_2 C_d L_2 R_{L2}^2 V_{C2} - 2 R I_o C_1 C_d L_2$$
$$R_{L2}^2 R_d V_{C2} + R^3 C_1 C_2 L_2 V_{C2}^2 + R^3 C_2 C_d L_2 V_{C2}^2 + 2 R^2 C_1 C_2 L_2 R_{L2} V_{C2}^2 + R^2 C_1 C_d L_2 R_d V_{C2}^2$$
$$+2 R^2 C_2 C_d L_2 R_{L2} V_{C2}^2 + R C_1 C_2 L_2 R_{L2}^2 V_{C2}^2 + 2 R C_1 C_d L_2 R_{L2} R_d V_{C2}^2 + R C_2 C_d L_2 R_{L2}^2 V_{C2}^2 + C_1 C_d L_2$$
$$R_{L2}^2 R_d V_{C2}^2\big) s^3 + \big(R^3 I_o^2 C_1 C_2 R_{L2}^3 + R^3 I_o^2 C_1 C_d R_{L2}^2 R_d + R^3 I_o^2 C_2 C_d R_{L2}^3 + R^3 I_o^2 C_2 C_d R_{L2}^2 R_d - R^3$$
$$I_{ref}^2 C_2 C_d R_{L1} R_{L2} R_d + R^2 I_o^2 C_1 C_d R_{L2}^3 R_d - 2 R^3 I_o C_1 C_2 R_{L2}^2 V_{C2} - 2 R^3 I_o C_1 C_d R_{L2} R_d V_{C2} - 2 R^3 I_o C_2 C_d$$
$$R_{L2}^2 V_{C2} - 2 R^3 I_o C_2 C_d R_{L2} R_d V_{C2} + R^3 I_{ref} C_2 C_d R_{L2} R_d V_g - 2 R^2 I_o C_1 C_2 R_{L2}^3 V_{C2} - 4 R^2 I_o C_1 C_d$$
$$R_{L2}^2 R_d V_{C2} - 2 R^2 I_o C_2 C_d R_{L2}^3 V_{C2} - 2 R^2 I_o C_2 C_d R_{L2}^2 R_d V_{C2} - 2 R I_o C_1 C_d R_{L2}^3 R_d V_{C2} - R^3 I_{ref}^2 C_2 L_2 R_{L1}$$
$$+R^3 C_1 C_2 R_{L2} V_{C2}^2 + R^3 C_1 C_d R_d V_{C2}^2 + R^3 C_2 C_d R_{L2} V_{C2}^2 + R^3 C_2 C_d R_d V_{C2}^2 + R^2 I_o^2 C_1 L_2 R_{L2}^2 + R^2$$
$$I_o^2 C_d L_2 R_{L2}^2 - R^2 I_{ref}^2 C_d L_2 R_{L1} R_d + 2 R^2 C_1 C_2 R_{L2}^2 V_{C2}^2 + 3 R^2 C_1 C_d R_{L2} R_d V_{C2}^2 + 2 R^2 C_2 C_d R_{L2}^2 V_{C2}^2$$
$$+2 R^2 C_2 C_d R_{L2} R_d V_{C2}^2 + R C_1 C_2 R_{L2}^3 V_{C2}^2 + 3 R C_1 C_d R_{L2}^2 R_d V_{C2}^2 + R C_2 C_d R_{L2}^3 V_{C2}^2 + R C_2 C_d R_{L2}^2 R_d$$
$$V_{C2}^2 + C_1 C_d R_{L2}^3 R_d V_{C2}^2 + R^3 I_{ref} C_2 L_2 V_g - 2 R^2 I_o C_1 L_2 R_{L2} V_{C2} - 2 R^2 I_o C_d L_2 R_{L2} V_{C2} + R^2 I_{ref} C_d L_2 R_d V_g$$
$$-2 R I_o C_1 L_2 R_{L2}^2 V_{C2} - 2 R I_o C_d L_2 R_{L2}^2 V_{C2} + R^2 C_1 L_2 V_{C2}^2 + R^2 C_d L_2 V_{C2}^2 + 2 R C_1 L_2 R_{L2} V_{C2}^2$$
$$+2 R C_d L_2 R_{L2} V_{C2}^2 + C_1 L_2 R_{L2}^2 V_{C2}^2 + C_d L_2 R_{L2}^2 V_{C2}^2\big) s^2 + \big(R^3 I_o^2 C_1 R_{L2}^2 + R^3 I_o^2 C_2 R_{L2}^2 + R^3 I_o^2 C_d R_{L2}^2$$
$$-R^3 I_{ref}^2 C_2 R_{L1} R_{L2} - R^3 I_{ref}^2 C_d R_{L1} R_d + R^2 I_o^2 C_1 R_{L2}^3 + R^2 I_o^2 C_d R_{L2}^3 + R^2 I_o^2 C_d R_{L2}^2 R_d - R^2 I_{ref}^2 C_d R_{L1} R_{L2} R_d$$
$$-2 R^3 I_o C_1 R_{L2} V_{C2} - 2 R^3 I_o C_2 R_{L2} V_{C2} - 2 R^3 I_o C_d R_{L2} V_{C2} + R^3 I_{ref} C_2 R_{L2} V_g + R^3 I_{ref} C_d R_d V_g$$
$$-4 R^2 I_o C_1 R_{L2}^2 V_{C2} - 2 R^2 I_o C_2 R_{L2}^2 V_{C2} - 4 R^2 I_o C_d R_{L2}^2 V_{C2} - 2 R^2 I_o C_d R_{L2} R_d V_{C2} + R^2 I_{ref} C_d R_{L2} R_d V_g$$
$$-2 R I_o C_1 R_{L2}^3 V_{C2} - 2 R I_o C_d R_{L2}^3 V_{C2} - 2 R I_o C_d R_{L2}^2 R_d V_{C2} + R^3 C_1 V_{C2}^2 + R^3 C_2 V_{C2}^2 + R^3 C_d V_{C2}^2 - R^2$$
$$I_{ref}^2 L_2 R_{L1} + 3 R^2 C_1 R_{L2} V_{C2}^2 + 2 R^2 C_2 R_{L2} V_{C2}^2 + 3 R^2 C_d R_{L2} V_{C2}^2 + R^2 C_d R_d V_{C2}^2 + 3 R C_1 R_{L2}^2 V_{C2}^2 + R C_2$$
$$R_{L2}^2 V_{C2}^2 + 3 R C_d R_{L2}^2 V_{C2}^2 + 2 R C_d R_{L2} R_d V_{C2}^2 + C_1 R_{L2}^3 V_{C2}^2 + C_d R_{L2}^3 V_{C2}^2 + C_d R_{L2}^2 R_d V_{C2}^2 + R^2 I_{ref} L_2 V_g\big) s$$
$$-R^3 I_{ref}^2 R_{L1} - R^2 I_{ref}^2 R_{L1} R_{L2} + R^2 R_{L2}^2 I_o^2 + R^3 I_{ref} V_g - 2 R^2 I_o R_{L2} V_{C2} + R^2 I_{ref} V_g R_{L2} - 2 R R_{L2}^2 I_o V_{C2} + R^2$$
$$V_{C2}^2 + 2 R R_{L2} V_{C2}^2 + R_{L2}^2 V_{C2}^2\Big)$$

References

[1] M. Guarnieri, "When Cars Went Electric, Part One [Historical]," *Industrial Electronics Magazine, IEEE,* vol. 5, pp. 61-62, 2011.

[2] M. Guarnieri, "When Cars Went Electric, Part 2 [Historical]," *Industrial Electronics Magazine, IEEE,* vol. 5, pp. 46-53, 2011.

[3] C. C. Chan, "The Rise & Fall of Electric Vehicles in 1828–1930: Lessons Learned [Scanning Our Past]," *Proceedings of the IEEE,* vol. 101, pp. 206-212, 2013.

[4] K. Rajashekara, "Present Status and Future Trends in Electric Vehicle Propulsion Technologies," *Emerging and Selected Topics in Power Electronics, IEEE Journal of,* vol. 1, pp. 3-10, 2013.

[5] R. K. Dixon, E. McGowan, G. Onysko, and R. M. Scheer, "US energy conservation and efficiency policies: Challenges and opportunities," *Energy Policy,* vol. 38, pp. 6398-6408, 2010.

[6] T. R. Hawkins, B. Singh, G. Majeau-Bettez, and A. H. Strømman, "Comparative Environmental Life Cycle Assessment of Conventional and Electric Vehicles," *Journal of Industrial Ecology,* vol. 17, pp. 53-64, 2013.

[7] E. J. Cairns and P. Albertus, "Batteries for Electric and Hybrid-Electric Vehicles," *Annual Review of Chemical and Biomolecular Engineering,* vol. 1, pp. 299-320, 2010.

[8] A. Ajanovic and R. Haas, "Technological, ecological and economic perspectives for alternative automotive technologies up to 2050," in *Sustainable Energy Technologies (ICSET), 2012 IEEE Third International Conference on*, 2012, pp. 129-134.

[9] N. Hill, C. Brannigan, R. Smokers, A. Schroten, H. v. Essen, and I. Skinner, "Developing a better understanding of the secondary impacts and key sensitivities for the decarbonisation of the EU's transport sector by 2050," European Commission Directorate-General Climate Action and AEA Technology plc, 2012.

[10] D. Anair and A. Mahmassani, "State of charge: Electric vehicles’ global warming emissions and fuel-cost savings across the United States," *Union of Concerned Scientists Report,* 2012.

[11] O. Lopez-Santos, L. Martinez-Salamero, G. Garcia, H. Valderrama-Blavi, and D. O. Mercuri, "Efficiency analysis of a sliding-mode controlled quadratic boost converter," *Power Electronics, IET,* vol. 6, pp. 364-373, 2013.

[12] Nissan, *2011 LEAF Owner's Manual*, 2011.

[13] M. D. Galus, R. A. Waraich, F. Noembrini, K. Steurs, G. Georges, K. Boulouchos, K. W. Axhausen, and G. Andersson, "Integrating Power Systems, Transport Systems and Vehicle Technology for Electric Mobility Impact Assessment and Efficient Control," *Smart Grid, IEEE Transactions on,* vol. 3, pp. 934-949, 2012.

[14] C. C. Chan, A. Bouscayrol, and K. Chen, "Electric, Hybrid, and Fuel-Cell Vehicles: Architectures and Modeling," *Vehicular Technology, IEEE Transactions on,* vol. 59, pp. 589-598, 2010.

[15] K. Rajashekara, "Parallel between More Electric Aircraft and Electric/Hybrid Vehicle Power Conversion Technologies," *Electrification Magazine, IEEE,* vol. 2, pp. 50-60, 2014.

[16] A. Emadi, L. Young Joo, and K. Rajashekara, "Power Electronics and Motor Drives in Electric, Hybrid Electric, and Plug-In Hybrid Electric Vehicles," *Industrial Electronics, IEEE Transactions on,* vol. 55, pp. 2237-2245, 2008.

[17] M. Ehsani, G. Yimin, and J. M. Miller, "Hybrid Electric Vehicles: Architecture and Motor Drives," *Proceedings of the IEEE,* vol. 95, pp. 719-728, 2007.

[18] A. Karaarslan and I. Iskender, "Average sliding control method applied on power factor correction converter for decreasing input current total harmonic distortion using digital signal processor," *Power Electronics, IET,* vol. 5, pp. 617-626, 2012.

[19] E. Sato, "Permanent magnet synchronous motor drives for hybrid electric vehicles," *IEEJ Transactions on Electrical and Electronic Engineering,* vol. 2, pp. 162-168, 2007.

[20] C. Mi, M. A. Masrur, and D. W. Gao, "Power Electronics in HEVs," in *Hybrid Electric Vehicles*, ed: John Wiley & Sons, Ltd, 2011, pp. 197-244.

[21] O. Hegazy, R. Barrero, J. Van Mierlo, P. Lataire, N. Omar, and T. Coosemans, "An Advanced Power Electronics Interface for Electric Vehicles Applications," *Power Electronics, IEEE Transactions on,* vol. 28, pp. 5508-5521, 2013.

[22] L. Zhu, "A Novel Soft-Commutating Isolated Boost Full-Bridge ZVS-PWM DC–DC Converter for Bidirectional High Power Applications," *Power Electronics, IEEE Transactions on,* vol. 21, pp. 422-429, 2006.

[23] A. Nahavandi, M. T. Hagh, M. B. B. Sharifian, and S. Danyali, "A Nonisolated Multiinput Multioutput DC–DC Boost Converter for Electric Vehicle Applications," *Power Electronics, IEEE Transactions on,* vol. 30, pp. 1818-1835, 2015.

[24] D. R. Northcott, S. Filizadeh, and A. R. Chevrefils, "Design of a bidirectional buck-boost dc/dc converter for a series hybrid electric vehicle using PSCAD/EMTDC," in *Vehicle Power and Propulsion Conference, 2009. VPPC '09. IEEE*, 2009, pp. 1561-1566.

[25] O. C. Onar, J. Kobayashi, D. C. Erb, and A. Khaligh, "A Bidirectional High-Power-Quality Grid Interface With a Novel Bidirectional Noninverted Buck–Boost Converter for PHEVs," *Vehicular Technology, IEEE Transactions on,* vol. 61, pp. 2018-2032, 2012.

[26] J. M. Blanes, R. Gutierrez, A. Garrigos, J. L. Lizan, and J. M. Cuadrado, "Electric Vehicle Battery Life Extension Using Ultracapacitors and an FPGA Controlled Interleaved Buck–Boost Converter," *Power Electronics, IEEE Transactions on,* vol. 28, pp. 5940-5948, 2013.

[27] S. Cuk and R. Middlebrook, "A new optimum topology switching dc-to-dc converter," in *Power Electronics Specialists Conference*, 1977, pp. 160-179.

[28] R. M. Schupbach and J. C. Balda, "Comparing DC-DC converters for power management in hybrid electric vehicles," in *Electric Machines and Drives Conference, 2003. IEMDC'03. IEEE International*, 2003, pp. 1369-1374 vol.3.

[29] R. P. Massey and E. C. Snyder, "High voltage single-ended DC-DC converter," in *Power Electronics Specialists Conference, 1977 IEEE*, 1977, pp. 156-159.

[30] A. Cantillo, A. De Nardo, N. Femia, and W. Zamboni, "Stability Issues in Peak-Current-Controlled SEPIC," *Power Electronics, IEEE Transactions on,* vol. 26, pp. 551-562, 2011.

[31] K. M. Tsang and W. L. Chan, "Multi-loop controller for wide operating range single-ended primary inductor DC/DC converter," *Power Electronics, IET,* vol. 4, pp. 891-898, 2011.

[32] A. Kavitha and G. Uma, "Comparative study between peak current mode and hysteretic current mode control of a single-ended primary inductance converter," *Power Electronics, IET,* vol. 5, pp. 1226-1235, 2012.

[33] I. Husain, *Electric and Hybrid Vehicles: Design Fundamentals*, 2nd ed.: Taylor & Francis, 2011.

[34] L. Albiol-Tendillo, E. Vidal-Idiarte, J. Maixe-Altes, J. M. Bosque-Moncusi, and H. Valderrama-Blavi, "Design and control of a bidirectional DC/DC converter for an Electric Vehicle," in *Power Electronics and Motion Control Conference (EPE/PEMC), 2012 15th International*, 2012, pp. LS4d.2-1-LS4d.2-5.

[35] S. Soylu, *Electric Vehicles – Modelling and Simulations*. Rijeka, Croatia: Intech Europe, 2011.

[36] T. C. Neugebauer and D. J. Perreault, "Computer-aided optimization of DC/DC converters for automotive applications," *Power Electronics, IEEE Transactions on,* vol. 18, pp. 775-783, 2003.

[37] S. De Breucker, K. Engelen, P. Tant, and J. Driesen, "Adaptive control scheme for a practical bidirectional DC-DC converter with a 80 kHz switching and a 10 kHz sampling frequency," in *Power Electronics, Machines and Drives (PEMD 2010), 5th IET International Conference on*, 2010, pp. 1-6.

[38] R. T. Naayagi, A. J. Forsyth, and R. Shuttleworth, "Bidirectional control of a dual active bridge DC-DC converter for aerospace applications," *Power Electronics, IET,* vol. 5, pp. 1104-1118, 2012.

[39] K. Hyosung, Y. Taesik, and C. Sewan, "Indirect Current Control Algorithm for Utility Interactive Inverters in Distributed Generation Systems," *Power Electronics, IEEE Transactions on,* vol. 23, pp. 1342-1347, 2008.

[40] K. Minho, O. Secheol, and C. Sewan, "High Gain Soft-Switching Bidirectional DC-DC Converter for Eco-Friendly Vehicles," *Power Electronics, IEEE Transactions on,* vol. 29, pp. 1659-1666, 2014.

[41] P. Junsung and C. Sewan, "Design and Control of a Bidirectional Resonant DC-DC Converter for Automotive Engine/Battery Hybrid Power Generators," *Power Electronics, IEEE Transactions on,* vol. 29, pp. 3748-3757, 2014.

[42] K. Engelen, S. De Breucker, P. Tant, and J. Driesen, "Gain scheduling control of a bidirectional dc-dc converter with large dead-time," *Power Electronics, IET,* vol. 7, pp. 480-488, 2014.

[43] J. A. Barrado, A. El Aroudi, H. Valderrama-Blavi, J. Calvente, and L. Martinez-Salamero, "Analysis of a Self-Oscillating Bidirectional DC-DC Converter in Battery Energy Storage Applications," *Power Delivery, IEEE Transactions on,* vol. 27, pp. 1292-1300, 2012.

[44] V. Utkin, J. Guldner, and J. Shi, *Sliding mode control in electro-mechanical systems*, 2nd ed.: Boca Raton,FL: CRC, 2009.

[45] L. Martinez-Salamero, G. Garcia, M. Orellana, C. Lahore, and B. Estibals, "Start-Up Control and Voltage Regulation in a Boost Converter Under Sliding-Mode Operation," *Industrial Electronics, IEEE Transactions on,* vol. 60, pp. 4637-4649, 2013.

[46] J. M. Miller and I. o. E. Engineers, *Propulsion Systems for Hybrid Vehicles*: Institution of Electrical Engineers, 2004.

[47] Z. Q. Zhu and D. Howe, "Electrical Machines and Drives for Electric, Hybrid, and Fuel Cell Vehicles," *Proceedings of the IEEE,* vol. 95, pp. 746-765, 2007.

[48] K. T. Chau, C. C. Chan, and L. Chunhua, "Overview of Permanent-Magnet Brushless Drives for Electric and Hybrid Electric Vehicles," *Industrial Electronics, IEEE Transactions on,* vol. 55, pp. 2246-2257, 2008.

[49] K. H. Nam, *AC Motor Control and Electrical Vehicle Applications*: CRC Press, 2010.

[50] I. Husain, *Electric and Hybrid Vehicles: Design Fundamentals, Second Edition*: Taylor & Francis, 2011.

[51] A. Emadi, A. Khaligh, C. H. Rivetta, and G. A. Williamson, "Constant power loads and negative impedance instability in automotive systems: definition, modeling, stability, and control of power electronic converters and motor drives," *Vehicular Technology, IEEE Transactions on,* vol. 55, pp. 1112-1125, 2006.

[52] Y. A. R. I. Mohamed, A. A. A. Radwan, and T. K. Lee, "Decoupled Reference-Voltage-Based Active DC-Link Stabilization for PMSM Drives With Tight-Speed Regulation," *Industrial Electronics, IEEE Transactions on,* vol. 59, pp. 4523-4536, 2012.

[53] A. M. Rahimi and A. Emadi, "An Analytical Investigation of DC/DC Power Electronic Converters With Constant Power Loads in Vehicular Power Systems," *Vehicular Technology, IEEE Transactions on,* vol. 58, pp. 2689-2702, 2009.

UNIVERSITAT ROVIRA I VIRGILI
DESIGN AND CONTROL OF A BIDIRECTIONAL DC/DC CONVERTER FOR AN ELECTRIC VEHICLE APPLICATION.
Laura Albiol Rendillo
Dipòsit Legal: T 1361-2015

[54] R. B. Ridley, "Secondary LC filter analysis and design techniques for current-mode-controlled converters," *Power Electronics, IEEE Transactions on,* vol. 3, pp. 499-507, 1988.

[55] R. W. Erickson and D. Maksimovic, *Fundamentals of Power Electronics*: Springer, 2001.

[56] R. Haroun, A. Cid-Pastor, A. El Aroudi, and L. Martinez-Salamero, "Synthesis of Canonical Elements for Power Processing in DC Distribution Systems Using Cascaded Converters and Sliding-Mode Control," *Power Electronics, IEEE Transactions on,* vol. 29, pp. 1366-1381, 2014.

[57] F. F. A. van der Pijl, M. Castilla, and P. Bauer, "Adaptive Sliding-Mode Control for a Multiple-User Inductive Power Transfer System Without Need for Communication," *Industrial Electronics, IEEE Transactions on,* vol. 60, pp. 271-279, 2013.

[58] A. Marcos-Pastor, E. Vidal-Idiarte, A. Cid-Pastor, and L. Martinez-Salamero, "Loss-Free Resistor-based Power Factor Correction using a Semi-bridgeless Boost Rectifier in Sliding-Mode Control," *Power Electronics, IEEE Transactions on,* vol. PP, pp. 1-1, 2014.

[59] R. Guzman, L. J. Garcia de Vicuna, J. Morales, M. Castilla, and J. Matas, "Sliding-Mode Control for a Three-Phase Unity Power Factor Rectifier Operating at Fixed Switching Frequency," *Power Electronics, IEEE Transactions on,* vol. PP, pp. 1-1, 2015.

[60] W. Rong-Jong and L. Chun-Yu, "Active Low-Frequency Ripple Control for Clean-Energy Power-Conditioning Mechanism," *Industrial Electronics, IEEE Transactions on,* vol. 57, pp. 3780-3792, 2010.

[61] J. Pegueroles-Queralt, F. D. Bianchi, and O. Gomis-Bellmunt, "A Power Smoothing System Based on Supercapacitors for Renewable Distributed Generation," *Industrial Electronics, IEEE Transactions on,* vol. 62, pp. 343-350, 2015.

[62] C. Evangelista, P. Puleston, F. Valenciaga, and L. M. Fridman, "Lyapunov-Designed Super-Twisting Sliding Mode Control for Wind Energy Conversion Optimization," *Industrial Electronics, IEEE Transactions on,* vol. 60, pp. 538-545, 2013.

[63] R. Haroun, A. El Aroudi, A. Cid-Pastor, G. Garica, C. Olalla, and L. Martinez-Salamero, "Impedance Matching in Photovoltaic Systems Using Cascaded Boost Converters and Sliding-Mode Control," *Power Electronics, IEEE Transactions on,* vol. 30, pp. 3185-3199, 2015.

[64] E. Mamarelis, G. Petrone, and G. Spagnuolo, "Design of a Sliding-Mode-Controlled SEPIC for PV MPPT Applications," *Industrial Electronics, IEEE Transactions on,* vol. 61, pp. 3387-3398, 2014.

[65] E. Bianconi, J. Calvente, R. Giral, E. Mamarelis, G. Petrone, C. A. Ramos-Paja, G. Spagnuolo, and M. Vitelli, "A Fast Current-Based MPPT Technique Employing Sliding Mode Control," *Industrial Electronics, IEEE Transactions on,* vol. 60, pp. 1168-1178, 2013.

[66] D. Gonzalez Montoya, C. Ramos, and R. Giral, "Improved design of sliding mode controllers based on the requirements of MPPT techniques," *Power Electronics, IEEE Transactions on,* vol. PP, pp. 1-1, 2015.

[67] R. Silva-Ortigoza, V. M. Hernandez-Guzman, M. Antonio-Cruz, and D. Munoz-Carrillo, "DC/DC Buck Power Converter as a Smooth Starter for a DC Motor Based on a Hierarchical Control," *Power Electronics, IEEE Transactions on,* vol. 30, pp. 1076-1084, 2015.

[68] B. Labbe, B. Allard, L.-S. Xuefang, and D. Chesneau, "An Integrated Sliding-Mode Buck Converter With Switching Frequency Control for Battery-Powered Applications," *Power Electronics, IEEE Transactions on,* vol. 28, pp. 4318-4326, 2013.

[69] A. Leon-Masich, H. Valderrama-Blavi, J. M. Bosque-Moncusi, J. Maixe-Altes, and L. Martinez-Salamero, "Sliding-Mode-Control-Based Boost Converter for High-Voltage–Low-Power Applications," *Industrial Electronics, IEEE Transactions on,* vol. 62, pp. 229-237, 2015.

[70] O. Lopez-Santos, L. Martinez-Salamero, G. Garcia, H. Valderrama-Blavi, and T. Sierra-Polanco, "Robust Sliding-Mode Control Design for a Voltage Regulated Quadratic Boost Converter," *Power Electronics, IEEE Transactions on,* vol. 30, pp. 2313-2327, 2015.

[71] M. Hao, L. Qinwei, and W. Yuxi, "Discrete pulse frequency modulation control with sliding-mode implementation on LLC resonant DC/DC converter via input-output linearisation," *Power Electronics, IET,* vol. 7, pp. 1033-1043, 2014.

[72] J. L. Sosa, M. Castilla, J. Miret, L. G. de Vicuna, and L. S. Moreno, "Sliding-Mode Input–Output Linearization Controller for the DC/DC ZVS CLL-T Resonant Converter," *Industrial Electronics, IEEE Transactions on,* vol. 59, pp. 1554-1564, 2012.

[73] L. Albiol-Tendillo, E. Vidal-Idiarte, J. Maixe-Altes, S. Mendez-Prince, and L. Martinez-Salamero. (2015, Seamless sliding-mode control for bidirectional boost converter with output filter for electric vehicles applications. *IET Power Electronics*. Available: http://digital-library.theiet.org/content/journals/10.1049/iet-pel.2014.0786

[74] P. J. Grbovic, *Ultra-Capacitors in Power Conversion Systems: Analysis, Modeling and Design in Theory and Practice*: Wiley, 2013.

[75] B. A. Miwa, "Interleaved Conversion Techniques for High Density Power Supplies," Massachusetts Institute of Technology, 1992.

[76] O. Hegazy, J. Van Mierlo, and P. Lataire, "Analysis, Modeling, and Implementation of a Multidevice Interleaved DC/DC Converter for Fuel Cell Hybrid Electric Vehicles," *Power Electronics, IEEE Transactions on,* vol. 27, pp. 4445-4458, 2012.

[77] D. De, C. Klumpner, C. Patel, K. Ponggorn, M. Rashed, and G. Asher, "Modelling and control of a multi-stage interleaved DC-DC converter with coupled inductors for super-capacitor energy storage system," *Power Electronics, IET,* vol. 6, pp. 1360-1375, 2013.

[78] W. Chien-Ming, L. Chang-Hua, H. Shih-Yung, L. Chien-Min, and L. Jyun-Che, "Analysis, design and performance of a zero-currentswitching pulse-width-modulation interleaved boost dc/dc converter," *Power Electronics, IET,* vol. 7, pp. 2437-2445, 2014.

[79] L. W. Zhou, B. X. Zhu, Q. M. Luo, and S. Chen, "Interleaved non-isolated high step-up DC/DC converter based on the diode-capacitor multiplier," *Power Electronics, IET,* vol. 7, pp. 390-397, 2014.

[80] A. Cid-Pastor, R. Giral, J. Calvente, V. I. Utkin, and L. Martinez-Salamero, "Interleaved Converters Based on Sliding-Mode Control in a Ring Configuration," *Circuits and Systems I: Regular Papers, IEEE Transactions on,* vol. 58, pp. 2566-2577, 2011.

[81] Control Techniques, "Unidrive SP Regen Installation Guide," ed, 2007.

[82] L. Yan-Fei and L. Xiaodong, "Recent developments in digital control strategies for DC/DC switching power converters," in *Power Electronics and Motion Control Conference, 2009. IPEMC '09. IEEE 6th International*, 2009, pp. 307-314.

[83] E. Vidal-Idiarte, A. Marcos-Pastor, G. Garcia, A. Cid-Pastor, and L. Martinez-Salamero, "Discrete-time sliding-mode-based digital pulse width modulation control of a boost converter," *Power Electronics, IET,* vol. 8, pp. 708-714, 2015.

[84] A. Marcos-Pastor, E. Vidal-Idiarte, A. Cid-Pastor, and L. Martinez-Salamero, "Digital control of a unidirectional battery charger for electric vehicles," in *Control and Modeling for Power Electronics (COMPEL), 2014 IEEE 15th Workshop on*, 2014, pp. 1-6.

[85] A. Marcos-Pastor, M. Bodetto, A. El Aroudi, E. Vidal-Idiarte, A. Cid-Pastor, and L. Martinez-Salamero, "Discrete-time sliding mode control of SEPIC and Ćuk converters supplying HBLEDs," in *Control and Modeling for Power Electronics (COMPEL), 2014 IEEE 15th Workshop on*, 2014, pp. 1-5.

[86] A. Marcos-Pastor, E. Vidal-Idiarte, A. Cid-Pastor, and L. Martinez-Salamero, "Digital Loss-Free Resistor for power factor correction applications," in *Industrial Electronics Society, IECON 2013 - 39th Annual Conference of the IEEE*, 2013, pp. 3468-3473.

[87] A. Marcos-Pastor, "Design and Control of a Battery Charger for Electric Vehicles," Doctoral Thesis, Universitat Rovira i Virgili, Tarragona, 2015.

[88] F. J. Chang, E. C. Chang, T. J. Liang, and J. F. Chen, "Digital-signal-processor-based DC/AC inverter with integral-compensation terminal sliding-mode control," *Power Electronics, IET,* vol. 4, pp. 159-167, 2011.

[89] E. Mamarelis, G. Petrone, and G. Spagnuolo, "An Hybrid Digital-Analog Sliding Mode Controller for Photovoltaic Applications," *Industrial Informatics, IEEE Transactions on,* vol. 9, pp. 1094-1103, 2013.

[90] E. Vidal-Idiarte, C. E. Carrejo, J. Calvente, and L. Martínez-Salamero, "Two-Loop Digital Sliding Mode Control of DC-DC Power Converters Based on Predictive Interpolation," *Industrial Electronics, IEEE Transactions on,* vol. 58, pp. 2491-2501, 2011.